THE ROLE OF NEUREXINS IN SEROTONIN SIGNALING AND COMPLEX BEHAVIORS

A Dissertation Presented

By

Amy Cheung

Submitted to the Faculty of the

University of Massachusetts Graduate School of Biomedical Sciences, Worcester

in partial fulfillment of the requirements for the degree of

DOCTOR OF PHILOSOPHY

April 27, 2021

Neuroscience

THE ROLE OF NEUREXINS IN SEROTONIN SIGNALING AND COMPLEX BEHAVIORS

A Dissertation Presented

By

Amy Cheung

This work was undertaken in the Graduate School of Biomedical Sciences

M.D./Ph.D. Program

Under the mentorship of

Kensuke Futai, Ph.D., Thesis Advisor

Andrew R. Tapper, Ph.D., Member of Committee

Christelle Anaclet, Ph.D., Member of Committee

Fen-Biao Gao, Ph.D., Member of Committee

Jacqueline N. Crawley, External Member of Committee

Gilles Martin, Ph.D., Chair of Committee

Mary Ellen Lane, Ph.D.,

Dean of the Graduate School of Biomedical Sciences

April 27, 2021

Dedication

To my mom and dad

for your unending support and wish for my happiness

To Kevin, my love and best friend

for encouraging me to embark on this adventure

Thank you for believing in me.

Acknowledgements

I've been on an incredible journey these past four years. I've met so many people and learned so many things that have helped shaped me into the person I am today. I would not be writing this thesis and immersing myself in the beauties and challenges of research if not for my thesis advisor, Dr. Kensuke Futai. From the beginning, Kenny gave me the independence and flexibility to explore my project in the ways I wanted to and opportunities to collaborate on some amazing projects. Kenny is one of the hardest working people I know. It's inspiring to see his passion for research and the remarkable efforts he makes to answer the scientific questions he pursues in his career. I am eternally grateful for his patience, guidance, and tenacity.

My TRAC meetings were moments I felt huge gains in my knowledge and confidence in my progress as a student. I am thankful for Gilles Martin, Andrew Tapper, Fen-Biao Gao, and Christelle Anaclet for serving on my TRAC and now my dissertation committee. They have always kept me on track and watched me grow every step of the way. I am excited and thankful to have Jacqueline Crawley, my behavioral neuroscientist idol, serve as my external committee member.

I had the opportunity to share my everyday life with wonderful lab members: Motokazu, Wenjie, Naoe, Julie, and Sabine. While they have moved on to new chapters in their lives, I am so happy that I could get to know these amazing people. I am grateful to Motokazu and Wenjie who both took the time to help me learn new techniques and think more critically when I first joined the lab.

I'm fortunate to have been able to share lab space with the Martin lab. I would like to thank Dr. Martin's lab members, Jenya, Timmy, and Pablo, for their bright attitudes that lift my spirits. In particular, Jenya has been a friend whom I could be honest with and discuss different perspectives on life and science.

For my scientific growth, I would like to thank people in the BNRI and in Dr. Veronica Alvarez's lab. Susanna from the Tapper lab is a talented behavioral neuroscientist whom I look up to and who has shared her expertise and advice on my project on numerous occasions. Aya and Roland from the Alvarez lab were instrumental in helping our lab establish fast scan cyclic voltammetry. I turned to Patrick in the Melikian lab and Jenya for advice on fast scan cyclic voltammetry. I would also like to thank the MD/PhD program and the National Institute of Mental Health for supporting my training.

I would like to thank the remarkable people who work behind-the-scenes including Chris, Mike G, Miranda, Jennifer, Tara, and Tracey. From ensuring our animal colonies are healthy and well to providing administrative, housekeeping, and lab support in the Department of Neurobiology, these were responsibilities that allowed our lab to run smoothly and effectively while I could focus on my research.

My friends in the Medical School Class of 2019, MD/PhD program, medical school and graduate school, Community Intervention Program, and outside of school, were there for me during both fun and difficult times. My medical school mentor, Philip Fournier, has known me since I first started medical school in 2015 and I look forward to our biannual meetings. He listens with an unbiased

perspective and helps me feel connected with more senior students by sharing what he's learned as a mentor. My close friend, Jingwen, shows me that distance does not matter in a friendship and we can always pick up where we last left off in our conversations. I have to give a special thanks to my dear friend Oghomwen, whom I can talk to candidly about our experiences as MD/PhD students and who continues to show me how to be resilient and compassionate.

Outside of my school life, the love and support from my mom and dad and my brothers Dan and David keep me motivated to push forward in my program. My parents repeatedly tell me two pieces of advice: be happy and work hard. They have sacrificed so much for my brothers and me to live comfortably and pursue our respective dreams. My weekly calls with my parents are relaxing ways to end my days because I know that all they want for me is to be healthy and strong.

I would like to thank my husband and best friend Kevin who gave me the confidence to begin this training program and persevere. He believed in me before I believed in myself and I wouldn't have been able to get through all of the challenging times in my program without his support. Kevin reminds me that there's more to life than work and I'm so thankful for all of the times we've had over the past 10 years.

Finally, I would like to thank you for reading my thesis and your interest in learning about what I've discovered during my PhD journey.

Abstract

Extensive serotonin (5-HT) fiber innervation throughout the brain corroborates 5-HT's modulatory role in numerous behaviors including social behavior, emotion regulation, and learning and memory. Abnormal brain 5-HT levels and function are implicated in Autism Spectrum Disorder (ASD) which often co-occurs with other neuropsychiatric conditions. While 5-HT therapeutics are used to treat ASD, variable improvements in symptomatology require further investigation of 5-HT-mediated pathology. Neurexins (Nrxns) are presynaptic cell adhesion molecules that maintain synapse function for proper neural circuit assembly. Given that aberrant Nrxn and 5-HT function independently contribute to signaling pathology and behavioral impairments, it is critical to understand how Nrxn-mediated 5-HT neurotransmission participates in pathological mechanisms underlying ASD.

Using fluorescence *in situ* hybridization, I found that the three Nrxn genes (*Nrxn1*, *Nrxn2*, and *Nrxn3*) are differentially expressed in 5-HT neurons in the dorsal raphe nucleus (DRN) and median raphe nucleus which contain the primary source of 5-HT neurons in the brain. Our lab generated a mouse model with selective deletion of Nrxns in 5-HT neurons to investigate the function of Nrxns in 5-HT signaling. The loss of Nrxns at 5-HT release sites reduced 5-HT release in the DRN and hippocampus and altered 5-HT innervation in specific brain regions. The lack of 5-HTergic Nrxns also reduced sociability and increased depressive-like behavior in males. This mouse model provides mechanisms to shed new light on 5-HT neurotransmission in the generation of complex behaviors.

Table of Contents

List of Tables

List of Figures

Chapter I

Chapter II

List of Copyrighted Materials Produced by the Author

Chapter II of this dissertation was previously published in:

Uchigashima, M.*, Cheung, A.*, Suh, J., Watanabe, M., & Futai, K. (2019). Differential expression of neurexin genes in the mouse brain. *J Comp Neurol, 527*(12), 1940-1965. https://doi.org/10.1002/cne.24664

* denotes co-first authors

List of Symbols, Abbreviations or Nomenclature

Chapters I, III-IV

5-HIAA	5-hydroxyindoleacetic acid
5-HT	serotonin
5-HTP	5-hydroxytryptophan
AADC	aromatic L-amino acid decarboxylase
ACC	anterior cingulate cortex
ADHD	attention-deficit/hyperactivity disorder
AMPA	α-amino-3-hydroxy-5-methyl-4-isoxazolepropionic acid
ASD	autism spectrum disorder
BLA	basolateral amygdala
BNST	bed nucleus of the stria terminalis
BTBR	Black and Tan BRachyury
Ca^{2+}	calcium
CNS	central nervous system
CNV	copy number variation
CT	computed tomography
DA	dopamine
dCA1	dorsal hippocampal CA1 subregion
dCA2	dorsal hippocampal CA2 subregion
dCA3	dorsal hippocampal CA3 subregion
DRN	dorsal raphe nucleus
E-I ratio	ratio between synaptic excitation and inhibition
FDA	Food and Drug Administration
FLX	fluoxetine
fMRI	functional magnetic resonance imaging
FSCV	fast scan cyclic voltammetry
GABA	gamma-aminobutyric acid
Gabrb3	gamma-aminobutyric acid type A receptor beta3 subunit
GFP	green fluorescent protein
GluA1	AMPA receptor subunit glutamate receptor 1
mEPSC	miniature excitatory postsynaptic current
mIPSC	miniature inhibitory postsynaptic current
mPFC	medial prefrontal cortex
MRN	median raphe nucleus
KI	knock-in
KO	knockout
Lmx1b	LIM homeodomain factor 1b
Lrrtm	leucine-rich repeat transmembrane protein
MAO	monoamine oxidase
MeA	medial amygdala
MRN	median raphe nucleus

NAc	nucleus accumbens
NAcc	nucleus accumbens core
NAcSh	nucleus accumbens shell
NMDA	N-methyl-D-aspartate receptor
Nrxn	neurexin
Nlgn	neuroligin
OCD	obsessive-compulsive disorder
PET	positron emission tomography
PLC	phosphoinositide-specific phospholipase C
PSD-95	postsynaptic density protein 95
retroAAV	retrograde adeno-associated virus
RFP	red fluorescent protein
Scn2A	voltage-gated sodium channel alpha subunit 2
SERT	serotonin transporter
Shank3	SH3 and multiple ankyrin repeat domains 3
SNRI	serotonin-norepinephrine reuptake inhibitor
SSRI	selective serotonin reuptake inhibitor
Syn	synapsin
TKO	triple knockout
TPH2	tryptophan hydroxylase 2
TTX	tetrodotoxin
vCA1	ventral hippocampal CA1
VGAT	vesicular GABA transporter
VGluT1	vesicular glutamate transporter type 1
VGluT3	vesicular glutamate transporter type 3
VMAT2	vesicular monoamine transporter 2
VTA	ventral tegmental area
WT	wildtype

Chapter II

3v	third ventricle
A1	primary auditory cortex
aq	cerebral aqueduct
Arc	arcuate nucleus
BA	basal nucleus of amygdala
BS	brainstem
CA	central nucleus of amygdala
CA1	field CA1 of hippocampus
CA2	field CA2 of hippocampus
CA3	field CA3 of hippocampus
Cb	cerebellum
Cl	claustrum
CM	centromedian thalamic nucleus

CPu	caudate-putamen
Cx	cortex
DG	dentate gyrus
DLL	dorsal nucleus of lateral lemniscus
DMH	dorsomedial hypothalamus
DMX	dorsal motor nucleus of vagus nerve
DRD	dorsal part of dorsal raphe nucleus
DRL	lateral part of dorsal raphe nucleus
DRV	ventral part of dorsal raphe nucleus
Epl	external plexiform layer of olfactory bulb
EW	Edinger-Westphal nucleus
Gl	glomerular layer of olfactory bulb
GrC	granule cell layer of cerebellum
GRN	gigantocellular reticular nucleus
GrO	granule cell layer of olfactory bulb
Hi	hippocampus
IC	inferior colliculus
ICj	islands of Calleja
IL	infralimbic cortex
IO	inferior olivary complex
IPN	interpeduncular nucleus
L1	cortical layer 1
L2/3	cortical layers 2/3
L4	cortical layer 4
L5	cortical layer 5
L6	cortical layer 6
LA	lateral nucleus of amygdala
LC	locus coeruleus
LD	laterodorsal thalamic nucleus
LDTg	laterodorsal tegmental nucleus
LEnt	lateral entorhinal cortex
LH	lateral hypothalamus
LHb	lateral habenula
LP	lateral posterior thalamic nucleus
LPB	lateral parabrachial nucleus
LRN	lateral reticular nucleus
LS	lateral septal nucleus
M1	primary motor cortex
MD	mediodorsal thalamic nucleus
MEnt	medial entorhinal cortex
MGN	medial geniculate nucleus
MHb	medial habenula
Mi	mitral layer of olfactory bulb
ML	molecular layer of cerebellum

MPB	medial parabrachial nucleus
MRN	medullary reticular nucleus
NAc	nucleus accumbens
ND	nucleus of Darkschewitsch
NDB	nucleus of diagonal band
NTB	nucleus of trapezoid body
NTS	nucleus of tractus solitarius
Ob	olfactory bulb
OT	olfactory tubercle
PAG	periaqueductal gray
PBG	parabigeminal nucleus
PCL	Purkinje cell layer of cerebellum
Pir	piriform cortex
PRN	pontine reticular nucleus
PrV	principal sensory nucleus of trigeminal nerve
PrL	prelimbic cortex
PVT	paraventricular thalamic nucleus
RSG	retrosplenial granular cortex
Rt	reticular thalamic nucleus
S1	primary somatosensory cortex
SC	superior colliculus
SNc	substantia nigra pars compacta
SNr	substantia nigra pars reticulata
SOP	paraolivary region of superior olivary complex
SpV	spinal nucleus of trigeminal nerve
STN	subthalamic nucleus
Su	subiculum
Th	thalamus
V1	primary visual cortex
VC	ventral cochlear nucleus
VII	facial nucleus
VMH	ventromedial hypothalamus
VPL	ventral posterolateral thalamic nucleus
VPM	ventral posteromedial thalamic nucleus
VTA	ventral tegmental area
XII	hypoglossal nucleus

Preface

The work presented in Chapter II was previously published in:

Uchigashima, M.*, Cheung, A.*, Suh, J., Watanabe, M., & Futai, K. (2019). Differential expression of neurexin genes in the mouse brain. *J Comp Neurol, 527*(12), 1940-1965. https://doi.org/10.1002/cne.24664

* denotes co-first authors

The work presented in Chapter III is unpublished and is in preparation for manuscript submission.

Cheung, A. Matsui, A., and Futai, K. (2021). Deletion of all neurexins in serotonin neurons compromises serotonin release and complex behaviors. *Under preparation*.

Chapter I

Introduction

Chapter I: Introduction

Autism Spectrum Disorder

The prevalence of autism spectrum disorder (ASD) continues to increase with each passing year. 1 in 132 children globally (Baxter et al., 2015) and 1 in 54 children in the United States are estimated to be living with ASD (Baio et al., 2018). ASD shows a male bias and is approximately 4x more common in boys than girls. The terminology and diagnostic criteria of ASD have changed over the years and most recently, ASD has become an umbrella term (e.g., for Asperger's syndrome and Pervasive Developmental Disorder) in the 5th edition of the Diagnostic and Statistical Manual of Mental Disorders. Multiple factors contribute to the rising prevalence rate including broad criteria for diagnosis, improved detection, and greater awareness of ASD in the community (Hansen et al., 2015; Rice et al., 2012).

Core diagnostic symptoms and comorbid conditions

To receive a diagnosis of ASD, a child must present with symptoms in two categories: persistent social communication and interaction challenges (e.g., abnormal social approach, lack of interest in peers) and restrictive, repetitive behaviors (e.g., patterned rituals, abnormal reactivity to sensory input) (American Psychiatric Association, 2013). Health care providers will also note the severity of ASD and associated conditions or factors, which highlight the spectrum of symptoms a child can present with.

Each person living with ASD has their own unique constellation of core symptoms with or without accompanying features. There is consensus in the literature that ASD is associated with numerous disorders. A study by *Levy et al.* of 2,568 children with ASD found that non-ASD developmental disorders such as language disorders, attention-deficit/hyperactivity disorder (ADHD), and intellectual disability co-occurred in 83% of the participants. Psychiatric diagnoses were found in 10% of cases, which included oppositional defiant disorder, anxiety disorder, obsessive-compulsive disorder (OCD), and depression. Neurological diagnoses like epilepsy, encephalopathy, and hearing loss were seen in 16% of the study cohort (Levy et al., 2010).

Doshi-Velez et al. identified four subgroups of comorbid disorders: seizures, multisystem disorders, psychiatric disorders, and disorders that could not be further resolved (Doshi-Velez et al., 2014). Seizures were present in 77.5% of individuals in one subgroup, while intellectual disability more often co-occurred in those with ASD with seizures or multisystem disorders. Children with less severe ASD were more frequently diagnosed with psychiatric disorders such as anxiety. Comorbidities may be difficult to recognize in individuals with more severe ASD who are nonverbal or have low language skills (Baghdadli et al., 2012). *Leyfer et al.* observed that the majority of children in the study (n = 109) had 1-2 psychiatric diagnoses, particularly anxiety disorders and ADHD (Leyfer et al., 2006). Taken together, the heterogeneity and complexity of ASD can be appreciated through the

core social deficits and restrictive behaviors necessary for diagnosis and the frequently overlapping presentation of neuropsychiatric conditions.

Pharmacological therapeutics

There is no cure for ASD and 1st line treatment is behavioral therapy. Currently, there are two FDA-approved drugs to treat irritability in ASD which are the second-generation antipsychotics risperidone and aripiprazole. Both risperidone and aripiprazole are commonly used to treat psychotic disorders like schizophrenia and bipolar disorder. Their primary mechanism of action is to antagonize serotonin 5-HT_{2A} receptors and dopamine D_2 receptors to alter activity in their respective pathways. Risperidone and aripiprazole can also bind to adrenergic (α_1 and α_2), 5-HT_{1A}, and histamine H_1 receptors, among other receptors (de Bartolomeis et al., 2015). Antagonism and agonism at numerous types of receptors with different binding affinities allow these antipsychotics to provide symptom relief but also contribute to side effects such as extrapyramidal symptoms, metabolic changes (e.g., weight gain), and sedation (Ucok & Gaebel, 2008).

Selective serotonin reuptake inhibitors (SSRIs) including fluoxetine (FLX) and citalopram are used to treat repetitive behaviors, anxiety, and aggression in people with ASD (Williams et al., 2013). Stimulants like amphetamine treat irritability and ADHD while anticonvulsants such as lamotrigine are used for seizures (Coleman et al., 2019). Of note, there is significant heterogeneity in therapeutic responses for different individuals (Hirsch & Pringsheim, 2016; Jesner

et al., 2007). Pharmacologic therapeutics provide variable relief for people with ASD and the benefited symptoms vs. adverse effects should be carefully considered when personalizing medicine for each patient.

Synaptic dysfunction

ASD is a neurodevelopmental disorder with complex etiology. Genetic and non-genetic influences contribute to susceptibility, although the relative contribution of these factors is under debate (Hallmayer et al., 2011; Taylor et al., 2020). Recent twin studies suggest that genetic effects play a major role in ASD (Bai et al., 2019; Hegarty et al., 2020). Rare and common genetic variants such as single nucleotide polymorphisms, copy number variations (CNVs) which describe structural variations in the genome, and epigenetic changes modulate phenotypic heterogeneity in ASD (de la Torre-Ubieta et al., 2016; Rylaarsdam & Guemez-Gamboa, 2019). Notably, synaptic proteins are consistently identified as ASD risk genes in large-scale genetic studies (De Rubeis et al., 2014; Grove et al., 2019; Pinto et al., 2014; Yuen et al., 2017; Zoghbi & Bear, 2012). These genes encode synaptic molecules that organize, stabilize, and confer identity and function at synapses. They include synaptic vesicle proteins (e.g., synapsin [Syn]), cell adhesion proteins (e.g., neurexins [Nrxns] and neuroligins [Nlgns]), ion transport proteins (e.g., voltage-gated sodium channel alpha subunit 2 [Scn2A]), scaffolding proteins (e.g., SH3 and multiple ankyrin repeat domains 3 [Shank3]), and receptor proteins (e.g., gamma-aminobutyric acid (GABA) type A receptor beta3 subunit

[Gabrb3]) (Giovedi et al., 2014; Rylaarsdam & Guemez-Gamboa, 2019; Won et al., 2013).

An increase in the ratio between synaptic excitation and inhibition (E-I ratio) is a central feature of ASD. Indeed, epilepsy commonly co-occurs in people with ASD (Levy et al., 2010) and a mouse model with knockout (KO) of the cell adhesion molecule CNTNAP2 (contactin associated protein 2) exhibited ASD-associated deficits and epileptic seizures (Penagarikano et al., 2011). Hyperexcitable cortical circuits have been described as consequences of impaired GABAergic neurotransmission due to fewer inhibitory synapses and reduced inhibitory synaptic transmission and feedback inhibition (Gibson et al., 2008; Han et al., 2012; Mao et al., 2015). However, increased inhibition has also been reported in mice with KO of Nlgn4 (Unichenko et al., 2018) and mutation of Nlgn3 (Tabuchi et al., 2007). This discrepancy could be due to examination of single genes in specific cell types and circuits that demonstrate a particular physiological phenotype to maintain synaptic homeostasis (Nelson & Valakh, 2015) or stabilize synapses (Antoine et al., 2019). Nevertheless, genes important for neurotransmitter signaling contribute to the development of ASD by modifying neural activity and synaptic structure/function.

Serotonin function

Serotonin (5-hydroxytryptamine, 5-HT) is a monoamine neurotransmitter that modulates electrochemical activity throughout the brain. 5-HT neurons reside in

the raphe nuclei located in the brainstem and send ascending and descending fibers to virtually all parts of the CNS. Rostral raphe nuclei project to the forebrain while caudal raphe nuclei project to the brainstem and spinal cord. There are approximately 350,000 5-HT neurons in the human brain and 25,000 5-HT neurons in the mouse brain (Charnay & Leger, 2010). The two largest raphe nuclei are the dorsal raphe nucleus (DRN) and median raphe nucleus (MRN) (**Figure 1.1**) which are part of the rostral group and contain roughly 9,000 and 2,000 5-HT neurons in mice, respectively (Ishimura et al., 1988). Of note, roughly 95% of 5-HT is found in the gut which regulates a variety of functions throughout the body (Berger et al., 2009). However, the focus of my thesis will be on 5-HT in the central nervous system (CNS).

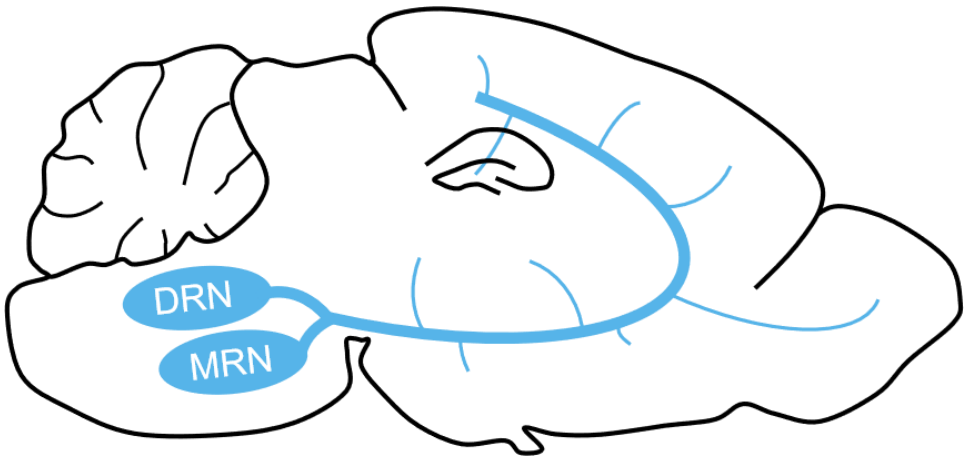

Figure 1.1 | Overview of 5-HT pathways in the mouse brain. The majority of 5-HT neurons innervating the brain are located in the dorsal raphe nucleus (DRN) and median raphe nucleus (MRN). As part of the rostral raphe nuclei, the DRN and MRN send diffuse projections to multiple brain regions.

There are seven families of 5-HT receptors which generate fourteen receptor subtypes. Apart from the ionotropic 5-HT_3 receptor, the remaining receptors (5-$HT_{1\text{-}2,4\text{-}7}$) are slower acting metabotropic G-protein coupled receptors that work through signaling pathways to modulate cellular activity, fast neurotransmission, and information propagation between cells. 5-HT receptors are expressed in a variety of cell types to relay 5-HT signals. 5-HT_1 receptors can act as autoreceptors and heteroreceptors which provide feedback on 5-HT activity by regulating 5-HT release or inhibitory responses to released 5-HT, respectively (Richardson-Jones et al., 2011). A list of 5-HT receptors and their distribution in the brain is shown in **Table 1.1** (Charnay & Leger, 2010; Francken et al., 1998; Grailhe et al., 2001; Gerard J. Marek, 2010; Pithadia & Jain, 2009; Pourhamzeh et al., 2021).

Table 1.1 | Overview of 5-HT receptors in the central nervous system

Receptor	Distribution	Effect
5-HT_{1A}	PFC, entorhinal cortex, hippocampus, amygdala, hypothalamus, raphe nuclei	Inhibitory (inhibits adenylyl cyclase)
5-HT_{1B}	ACC, NAc, hippocampus, substantia nigra, VTA, caudate putamen, ventral pallidum, raphe nuclei	Inhibitory (inhibits adenylyl cyclase)
5-HT_{1D}	Hippocampus, olfactory cortex, globus pallidus, striatum, substantia nigra, DRN	Inhibitory (inhibits adenylyl cyclase)
5-HT_{1E}	Frontal cortex, entorhinal cortex, hippocampus, amygdala, striatum, globus pallidus	Inhibitory (inhibits adenylyl cyclase)
5-HT_{1F}	Cingulate cortex, entorhinal cortex, hippocampus, DRN	Inhibitory (inhibits adenylyl cyclase)
5-HT_{2A}	PFC, cerebral cortex, claustrum, olfactory tubercle, striatum, NAc	Excitatory (stimulates adenylyl cyclase)
5-HT_{2B}	Hippocampus, hypothalamus, amygdala, septum, cerebellum	Excitatory (stimulates PLC)
5-HT_{2C}	Piriform cortex, hippocampus, substantia nigra, VTA, striatum, amygdala, striatum, NAc, global pallidus, DRN	Excitatory (stimulates PLC)
5-HT_{3}	PFC, hippocampus, entorhinal cortex, amygdala, NAc, solitary tract nerve, trigeminal nerve	Excitatory (ligand-gated cation channel)
5-HT_{4}	Frontal cortex, hippocampus, striatum, olfactory tubercle, amygdala, substantia nigra, VTA	Excitatory (stimulates adenylyl cyclase)
5-HT_{5A}	Cerebral cortex, hippocampus, habenula, thalamus, striatum, amygdala, DRN, cerebellum	Inhibitory (inhibits adenylyl cyclase)
5-HT_{5B}	Does not encode a functional protein in humans	
5-HT_{6}	Frontal cortex, entorhinal cortex, caudate putamen, olfactory tubercle, hippocampus, striatum, hypothalamus, NAc, VTA, cerebellum	Excitatory (stimulates adenylyl cyclase)
5-HT_{7}	ACC, cerebral cortex, thalamus, hypothalamus, hippocampus, amygdala, substantia nigra, VTA, DRN	Excitatory (stimulates adenylyl cyclase)

Abbreviations: anterior cingulate cortex (ACC); dorsal raphe nucleus (DRN); nucleus accumbens (NAc); prefrontal cortex (PFC); ventral tegmental area (VTA).

Brain-wide circuits and associated behaviors

5-HT pathways have an extensive presence in regulating processes related to mood, memory, reward, social behavior, sleep, and stress (Berger et al., 2009). Networks of connected brain areas interact with one another to participate in the

generation of complex behaviors. At rest, positron emission tomography (PET) imaging of the DRN and MRN show serotonin transporter (SERT) functional connectivity with cortical (e.g., medial prefrontal cortex [mPFC], anterior cingulate cortex [ACC]) and limbic structures (e.g., amygdala, hippocampus, thalamus), basal ganglia, and cerebellum (Beliveau et al., 2015). Brain-wide anterograde tracing of SERT-labeled 5-HT fibers arising from rostral raphe nuclei demonstrated distinct patterns of connectivity among 5-HT neuron subgroups (Muzerelle et al., 2016). For example, the DRN largely projects to mPFC, amygdala, and striatum, while MRN projections send major inputs to the hippocampus, lateral septum, and interpeduncular nucleus.

5-HT influences social behavior by modifying activity in the amygdala, hippocampus, and somatosensory cortex, among other connected areas (Kiser et al., 2012). Differing functions between the DRN and MRN on social behavior have been identified in animal studies. DRN has been shown to encode information for rewards with positive valence (social interaction, sucrose, food, sex) but not for aversive stimuli (quinine, foot shock) through 5-HT neuron activation and GABA neuron inhibition (Li et al., 2016). Another study found that acute activation of the DRN increased social interaction, while stimulation of the MRN reduced aggressive behaviors with no effect on social interaction (Balazsfi et al., 2018).

5-HT activity has been associated with learning and memory processes. Drugs that act on 5-HT receptors have altered memory consolidation in associative learning tasks (Meneses, 2003). 5-HT_{1A} receptor activation using the agonist 8-

OH-DPAT enhanced learning acquisition and short- and long- term memory in rats tested in the Morris water maze test (Haider et al., 2012). Tryptophan hydroxylase 2 (TPH2) KO mice that lack the ability to synthesize brain 5-HT showed enhanced learning acquisition, contextual fear memory, and heightened locomotor responses to foot shock with increased c-Fos expression in the hippocampus (Waider et al., 2019). Depletion of 5-HT using Pet-1 KO mice demonstrated that hippocampal inputs from the MRN but not the DRN are important for object memory (Fernandez et al., 2017).

5-HT signaling contributes to the regulation of emotional behaviors. The DRN-mPFC circuit (Garcia-Garcia et al., 2017) and SERT variants (Canli & Lesch, 2007) are involved in depressive-like phenotypes. 5-HT neuron activity in the DRN and MRN have both been linked to stress responses (Nishitani et al., 2019; Teissier et al., 2015). Additionally, 5-HT receptors provide a link between 5-HT signaling and sleep. 5-HT_7 receptor blockade altered circadian rhythms by increasing the latency to rapid eye movement (REM) and decreasing the total amount of REM sleep (Thomas et al., 2003). Altogether, 5-HT neuron activity and connectivity have remarkable modulatory effects on behavioral functions.

Neuropsychiatric disorders with serotonin dysfunction

Perturbations in the 5-HT system are associated with a variety of neuropsychiatric conditions, notably mood disorders, depression, OCD, ASD, and schizophrenia. Human PET and functional magnetic resonance imaging (fMRI) studies of

participants with anxiety disorders and depression revealed functional abnormalities in the nucleus accumbens (NAc), PFC, ACC, amygdala, hippocampus, and dorsomedial thalamus (Martin et al., 2009; Pandya et al., 2012). Activation of MRN but not DRN 5-HT neurons increased anxiety-like behaviors in mice (Ohmura et al., 2014). *Abela et al.* also showed that anxiety-related behavior could be enhanced by stimulating MRN-hippocampal inputs (Abela et al., 2020). SERT KO mice demonstrated increased anxiety-like behavior, which could be reversed with administration of the 5-HT_{1A} receptor antagonist WAY 100635 (Holmes et al., 2003). Additionally, the cortico-striato-thalamo-cortical pathway has been described in the pathophysiology of OCD. PET and MRI imaging revealed that adults with OCD have reduced SERT binding in the orbitofrontal cortex (an area of the PFC) and insular cortex (Matsumoto et al., 2010).

A meta-analysis of MRI and computed tomography (CT) studies on structural brain changes in people with depression found that smaller volumes of the hippocampus, frontal lobe, basal ganglia, thalamus, orbitofrontal cortex, and gyrus rectus correlated with greater disorder severity (Kempton et al., 2011). Reduced SERT binding and neuron density were also observed in the PFC (Arango et al., 2002). The short form of the SERT gene (i.e., low-expressing variant) has been linked to decreased SERT expression and poor clinical outcomes due to greater vulnerability to stress and poor response to antidepressants (Canli & Lesch, 2007). The 5-HT hypothesis of depression postulates that reduced 5-HT levels predispose individuals to depression. TPH2 knock-in (KI) mice, which show a 60-

80% reduction in brain 5-HT, were more susceptible to social defeat stress and less sensitive to FLX in reversing stress-induced social avoidance (Sachs et al., 2015). Activation of DRN 5-HT neurons produced antidepressant effects while their inhibition increased anxiety-like behavior (Nishitani et al., 2019). *Teissier et al.* correlated increased anxiety and depressive-like behaviors in a mouse model with altered emotional behaviors with reduced DRN and increased MRN 5-HT neuron activity (Teissier et al., 2015).

5-HT was the first biomarker identified in ASD (C. L. Muller et al., 2016) and remains one of the most consistent neurochemical findings in this disorder. While 5-HT is used as a signal to modulate neural circuit formation, neuronal migration, dendritic maturation, axon branching, and neurogenesis during development (Gaspar et al., 2003), its precise contribution to the neurodevelopmental trajectories of ASD is not well understood. Given that the pathophysiology of ASD is driven by numerous factors, many studies focus on postnatal observations and correlations between the 5-HT system and ASD. A meta-analysis found that more than 25% of the study participants had elevated blood 5-HT levels (Gabriele et al., 2014). Reduced SERT activity has been identified in gene (Adamsen et al., 2014; Cook et al., 1997) and imaging studies (Andersson et al., 2020; Makkonen et al., 2008; Nakamura et al., 2010) with significant association in areas like the mPFC, NAc, anterior and posterior cingulate cortices, putamen, and thalamus.

Schizophrenia has long been associated with dysfunction in the 5-HT system. The pathophysiology of schizophrenia likely involves alterations in multiple

pathways including 5-HT, DA, and glutamate neurotransmission (Patel et al., 2014). 5-HT receptors have been found to play a role in influencing negative symptoms of schizophrenia (e.g., flat affect, anhedonia) with much focus placed on 5-HT_{1A} and 5-HT_{2A} receptors (Pourhamzeh et al., 2021; Selvaraj et al., 2014).

Serotonin therapeutics

Medications that target the 5-HT system enhance 5-HT levels or rebalance 5-HT activity (**Table 1.2**) and often take weeks to demonstrate therapeutic effect. Antidepressants were named for their ability to treat depression, although they are also used to treat other disorders with 5-HT dysfunction like anxiety disorders, ASD, and OCD. Major classes of antidepressants include SSRIs, serotonin-norepinephrine reuptake inhibitors (SNRIs), atypical antidepressants, monoamine oxidase (MAO) inhibitors, and tricyclic antidepressants (Pourhamzeh et al., 2021). Additionally, antipsychotics target 5-HT and/or DA receptors to modify neuromodulatory neurotransmission. While best known to treat schizophrenia and other psychotic disorders, they are used for symptom relief in a variety of neuropsychiatric disorders such as depression and anxiety. Multimorbidity alludes to shared pathogenesis which allows for overlapping treatment options.

Table 1.2 | Drugs that modulate 5-HT activity

	Mechanism of action	Examples
Antidepressants		
SSRIs	Block 5-HT reuptake	Escitalopram, fluoxetine, fluvoxamine, sertraline
SNRIs	Block 5-HT and norepinephrine reuptake	Duloxetine, venlafaxine
Atypical antidepressants	Primarily block α_2 receptors	Mirtazapine, bupropion, trazadone
Tricyclic antidepressants	Primarily block 5-HT and norepinephrine reuptake	Amitriptyline, clomipramine, imipramine
MAO inhibitors	Block breakdown of 5-HT	Phenelzine, selegiline
Antipsychotics		
First-generation (typical)	Primarily block D_2 receptors	Chlorpromazine, fluphenazine, haloperidol
Second-generation (atypical)	Primarily block 5-HT_{2A} and D_2 receptors	Aripiprazole, olanzapine, quetiapine, risperidone

Abbreviations: monoamine oxidase (MAO); selective serotonin reuptake inhibitors (SSRIs); serotonin-norepinephrine reuptake inhibitors (SNRIs).

Serotonin neurotransmission

5-HT is released from vesicles at presynaptic terminals, varicosities on axons, and from cell bodies and dendrites (Colgan et al., 2012; Quentin et al., 2018) to act on postsynaptic receptors through volume transmission or directly across the synaptic cleft in synaptic dyads or triads (Belmer et al., 2017). While the molecular architecture of 5-HT release sites is not well-defined, work in the DA system demonstrates that varicosities on DA axons serve as active zone-like sites with release machinery including scaffolding proteins bassoon and ELKS (Liu et al., 2018). 5-HT release sites may exhibit similar structural mechanisms for secretion.

5-HT neurons can be identified by genes that encode proteins critical for their development and function in neurotransmission. These include TPH2,

aromatic L-amino acid decarboxylase (AADC), SERT, vesicular monoamine transporter 2 (VMAT2), MAO, transcription factor Fev (rodent orthologue, Pet-1), and LIM homeodomain factor 1b (Lmx1b) (E. S. Deneris & Wyler, 2012). Fev and Lmx1b serve as early markers that specify 5-HT neuron differentiation (Ding et al., 2003; Hendricks et al., 1999). The synthesis of 5-HT requires TPH to convert tryptophan to 5-hydroxytryptophan (5-HTP) and AADC to convert 5-HTP to 5-HT. VMAT2 transports intracellular 5-HT into vesicles to prepare for release. SERT regulates the availability of extracellular 5-HT by transporting 5-HT back into 5-HT release sites. The metabolism of 5-HT requires MAO to convert 5-HT to 5-hydroxyindoleacetic acid (5-HIAA).

Examining sex differences are becoming more standard in research studies. PET and MRI imaging of healthy male and female participants showed that the rate of 5-HT synthesis was uniform throughout the brain (regions studied included frontal cortex, thalamus, and hippocampus) and was higher in males than females (Nishizawa et al., 1997). It is possible that lower rates of serotonin synthesis could be associated with the higher prevalence of depressive disorders in women. In contrast, the prevalence of ASD is higher in males than females. A PET study found that adult men with ASD had lower SERT availability in the brainstem and in cortical and subcortical areas compared with men without ASD, suggesting mechanisms that reduce 5-HT innervation or compensate for changes in other components of 5-HT signaling (Andersson et al., 2020). Both testosterone (L. Zhang et al., 1999) and estrogen (Hernandez-Hernandez et al., 2019) have been

shown to regulate the expression of genes involved in 5-HT signaling. Taken together, sex-specific differences are essential to characterize neuropsychiatric disorders with abnormal 5-HT function.

Volume transmission

Decades of work examining ultrastructural features of 5-HT release sites highlight that volume transmission is the predominant mode of 5-HT release in the CNS and that 5-HT is extrasynaptically released from 5-HT neuron axons, cell bodies, and dendrites. The percentage of junctional complexes varies across brain regions, however, most areas including cortical structures, hippocampus, striatum, and entorhinal cortex show low (less than 40%) synaptic incidence (Martin Parent & Descarries, 2020). Regions like the BLA (J. F. Muller et al., 2007) and subthalamic nucleus (M. Parent et al., 2010) contain around 40-80% terminals that form synaptic junctions. The contribution of different raphe nuclei demonstrates different connection patterns. In the hippocampus, MRN fibers form synapses with interneurons (Varga et al., 2009) and are characterized by axons with large spherical varicosities (type M). Axons from the DRN show fine beaded or small fusiform varicosities (type D) (Kosofsky & Molliver, 1987).

5-HTergic Retzius neurons in the leech *Hirudo medicinalis* contain vesicles that cluster at the plasma membrane following electrical stimulation to induce somatic release (De-Miguel et al., 2015). Cultured Retzius cells contained small synaptic vesicles exclusively in axons and large dense-core vesicles in both axons

and somas (Bruns et al., 2000). Approximately 17x less 5-HT was found to be released from small synaptic vesicles compared with large dense-core vesicles. However, small synaptic vesicles released 5-HT more rapidly and frequently to single action potentials than large dense-core vesicles (Bruns & Jahn, 1995). *Colgan et al.* showed that VMAT2 is located in 5-HT dendrites associated with clusters of clear vesicles and large dense-core vesicles. Dendritic but not somatic 5-HT exocytosis was found to be action potential-independent and could be induced by N-methyl-D-aspartate receptor (NMDA) receptor activation. Moreover, somatic and dendritic release exhibited different responses to FLX (Colgan et al., 2012). Taken together, extrasynaptic neurotransmission allows 5-HT to function on timescales of milliseconds (fast) to minutes (slow) in close apposition (nanometers) to postsynaptic specializations or micrometers away from postsynaptic targets. 5-HT diffused throughout the extracellular milieu can exert differing actions on 5-HT signaling components like receptors and transporters to modulate effective communication within innervated circuits.

Serotonin synapses

5-HT varicosities make symmetric and asymmetric contacts primarily with dendrites of postsynaptic cells. Brain areas show differing innervation configurations related to the proportion of asymmetric vs. symmetric synapses, extrasynaptic vs. synaptic sites, and precise distribution of synapses (Martin Parent & Descarries, 2020). For example, most synaptic 5-HT varicosities form

asymmetric junctions with dendritic shafts or spines in the hippocampus (Oleskevich et al., 1991). 76% of varicosities form synaptic junctions in the amygdala which are mostly symmetric and mainly target spines and dendrites of pyramidal cells (J. F. Muller et al., 2007). In the mPFC, SERT-labeled terminals are typically asymmetric and more frequently target dendritic spines in the superficial layers (Miner et al., 2000).

SERT-positive axons were found to form synaptic triads with excitatory and inhibitory synapses (Belmer et al., 2017). *Belmer et al.* showed that SERT-labeled fibers that express synaptic vesicle protein synaptophysin (5-HT varicosity) were closely apposed to SERT-negative synaptophysin (presynaptic terminal) and postsynaptic density protein 95 (PSD-95)-associated excitatory or gephyrin-associated inhibitory (postsynaptic) sites. In the limbic regions examined, extra-triadic boutons were the predominant innervation configuration while the percentage of excitatory and inhibitory triads differed. For instance, excitatory triads were more frequent in the mPFC whereas inhibitory triads predominated in the amygdala. No differences in the ratio between excitatory and inhibitory triads were observed in the NAc, bed nucleus of the stria terminalis (BNST), and hippocampus.

5-HT neurons in the DRN have been found to co-release 5-HT and glutamate (H. L. Wang et al., 2019). In the ventral tegmental area (VTA), SERT terminals that co-express vesicular glutamate transporter type 3 (VGluT3) make asymmetric synapses on DA neurons and activation of SERT fibers enhanced

conditioned place preference. Moreover, a DRN-VTA-NAc circuit was identified in which DRN 5-HT neuron-mediated release of glutamate and 5-HT in the VTA increased DA neuron firing which evoked DA release in the NAc.

While it is challenging to differentiate extrasynaptic vs. synaptic contributions, 5-HT signaling has a clear role in regulating excitatory and inhibitory transmission. *Teixeria et al.* demonstrated that activation of 5-HT terminals in the CA1 subregion of the hippocampus potentiated CA3-to-CA1 synaptic inputs and enhanced spatial memory performance in the Morris water maze test. In contrast, inhibiting CA1 5-HT terminals impaired memory formation. The 5-HT_4 receptor was found to modulate these electrophysiological and behavioral effects (Teixeira et al., 2018). Additionally, 5-HT has been shown to inhibit excitatory postsynaptic currents (EPSCs) and reduce presynaptic glutamate release in the ACC (Tian et al., 2017). In the medial preoptic area of the hypothalamus, 5-HT decreased the frequency of inhibitory postsynaptic currents (IPSCs) (Lee et al., 2008).

Serotonin mouse models with autism-relevant phenotypes

ASD has been associated with reduced levels of 5-HT's major metabolite 5-HIAA (Adamsen et al., 2014) and 5-HT synthesis capacity (Chugani et al., 1999) in humans and 5-HT and 5-HIAA (Kane et al., 2012; Nakai et al., 2017) in mouse models. Deletion of TPH2 produced mice with deficits in social behavior (e.g., social memory, social olfactory discrimination) and repetitive behaviors (Kane et al., 2012). In contrast, SERT KO mice with high brain 5-HT levels exhibited social

deficits and enhanced anxiety, which could be reversed when put on a tryptophan-free diet (Tanaka et al., 2018). A fuller understanding of 5-HT dysfunction will require an examination of molecular and physiological properties underlying 5-HT signaling especially in the context of altered 5-HT levels.

Particular CNVs have been linked to ASD pathogenesis (Vicari et al., 2019). 15q11-13 mice display reduced 5-HT in the DRN and impaired social approach, which could be restored with fluoxetine treatment (Nakai et al., 2017). The mouse model also showed fewer inhibitory synapses and hyperexcitable pyramidal neurons in the somatosensory cortex, alluding to a characteristic increase in E-I ratio often seen in ASD. In a different study, 15q11-13 pups (postnatal days 7 to 21) that were treated with oxytocin or the 5-HT_{1A} receptor agonist 8OH-DPAT exhibited improved social behavior (Nagano et al., 2018). Mice with specific 16p11.2 deletion in DRN 5-HT neurons showed decreased 5-HT neuron activity and reduced sociability, which could be rescued by 5-HT terminal stimulation in the NAc (Walsh et al., 2018). Activation of NAc 5-HT_{1B} receptors were sufficient to rescue these social behavior deficits.

Black and Tan BRachyury (BTBR) mice are a well-known mouse model of ASD which were investigated for alterations in 5-HT signaling (Gould et al., 2011). *Gould et al.* found that BTBR mice display reduced SERT binding in areas like the hippocampus, basolateral amygdala (BLA), and DRN. Both fluoxetine and buspirone, a 5-HT_{1A} receptor partial agonist, improved sociability whereas risperidone improved repetitive behaviors. Additionally, 5-HT neurotransmission

was investigated in Shank3 KO mice. Optogenetic stimulation of DRN 5-HT neurons, but not VTA DA neurons, enhanced social interaction indicating that 5-HT signaling is involved in social processes (J. Luo et al., 2017).

Synaptic neurexins

As the primary sites of communication between cells in the brain, synapses require proteins to promote their discrete identities and bring together pre- and post-synaptic components. Nrxns are presynaptic cell adhesion molecules that are among the most well-studied genes critical for synaptic function (J. H. Kim & Huganir, 1999; Sudhof, 2017). In the developing brain, Nrxns are expressed before synapses are extensively formed and are speculated to act as cell recognition molecules in preparation for synapse assembly (Harkin et al., 2017; Puschel & Betz, 1995). There are three Nrxn genes (Nrxn1, Nrxn2, Nrxn3) which are under the control of three promoters (α, β, γ). γNrxns are the shortest isoforms and are transcribed only from the Nrxn1 gene (**Figure 1.2**). The longer αNrxns and shorter βNrxns generate six principal isoform variants (αNrxn1-3, βNrxn1-3). Nrxns have six canonical splice sites and undergo extensive alternative splicing to generate thousands of Nrxn variants that can potentially govern synapse dynamics (Aoto et al., 2013; Reissner et al., 2008; Schreiner et al., 2014; Ullrich et al., 1995). My thesis focuses on the six major Nrxn isoforms to examine their diverse expression profiles and capabilities in organizing circuits.

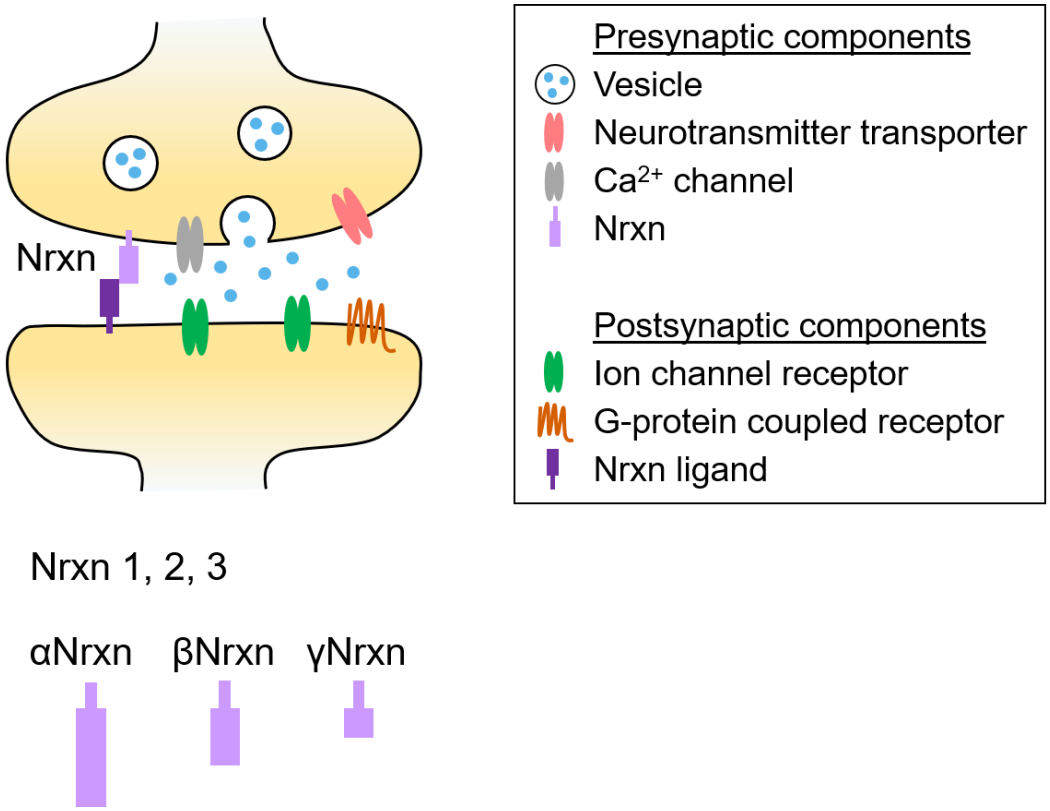

Figure 1.2 | Overview of neurexins at the synapse. Neurexins (Nrxns) are presynaptic cell adhesion molecules that are encoded by three genes (Nrxn1-3) and use three promoters to generate α, β, and γNrxns. The functions of Nrxns can be considered based on their roles on the presynaptic and postsynaptic sides. On the presynaptic side, Nrxns are important for neurotransmitter release by coupling calcium (Ca^{2+}) channels to presynaptic machinery. On the postsynaptic side, Nrxn ligands which include other cell adhesion molecules provide Nrxns with a signaling platform to modify synaptic properties.

Functional role at synapses

Presynaptic Nrxns interact with proteins across the synapse to regulate synaptic properties. Nrxn ligands include postsynaptic cell adhesion proteins (e.g., Nlgn1-4, dystroglycan, and calsyntenin-3), leucine-rich repeat transmembrane proteins (LRRTM1-4), secreted proteins (cerebellin-1 and neurexophilins), adhesion G-protein coupled receptors (latrophilins), and carbonic anhydrase-related proteins (CA10, CA11) (Gomez et al., 2021; Sudhof, 2017). Trans-synaptic interactions

allow Nrxns to provide signaling platforms for ligand partners and modify pre- and/or post- synaptic functions. Moreover, Nrxns have an important role in presynaptic dynamics. A recent study demonstrated that pan-Nrxn deletion at the calyx of Held synapse impaired calcium (Ca^{2+})-dependent fast neurotransmitter release and had no impact on synapse formation or the release machinery itself (F. Luo et al., 2020). Using super-resolution microscopy, *Trotter et al.* demonstrated that Nrxn1 concentrates into nanoclusters and synapses containing multiple Nrxn1 nanoclusters were associated with more α-amino-3-hydroxy-5-methyl-4-isoxazolepropionic acid (AMPA) receptor subunit glutamate receptor 1 (GluA1) and active vesicle exocytosis (Trotter et al., 2019). Nrxn1 ectodomain cleavage but not synaptic activity was found to regulate Nrxn1 nanocluster content.

Many of the functions of Nrxns have been discovered through their removal at synapses. Global αNrxn triple knockout (TKO) mice do not survive more than several days after birth and show reduced excitatory and inhibitory neurotransmitter release by impairing presynaptic Ca^{2+} influx (Missler et al., 2003). Single αNrxn2 KO mice exhibited no alterations in survival and were used as “WT controls” in this study. A concurrent decrease in inhibitory synapses was also observed. Collectively, *Missler et al.* demonstrated that Nrxns control neurotransmitter release by coupling Ca^{2+} channels to presynaptic machinery. αNrxns were found to modulate acetylcholine release at neuromuscular junctions, indicating that Nrxns do not require a postsynaptic neuron target to generate physiological effects (Sons et al., 2006). Additionally, conditional removal of all

Nrxns resulted in synapse-specific functions (L. Y. Chen et al., 2017). Presynaptic climbing fibers from the cerebellar cortex with sparse Nrxn deletion exhibited blunted axons and no effect on excitatory responses with postsynaptic Purkinje cells. In contrast, global deletion of Nrxns in inferior olive neurons caused no alterations in climbing fiber axons but impaired excitatory synaptic transmission. Pan-Nrxn deletion in two interneuron cell types in the mPFC also generated different synaptic deficits, ranging from reductions in the size of presynaptic inhibitory synapses and density of presynaptic excitatory synapses to decreases in inhibitory synaptic strength and GABA release.

Gene- and promoter- specific Nrxn KO mice reveal a variety of synaptic effects depending on the Nrxn isoform removed and specific circuit investigated. βNrxns have been found to regulate excitatory but not inhibitory synaptic neurotransmitter release in the hippocampus and influence endocannabinoid signaling (Anderson et al., 2015). Conditional βNrxn KO in hippocampal CA1 neurons reduced excitatory synaptic strength at subiculum synapses and impaired contextual but not cued fear memory. *Aoto et al.* showed that Nrxn3 is involved in circuit-dependent roles at excitatory and inhibitory synapses. General features of Nrxn3 KO mice included impaired survival, reduced body weight, ataxia, and hyperactivity. Conditional deletion of Nrxn3 in hippocampal CA1 neurons impaired postsynaptic AMPA-mediated responses in subiculum synapses while Nrxn3 removal in the olfactory bulb reduced GABA release without affecting excitatory responses (Aoto et al., 2015). In contrast, mice with global Nrxn3 KI or Nrxn3 KO

in somatostatin-positive interneurons in the ACC (SST-Nrxn3 KO) showed enhanced observational fear learning and memory. SST-Nrxn3 KO mice also exhibited impaired GABA release (Keum et al., 2018). Taken together, Nrxns are critical organizers of synapse properties that drive non-canonical, circuit-specific phenotypes by modifying pre- and/or post- synaptic signaling.

Neuropsychiatric disorders with neurexin dysfunction

Human genetic studies of Nrxns have revealed an association between Nrxn variants and neuropsychiatric disorders, particularly ASD and schizophrenia (Kasem et al., 2018; Yuen et al., 2017). Multiple genetic and environmental risk factors contribute to the etiology of neuropsychiatric conditions and while each disorder is phenotypically complex, similar behavioral characteristics and responses to treatment hint at overlapping pathophysiology. Nrxn variants have been observed in approximately 1-2% of people with ASD or schizophrenia (Kasem et al., 2018). A recent connectome-wide association study examined rare 16p11.2 and 22q11.2 CNVs that increase risk for ASD, schizophrenia, and ADHD (Moreau et al., 2020). Similar functional connectivity signatures were found in the thalamus, somatomotor, posterior insula, and ACC between ASD and schizophrenia but not for ADHD. All three Nrxn genes have been implicated in ASD. Mutations in αNrxn1 (Autism Genome Project et al., 2007; H. G. Kim et al., 2008; Yan et al., 2008) and βNrxn1 (Feng et al., 2006) were among the earliest evidence to describe Nrxns as ASD risk genes. Nrxn2 (Gauthier et al., 2011) and Nrxn3

(Vaags et al., 2012) mutations were also identified but at a lower frequency than Nrxn1. In contrast, only Nrxn1 variants have been associated with schizophrenia (Hu et al., 2019; Kirov et al., 2008; Vrijenhoek et al., 2008), intellectual disability (Guilmatre et al., 2009; Zweier, 2012), bipolar disorder (D. Zhang et al., 2009), ADHD (Bradley et al., 2010), and Tourette syndrome (Nag et al., 2013).

Knockout mouse models with autism-relevant phenotypes

A variety of social and repetitive behavioral tests evaluate behavioral phenotypes relevant to ASD. Moreover, the frequent presence of comorbid conditions warrants investigation of other complex behaviors such as emotional behaviors, learning and memory, sensorimotor gating, and exploratory activity (Silverman et al., 2010). αNrxn1 KO mice display impaired prepulse inhibition, increased grooming behavior, and impaired nest building with no effect on social behaviors (Etherton et al., 2009). They also showed decreased excitatory synaptic strength in the CA1 subregion of the hippocampus. Another study explored the behaviors of a different αNrxn1 KO mouse line (Grayton et al., 2013). Both male and female αNrxn1 KO mice exhibited increased social novelty preference and impaired nest building. Male αNrxn1 KO mice showed elevated anxiety and aggression which correlated with reduced direct investigation of a juvenile conspecific. Reduced locomotor activity was observed only in female αNrxn1 KO mice. Inconsistent findings were found between the *Etherton et al.* and *Grayton et al.* studies, although both lines showed poor nest building behavior. Additionally, heterozygous deletion of αNrxn1

led to impaired social memory and enhanced associative fear memory (Dachtler et al., 2015). Other studies of αNrxn1 KO mice displayed behaviors unrelated to core ASD deficits (Asede et al., 2020; Esclassan et al., 2015; Laarakker et al., 2012; Twining et al., 2017).

αNrxn2 KO mice exhibited decreased sociability and social memory and increased anxiety (Dachtler et al., 2014). Another study of αNrxn2 KO mice reported elevated anxiety in both sexes and a female-specific increase in repetitive behaviors and decrease in sociability and social novelty preference (Born et al., 2015). These behavioral effects correlated with reduced glutamate release and impaired short-term plasticity at excitatory synapses. Additionally, *Dachtler et al.* investigated the impact of heterozygous deletion of αNrxn2 and showed that αNrxn2 heterozygous mice poorly discriminated social and nonsocial stimuli although no differences in investigation of social conspecifics were observed compared with WT mice (Dachtler et al., 2015). αNrxn2 heterozygous mice also exhibited poor object recognition memory and a female-specific impairment in associative fear memory.

Inducible βNrxn1 KO after the first two postnatal weeks caused increased grooming, impaired social interaction, and reduced preference for social odors (Rabaneda et al., 2014). βNrxn1 KO mice also displayed reduced miniature EPSC (mEPSC) and miniature IPSC (mIPSC) frequency in the somatosensory cortex, indicating impaired excitatory and inhibitory neurotransmitter release. GABAergic neurons were not affected by βNrxn1 KO and the decrease in mIPSC frequency

appeared to be a compensatory mechanism to stabilize the reduction in excitation. Taken together, differences in experimental conditions and genetic backgrounds likely contribute to study-specific findings especially in αNrxn1 and αNrxn2 KO mice. Other mouse models of ASD also show differences in the range of behaviors demonstrated, which could reflect the diverse presentations of ASD itself (Silverman et al., 2010). KO of αNrxn1, αNrxn2, and βNrxn1 reduced excitatory synaptic transmission which contrasts the expected increase in E-I ratio seen in ASD. Of note, E-I ratio was not precisely measured and inhibitory synaptic transmission was not explored in the αNrxn1 and αNrxn2 KO mouse studies.

Standing questions and scope of dissertation

My thesis explores Nrxns through two different perspectives to better understand how they contribute to neurotransmission: brain-wide expression of Nrxns in the adult mouse brain (Chapter II) and Nrxns expressed in the neuromodulatory 5-HT system (Chapter III). The diverse functions of Nrxns can be attributed to their isoforms which are differentially expressed in specific circuits and brain regions. Each isoform organizes synapses based on Ca^{2+} channel-mediated control of neurotransmitter release and/or interaction with trans-synaptic partners to regulate synaptic properties. An unbiased approach to examining Nrxn expression throughout the brain remains to be performed. Additionally, Nrxns are extensively studied in excitatory and inhibitory neurons which have led to the discovery of new interacting partners and physiological roles in a variety of circuits. Specific

matching of Nrxn splice variants with trans-synaptic proteins (i.e., molecular codes) are also being scrutinized. Such detailed investigation of Nrxns exists, yet their function in other cell types is underexplored.

What is the pattern of Nrxn isoform expression in the brain? Chapter II investigates the precise distribution of the six principal Nrxn isoforms in different brain regions, subregions, and cell types. Using chromogenic and fluorescence *in situ* hybridization, we demonstrate that the mRNA profiles of Nrxns are highly diverse and expressed in neuromodulatory cell types and non-neuronal cells.

How do Nrxns impact 5-HT signaling? Chapter III examines the expression of Nrxns in 5-HT neurons and the effect of their removal on 5-HT neurotransmission. Using physiological, molecular, and behavioral approaches, we show that 5-HTergic Nrxns control efficient 5-HT release and modulate 5-HT fiber connectivity and sex-specific behaviors.

Finally, Chapter IV presents a summary of findings through these two viewpoints with a particular focus on the significance, limitations, and future studies of the work conducted in Chapter III. Understanding how cells communicate with each other at synapses is essential to connect biological mechanisms to the generation of complex behaviors. A continuum of behavioral alterations is present in ASD and my thesis work aims to contribute another piece to the ASD puzzle through an examination of Nrxns as synapse organizers throughout the brain and key players in 5-HT signaling.

Chapter II

Differential expression of neurexin genes in the mouse brain

Chapter II: Differential expression of neurexin genes in the mouse brain

Motokazu Uchigashima[1,2,*], Amy Cheung[1,*], Julie Suh[1], Masahiko Watanabe[2], Kensuke Futai[1]

1. Department of Neurobiology, Brudnick Neuropsychiatric Research Institute, University of Massachusetts Medical School, Worcester, Massachusetts.
2. Department of Anatomy, Hokkaido University Graduate School of Medicine, Sapporo, Hokkaido, Japan.

* Contributed equally to this work.

Roles of authors

M.U., A.C. and K.F. designed research; M.U., A.C., J.S. and K.F. carried out experiments; M.U., and A.C. analyzed data; M.U., A.C., M.W. and K.F. wrote the paper.

Abstract

Synapses, highly specialized membrane junctions between neurons, connect presynaptic neurotransmitter release sites and postsynaptic ligand-gated channels. Neurexins (Nrxns), a family of the presynaptic adhesion molecules, have been characterized as major regulators of synapse development and function. Via their extracellular domains, Nrxns bind to different postsynaptic proteins, generating highly diverse functional readouts through their postsynaptic binding partners. Not surprisingly given these versatile protein interactions, mutations and deletions of Nrxn genes have been identified in patients with autism spectrum disorders, intellectual disabilities and schizophrenia. Therefore, elucidating the expression profiles of the Nrxns in the brain is of high significance. Here, using chromogenic and fluorescence in situ hybridization, we characterize the expression patterns of Nrxn isoforms throughout the brain. We found that each Nrxn isoform displays a unique expression profile in a region-, cell type- and sensory system- specific manner. Interestingly, we also found that αNrxn1 and αNrxn2 mRNAs are expressed in non-neuronal cells, including astrocytes and oligodendrocytes. Lastly, we found diverse expression patterns of genes that encode Nrxn binding proteins, such as Neuroligins (Nlgns), Leucine-rich repeat transmembrane neuronal protein (Lrrtms) and Latrophilins (Adgrls), suggesting that Nrxn proteins can mediate numerous combinations of trans-synaptic interactions. Together, our anatomical profiling of Nrxn gene expression reflects the diverse roles of Nrxn molecules.

Introduction

Neurexin (Nrxn) is a presynaptic cell adhesion molecule that was originally identified as an α-latrotoxin receptor (Ushkaryov et al., 1992). In mammals, three Nrxn genes (*Nrxn1*, *Nrxn2*, and *Nrxn3*) are transcribed as longer alpha (*αNrxn1*, *αNrxn2*, *αNrxn3*), shorter beta (*βNrxn1*, *βNrxn2*, *βNrxn3*), and *Nrxn1*-specific gamma *(γNrxn1*) isoforms from two different promoters (Sterky et al., 2017; Tabuchi & Sudhof, 2002). The longer isoforms, αNrxns, have six extracellular laminin/neurexin/sex-hormone-binding globulin (LNS) domains, three interspersed epidermal growth factor-like repeats, an O-linked sugar modification sequence, a cysteine loop, a transmembrane region, and a short intracellular carboxyl terminal. Shorter isoforms, βNrxns, contain a unique β isoform-specific domain with the sixth LNS and intracellular domain of αNrxns (Sudhof, 2017). *Nrxn* isoforms also have six alternative splicing sites, resulting in thousands of potential Nrxn variants (Gorecki et al., 1999; Puschel & Betz, 1995; Schreiner et al., 2014; Treutlein et al., 2014; Ullrich et al., 1995).

The diversity of the Nrxn isoforms are thought to encode synapse specification (Sudhof, 2017). In fact, they can bind to various postsynaptic binding partners at different extracellular sites in the presence or absence of splicing sites (Boucard et al., 2005; Koehnke et al., 2010; Reissner et al., 2008). Neuroligins (Nlgns) (Ichtchenko et al., 1995; Ichtchenko et al., 1996), LRRTMs (leucine rich repeat transmembrane neuronal protein) (de Wit et al., 2009; Ko et al., 2009), $GABA_A$ receptors (C. Zhang et al., 2010), cerebellins (Uemura et al., 2010),

SPARCL1 (secreted protein acidic and rich in cysteines 1, also referred to as Hevin) (Singh et al., 2016), and latrophilins (Boucard et al., 2012) can bind to the sixth LNS domain shared with both αNrxns and βNrxns. Emerging evidence reveals that interactions of Nrxns with Nlgns play a key role in synaptogenesis and excitatory and inhibitory synaptic transmission (Boucard et al., 2005; Chih et al., 2006; Futai et al., 2013; Futai et al., 2007; Graf et al., 2004; Kang et al., 2008; Nam & Chen, 2005). Interestingly, a variety of molecules critical for synaptogenesis have been reported to bind to specific Nrxn isoforms. For example, neurexophilins (Missler et al., 1998) and dystroglycan (Sugita et al., 2001) bind to the second LNS domain specific to αNrxns. IgSF21 can promote presynaptic differentiation of inhibitory synapses through the first LNS domain of αNrxn2 (Tanabe et al., 2017). C1ql2/3 can interact with the fifth splicing site of α/βNrxn3, and recruit kainate receptors to synaptic sites (Matsuda et al., 2016). These findings suggest isoform-specific roles of Nrxns in synapse specification.

Mutations and deletions of *Nrxn* loci have been associated with neuropsychiatric and neurodevelopmental disorders. Copy number alterations (Sebat et al., 2007; Szatmari et al., 2007) and deleterious (Yan et al., 2008; Zahir et al., 2008) mutations in *αNrxn1* are the most commonly reported Nrxn isoform-specific modifications predisposing people to autism spectrum disorder (ASD), attention deficit hyperactivity disorder (ADHD), intellectual disability, schizophrenia, and Tourette syndrome (Ching et al., 2010; Clarke et al., 2012; H. G. Kim et al., 2008). Increasing genetic evidence, including deletions in chromosome 2p16.3

where *Nrxn1* is located, reveals an overlap between ASD and schizophrenia comorbidity and symptomatology (Autism Spectrum Disorders Working Group of The Psychiatric Genomics, 2017; Vinas-Jornet et al., 2014). Mutations in *Nrxn3* have also been identified in rare ASD cases (RK et al., 2017; Vaags et al., 2012). Taken together, these findings suggest that Nrxn expression should prevail in brain regions that coordinate higher cognitive functions. However, brain region- and cell type- specific expression of Nrxns is poorly understood.

The three *Nrxn* genes are transcribed in the brain, but display differential expression patterns, with the abundance of *αNrxn*s exceeding that of *βNrxn*s (Ullrich et al., 1995). Some studies have revealed cell type-specific *Nrxn* expression and distinct expression of *Nrxn* mRNA splice variants in a given cell by single cell RT-PCR or RNA-Seq (Schreiner et al., 2014; Treutlein et al., 2014). Proteomic analysis highlights the specificity of Nrxn splice isoform expression in different brain regions (Schreiner et al., 2015). However, our knowledge of Nrxn expression in different brain regions and subregions is still limited. To fill this current knowledge gap, we conducted brain-wide mapping of α and β isoforms of *Nrxn1*, *Nrxn2*, and *Nrxn3* by *in situ* hybridization, and report region- and cell type-dependent expression of *Nrxn* isoforms in the mouse brain.

Materials and Methods

Animals and section preparations

All animal protocols were approved by the Institutional Animal Care and Use Committee (IACUC) at the University of Massachusetts Medical School. C57BL6 male mice at postnatal day 28 were used, which represents the age when the expression levels of major synaptic proteins have stabilized (Gonzalez-Lozano et al., 2016). For chromogenic *in situ* hybridization, mice were transcardially perfused with 4% paraformaldehyde/0.1M phosphate buffer (PB, pH 7.2) under isoflurane anesthesia and postfixed for 3 days with the same fixatives. For double fluorescent *in situ* hybridization (FISH), brains were freshly obtained under isoflurane anesthesia and immediately frozen with powdered dry ice. Sections (20 μm) were prepared on a cryostat (CM3050S; Leica Microsystems). Fresh frozen sections were further mounted on silane-coated slides.

Plasmids

Total RNA was extracted from hippocampal primary cultures (days in vitro 14) using RNAqueous Micro Kits (Ambion) and reverse-transcribed using SuperScript III kits (Invitrogen). Nrxn, tyrosine hydroxylase (Th), P2Y purinoceptor 12 (P2ry12), Nlgn, Lrrtm, and Adgrl fragments listed in **Table 2.1** were PCR amplified and sub-cloned into the pBluescript-SK(-) vector (Stratagene). We obtained the Nlgn3 probe from Dr. Tanaka (Tanaka et al., 2010). All Nrxn probes were designed for

the coding regions and/or 5´-untranslated regions (5´-UTRs) to detect all splice variants for each Nrxn isoform.

Preparation of cRNA probes

Chromogenic and double fluorescent *in situ* hybridization were performed as previously described (Kudo et al., 2012; Yamasaki et al., 2010; Yamasaki et al., 2001). cRNA probes used in the present study are shown in **Table 2.1**. By using linearized pBluescript-SK(-) clones as templates, fluorescein- or digoxigenin (DIG)- labeled cRNA probes were transcribed with RNA labeling kit (Sigma) and T3 or T7 RNA polymerase (Promega). cRNA probes were suspended in 50% formamide.

Chromogenic *in situ* hybridization

All experiments were carried out at room temperature, unless otherwise noted. Sections were pretreated as follows: acetylation with 0.25% acetic anhydride/0.1M triethanolamine-HCl (pH 8.0) for 10 min, wash with 2x SSC (1x SSC is composed of 150 mM NaCl and 15 mM sodium citrate) in 0.1% Tween 20 for 10 min, and prehybridization with hybridization buffer (50% formamide, 33 mM Tris-HCl [pH 8.0], 0.1% N-Laurosylsarcosine sodium salt, 1x Denhardt's solution, 0.6 M NaCl, 200 μg/ml of tRNA, 1 mM EDTA, 10% dextran sulfate) for 30 min. Hybridization was carried out at 63.5 or 75°C in a 1:1,000 or 1:10,000 dilution of DIG-labeled cRNA probe (see **Table 2.1**) supplemented with hybridization buffer. Successive

post-hybridization washing was done at 61 or 75°C; 5x SSC, 0.0005% Tween 20 for 20 min, 4x SSC, 50% formamide, 0.001% Tween 20 for 40 min, 2x SSC, 50% formamide, 0.001% Tween 20 for 40 min, and 0.1x SSC, 0.0005% Tween 20 for 20 min. For Nrxn1β mRNA, sections were alternatively washed with 2x SSC, 0.1% Tween 20 at 75°C for 30 min twice, 20 μg/ml RNase, 0.5M NaCl, 10 mM Tris-HCl (pH 8.0), 1 mM EDTA at 37°C for 30 min, and 0.2x SSC, 0.1% Tween 20 at 37°C for 30 min. Sections were incubated with 20 μM iodoacetamide, 0.5 M NaCl, 0.01 M Tris-HCl [pH 8.0], 5 mM EDTA, 0.0005% Tween 20 for 30 min, DIG blocking solution (1% DIG blocking reagent [Sigma] in maleinic acid buffer [pH 7.5]) for 30 min, and alkaline phosphatase-conjugated anti-DIG antibody (1:500, Roche Diagnostics) in DIG blocking buffer for 2 hours. After washing with TNT buffer (0.1 M Tris-HCl [pH 7.5] and 0.15 M NaCl) three times, sections were incubated with NBT/BCIP solution (1:50; Roche Diagnostics) in 0.01M Tris-HCl (pH 9.5), 0.01M MgCl2 at 4°C for up to 3 days. Sections were mounted on gelatin-coated slides and dehydrated in 100% methanol for 10 min, 100% ethanol two times for 10 min each, 100% Xylene three times for 10 min each, and embedded with Entellan New (Millipore). The specificity of cRNA probes against each Nrxn isoform mRNA was validated by the identical signal pattern obtained by two different probes and lack of hybridization signals with their sense probes (**Figure 2.1**).

Double-labeled fluorescent *in situ* hybridization

Fresh frozen sections were fixed with 4% paraformaldehyde, 0.1M PB for 30 min, acetylated with 0.25% acetic anhydride in 0.1M triethanolamine-HCl (pH 8.0) for 10 min, and prehybridized with hybridization buffer for 30 min. After dehydration, hybridization was then performed with a mixture of fluorescein- or DIG-labeled cRNA probes at a dilution of 1:1,000 or 1:10,000 (see **Table 2.1**) in hybridization buffer. Post-hybridization washing was performed as described for chromogenic *in situ* hybridization. To visualize signals, we adopted a two-step detection method. For the first detection, sections were blocked with DIG blocking solution for 30 min and 0.5% tryamide signal amplification (TSA) blocking reagent in TNT buffer for 30 min, and incubated with peroxidase-conjugated anti-fluorescein antibody (1:500, Roche Diagnostics) for 1 hour. After washing with TNT buffer three times, sections were incubated by using TSA Plus Fluorescein amplification kit (PerkinElmer) for 10 min. Residual peroxidase activity was inactivated with 3% H_2O_2 in TNT buffer for 30 min. For the second detection, sections were again blocked with DIG blocking solution and 0.5% TSA blocking reagent in TNT buffer for 30 min each, and incubated with peroxidase-conjugated anti-DIG antibody (1:500 Roche Diagnostics) for 1 hour. After washing with TNT buffer three times, signals were visualized with TSA Plus Cy3 amplification kit (PerkinElmer) for 10 min. Nuclear counterstaining was performed with DAPI (1:5000, Sigma-Aldrich) for 10 min. The specificity of cRNA probes for *Th* and *P2ry12*, which were newly generated in this study, were validated by unique signal patterns with labeled cells distributed

selectively in catecholaminergic nuclei (**Figures 2.14 and 2.15**) and scattered in the neuropil region (**Figures 2.16 and 2.17**), respectively.

Table 2.1 | List of cRNA probes used in the present study

Molecule	Sequence	Accession # (Genebank or NCBI)	Dilution	Hybridization Temperature (°C)	Reference
αNrxn1#1	186–631	NM_020252.3	1:1,000	63.5	this study
	AAGGGGAATAACCAGGCAGATTTCTGAGTTCTTATAAACGTCAAAATAAAATCAAAATGCATCACCAACATACAACCAACTGACATGCTGGAG TCTTAGGGTGGCCTTGCAGAGACAGAAAAAAGAAGAGTTTGAGGGATTGATTTCACCATCTAACAGCTTCTGGCTACTTCACAGCAGGGTTTG AGACCTACCTACAGGGCTCCTAAACATAAAGCGAATCAGCCTGGGAGGGCATGCACAGGAAATTTGGCCTTGGCTTTAGTGGTGCTGGAAG CCCATGATATGACAGAAGTAGGCCTCTGAAGCTATTCTGGTGTCTCACTCTGTCCTTTCTCCTTCTGTGCTTGGAGCCAACATCTGGAGGGG CCTCGAGGCCTGCCAAGCAGCCAAAGATCCTGGCTCAGTGTTGACTTCGTGTTCCTCTCCGAGAAAAGTGTGTTTCT				
αNrxn1#2	631–1132	NM_020252.3	1:10,000	63.5	this study
	TTCCGATTCTGCTCTCCTACTGCTGGCACCGCGCCGGTGGTACTTTGAAGGTTTTGGTCCTGGGATAGTTGAAGTACCTGTTGGTGCCACAG ATGCCCTCACTTAAACATCATCGGATGCAAATGGATCAGTGATCGCTCTTGAGCCTCGGTGGCCCTCTTTTTCAGAACGTTGCCTCCAAAGTG TATCCCCCCTTTGGCCTGGAAGTTCTGCAGCTATCCCATAGGACTGGGGTCTCCGCTTTCCAGTTGGAAGGAGACTACTGGGAGAGAGGAA GGGGCTGCTGGAAGAGAAGAAGAAGGAAAAAAGAGCTGAAGGAGGGTGCGCCCCTCCCACTGCCGCCTCCCCCCTCCCTCCCACTCCTCT GCGGACCCCCATTTCTCTGTGAAGGTGTCCAGGACCGCTTCGACCCTGTCGCCCCCGGCTCCCCCCCCGCCGCACCCCAGCCCCGAGCATG GGGACGGCGCTGGTCCAGCGCGGGGGCTGCTGTCTCCTCTGCCTGT				
βNrxn1#1	379–824	XM_006523818.2	1:10,000	75	this study
	GCTCTTTCATCTGCCCCTGCTTTTCCTCCGCTCGCTTTCCCCAGTTCGATCCCTGCTGTCTTCACGAGGGTGCCCACTTCCCTCTGAACCCAT CGTCGGGCGTAGTGTCAGGAGGCGGCGGACTCGGAGATTGCCTCTGGAGCAGGCGATGCGCGCCGCTGCTCTGCGCGCTGCCCGGGTGA GGCTGGCGGGAGCTGGAGAGCTGGCCAGGGCTGAATGGAGGGACAGGGTGCCTTGCGTCCATGGGGTCTGCTTCTTTCCTGAAAGGAGG CTGGACCGGCGAAGTGGTCTCCCAGTTCCCCGCGCACAATGCTAAATGGATTTACCTAGTGGATTCCCGGTGGATGGCTGTCATGTAGAAGT GAAGACCCTCCGGGAGGAGCTTTAAACAATTTCCAGGCTCCCCAACCCCGGCACACACTCTCGCCCGAAACTCTTGGGGAGTA				
βNrxn1#2	882–1490	XM_006523818.2	1:10,000	75	this study
	TGTTCTTCGGGTCTGCTTTTCCGGACAAGTCCTCCGGCCAGCTACATTCACCTCGGCTATGTTTCGGATTGTTTGGGGTACTGTTGTAGGGC ACTGCAGACTCCAGGACCCTGAGAAGACTGTCCGAAGGAGGGAGAGGATGGCTGCCCTGGCGCGGTAAGGCGGCCAATCCAGCAGCCAAC CGCGAGCCGCCCGATCCCCGGCTTCCTCTTCTCTTCTTGTGCCCCAAACTTTGCCTCCCGCGGCGGCTGCCCCTTGGCGGGCGCCCCGCC ATGTACCAGAGGATGCTTCGGTGCGGCGCCGATCTGGGATCGCCCGGGGGCGGCAGTGGCGGCGGCGCAGGGGGGCGCCTGGCCCTGA TCTGGATAGTCCCGCTCACCCTCAGCGGCCTCCTAGGAGTGGCCTGGGGGGCATCCAGTTTGGGAGCGCACCACATCCACCATTTCCATGG CAGCAGCAAGCATCATTCAGTGCCTATTGCAATCTACAGGTCACCAGCATCCTTGCGAGGCGGACACGCTGGGACAACATATATCTTTAGCA AAGGTGGTGGACAGATTACATATAAGTGGCCTCCCAATGACCGCCCCAGTACACGAGCAGACAGGC				
αNrxn2#1	120–370	NM_001205234	1:1,000	63.5	this study
	GACCAGGAGGCGCGAGGCAGCCGATATCGCTGGCCCAGGATCTGTTACCTGCCGTAGACCCAGCGGTCTCTAGGCTCGGATCCCTACCCT TCAGCTCCTGGCGCCCCCAAAACCAGGCGTCCCTCCCCCACCTTCCATACGAGCCCGCCGCGGGGGAGGGGCTCCACCACCGCAGCCGC CGTCGTTGCCTTCCGGGGACGTGGACACGTGAGCCCCGGCTACTGAGTCCATGGCACTGTGAATCGGCGAGG				

Molecule	Sequence	Accession # (Genebank or NCBI)	Dilution	Hybridization Temperature (°C)	Reference
αNrxn2#2	894–1209	NM_001205234	1:1,000	63.5	this study
	TCAAAGCGGCGCGAGATGCAGGTGGCCAGCGACCTGTTCGTGGGCGGCATCCCTCCCGACGTGCGCCTATCTGCACTCACGCTCAGCACC GTCAAGTACGAGCCGCCTTTCCGCGGCCTTCTGGCCAACCTGAAGCTGGGCGAGCGGCCGCCGGCGCTGCTGGGTAGCCAGGGTCTGCG CGGTGCGGCCGCCGACCCTCTGTGTGCGCCTGCGCGCAATCCCTGCGCCAACGGCGGTCTCTGCACCGTGCTAGCCCCCGGCGAGGTGG GCTGCGACTGCAGCCACACTGGATTTGGCGGCAAGTTCTGCAGTGAAG				
βNrxn2#1	188–375	AK163904.1	1:1,000	63.5	this study
	TGAGGGGGGACCCCTAGCCGCCCGCGATGGATCCAGGCTTCACGGACCTTGGCCTTCCCGCTGCGCGTACCCCGGATTCCCCGGCGGGA TCCAGTTGATTTGCTTGGCTCCGGACTGAGGCTCGGGCTCTGGTTTTCCTTCGCTTCACCCCTACCCCCCTCTCGGAGCTCGCAACCGGAG GGGGGCTT				
βNrxn2#2	543–714	AK163904.1	1:1,000	63.5	this study
	TTCTGCTGGGGCTGCTGCTGCTGCTGGGGGCGGCTGAGGGGGCCCGGGTCTCGTCCAGCCTCAGCACCACCCACCACGTCCACCACTTCC ACAGCAAGCACGGCACCGTGCCCATCGCCATCAACCGCATGCCCTTCCTCACCCGCAGCGGGCACGCTGGGACCACATACAT				
αNrxn3#1	207–795	NM_001198587	1:1,000	63.5	this study
	CCTCCCGATTACTCCTCCTCCATTACAGCACCCTGAGCCCCAGCCCTGTCCTTGGTCTTCCTGGCTAGGACGCATTTGCCGGGAGGAAGACA TTACGGAAGGCTTATTCCCACCCTGGGCTCCTTCTCCTCCTTGAATCAAGGCCTCCGGATCCACATGGATAGCTGAGATCTTTTCTTGGAGAA AGATACTTCTTCCTCGCCTCATCCCTGATTTGCCTCACCCGACAAATCCCCTGTCTGTTTCGTCTCCCTCTTTATGGGATTTCTTGCTTGTGTG CCTATCTAGGGCCGTGTTGTCCTTTTTCCTCTCCTTCCCCTTTCCTCCTAACATTCCTGTGTGTGTTCTTCTTGTGTCTTCTCTTGTACCACTCT GTTTTCCCTCTTTGCCCTCACAATCACCTATCCCCTGCCTCCCGCTCCCACGGCTGATACCTGGCCTACCTGCTCCTCTGTGCTCTGACCCA GCAGGCACCATGAGCTTTACCCTCCACTCAGTTTTCTTCACCTTGAAGGTGAGCATCTTTCTGGGCTCCCTGGTGGGGCTTTGCCTGGGTCT GGAGTTCATGGGCCTTCCTAACCAGTGGGCC				
αNrxn3#2	796–1782	NM_001198587	1:1,000	63.5	this study
	CGCTACCTGCGTTGGGATGCAAGCACGCGCAGTGACCTGAGCTTCCAGTTCAAGACCAATGTTTCCACTGGGCTGCTCCTGTATTTGGATGA TGGTGGTGTCTGTGACTTCCTCTGTCTCTCCCTGGTGGATGGCCGCGTTCAGCTCCGCTTTAGCATGGACTGTGCCGAGACCACTGTGCTAT CCAACAAGCAGGTGAACGACAGCAGTTGGCACTTCCTCATGGTGAGCCGTGATCGTGTGCGCACTGGGCTGGTGATTGATGGTGAGGGCCA GTCTGGAGAGCTACGGCCCCAGCGGCCTTATATGGATGTGGTCAGTGATTTGTTCCTCGGTGGCGTCCCCGCTGACATTCGACCTTCTGCC CTGACCCTCGATGGAGTACAGAGCATGCCTGGCTTTAAGGGATTAATGCTGGATCTCAAGTATGGCAACTCGGAACCTCGGCTTCTGGGGA GCCAGAGCGTCCAGTTAGAAGCAGAGGGACCCTGTGGCGAGCGTCCCTGTGAAAATGGTGGGATCTGCTTCCTCTTGGATGGTCATCCCAC CTGTGACTGTTCTACCACTGGCTATGGTGGCACACTCTGCTCAGAAGATGTCAGTCAAGGTCCAGGCCTCTCCCATCTTATGATGAGTGAAC AAGCACGAGAGGAGAACGTGGCCACCTTCCGAGGCTCAGAGTATCTGTGCTATGACCTGTCCCAGAACCCCATCCAGAGCAGCAGCGACGA AATCACCCTTTCCTTTAAGACCTGGCAACGCAATGGGCTCATCCTCCACACTGGCAAGTCGGCCGACTATGTTAACCTGGCTCTGAAGGATG GTGCGGTCTCCTTGGTCATTAACCTGGGGTCCGGGGCCTTTGAGGCCATTGTGGAGCCAGTGAATGGGAAATTCAACGACAACGCCTGGCA TGATGTCAAAGTGACACGCAATCTTCGGCAGGTGACAATCTCTGTGGATGGCATCCTAACCACAACGGGCTAC				

Molecule	Sequence	Accession # (Genebank or NCBI)	Dilution	Hybridization Temperature (°C)	Reference
βNrxn3#1	85–530	NM_001252074	1:1,000	63.5	this study
	CTGCTCCTCTCCACCTTCTGCTACGTTGGTCTGGGTGGCTAGCTCAGTGCTGTTTCTTTTCCTCTGGCCCTTCTTGATCCCTTTCTCTGGCTA CTGCTGCTGGCTGATTTTCAACCTATTGGGAACTCAGGACTTAAGGCGGCTGCACCGTGGCGCTCATCCAGGACACTCAGGGTTAACAGCCT CCGCGCCCATCCACAGAGACTCCCGGGAGCAGAACTCTTCCACCTGCAGCCCCCTTTTGCCTGGCAGTTCTGCATTGCATCGCTTGGAAGT CGAAACAAGAAAGAAAGAAAGAAAGAAAAATGTCCAAACTCCTTGGATGTTGGGAAAAACTAGCGTGAATTTACTTGGTTTTTTCCTGCTCTGT CTTCTCTCTCCGTTTCCACCTTTCCCCAGTGGCTTTCCAGAGTATGCAGCTAGTACATCGGACTTGAAGTACCAAG				
βNrxn3#2	771–1235	NM_001252074	1:1,000	63.5	this study
	TTCCCCGAAAGCTTTTATTGCTTCCCTCATCCCCAAATTGAACAACTCTTCCTCCTGCTATGATGGGCCTCTGGGCATCATGAACTTCGTTATT GCTCACTGGCTGGAATTTAAACTGCCCATCTGTAGTGGTCCAGTGCGTTGACCATGCACCTGAGAATCCACCCAAGACGGAGCCCTCCTCGC CGGCCGGCCTGGACGCTTGGGATCTGGTCCCTCTTCTGGGGATGTATCGTCAGCTCTGTGTGGAGTTCTTCTAATGTAGCCTCCTCCTCCTC TTCCTCTCCGGGATCTCACTCTCAGCAGGAACACCATTTCCACGGCAGCAAGCACCACTCTGTGCCTATTTCTATCTATCGCTCCCCTGTTTC CCTTCGAGGAGGGCACGCTGGTGCAACATACATCTTTGGGAAAAGCGGTGGCCTCATCCTCTATACCTGGCCAGCAAATGACAGACCCAGC ACA				
Vglut1	301–1680	BC054462	1:1,000	63.5	(Yamasaki et al., 2010) (Mao et al., 2018)
	ACATGGCTCCTTTTTCTGGGGCTACATTGTCACTCAGATTCCTGGAGGATTTATCTGCCAAAAATTCGCAGCCAACAGGGTCTTTGGCTTTGC CATTGTGGCTACCTCCACCCTAAACATGTTGATCCCTTCAGCAGCCCGCGTTCACTATGGCTGTGTCATCTTCGTGAGGATCCTTCAGGGATT GGTGGAGGGGGTCACATACCCTGCTTGCCATGGCATCTGGAGCAAATGGGCCCCTCCCTTAGAACGGAGTCGGCTGGCAACGACAGCCTTT TGCGGTTCCTATGCTGGGGCGGTGGTTGCCATGCCCTTGGCTGGGGTCCTTGTGCAGTATTCAGGATGGAGTTCTGTCTTCTATGTCTATGG CAGCTTCGGGATCTTTTGGTACCTGTTCTGGTTGCTTGTCTCCTATGAGTCACCGGCACTGCACCCCAGCATCTCTGAGGAGGAGCGCAAAT ACATTGAGGATGCCATCGGGGAGAGCGCCAAGCTCATGAACCCTGTTACGAAGTTTAACACACCCTGGAGGCGCTTCTTTACGTCCATGCCC GTCTATGCCATCATCGTTGCGAACTTTTGCCGCAGCTGGACCTTCTACCTGCTCCTCATCTCTCAGCCCGCCTACTTTGAAGAAGTGTTCGGC TTTGAGATCAGCAAGGTGGGGCTGGTGTCGGCGCTGCCTCACCTTGTCATGACCATCATCGTACCCATTGGAGGCCAGATCGCTGACTTTTT GCGCAGTCGTCACATAATGTCCACTACCAACGTGCGAAAGCTCATGAACTGCGGGGGTTTCGGGATGGAAGCCACGCTGCTGCTGGTGGTC GGATACTCGCACTCCAAGGGCGTGGCCATCTCCTTCCTGGTCCTGGCTGTGGGCTTCAGTGGCTTTGCCATCTCTGGGTTTAACGTGAACCA CTTGGACATCGCCCCTCGCTATGCCAGCATCTTGATGGGCATTTCCAATGGCGTGGGCACACTGTCTGGGATGGTGTGCCCCATCATCGTG GGTGCAATGACCAAGCACAAGACGCGGGAGGAGTGGCAGTACGTGTTCCTCATAGCCTCCCTGGTGCACTACGGCGGTGTCATCTTCTATG GGGTCTTTGCTTCGGGAGAGAAGCAGCCGTGGGCAGAGCCGGAGGAGATGAGCGAGGAGAAGTGTGGCTTTGTTGGCCACGACCAGCTG GCTGGCAGTGACGAAAGTGAAATGGAGGACGAGGCTGAGCCCCCAGGGGCGCCCCCCGCGCCGCCTCCGTCCTACGGGGCCACACACAG CACAGTGCAGCCTCCGAGGCCCCCGCCCCCTGTCCGGGACTACTGACCACGGGCCTCCCACTGTGGGGCAGTTTCCAGGACTTCCACTCC ATACACCTC				

Molecule	Sequence	Accession # (Genebank or NCBI)	Dilution	Hybridization Temperature (°C)	Reference
Gad1	1036–2015	NM_008077	1:1,000	63.5	(Yamasaki et al., 2010) (Mao et al., 2018)
	GTACAGCATCATGGCTGCTCGTTACAAGTACTTCCCAGAAGTGAAGACAAAAGGCATGGCGGCTGTGCCCAAACTGGTCCTCTTCACCTCAG AACACAGTCACTATTCCATAAAGAAAGCCGGGGCTGCGCTTGGCTTTGGAACCGACAATGTGATTTTGATAAAGTGCAATGAAAGGGGGAAG ATAATTCCGGCTGATTTAGAGGCAAAAATTCTTGATGCCAAACAAAAGGGCTATGTTCCCCTTTATGTCAATGCAACCGCAGGCACGACTGTT TACGGAGCATTCGATCCAATCCAGGAAATTGCGGACATATGTGAGAAATACAACCTTTGGCTGCATGTGGATGCTGCCTGGGGTGGTGGACT GCTCATGTCCCGGAAGCACCGCCACAAACTCAGCGGCATAGAAAGGGCCAATTCAGTCACCTGGAACCCTCACAAGATGATGGGCGTGCTG CTCCAGTGCTCTGCCATTCTGGTCAAGGAAAAGGGTATACTCCAAGGATGCAACCAGATGTGTGCAGGCTACCTCTTCCAGCCAGACAAGCA GTATGACGTCTCCTATGACACCGGGGACAAGGCGATTCAGTGTGGCCGCCATGTGGACATCTTCAAGTTCTGGCTGATGTGGAAAGCAAAG GGCACCGTGGGATTTGAAAACCAGATCAACAAATGCCTGGAGCTGGCTGATTACCTCTACGCCAAGATTAAAAACAGAGAAGAGTTTGAGAT GGTTTTCGATGGTGAGCCTGAGCACACAAATGTCTGTTTCTGGTACATTCCACAAAGCCTTCGAGGGGTTCCAGATAGCCCTGAGCGACGAG AAAAGCTACACAGGGTGGCTCCCAAGATCAAAGCTCTGATGATGGAGTCAGGAACAACCATGGTGGGCTACCAGCCTCAAGGGGACAAGGC CAACTTCTTCCGGATGGTCATCTCTAACCCAGCCGCCACCCAGTCTGACATCGATTTCCTCA				
Th	1–1025	AY855842	1:1,000	63.5	this study
	ATGCCCACCCCCAGCGCCTCCTCGCCACAGCCCAAGGGCTTCAGAAGAGCCGTCTCAGAGCAGGATACCAAGCAGGCCGAGGCTGTCACG TCCCCAAGGTTCATTGGACGGCGGCAGAGTCTCATCGAGGATGCCCGCAAGGAGCGGGAGGCAGCAGCAGCTGCAGCAGCAGCAGCGGT AGCCTCCTCGGAACCTGGGAACCCACTGGAGGTTGTGGTATTTGAGGAGAGGGATGGGAATGCTGTTCTCAACCTGCTCTTCTCCCTGAGG GGTACAAAACCCTCCTCCTTGTCTCGGGCTGTAAAAGTATTTGAGACATTTGAAGCCAAAATTCACCACTTAGAGACCCGGCCTGCCCAGAG GCCACTGGCAGGAAGCCCCCACCTGGAGTATTTTGTGCGCTTCGAGGTGCCCAGTGGAGACCTGGCTGCCCTCCTCAGCTCTGTGCGTCG GGTGTCTGACGACGTGCGCAGTGCCAGAGAGGACAAGGTCCCCTGGTTCCCAAGAAAAGTGTCGGAATTGGACAAGTGTCACCACCTGGTC ACCAAGTTTGACCCTGATCTGGACCTGGACCACCCGGGCTTCTCTGACCAGGTGTATCGCCAGCGTCGGAAGCTGATTGCAGAGATTGCCT TCCAGTACAAGCACGGTGAACCAATTCCCCATGTGGACTACACAGCGGAAGAGATTGCTACCTGGAAGGAGGTATATGCCACGCTGAAGGG CCTCTATGCTACCCATGCCTGCCGGGAGCACGTGGAGGGTTTCCAGCTTCTGGAACGGTACTGTGGCTACCGAGAGGACAGCATCCCACAG CTGGAGGACGTGTCCCGCTTCTTGAAGGAGCGGACTGGCTTCCAGCTGCGACCCGTGGCCGGTCTACTGTCCGCCCGTGATTTTCTGGCCA GTCTGGCCTTCCGCGTGTTTCAATGCACCCAGTATATCCGCCATGCCTCCTCACCTATGCATTCACCTGAGCCGGACTGCTGCCATGAGCTG TTGGGACATGTACCCATGTTGGCTGA				
Glast	1571–2473	AF330257	1:1,000	63.5	(Yamasaki et al., 2010) (Mao et al., 2018)
	TGAAGAACCGAGATGTTGAAATGGGGAACTCGGTGATTGAGGAGAACGAAATGAAGAAGCCGTATCAGCTGATTGCCCAGGACAATGAACC GGAGAAACCCGTGGCAGACAGCGAAACCAAGATGTAGACGGACAGAGAAGTGCTTTCTTAAGCACCAAGTGTTGGAAACTGTTCTACAATGT ATCCATCTCCCTGGGCTCACTTTCCCAGTGAGCTCCTCTTTCCTCCCTACTCTGATAGGATTGGAAAACGGCCAAACACAAAGGAGGGCTCT GCAGCAGCCCAAACCTATCGGTTTTAGCCTACATTTGAAAATTTTAAGTCATTTCATATTATTCTTACCAAGTAAGCTACTACAATCAAACACAG TTTCGATATTACCAATTTAGGTGGCAAACGATCCTGTGCCATTGCTCTGTAAGTAAAAGAATTAAGCAAATGATAGGCTACCGAAAAAAAAAGT TTTAAAATCAACTTTCAAGATGTAAAAATCCTTCAGAATGCAACTGAGTTTTAATCTTAAAACATTACAACTTGATGAGCAATTATCAGTTACCCA TTGAGTAGCTGAGAGGTTCCCATTTCTTCTGACTCCTGCCCTGACTTTGTCAGCATCAGGGCAATCCCCACATGCACACAGCACAGCTGTGA GGAGGAGCGGAGAGTGAGGCTCCCAAATGGTCTAGAGTGAGCCTTGTCTCATCCATTGGCCTCAGTGTTCTCATCCGGAAAATGAGTGACT CCTAGACAGGCCTCTCTAGCCCAAACTTCTGGAACATCAGGAAGGACCCTGCCCCTGTACACCATGAGGATCTCAGACAGGACACTTATTGG GAATGGACATTTCTCTCTAGGGGCAGGCTGTGTGTGGCTCACTAGATCCTGGGTTCAAAATGTTCGTT				

Molecule	Sequence	Accession # (Genebank or NCBI)	Dilution	Hybridization Temperature (°C)	Reference
Plp	1–1359	NM_011123	1:1,000	63.5	(Yamasaki et al., 2001)
	CTTTTCATTGCAGGAGAAGAGGACAAAGATACTCAGAGAGAAAAAGTAAAGGACAGAAGAAGGAGACTGGAGAGACCAGGATCCTTCCAGCT GAGCAAAGTCAGCCGCAAAACAGACTAGCCAACAGGCTACAATTGGAGTCAGAGTGCCAAAGACATGGGCTTGTTAGAGTGTTGTGCTAGAT GTCTGGTAGGGGCCCCCTTTGCTTCCCTGGTGGCCACTGGATTGTGTTTCTTTGGAGTGGCACTGTTCTGTGGATGTGGACATGAAGCTCTC ACTGGTACAGAAAAGCTAATTGAGACCTATTTCTCCAAAAACTACCAGGACTATGAGTATCTCATTAATGTGATTCATGCTTTCCAGTATGTCA TCTATGGAACTGCCTCTTTCTTCTTCCTTTATGGGGCCCTCCTGCTGGCTGAGGGCTTCTACACCACCGGCGCTGTCAGGCAGATCTTTGGC GACTACAAGACCACCATCTGCGGCAAGGGCCTGAGCGCAACGGTAACAGGGGGCCAGAAGGGGAGGGGTTCCAGAGGCCAACATCAAGCT CATTCTTTGGAGCGGGTGTGTCATTGTTTGGGAAAATGGCTAGGACATCCCGACAAGTTTGTGGGCATCACCTATGCCCTGACTGTTGTATG GCTCCTGGTGTTTGCCTGCTCGGCTGTACCTGTGTACATTTACTTCAATACCTGGACCACCTGTCAGTCTATTGCCTTCCCTAGCAAGACCTC TGCCAGTATAGGCAGTCTCTGCGCTGATGCCAGAATGTATGGTGTTCTCCCATGGAATGCTTTCCCTGGCAAGGTTTGTGGCTCCAACCTTC TGTCCATCTGCAAAACAGCTGAGTTCCAAATGACCTTCCACCTGTTTATTGCTGCGTTTGTGGGTGCTGCGGCCACACTAGTTTCCCTGCTCA CCTTCATGATTGCTGCCACTTACAACTTCGCCGTCCTTAAACTCATGGGCCGAGGCACCAAGTTCTGAGCTCCCATAGAAACTCCCCTTTGTC TAATAGCAAGGCTCTAACCACACAGCCTACAGTGTTGTGTTTTAACTCTGCCTTTGCCACTGATTGGCCCTCTTCTTACTTGATGAGTATAACA AGAAAGGAGAGTCTTGCAGTGATTAATCTCTCTCTGTGGACTCTCCCTCTTAGTACCTCTTTTAGTCATTTTGCTCCACAGCAGGCTCCTGCTA GAAATGGGGGATGCCTGAGAAGGTGACTCCCCAGCTGCAAGTCGCAGAGGAGTGAAAGCTCTAATTGATTTTGCAAGCATCTCCTGAAGAC CAGGATGTGCTTCCTTCTCAAAGGGCACTTCCAACTGAGGAGAGCAGAACGGAAAGGTTCTCAGG				
P2ry12	347–846	NM_027571	1:1,000	63.5	this study
	ACTCAAGGCTGCCTTGCTGAAGTCTCTGCAGAGTCTCTATCACAGAGGGCTTTGGGAACTTATGCAAGTCACTGAGAAGAAAGCAACAGATG CCAGTCTGCAAGTTCCACTAACTAGTATTCCCGGAGACACTCATATCCTTCAGATTCAGCAGAACCAGGACCATGGATGTGCCTGGTGTCAA CACCACCTCAGCCAATACCACCTTCTCCCCTGGGACCAGCACCCTGTGCGTCAGAGACTACAAGATCACCCAGGTTCTCTTCCCATTGCTGT ACACCGTCCTGTTCTTTGCTGGGCTCATCACGAACAGCTTGGCAATGAGGATTTTCTTTCAGATCCGCAGTAAATCCAACTTCATCATTTTTCT TAAGAACACGGTCATCTCTGATCTACTAATGATTCTAACTTTTCCATTTAAAATTCTTAGTGATGCTAAACTGGGAGCCGGGCCTCTGAGAACC TTGGTGTGCCAAGTTACTTCAGTCACATTTTATTTT				
Nlgn1	3098-3790	NM_138666	1:1,000	63.5	this study
	CCAGAAAGACCAGCTTTATCTCCATATTGGATTAAAACCGAGAGTTAAAGAGCATTACAGAGCCAATAAGGTAAATCTCTGGCTGGAGCTGGT ACCTCATCTGCATAATCTCAATGACATTTCTCAGTATACCTCGACAACAACTAAAGTGCCATCCACGGACATCACTCTCAGACCTACAAGGAA GAATTCCACACCAGTCACATCAGCCTTTCCCACTGCCAAACAGGATGATCCCAAGCAACAACCAAGCCCCTTCTCGGTGGATCAGAGGGACT ACTCCACAGAGCTAAGTGTCACTATCGCAGTGGGGGCCTCTCTGCTGTTTCTCAACATCTTGGCTTTTGCAGCCCTGTACTACAAGAAGGATA AGAGGAGACATGATGTCCACCGGAGGTGCAGCCCTCAGCGCACGACCACCAACGACCTAACCCATGCTCCAGAAGAGGAAATTATGTCTCT CCAAATGAAGCACACTGACTTGGATCACGAGTGTGAGTCCATCCATCCACATGAGGTGGTTCTTCGGACCGCCTGTCCCCCAGATTATACTC TAGCTATGAGGAGGTCACCTGATGATATTCCACTAATGACACCTAACACCATCACAATGATTCCCAACACTATACCAGGGATTCAGCCCTTAC ATACATTCAACACATTTACTGGAGGACAGAATAATACACTGCCCCA				

Molecule	Sequence	Accession # (Genebank or NCBI)	Dilution	Hybridization Temperature (°C)	Reference
Nlgn2	2041-2895	NM_198862	1:1,000	75	this study
	ACTGGTGACCCCAACCAGCCTGTGCCACAGGACACCAAGTTCATCCACACCAAGCCCAACCGCTTTGAAGAGGTAGTGTGGAGCAAGTTCA ACAGCAAGGAAAAGCAGTATCTGCACATAGGCTTGAAACCACGCGTGCGCGACAACTACCGTGCCAACAAGGTGGCCTTCTGGCTGGAGCT CGTGCCCCACCTGCACAACCTGCACACAGAGCTCTTCACCACCACCACTCGCCTGCCTCCCTATGCCACACGCTGGCCACCTCGCACACCT GGTCCTGGCACTTCCGGCACACGCCGTCCTCCCCCACCTGCCACTCTGCCACCTGAGTCTGATATTGACCTAGGCCCAAGGGCCTATGACC GCTTCCCCGGTGACTCGAGGGACTACTCCACGGAGCTAAGCGTGACTGTGGCAGTGGGTGCCTCCCTCCTCTTCCTCAACATCCTTGCCTTT GCCGCCCTCTATTACAAGCGGGACCGGCGCCAGGAGCTGCGGTGCCGGAGGCTTAGCCCACCAGGAGGCTCAGGCTCAGGTGTGCCTGG TGGGGGCCCCCTGCTTCCCACTGCTGGCCGTGAGCTACCCCCGGAGGAGGAGCTAGTATCGCTGCAGCTGAAGCGGGGTGGTGGTGTTG GGGCGGACCCTGCTGAGGCCCTGCGCCCTGCCTGTCCACCCGACTATACCCTGGCCTTGCGCCGGGCACCGGACGATGTGCCTCTCTTGG CCCCCGGGGCCCTAACCCTGCTGCCTAGTGGCCTGGGGCCCCCGCCCCCGCCCCCACCCCCTTCTCTCCATCCCTTTGGGCCCTTCCCAC CCCCACCCCCTACTGCTACCAGCCACAACAACACGCTACCC			
Nlgn3	2939-3782	NM_172932	1:1,000	63.5	(Tanaka et al., 2010)
	ATGCACCCGCATGTACAAAAACACAAATCCAGACGTGAACCTGAATAGGCCCTTCAAATGGGGACACATACGAGTCCTTGGTACCAAGGGCC CATGGAACAGCAGCTGGAACCAGCTCCTTGAGCCCGACCACAGACACTCCTGGGGCCCTGGAAGCCACAGCCGGACACCCCCTTGGTGCT TGCCTTCTCGGAACTGCACCTCTACCAACTGCAGACTCGGGAGCTTTAAAGAGCAGGATAGCTCTTCCTCCCCCAGACTTGGTCTTTTCTCTG GGTCTTGTTTTTGTTGATTTTTTTCATTTTTAAATTGGAACCAATGCTTTTCCAACCCATTGAGTGCTAAGCAGCTCTGGAAGGGAGGGCTCCA AGATCAGGACGCTCTGGCTCTGGGACTCCCAATGTTCATACAATCAGACCAAGGAGAAGGACCTTCCAAGACAGTGACAGATGGGCACAAG ACTATGGGGTAAGAGGAGGAAGAGGCTAGCAATGGATGGGGCTTGAGGGCCAGCAAGGACAGAGCACCAACTGGCTCTGGGCCTCCCAGA GAGGACTACAGAGCCTACAGGGTGACCTGCTTCTGCAAAGGCCAGCAGCAGCAGCCTGCCTGGAGAAGCCTAGGTTTGATGAACTAAGTAC TGTGGAGGCCCTGACCTTATTGGGCCCCTGGGTATATAATCTGGGTTCTGCCTCTGCCCTTGGGGACATGATATCAGAAATTTGCCCCATTTT CTTTACAGTCTCTTTGTGTCTGTCATTTCTCTTTCAAAACAACAGTGTTTTGGTTTTTTTTTTTTTTTCGGTTGTTGTTGGCTTTTTTTTTTTTTTT TTTTTAAGAAAA			
Lrrtm1	1286-2134	NM_028880.3	1:1,000	75	this study
	AGGCGGAATAAGGTTGCCATTGTGGTCAGCTCTCTCGACTGGGTTTGGAATTTGGAGAAAATGGACTTGTCTGGGAACGAGATCGAATACAT GGAGCCCCATGTGTTCGAGACCGTTCCCTACCTGCAGACCCTGCAGCTGGACTCCAACCGCCTCACCTACATTGAGCCCCGTATTCTCAACT CCTGGAAGTCCCTTACGAGCATCACTCTGGCCGGGAACCTGTGGGACTGCGGGCGCAACGTGTGTGCTCTAGCTTCCTGGCTCAGCAACTT CCAGGGACGTTACGATGCTAACTTGCAGTGCGCCAGCCCAGAGTACGCACAGGGCGAGGACGTCTTGGATGCAGTGTATGCTTTCCACCTG TGTGAGGATGGGGCCGAGCCCACCAGCGGCCACCTCCTGTCGGTGGCCGTCACTAACCGCAGTGACCTAACGCCCCCAGAGAGCTCAGCC ACGACTCTGGTGGACGGTGGGGAGGGGCACGATGGCACGTTTGAGCCCATCACTGTGGCTCTTCCAGGCGGCGAGCACGCAGAGAACGCT GTGCAAATCCACAAAGTGGTCACTGGCACCATGGCCCTCATCTTCTCCTTCCTCATCGTGGTCCTCGTACTCTACGTATCCTGGAAGTGTTTC CCAGCCAGCCTCAGGCAGCTCAGACAGTGCTTTGTCACGCAGCGCAGGAAGCAGAAGCAGAAACAGACCATGCATCAGATGGCTGCTATGT CTGCCCAGGAATACTATGTTGATTACAAACCTAACCACATCGAGGGGGCCCTGGTTATCATCAACGAGTACGGTTCGTGTACCTGTCACCAG CAGCCTGCGAGGGAATGCGAGGTGTGA			

Molecule	Sequence	Accession # (Genebank or NCBI)	Dilution	Hybridization Temperature (°C)	Reference
Lrrtm2	183-682	NM_178005.4	1:1,000	63.5	this study
	TATTAACTTATAATCAAAGCCGGTTTAGGGGATCAGAGCACAGGGAAAATGACACCAGTGCTTTCCAGAGGAATATCCTAAGGGAAAAAACAA TTCACCCTGATAGACTTGAATTTTACTTGAAAAGCCTGGGGCACAGAAAACAGGAAACTGGTCAAAGGCTCCTGCATGTTAGAGCCTTTTACA GACTCACTGCGTTGAGTCTGACAACCTCGACTGAATGCAGCCTCCAATGTGCTCAGAAGAATGGGCTTACATTTCAAGTGGCCATTAGGGGC CCCTATGCTGGCAGCAATATATGCAATGAGTGTGGTATTAAAAATGCTGCCTGCCCTGGGTATGGCGTGTCCACCTAAATGCCGCTGTGAGA AGCTGCTATTCTACTGCGACTCTCAGGGCTTCCACTCAGTGCCAAACGCCACAGACAAGGGTTCTTTGGGTCTGTCCCTGAGGCACAATCAC ATCACAGCGCTTGAAAGAGATCAATTTGCCAGCTTCAG				
Lrrtm3	1882-2281	NM_178678	1:1,000	63.5	this study
	CCGCGAGCATGAAGCAGCTGCAGCAGCGCTCCCTCATGCGAAGGCACCGGAAGAAGAAACGGCAATCGCTCAAGCAGATGACTCCAGGCA CCCAGGAATTTTATGTAGATTATAAACCCACCAACACGGAGACCAGCGAGATGCTGCTGAACGGAACGGGACCCTGCACCTATAGCAAATCA GGCTCCAGGGAATGTGAGATACCTTTATCAATGAATGTGTCAACCTTTCTGGCATATGACCAGCCCACAATAAGTTACTGTGGGGTCCATCAT GAACTCCTCTCCCATAAGTCCTTTGAAACGAATGCACAGGAAGACACGATGGAAAGCCACCTAGAGACTGAGCTGGACTTGAGCACAATCAC GTCAGCTGGCCGCATCAGTGACCATAAACCACA				
Lrrtm4	1608-2107	NM_001134743	1:1,000	63.5	this study
	CTCCGTGGCCATGATTCTCCTGGTGATCTATGTGTCTTGGAAACGGTACCCAGCCAGCATGAAACAACTCCAACAGCACTCACTTATGAAGA GGAGACGGAAAAAGGCGAGGGAGTCGGAGAGACAGATGAATTCCCCTTTACAGGAATACTACGTGGACTACAAACCGACGAACTCTGAGAC CATGGATATATCGGTTAATGGATCTGGTCCCTGCACATATACCATCTCTGGCTCCAGGGAGTGTGAGATACCCCACCATGTGAAGCCCCTGC CGTATTACAGCTATGACCAACCAGTGATTGGGTACTGCCAGGCCCACCAGCCTCTCCACATCAACAAGGCTTATGAAGCTGTGTCTATAGAA CAGGATGACAGCCCCAGTTTGGAGCTTGGGAGAGACCACAGCTTCATTGCCACCATAGCCAGGTCGGCTGCACCTGCCATTTATCTGGAGA GAATAACAAACTAACAGCGAAACTAACTTCTAGATGAAGAGC				
Adgrl1	2943-3392	NM_181039	1:1,000	63.5	this study
	TCCTGGAGGTAACTGTGCTGAACACGGAGGGCCAAGTGCAGGAGTTGGTGTTCCCCCAAGAGTATCCCAGTGAGAACTCCATTCAGCTCTC CGCCAACACCATCAAGCAGAACAGCCGCAACGGTGTGGTGAAAGTTGTCTTCATTCTCTACAACAACCTGGGCCTCTTCTTGTCCACGGAGA ATGCCACAGTGAAGCTGGCAGGTGAGGCAGGGACAGGTGGCCCTGGAGGTGCCTCCCTGGTGGTCAACTCACAGGTCATCGCAGCATCTA TCAATAAGGAGTCTAGCCGCGTCTTCCTCATGGACCCTGTCATCTTTACTGTAGCCCACTTGGAGGCCAAGAACCACTTCAATGCAAACTGCT CCTTCTGGAACTACTCAGAGCGCTCCATGCTGGGCTACTGGTCAACCCAGGGCTGCCGATTGGTGGAGTCCAATAAGACCCATA				
Adgrl2	1834-2233	NM_001081298	1:1,000	63.5	this study
	GCAATTGTGGACACGGTAGACAACCTTCTGAGAGCTGAGGCTTTGGAATCCTGGAAACACATGAATTCTTCAGAGCAGGCGCACACAGCCAC AATGTTGTTGGATACCTTGGAAGAAGGAGCATTCGTCCTAGCAGACAACCTTTTGGAACCAACCAGGGTCTCCATGCCAACAGAAAATATTGT TTTAGAAGTTGCTGTCCTCAGCACGGAAGGGCAGGTCCAAGACTTTAAATTCCCTCTGGGCTTAAAGGGGTTGGGCAGCTCCATCCAGCTCT CTGCCAACACGGTCAAACAGAACAGCAGGAATGGGCTGGCCAAGCTGGTATTCATCATTTACCGGAGCCTGGGACAATTCCTAAGCACTGA GAACGCAACCATAAAGCTGGGTGCAGACCTCA				

Molecule	Sequence	Accession # (Genebank or NCBI)	Dilution	Hybridization Temperature (°C)	Reference
Adgrl3	2410-2809	NM_001347367	1:1,000	63.5	this study
	CTGGATAGTAGATCAGGGCCGGTACATCATGGACAAGTCTCCTACATCTCTCCACCAATTCACCTCGACTCTGAACTAGAAAGGCCCCCTGT CAGAGGGATTTCTACCACAGGATCCCTGGGTATGGGAAGCACGACCACCAGCACCACCCTCCGGACCACAACCTGGAACATAGGCAGGAGT ACCACCGCATCCTTGCCGGGCAGAAGAAACCGCAGTACCAGCACGCCATCCCCCGCGGTAGAGGTGCTGGATGACGTCACCACACACCTG CCCTCGGCAGCCTCCCAAATCCCAGCTATGGAAGAGAGCTGCGAGGCTGTGGAAGCCCGAGAAATCATGTGGTTTAAGACCAGACAGGGG CAGGTAGCAAAGCAGCCATGCCCAGCAGGAACCATAG				

Image acquisition, analysis and quantification

Chromogenic images were acquired with a dissecting microscope (SZX16, Olympus) equipped with a CCD digital camera (INFINITY3-1UC, Lumenera) or a fluorescence microscope (BZ-X710, Keyence) with a 20x objective lens (NA 0.75). Images were analyzed with ImageJ software (SCR_003070). Briefly, images were converted to grayscale with the dark background. The mean *Nrxn* signal intensity in a given region was measured and normalized to the mean intensity in the pyramidal cell layer of the piriform cortex, which exhibited high signals for all isoforms (**Figures 2.2g-l and 2.3a-f**). The background noise was defined as the mean intensity outside the section and subtracted from each density before normalization. We scored >70% of the normalized intensity as strong (+++), 30-70% as moderate (++), 10-30% as weak (+), and <10% as very weak or not detected (-) (**Table 2.2**). FISH images were acquired with a fluorescence microscope (BZ-X710, Keyence) with a 20x objective lens (NA 0.75) or a confocal microscope (FV1200, Olympus) with a UPlanSapo 20x objective (NA 0.75). The images were captured with exposure times respective to each Nrxn isoform. On the confocal, the size of images was 800 x 800 or 1000 x 1000 pixels. For quantification, simultaneously stained sets of cells on the same slide were imaged using identical settings. Measurements were performed with one section from each brain by using ImageJ software. Briefly, background levels were determined with the signal intensity in DAPI-negative neuropil regions, and subtracted from each image. The same circular region of interest (ROI) was applied to cell bodies

containing DAPI+ nuclei with or without labeling for cell type-specific markers, and the mean signal intensity was measured.

The expression of *Nrxns* in glutamatergic and GABAergic neurons were examined with double FISH sections for glutamic acid decarboxylase 1 (*Gad1*), a marker of GABAergic neurons, and *Nrxn* mRNAs. In the somatosensory cortex, most DAPI+ nuclei were divided into two types: large and pale nuclei containing a few heavily stained puncta for DAPI, reflecting decondensed chromatin (arrowheads in **Figure 2.8a, b**), and small and dark nuclei (arrows in **Figure 2.8a, b**). The former DAPI+ nuclei were classified as neuronal nuclei, and the latter as non-neuronal nuclei (Yu et al., 2015). Most glutamatergic and GABAergic neurons, identified by type 1 vesicular glutamate transporter (*Vglut1*) and *Gad1* mRNA expression, respectively, displayed large and pale DAPI signals (*Vglut1*: 99.2% /total 249 *Vglut1*+ nuclei; *Gad1*: 98.8% /84). All cells with small and dark DAPI+ nuclei (n = 134 nuclei) did not express *Vglut1* or *Gad1*. Thus, *Gad1*(-) cells with large and pale DAPI+ nuclei were analyzed as glutamatergic neurons. Occasionally, cells with small and dark DAPI+ nuclei were found, but not used for quantitative analysis. In the hippocampus and cerebellar cortex, glutamatergic neurons were densely distributed in pyramidal or granule cell layers, and predominate over other types of cells. Thus, *Gad1*(-) cells in these cell layers were classified as glutamatergic neurons.

Statistical analyses

The data were obtained from two mice and pooled. Results are reported as means ± SEM. For comparison between two neuronal types, Mann-Whitney non-parametric test was performed. For multiple comparisons, Kruskal-Wallis non-parametric ANOVA followed by Dunn's post hoc test were performed using Prism 5 (Graph Pad Software). Statistical significance was set at $p < 0.05$.

Results

1. Overall expression in the brain and validation of ISH probes

Two non-overlapping antisense probes for the unique amino terminus and/or 5´-UTR region of each *Nrxn* isoform (total, 12 probes) were used to determine overall expression in the brain (**Figure 2.1**). Chromogenic *in situ* hybridization with sagittal brain sections showed distinct signal patterns for each isoform. Strong signals for *αNrxn1*, *αNrxn2*, and *βNrxn2* mRNAs were distributed in the olfactory bulb, neocortex, hippocampus, and cerebellum (**Figure 2.1a-d, i, j**). Expression of *βNrxn1* mRNA was high in the neocortex, hippocampus, and cerebellum (**Figure 2.1g, h**). High expression of *αNrxn3* mRNA was observed in the olfactory bulb, neocortex, hippocampus, and caudate-putamen (**Figure 2.1e, f**), while *βNrxn3* mRNA was enriched in the olfactory bulb and cerebellum (**Figure 2.1k, l**). In the thalamus and brainstem, all isoforms of *Nrxn* mRNAs were differentially expressed at low to moderate levels. Two cRNA probes for each isoform yielded somewhat different intensities, particularly for *αNrxn3* and *βNrxn1* labeling, but importantly,

exhibited the same spatial patterns of labeling. Furthermore, no signals were found with the sense cRNA probes (**Figure 2.1m-x**). These results indicate the specificity of cRNA probes and hybridizing signals with use of them.

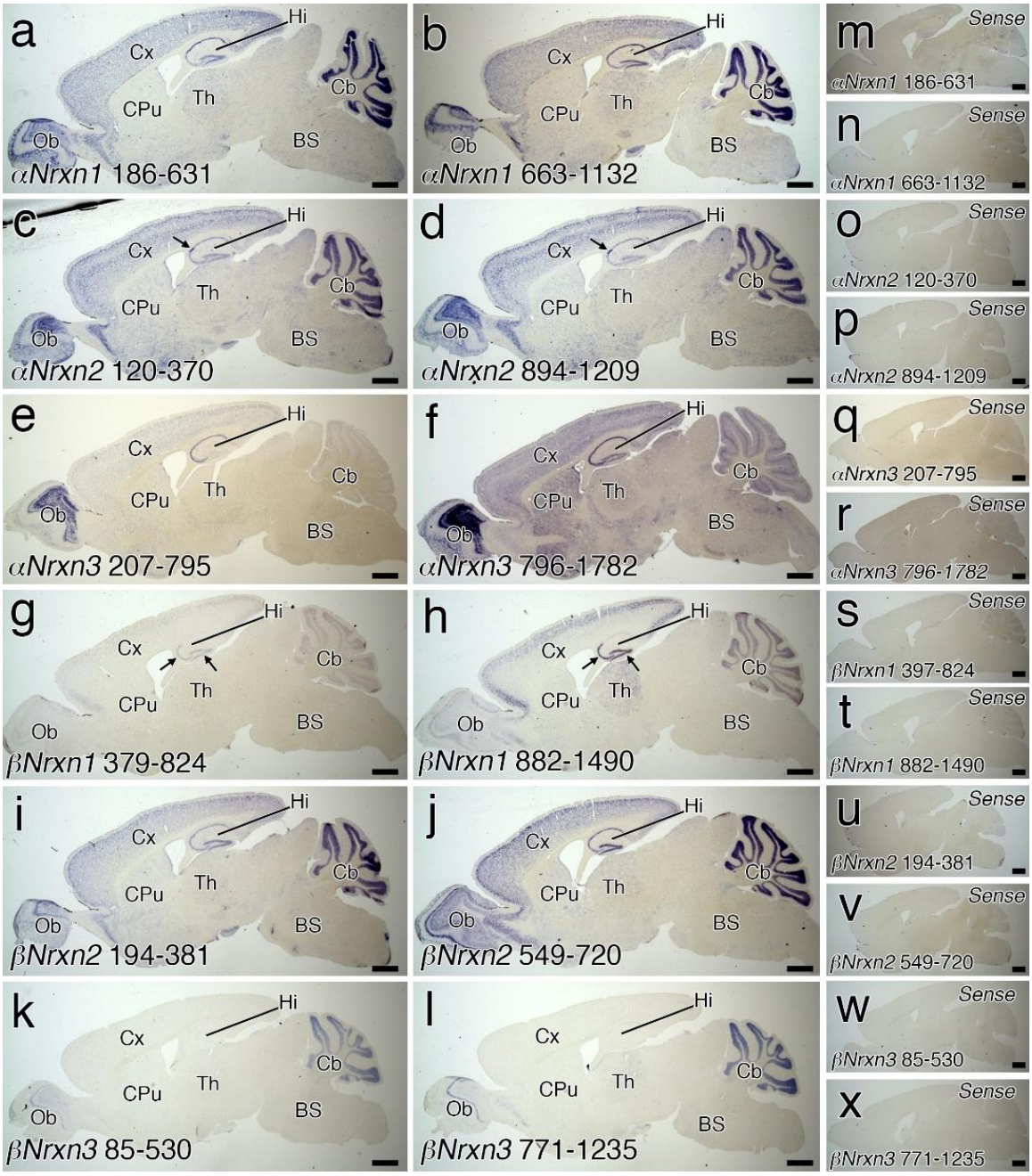

Figure 2.1 | **Validation of Nrxn ISH probes in the brain.** (a-l) Whole brain sagittal views of chromogenic hybridization signals with Nrxn-isoform-specific antisense cRNA probes. Two cRNA probes are prepared for *αNrxn1* (a, b), *αNrxn2* (c, d), *αNrxn3* (e, f), *βNrxn1* (g, h), *βNrxn2* (i, j), and *βNrxn3* (k, l) mRNAs. Arrows indicate dense staining patterns in the CA2 for *αNrxn2* mRNA (c, d) and in the CA3 and dentate gyrus for *βNrxn1* mRNA (g, h). (m-x) Whole brain sagittal views of chromogenic hybridization signals with two sense cRNA probes lacking signal for *αNrxn1* (m, n), *αNrxn2* (o, p), *αNrxn3* (q, r), *βNrxn1* (s, t), *βNrxn2* (u, v), and *βNrxn3* (w, x) mRNAs. For abbreviations, see list. Scale bars, 1 mm.

2. Region-specific expression of Nrxn isoforms

To map the expression of each *Nrxn* isoform in the brain, we used coronal sections of mouse brains at the age of one month. In the following analysis, two non-overlapping cRNA probes were used in mixture to increase the intensity of hybridizing signals. The expression levels of each *Nrxn* isoform were assessed based on signal intensity (**Table 2.2**).

Table 2.2 | Expression levels of six isoforms of Nrxn mRNAs in individual regions

Region	*Nrxn* mRNA expression *αNrxn1*	*αNrxn2*	*αNrxn3*	*βNrxn1*	*βNrxn2*	*βNrxn3*	Figures
Telencephalon							
Olfactory bulb (Ob)							
Glomerular layer (Gl)	+++	+	+++	+	++	+	2.2
Mitral cell layer (Mi)	+++	++	+++	++	+++	+++	2.2
Granule cell layer (GrO)	+++	++	+++	+	++	++	2.2
Neocortex (Primary somatosensory cortex: S1)							
Layer 1	+	+	+	–	–	+/–	2.3, 2.8, 2.9
Layers 2/3	++	++	++	++	++	+	2.3, 2.8, 2.9
Layer 4	++	+	+	++	+	++	2.3, 2.8, 2.9
Layer 5	++	++	++	++	+	+	2.3, 2.8, 2.9
Layer 6	++	+	++	+	+	+	2.3, 2.8, 2.9
Neocortex (primary motor cortex: M1)							
Layer 1	+	+	+	–	–	–	2.2
Layers 2/3	++	++	++	++	++	+[a]	2.2
Layer 5	++	++	++	+	+	+	2.2
Layer 6	++	+	++	+	+	+	2.2
Neocortex (Primary auditory cortex: A1)							
Layer 1	+	+	+	+	–	–	2.3, 2.4
Layers 2/3	++	++	++	++	++	++	2.3, 2.4
Layer 4	++	+	++	++	+	++	2.3, 2.4
Layer 5	++	++	++	+	+	+	2.3, 2.4
Layer 6	++	+	++	+	+	+	2.3, 2.4
Retrosplenial granular cortex (RSG)	++	++	++	++	+	+	2.3, 2.4
Piriform cortex (Pir)	+++	+++	+++	+++	+++	+++	2.2, 2.3

Lateral entorhinal cortex (LEnt)	++	++	++	++	++	++	2.4, 2.5
Medial entorhinal cortex (MEnt)	++	++	+	++	++	+	2.5
Olfactory tubercule (OT)	+	+	+++	+	+	++	2.2
Hippocampus							
CA1	+++	++	+++	+	+++	++	2.3, 2.4, 2.10, 2.11
CA2	+++	+++	+++	+++	+++	++	2.3, 2.4, 2.10, 2.11
CA3	+++	++	+++	+++	+++	++	2.3, 2.4, 2.10, 2.11
Subiculum (Su)	++	++	++	+	+	+	2.4
Dentate gyrus (DG)	+++	++	++	+++	+++	+	2.3, 2.4, 2.10, 2.11
Caudate-putamen (CPu)	+	+	+++	+	+	++	2.2
Nucleus accumbens (NAc)	+	+	+++	+	+	++	2.2
Island of Calleja (ICj)	++	+++	+++	+++	+	+++	2.2
Lateral septal nucleus (LS)	+	++	++	+	+	+	2.2
Nucleus of the diagonal band (NBD)	++	++	++	+	+	+	2.2
Amygdala							
Lateral nucleus (LA)	++	++	++	++	++	+	2.3
Basal nucleus (BA)	++	++	++	+	++	+	2.3
Central nucleus (CA)	++	++	++	+	++	++	2.3
Claustrum (CI)	++	+	+++	++	++	+	2.3
Diencephalon							
Epithalamus							
Lateral habenular nucleus (LHb)	++	+	+	–	+	+	2.3
Medial habenular nucleus (MHb)	+++	+++	+[a]	–	++	–	2.3
Thalamus							
Ventral posteromedial nucleus (VPM)	++	+	+	+	+	++	2.3
Ventral posterolateral nucleus (VPL)	++	+	+	+	+	++	2.3
Lateral dorsal nucleus (LD)	++	+	+	++	+	++	2.3
Lateral posterior nucleus (LP)	++	+	+	++	+	++	2.3

Mediodorsal nucleus (MD)	++	+	+	++	+	++	2.3
Centromedian nucleus (CM)	++	+	+	++	+	++	2.3
Paraventricular nucleus (PVT)	++	++	+	+	++	+	2.3
Medial geniculate nucleus (MGN)	++	+	+	++	+	++	2.4
Reticular thalamic nucleus (Rt)	+	+	++	–	+	+	2.3
Subthalamic nucleus (STN)	++	+	+	–	+	+	2.3
Hypothalamus							
Lateral area (LH)	++	++	+	–	+	+	2.3
Dorsomedial nucleus (DMH)	+++	+++	++	–	++	++	2.3
Ventromedial nucleus (VMH)	++	+++	+	–	+	+	2.3
Arcuate nucleus (Arc)	+++	++	+++	+	++	+	2.3
Midbrain							
Superior colliculus (SC)	++	++	+[a]	–	+	+[a]	2.4, 2.5
Inferior colliculus (IC)	++	+	+[a]	+	++	+[a]	2.5, 2.6
Parabigeminal nucleus (PBG)	++	++	+	+	+	+	2.5
Periaqueductal gray (PAG)	++	+	+	+	+	–	2.4, 2.5
Nucleus of Darkschewitsch (ND)	+	++	+++	–	+	+	2.4
Edinger-Westphal nucleus (EW)	+	++	+	–	+	+	2.4
Dorsal raphe nucleus							
Dorsal part (DRD)	++	++	+	–	++	+	2.5
Ventral part (DRV)	++	++	+	–	++	+	2.5
Lateral part (DRL)	++	++	++	–	+	+	2.5
Substantia nigra parts reticulata (SNr)	+	+	+	–	+	+	2.4
Substantia nigra parts compacta (SNc)	+	++	++	–	+	+	2.4, 2.14, 2.15
Ventral tegmental area (VTA)	++	++	++	–	+	+	2.4
Interpeduncular nucleus (IPN)	++	++	++	+	+	+	2.4
Pons							
Dorsal nucleus of lateral lemniscus (DLL)	+	+	++[a]	–	–	+	2.5

Nucleus of trapezoid body (NTB)	+	–	++[a]	–	–	–	2.5
Paraolivary region of superior olivary complex (SOP)	+	–	+[a]	–	–	+	2.5
Pontine reticular nucleus (PRN)	+	–	+[a]	–	–	+[a]	2.5
Laterodorsal tegmental nucleus (LDTg)	++	++	++	–	+	+	2.6
Locus coeruleus (LC)	+	++	+	–	++	+	2.6, 2.14, 2.15
Lateral parabrachial nucleus (LPB)	++	+	+	–	+	+[a]	2.6
Medial parabrachial nucleus (MPB)	+	+	+	–	+	+	2.6
Ventral cochlear nucleus (VC)	+	–	+[a]	–	+	+[a]	2.6
Facial nucleus (VII)	+	++	–	–	+	–	2.6
Principal sensory nucleus of trigeminal nerve (PrV)	+	–	+[a]	–	+	+[a]	2.6
Medulla							
Gigantocellular reticular nucleus (GRN)	+	+	++[a]	–	–	+[a]	2.6
Spinal nucleus of trigeminal nerve (SpV)	+	+	+	+	+	+	2.7
Nucleus of the tractus solitarius (NTS)	++	++	++	+	++	++	2.7, 2.14, 2.15
Dorsal motor nucleus of vagus nerve (DMX)	++	++	++	+	++	+	2.7
Hypoglossal nucleus (XII)	+	++	+	–	++	+	2.7
Inferior olivary complex (IO)	+	+	–	+	++	–	2.7
Medullary reticular nucleus (MRN)	+	+	+[a]	–	+	+	2.7
Lateral reticular nucleus (LRN)	+	+	+	–	+	+	2.7
Cerebellum							
Purkinje cell layer (PCL)	+	++	+++	+	++	+	2.6, 2.7, 2.12, 2.13
Granule cell layer (GrC)	+++	++	+[a]	+++	+++	+++	2.6, 2.7, 2.12, 2.13
Molecular layer (ML)	+	+	+[a]	–	–	–	2.6, 2.7, 2.12, 2.13

+++, strong; ++, moderate; +, weak; –, very weak or not detected. See Materials and Methods for the criteria to determine the expression levels of *Nrxn* isoforms in individual regions.

[a] Regions including sparse cells highly expressing *Nrxn* isoforms.

2.1. Telencephalon

2.1.1 Olfactory bulb

All six *Nrxn* isoforms were detected in the olfactory bulb (**Figure 2.2a-f**), consistent with a previous study (Ullrich et al., 1995). *αNrxn1* and *αNrxn3* mRNAs were highly expressed in each neuronal layer, i.e., the glomerular, mitral cell, and granule cell layers, while *αNrxn2* mRNA was more enriched in the mitral and granule cell layers than in the glomerular layer. All three *βNrxn* mRNAs were, though generally low compared with *αNrxn*s, dominantly expressed in the mitral cell layer.

2.1.2 Neocortex

In the neocortex, distinct laminar patterns were observed (**Figures 2.2g-l, 2.3, and 2.4**), as previously described in rat brains (Ullrich et al., 1995). Among six isoforms, *αNrxn1* mRNA was expressed uniformly in cortical layers 2-6 (**Figures 2.2g, 2.3a, and 2.4a**), while others varied among cortical layers. *αNrxn2* mRNA peaked in layers 2/3 and 5 (**Figures 2.2h and 2.3b**), *αNrxn3* mRNA peaked in layers 5 and 6 (**Figures 2.2i, 2.3c, and 2.4c**), and *βNrxn1* and *βNrxn2* mRNAs were dominantly expressed in layers 2/3 and 4 (**Figures 2.2j, k, 2.3d, e, and 2.4d, e**). Layers with the highest level of *βNrxn3* mRNA varied in different neocortical areas: layers 2/3 in the primary motor (**Figure 2.2l**), layer 4 in the primary somatosensory (**Figure 2.3f**), and layers 2/3 and 4 in the primary auditory cortex (**Figures 2.3f and 2.4f**).

High expression of all six isoforms was found in the pyramidal cell layer of the piriform cortex (**Figures 2.2g-l and 2.3a-f**). Similarly, all six isoforms were

highly expressed in the upper layers of the lateral entorhinal cortex at rostral levels (**Figure 2.4a-f**). At more caudal levels, *αNrxn3* and *βNrxn3* mRNA signal intensities were lower in the lateral and medial entorhinal cortex (**Figure 2.5c, f**), whereas expression levels were maintained there for other isoforms (**Figure 2.5a, b, d, e**). This suggests a rostrocaudal gradient of *αNrxn3* and *βNrxn3* expression within the entorhinal cortex.

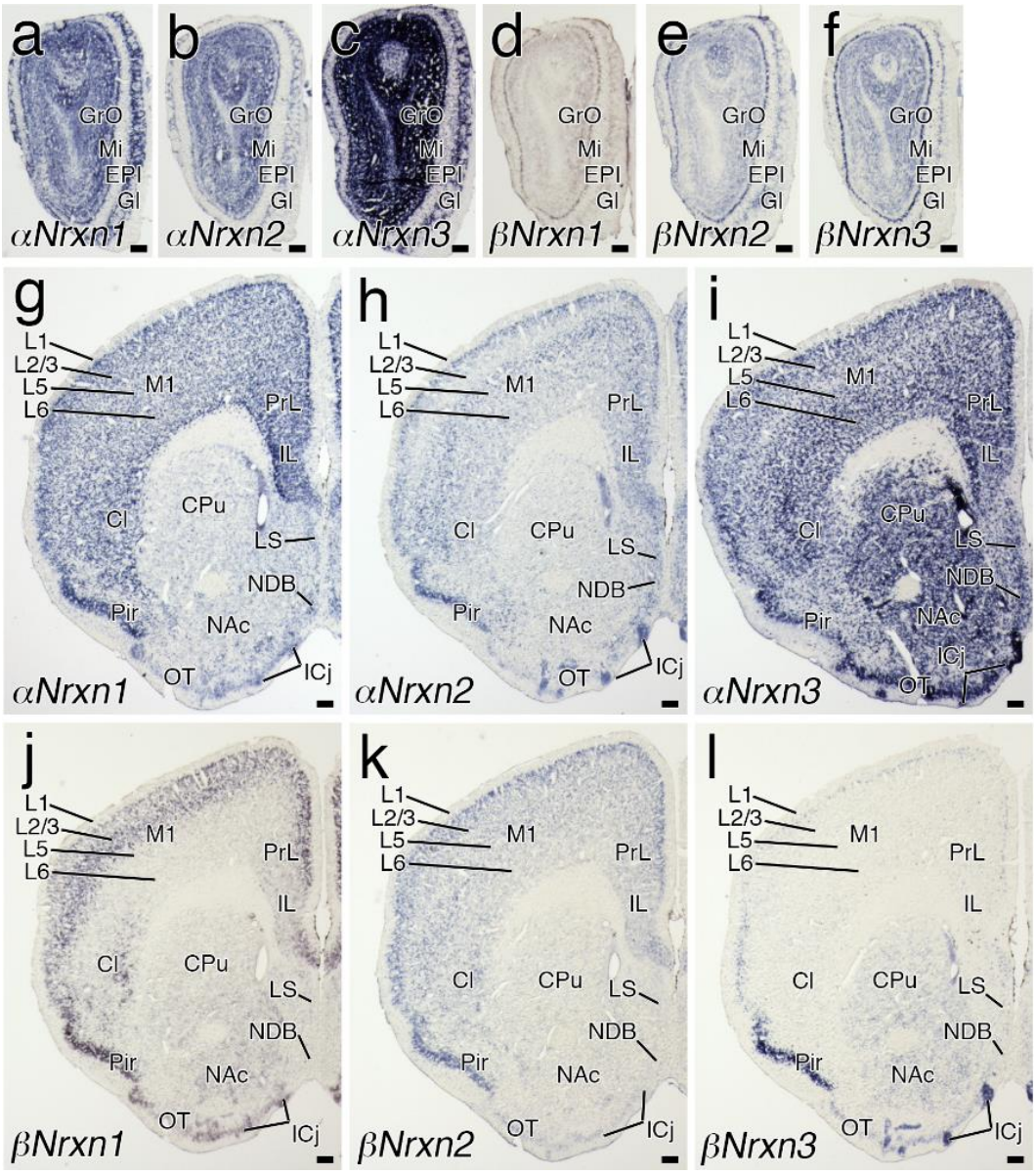

Figure 2.2 | **Region-specific expression of *Nrxn* mRNAs in the telencephalon and diencephalon.** Coronal views of chromogenic hybridization signals for *αNrxn1* (a, g), *αNrxn2* (b, h), *αNrxn3* (c, i), *βNrxn1* (d, j), *βNrxn2* (e, k), and *βNrxn3* (f, l) mRNAs in the mouse brain. For abbreviations, see list. Scale bars, 200 μm.

2.1.3 Hippocampus

The hippocampal formation, including the Ammon's horn (CA1-CA3), subiculum, and dentate gyrus, was one of the regions with the highest signals for each isoform

in the brain (**Figures 2.3a-f and 2.4a-f**). Consistent with previous studies (Nguyen et al., 2016; Ullrich et al., 1995), expression patterns in neuronal cell layers varied by *Nrxn* isoforms and hippocampal subregion. *αNrxn1* and *βNrxn2* mRNAs were uniformly expressed across different subregions (**Figures 2.3a, e and 2.4a**, **e**). In contrast, *αNrxn2* mRNA expression peaked in the CA2 (**Figure 2.3b**), *αNrxn3* mRNA in the CA1-CA3 (**Figures 2.3c and 2.4c**), and *βNrxn1* mRNA in the CA3 and dentate gyrus (**Figures 2.3d and 2.4d**). The expression pattern of *βNrxn3* mRNA was unique, in that it was hardly detected in the rostral portion of the dentate gyrus (**Figure 2.3f**), but expressed in more caudal portions of the dentate gyrus, particularly its ventral part (**Figure 2.4f**), suggesting a septotemporal gradient of *βNrxn3* expression within the dentate gyrus. In neuropil layers, some scattered cells were labeled for *αNrxn1-3* and *βNrxn3* mRNAs, suggesting their expression in interneurons (arrows in **Figure 2.4a-c, f**).

2.1.4 Cerebral nuclei

In the caudate-putamen and nucleus accumbens, *αNrxn3* mRNA was predominantly expressed (**Figure 2.2i**). The island of Calleja showed intense signals for *αNrxn2*, *αNrxn3*, *βNrxn1*, and *βNrxn3* mRNAs (**Figure 2.2h-j, l**). In the lateral septal nucleus and nucleus of the diagonal band, three *αNrxn* isoforms were discernible, but *βNrxn* isoforms were at low or undetectable levels (**Figure 2.2g-l**). In the amygdala, *αNrxn1*, *αNrxn2*, *αNrxn3*, and *βNrxn2* mRNAs were uniformly expressed in three subnuclei, the lateral, basal and central nuclei, while *βNrxn2*

and *βNrxn3* mRNAs were more enriched in the lateral or central nucleus, respectively (**Figure 2.3a-f**).

2.2. Diencephalon

In the medial habenular nucleus, high to moderate expression was noted for *αNrxn1*, *αNrxn2*, and *βNrxn2* mRNAs, and *αNrxn3* mRNA expression was confined to its dorsomedial portion (**Figure 2.3a-c, e**). Expression levels were generally low in the lateral habenular nucleus, with relatively higher levels for *αNrxn1* mRNA (**Figure 2.3a**). In the thalamus, *αNrxn1*, *βNrxn1*, and *βNrxn3* mRNAs were expressed widely and highly, as exemplified by ventral posteromedial and posterolateral nuclei, mediodorsal nucleus, and medial geniculate nucleus (**Figures 2.3a-f and 2.4a-f**). In the subthalamic nucleus and reticular thalamic nucleus, *αNrxn1* or *αNrxn3* mRNA, respectively, was a predominant isoform (**Figure 2.3a, c**). In the hypothalamus, three *αNrxn* isoforms were predominantly expressed, with some different intensities among the lateral, dorsomedial, ventromedial, and arcuate nuclei (**Figure 2.3a-f**). A moderate expression level was also found for *βNrxn2* mRNA in the arcuate nucleus (**Figure 2.3e**).

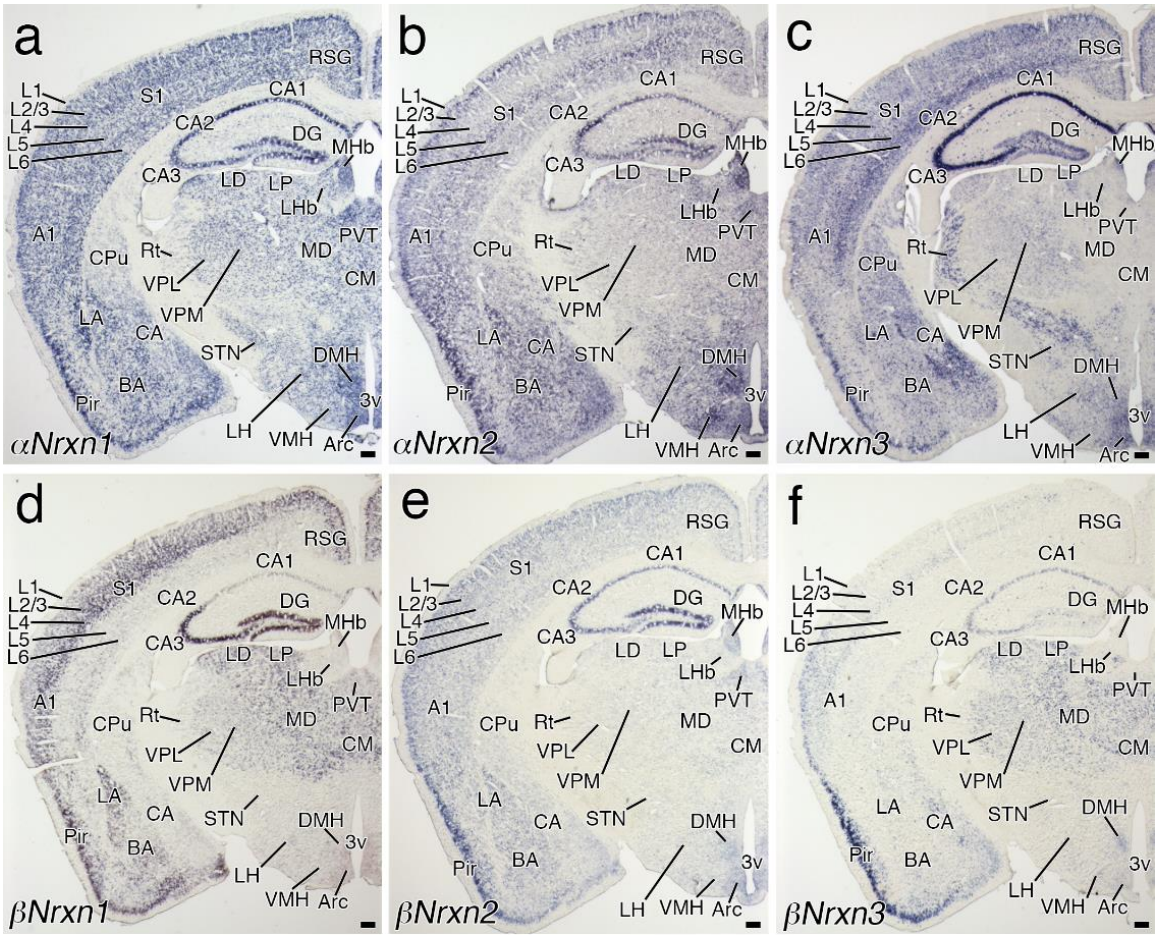

Figure 2.3 | Region-specific expression of *Nrxn* mRNAs in the telencephalon and diencephalon. Coronal views of chromogenic hybridization signals for *αNrxn1* (a), *αNrxn2* (b), *αNrxn3* (c), *βNrxn1* (d), *βNrxn2* (e), and *βNrxn3* (f) mRNAs in the mouse brain. For abbreviations, see list. Scale bars, 200 μm.

2.3. Midbrain

Three *αNrxn* isoforms were widely and predominantly expressed in the midbrain, showing heterogeneous regional patterns (**Figures 2.4a-c, 2.5a-c, and 2.6a-c**). *αNrxn2* mRNA was predominant in the Edinger-Westphal nucleus (**Figure 2.4b**) and the dorsal raphe nucleus (**Figure 2.5b**), while *αNrxn3* mRNA was predominant in the substantia nigra pars compacta, ventral tegmental area, Nucleus of

Darkschewitsch, and lateral part of the dorsal raphe nucleus (**Figures 2.4c and 2.5c**). Sparse cells within the inferior colliculus expressed *αNrxn3* mRNA at high levels (**Figure 2.6c**). Expression levels of three *βNrxn* isoforms were generally low or undetectable in the midbrain (**Figures 2.4d-f, 2.5d-f, and 2.6d-f**), but *βNrxn3* mRNA was detected in some sparse cells in the inferior colliculus (**Figure 2.6f**) and other midbrain regions.

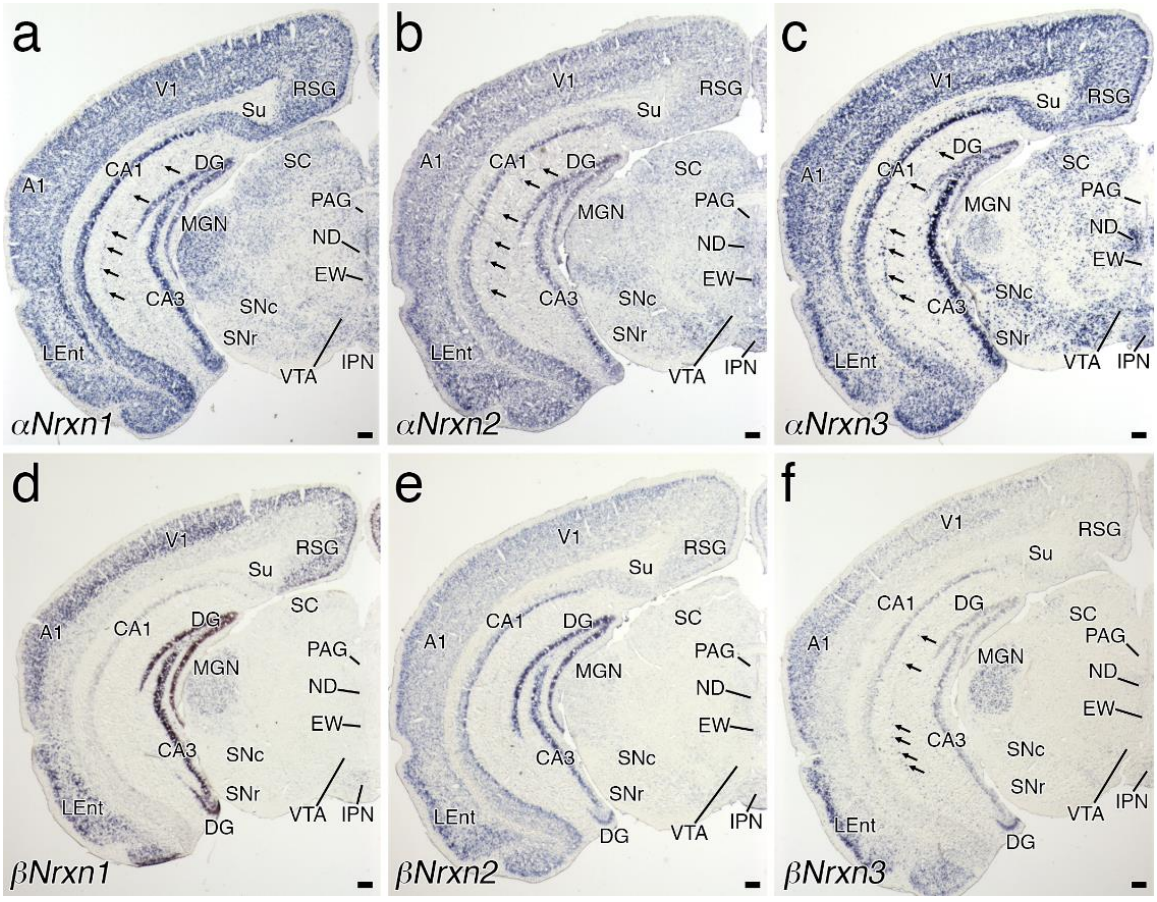

Figure 2.4 | Region-specific expression of *Nrxn* mRNAs in the midbrain. Coronal views of chromogenic hybridization signals for *αNrxn1* (a), *αNrxn2* (b), *αNrxn3* (c), *βNrxn1* (d), *βNrxn2* (e), and *βNrxn3* (f) mRNAs in the mouse brain. Arrows indicate cells expressing *αNrxn1* (a), *αNrxn2* (b), *αNrxn3* (c), and *βNrxn3* (f) mRNAs in the neuropil layer of the hippocampus. For abbreviations, see list. Scale bars, 200 µm.

2.4. Pons

In the pons, *αNrxn3* mRNA was predominant in many nuclei (**Figures 2.5c and 2.6c**), with the strongest signals in the nucleus of the trapezoid body (**Figure 2.5c**) and the lowest signals in the facial nucleus (**Figure 2.6c**). *αNrxn1* and *αNrxn2* mRNAs were expressed at low to moderate levels in the pontine tegmentum, including the lateral and medial parabrachial nuclei, locus coeruleus (LC), and laterodorsal tegmental nucleus (**Figure 2.6a, b**). In addition, *αNrxn2* mRNA expression was moderately expressed in the facial nucleus (**Figure 2.6b**). Three *βNrxn* mRNAs were generally low in the pons, except for moderate expression of *βNrxn2* mRNA in the LC (**Figure 2.6e**) and *βNrxn3* mRNA in the dorsal part of the lateral parabrachial nucleus (**Figure 2.6f**). Cells expressing *βNrxn3* mRNA were scattered over the pons, such as in the ventral cochlear nucleus and principal sensory nucleus of trigeminal nerve (**Figure 2.6f**).

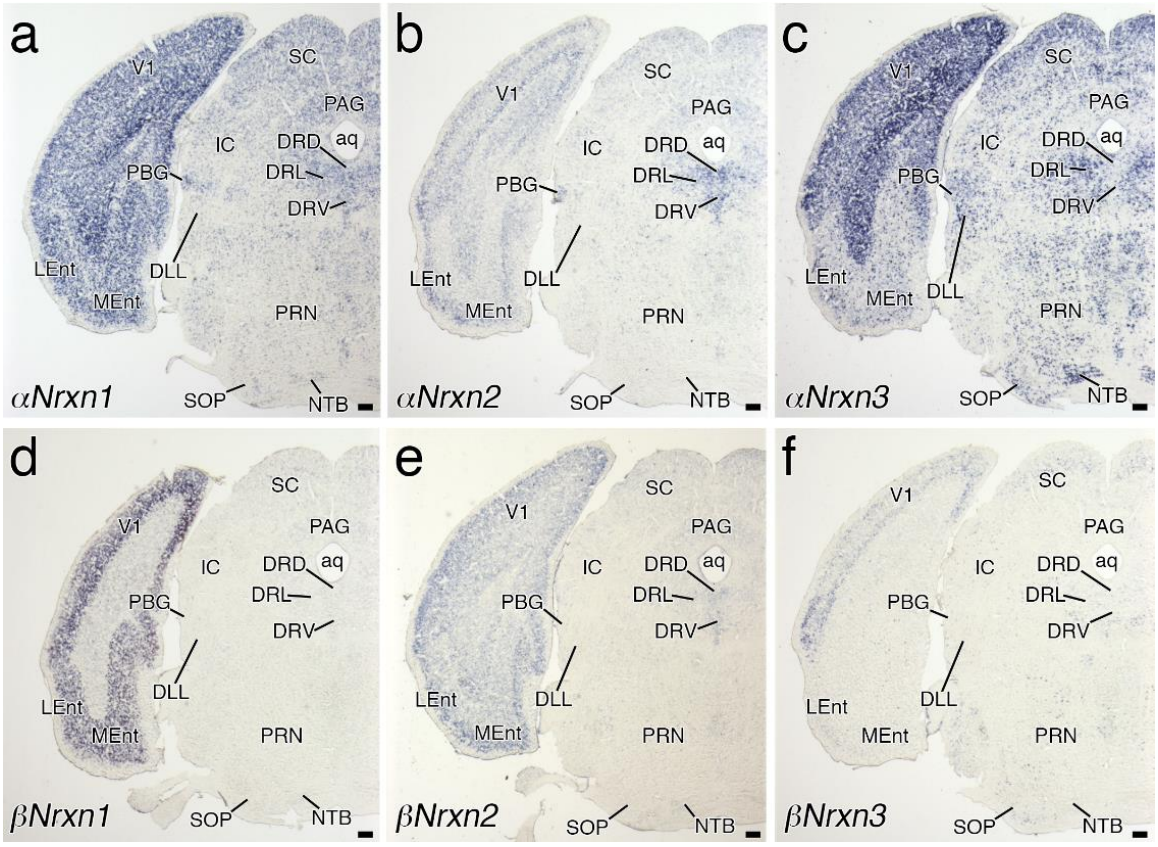

Figure 2.5 | **Region-specific expression of *Nrxn* mRNAs in the pons.** Coronal views of chromogenic hybridization signals for *αNrxn1* (a), *αNrxn2* (b), *αNrxn3* (c), *βNrxn1* (d), *βNrxn2* (e), and *βNrxn3* (f) mRNAs in the mouse brain. For abbreviations, see list. Scale bars, 200 µm.

2.5. Medulla

Like in the pons, *αNrxn3* mRNA was most prevalent in the medulla (**Figures 2.6c and 2.7c**). However, *αNrxn3* mRNA was not detected in the inferior olivary complex, where *αNrxn1*, *αNrxn2*, *βNrxn1*, and *βNrxn2* mRNAs were weakly expressed (**Figure 2.7a, b, d, e**). The nucleus of the tractus solitarius (NTS) and dorsal motor nucleus of vagus nerve expressed high levels of all three *αNrxn* isoforms and low to moderate levels of all three *βNrxn* isoforms (**Figure 2.7a-f**).

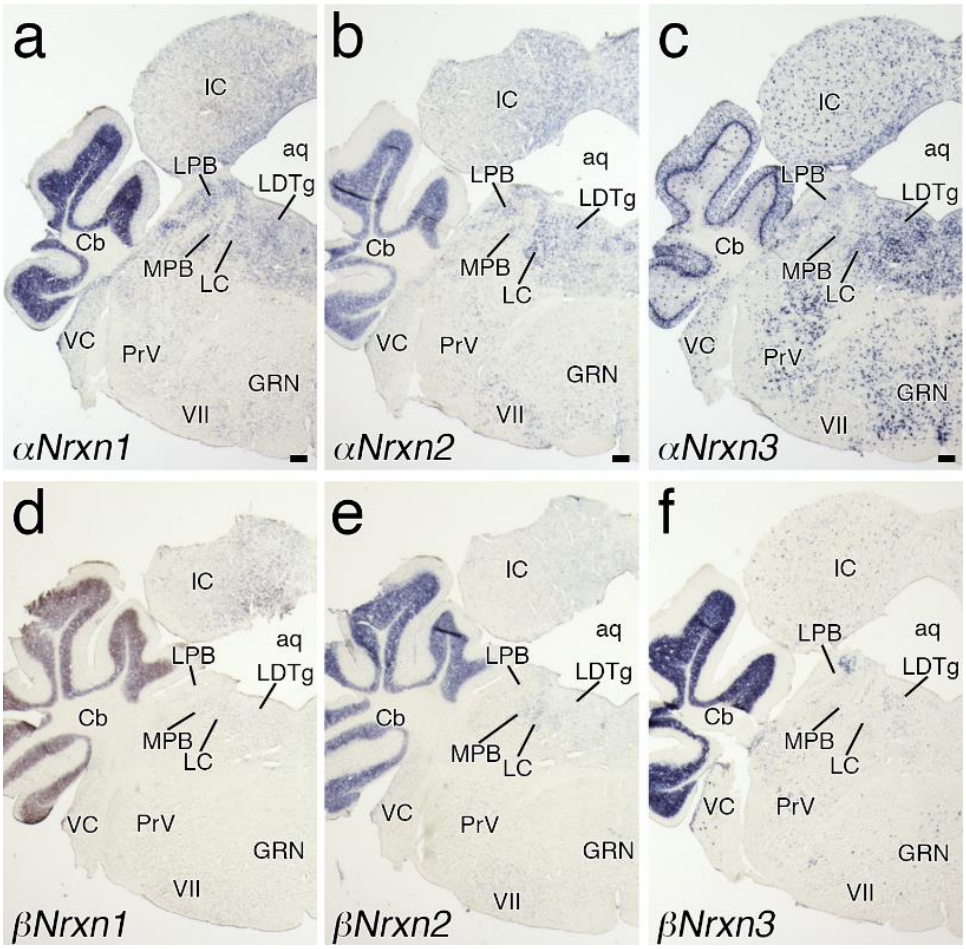

Figure 2.6 | Region-specific expression of *Nrxn* mRNAs in the anterior medulla. Coronal views of chromogenic hybridization signals for *αNrxn1* (a), *αNrxn2* (b), *αNrxn3* (c), *βNrxn1* (d), *βNrxn2* (e), and *βNrxn3* (f) mRNAs in the mouse brain. For abbreviations, see list. Scale bars, 200 µm.

2.6. Cerebellum

In the cerebellar cortex, all six *Nrxn* isoforms were highly expressed in the granule cell layer, where *αNrxn3* mRNA was restricted to a few scattered cells and the rest were expressed diffusely (**Figures 2.6 and 2.7**). In the molecular layer, *αNrxn3* mRNA was expressed predominantly in scattered cells (**Figures 2.6c and 2.7c**).

Various isoforms were less expressed in the Purkinje cell layer, with the highest level for *αNrxn3* mRNA.

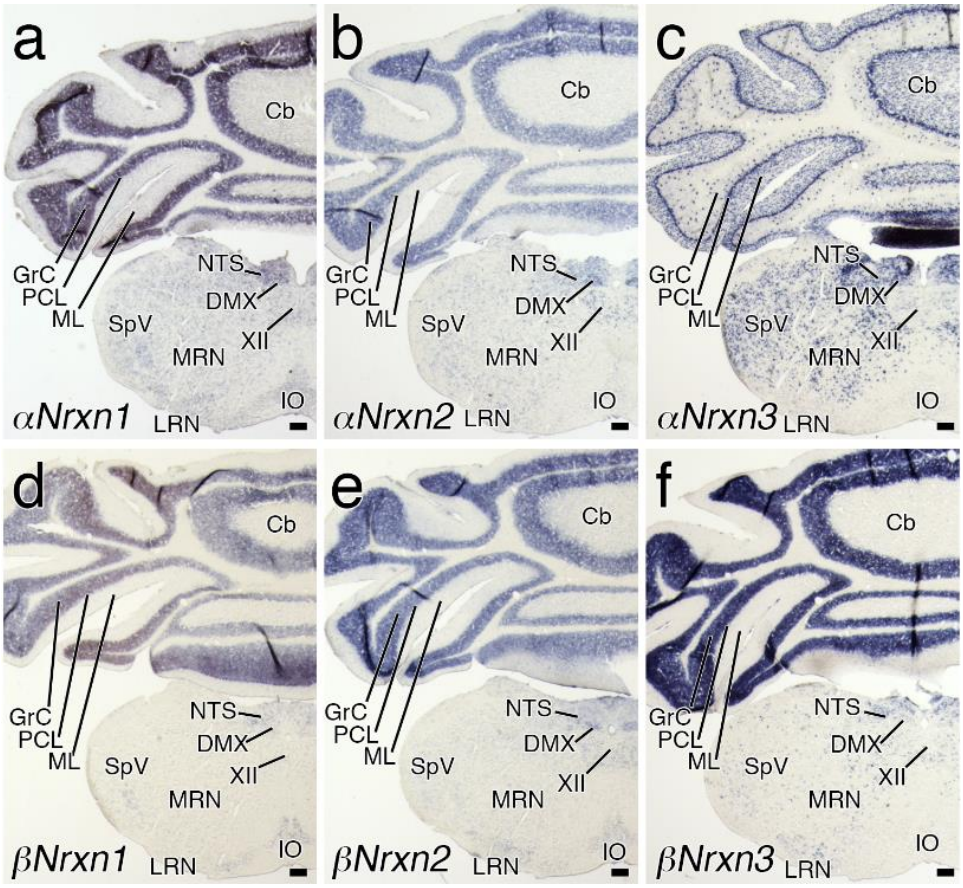

Figure 2.7 | Region-specific expression of *Nrxn* mRNAs in the posterior medulla. Coronal views of chromogenic hybridization signals for *αNrxn1* (a), *αNrxn2* (b), *αNrxn3* (c), *βNrxn1* (d), *βNrxn2* (e), and *βNrxn3* (f) mRNAs in the mouse brain. For abbreviations, see list. Scale bars, 200 μm.

3. Cell type-specific expression of Nrxn isoforms

To address the type of cells expressing each *Nrxn* isoform, we employed double FISH for *Nrxns* and cellular markers, and measured the fluorescent intensity of each *Nrxn* isoform in given types of cells.

3.1. Glutamatergic and GABAergic neurons

Using *Gad1* mRNA as a neuronal marker of GABAergic neurons, we measured the signal intensity of *Gad1*(+) GABAergic and *Gad1*(-) glutamatergic neurons in the primary somatosensory cortex (**Figures 2.8 and 2.9**), hippocampus (**Figures 2.10 and 2.11**), and cerebellar cortex (**Figures 2.12 and 2.13**). Indeed, in the primary somatosensory cortex, cells that had large and DAPI-pale nuclei expressed either *Vglut1*, which is selectively expressed in cortical glutamatergic neurons (arrowheads in **Figure 2.8a**), or *Gad1* (arrowheads in **Figure 2.8b**) mRNA, thus being assigned as glutamatergic and GABAergic neurons, respectively. Cells having small and DAPI-dark nuclei without *Vglut1* or *Gad1* mRNA are likely glial cells (arrows in **Figure 2.8a, b**; See **Materials and Methods**) (Yu et al., 2015). The mean intensity in each neuronal layer of the primary somatosensory cortex was calculated for glutamatergic and GABAergic neurons (**Figures 2.8c-h and 2.9a-f**). The mean fluorescent intensity in glutamatergic neurons (blue dots in **Figures 2.8d, f, h and 2.9b, d, f**) was comparable to optical intensity by chromogenic *in situ* hybridization (**Figure 2.3a-f**). Compared to glutamatergic neurons, *Nrxn* expression in GABAergic neurons exhibited different laminar patterns (red dots in **Figures 2.8d, f, h and 2.9b, d, f**). Significantly higher levels in GABAergic neurons than in glutamatergic neurons in the same layer were noted for *αNrxn2* mRNA in layers 4 and 6 (**Figure 2.8e, f**), *αNrxn3* mRNA in layers 4-6 (**Figure 2.8g, h**), *βNrxn1* mRNA in layer 6 (**Figure 2.9a, b**), *βNrxn2* mRNA in layers 4 and 6 (**Figure 2.9c, d**), and *βNrxn3* mRNA in layers 2/3, 5, and 6 (**Figure 2.9e,**

f). Conversely, significantly lower levels were noted for *Nrxn1* mRNA in layers 4 and 5 (**Figure 2.8c, d**) and *βNrxn1* mRNA in layers 2-4 (**Figure 2.9a, b**).

In the dorsal hippocampus, the pattern of mean *Nrxn* fluorescent intensity in *Gad1*(-) glutamatergic neurons among different subregions (**Figures 2.10 and 2.11**) was generally comparable to that of chromogenic signals (**Figure 2.3a-f**). In the CA1-CA3 subregions, GABAergic neurons tended to be significantly lower in *Nrxn* mRNA expression than glutamatergic neurons. In the dentate gyrus, by contrast, GABAergic neurons expressed significantly higher levels for all three *αNrxn* and *βNrxn3* mRNAs (**Figure 2.11a, b**).

In the cerebellar cortex, distinct neuron type-dependent expression, as suggested from distinct layer labeling and sparse vs. diffuse labeling (**Figures 2.6 and 2.7**), was substantiated by double FISH (**Figures 2.12 and 2.13**). GABAergic interneurons in the molecular layer mainly expressed *αNrxn3* mRNA, with additional very low signals for *αNrxn1*, *αNrxn2*, *βNrxn1*, and *βNrxn2* mRNAs. GABAergic Purkinje cells expressed *αNrxn3* mRNA at the highest level, and more or less expressed the other isoforms. On the other hand, all six *Nrxn* isoforms were highly expressed in GABAergic Golgi cells. Granule cells highly expressed all six *Nrxn* isoforms except for *αNrxn3* mRNA.

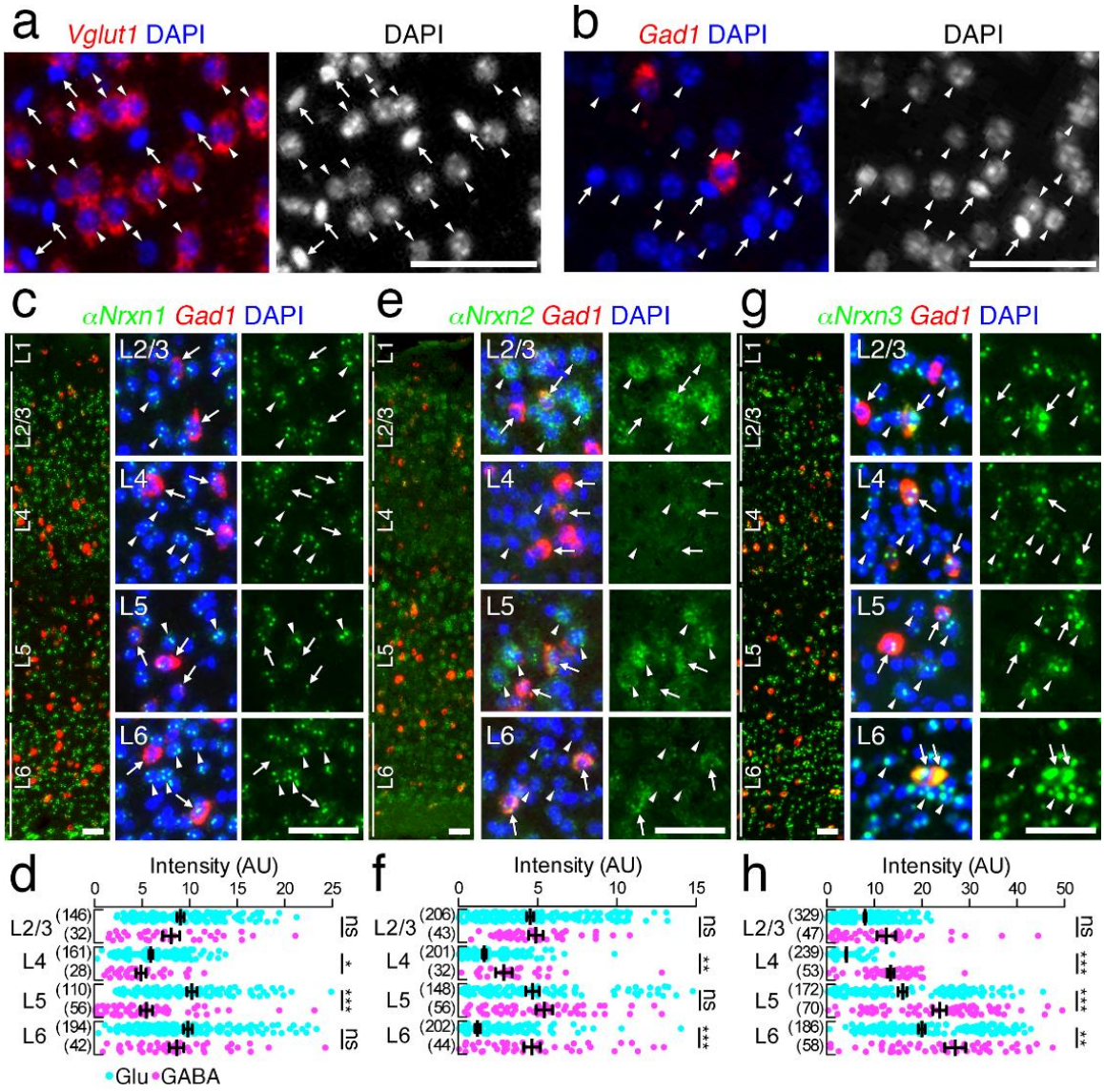

Figure 2.8 | Layer-specific expression of *αNrxn* mRNAs in the primary somatosensory neocortex. (a, b) Single FISH for *Vglut1* (red, a) and *Gad1* (red, b) mRNAs with DAPI staining (blue and gray on the left and right, respectively). Note that *Vglut1* (a) or *Gad1* (b) mRNA-expressing neurons have large and pale DAPI+ nuclei (arrowheads), but not small and dark DAPI+ nuclei (arrows). (c, e, g) Double FISH for *αNrxn1* (c), *αNrxn2* (e), *αNrxn3* (g) and *Gad1* mRNAs showing distinct laminar-specific patterns of *Nrxn* mRNAs (green) between *Gad1*(+) GABAergic (red, arrows) and *Gad1*(-) glutamatergic (arrowheads) neurons. The left panel presents a low power-magnified image including the entire cortical layers, and the middle and right panels present high power-magnified images of layers 2/3, 4, 5, and 6 (L2/3, L4, L5, and L6) in order from the top. Note that the signals for *Nrxns* in GABAergic neurons tend to be variable. Nuclei were stained with DAPI (blue). (d, f, h) Summary scatter plots for *αNrxn1* (d), *αNrxn2* (f), or *αNrxn3* (h) mRNA in glutamatergic (aqua) and GABAergic (magenta) neurons. The

numbers of cells analyzed are indicated in the parenthesis to the left of each column. Data are represented as means ± SEM. ns, not significant; * P < 0.05; ** P < 0.01; *** P < 0.001 (Mann-Whitney test). Scale bars, 50 µm.

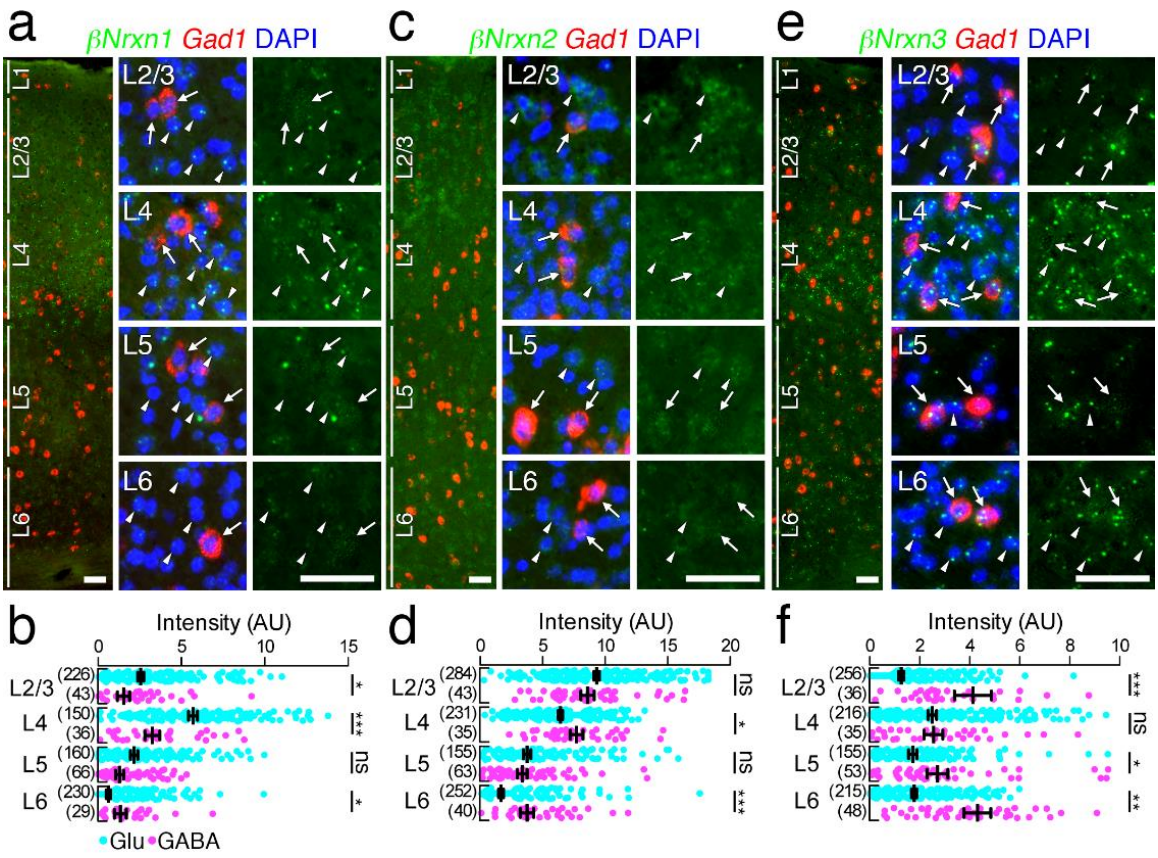

Figure 2.9 | Layer-specific expression of *βNrxn* mRNAs in the primary somatosensory neocortex. (a, c, e) Double FISH for *βNrxn1* (a), *βNrxn2* (c), or *βNrxn3* (e) and *Gad1* mRNAs showing distinct laminar-specific patterns of *Nrxn* mRNAs (green) between *Gad1*(+) GABAergic (red, arrows) and *Gad1*(-) glutamatergic (arrowheads) neurons. The left panel presents a low power-magnified image including the entire cortical layers, and the middle and right panels present high power-magnified images of layers 2/3, 4, 5, and 6 (L2/3, L4, L5, and L6) in order from the top. Note that the signals for *Nrxns* in GABAergic neurons tend to be variable. Nuclei were stained with DAPI (blue). (b, d, f) Summary scatter plots for *βNrxn1* (b), *βNrxn2* (d), or *βNrxn3* (f) mRNA in glutamatergic (aqua) and GABAergic (magenta) neurons. The numbers of cells analyzed are indicated in the parenthesis to the left of each column. Data are represented as means ± SEM. ns, not significant; * P < 0.05; ** P < 0.01; *** P < 0.001 (Mann-Whitney test). Scale bars, 50 µm.

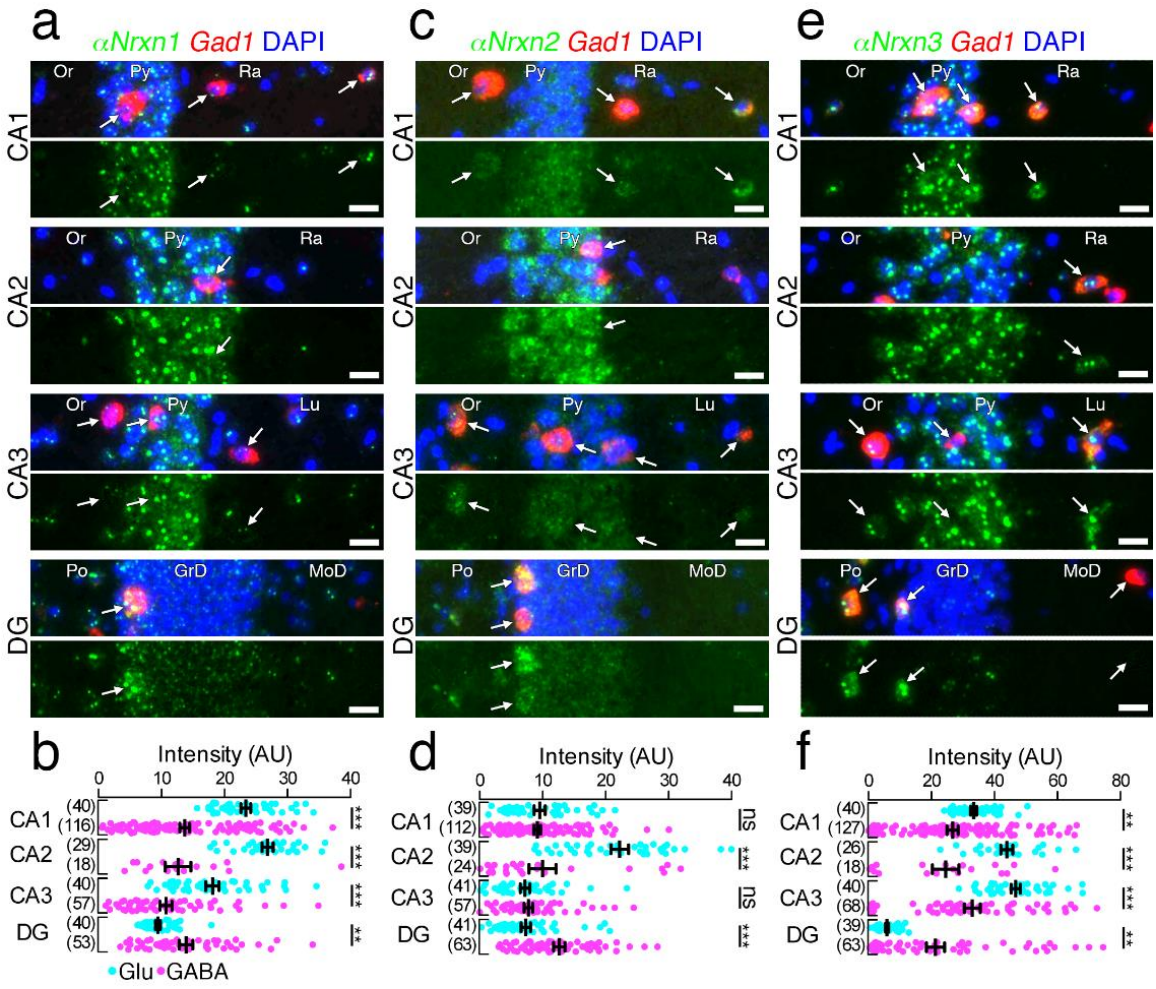

Figure 2.10 | Hippocampal subregion-specific expression of *αNrxn* mRNAs.
(a, c, e) Double FISH for *αNrxn1* (a), *αNrxn2* (c), or *αNrxn3* (e) and *Gad1* mRNAs in the hippocampus showing different subregion-specific patterns of *Nrxn* mRNAs (green) between *Gad1*(+) GABAergic (red, arrows) and *Gad1*(-) glutamatergic neurons. The four pairs of panels show the CA1, CA2, CA3, and dentate gyrus (DG) in order from the top. Note that the signal intensity in individual GABAergic neurons is variable, compared with that in glutamatergic neurons. Nuclei were stained with DAPI (blue). Or, stratum oriens; Py, Pyramidal cell layer; Ra, stratum radiatum; Lu, stratum lucidum; Po, polymorphic layer; GrD, granule cell layer; MoD, molecular layer. (b, d, f) Summary scatter plots for *αNrxn1* (b), *αNrxn2* (d), or *αNrxn3* (f) mRNA in glutamatergic (aqua) and GABAergic (magenta) neurons. The number in the parentheses next to each column indicates the number of cells analyzed. Data are represented as means ± SEM. ns, not significant; * $P < 0.05$; ** $P < 0.01$; *** $P < 0.001$ (Man-Whitney test). Scale bars, 20 μm.

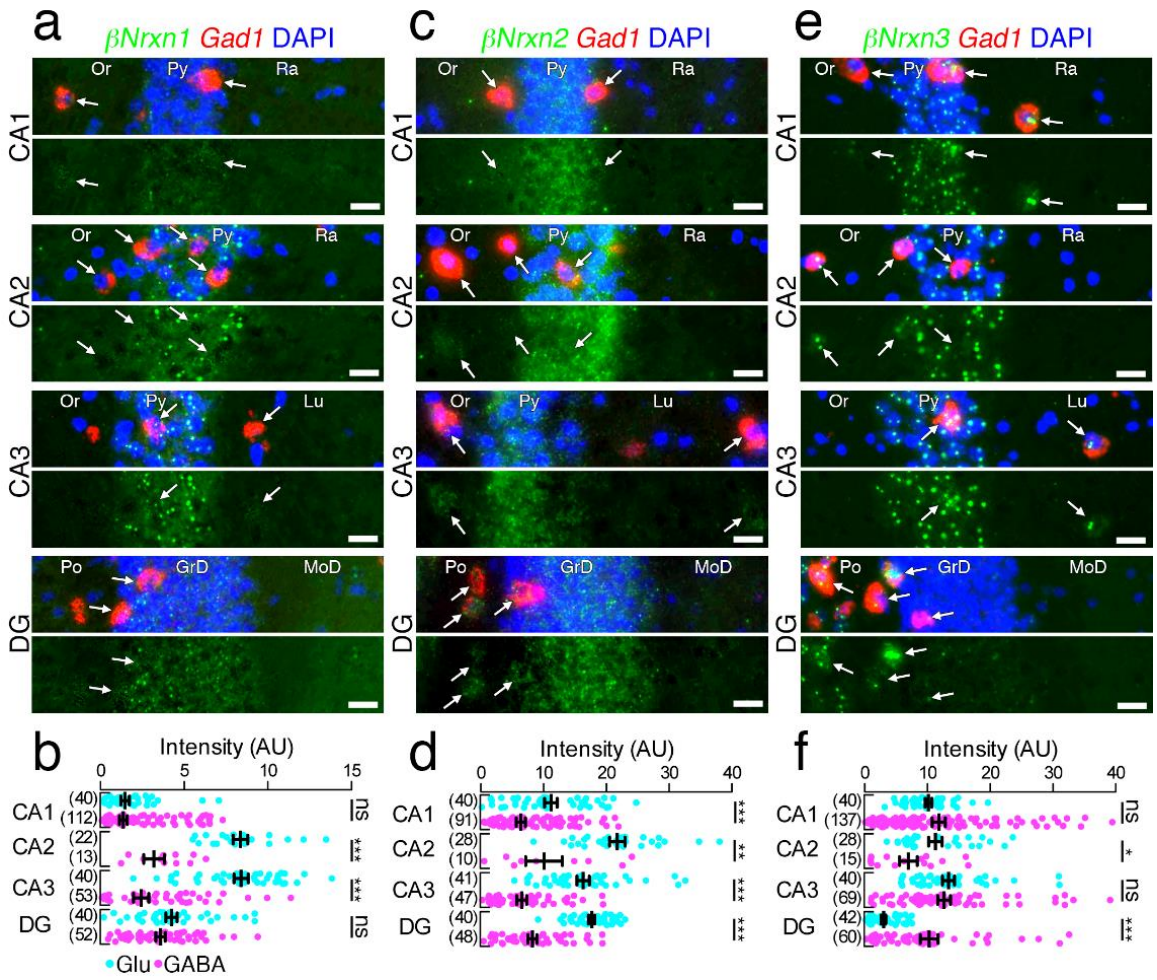

Figure 2.11 | **Hippocampal subregion-specific expression of *βNrxn* mRNAs.**
(a, c, e) Double FISH for *βNrxn1* (a), *βNrxn2* (c), or *βNrxn3* (e) and *Gad1* mRNAs in the hippocampus showing different subregion-specific expression patterns of *Nrxn* mRNAs (green) between *Gad1*(+) GABAergic (red, arrows) and *Gad1*(-) glutamatergic neurons. The four pairs of panels show the CA1, CA2, CA3, and dentate gyrus (DG) in order from the top. Note that the signal intensity in individual GABAergic neurons is variable, compared with that in glutamatergic neurons. Nuclei were stained with DAPI (blue). Or, stratum oriens; Py, Pyramidal cell layer; Ra, stratum radiatum; Lu, stratum lucidum; Po, polymorphic layer; GrD, granule cell layer; MoD, molecular layer. (b, d, f) Summary scatter plots for *βNrxn1* (b), *βNrxn2* (d), or *βNrxn3* (f) mRNA in glutamatergic (aqua) and GABAergic (magenta) neurons. The number in the parentheses next to each column indicates the number of cells analyzed. Data are represented as means ± SEM. ns, not significant; * $P < 0.05$; ** $P < 0.01$; *** $P < 0.001$ (Man-Whitney test). Scale bars, 20 μm.

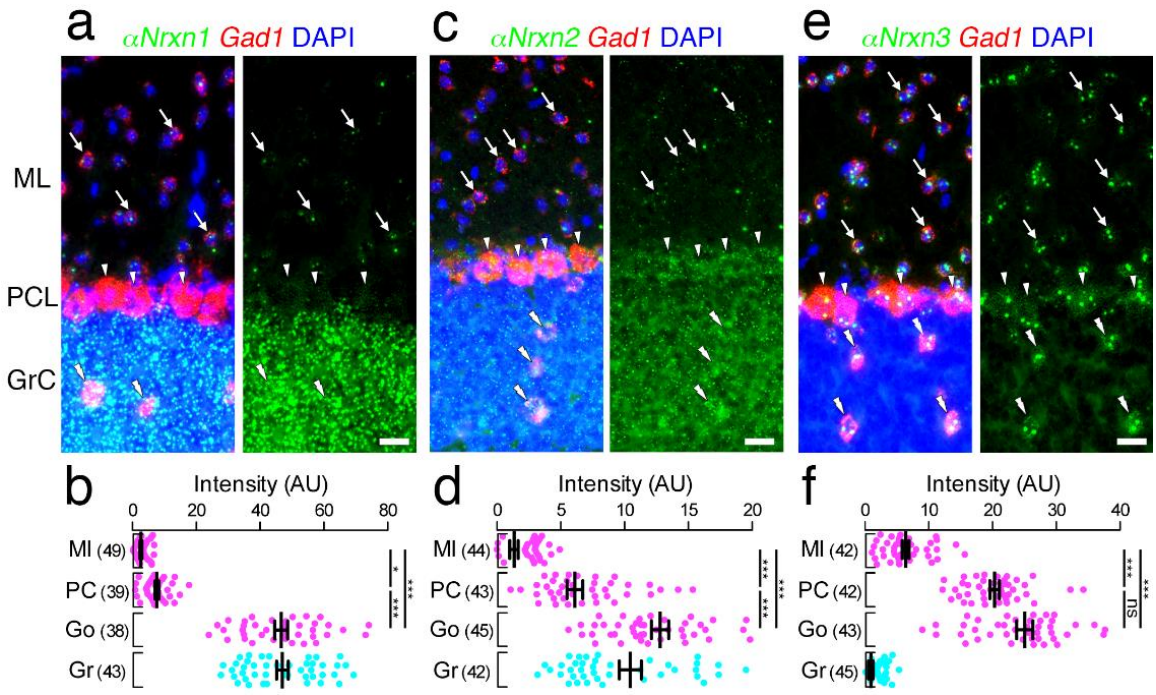

Figure 2.12 | Cell type-dependent expression of *αNrxn* mRNAs in the cerebellar cortex. (a, c, e, g, i, k) Double FISH for *αNrxn1* (a), *αNrxn2* (c), or *αNrxn3* (e) and *Gad1* mRNAs in the cerebellar cortex showing different expression patterns of Nrxn mRNAs (green) in *Gad1* mRNA (red)-labeled molecular layer interneurons (arrows), Purkinje cells (arrowheads), and Golgi cells (double arrowheads) and *Gad1* mRNA-unlabeled granule cells. Nuclei were stained with DAPI (blue). (b, d, f) Summary scatter plots for *αNrxn1* (b), *αNrxn2* (d), or *αNrxn3* (f) mRNA in molecular layer interneurons (magenta, MI), Purkinje cells (magenta, PC), Golgi cells (magenta, Go), and granule cells (aqua, Gr). The number in the parentheses next to each column indicates the number of cells analyzed. Data are represented as means ± SEM. ns, not significant; * $P < 0.05$; ** $P < 0.01$; *** $P < 0.001$ (Kruskal-Wallis test with post hoc Dunn's test). Scale bars, 20 μm.

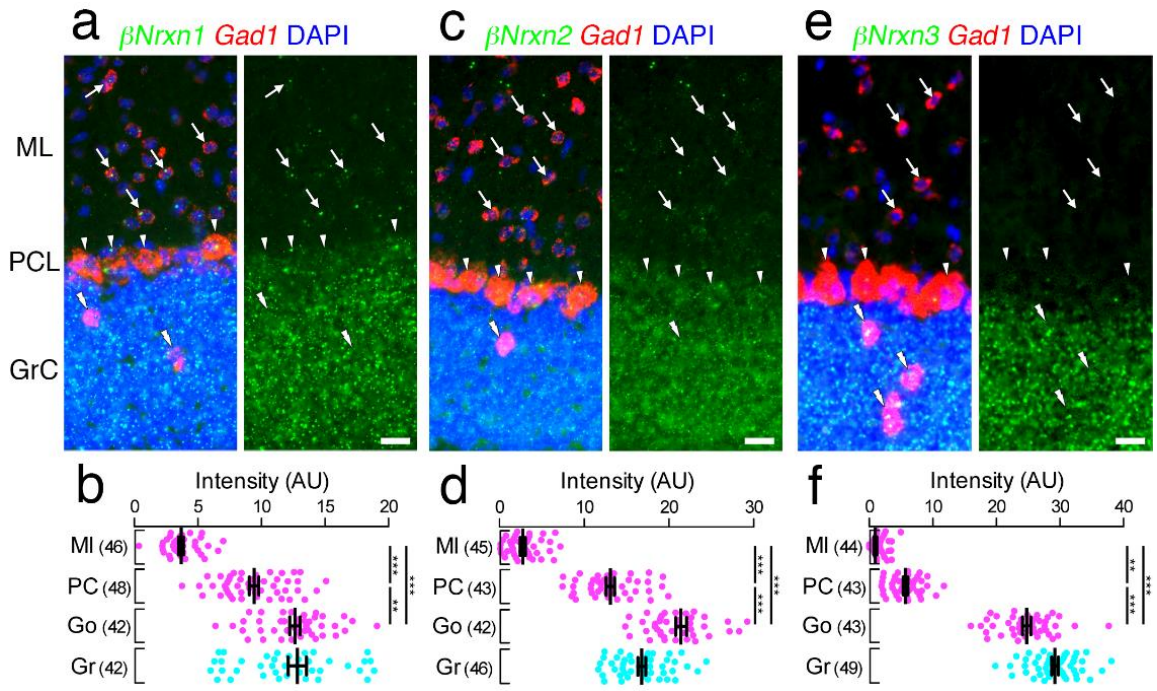

Figure 2.13 | Cell type-dependent expression of *βNrxn* mRNAs in the cerebellar cortex. (a, c, e) Double FISH for *βNrxn1* (a), *βNrxn2* (c), or *βNrxn3* (e) and *Gad1* mRNAs in the cerebellar cortex showing different expression patterns of Nrxn mRNAs (green) in *Gad1* mRNA (red)-labeled molecular layer interneurons (arrows), Purkinje cells (arrowheads), and Golgi cells (double arrowheads) and *Gad1* mRNA-unlabeled granule cells. Nuclei were stained with DAPI (blue). (b, d, f) Summary scatter plots for *βNrxn1* (b), *βNrxn2* (d), or *βNrxn3* (f) mRNA in molecular layer interneurons (magenta, MI), Purkinje cells (magenta, PC), Golgi cells (magenta, Go), and granule cells (aqua, Gr). The number in the parentheses next to each column indicates the number of cells analyzed. Data are represented as means ± SEM. ns, not significant; * $P < 0.05$; ** $P < 0.01$; *** $P < 0.001$ (Kruskal-Wallis test with post hoc Dunn's test). Scale bars, 20 μm.

3.2. Catecholaminergic neurons

We also examined the expression patterns of *Nrxn* mRNAs in catecholaminergic neurons including dopaminergic (DA) neurons in the midbrain and noradrenergic neurons in the LC and NTS (**Figures 2.14 and 2.15**). Catecholaminergic neurons were identified as cells positive for tyrosine hydroxylase (*Th*) mRNA, the rate-limiting enzyme for catecholamine biosynthesis. *αNrxn1* mRNA was expressed at

higher levels in midbrain DA neurons and NTS NA neurons than in LC NA neurons (**Figure 2.14a, b**). In contrast, *αNrxn2* mRNA was expressed at higher levels in both NA neurons than in midbrain DA neurons (**Figure 2.14c, d**). *αNrxn3* mRNA expression is the highest in midbrain DA neurons (**Figure 2.14e, f**). *βNrxn1* mRNA was hardly detected in the three catecholaminergic neurons analyzed (**Figure 2.15a, b**). *βNrxn2* and *βNrxn3* mRNAs were expressed at the highest level in locus coeruleus NA neurons and midbrain DA neurons, respectively (**Figure 2.15c-f**). Taken together, our double FISH data demonstrate that *Nrxn* expression in given neural regions is highly variable depending on neuron types and subregions, but that there is no specific or preferential assignment of given *Nrxn* isoforms to neurochemical types of neurons.

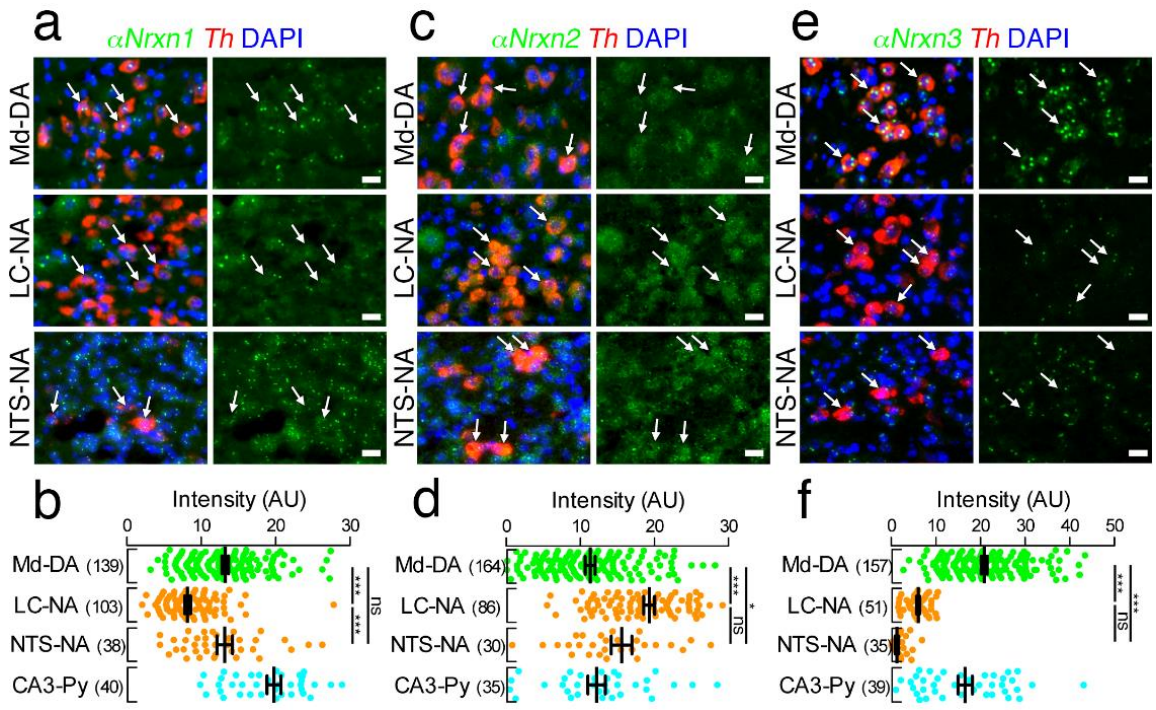

Figure 2.14 | Distinct expression of *αNrxn* mRNAs in catecholaminergic neurons. (a, c, e) Double FISH for *αNrxn1* (a), *αNrxn2* (c), or *αNrxn3* (e) and *Th* mRNAs showing distinct expression patterns of Nrxn mRNAs (green) in *Th* mRNA (red)-labeled DA neurons in the midbrain (Md-DA, top) and NA neurons in the LC (LC-NA, middle) and NTS (NTS-NA, bottom). Arrows indicate catecholaminergic neurons. Nuclei were stained with DAPI (blue). (b, d, f) Summary scatter plots for *αNrxn1* (b), *αNrxn2* (d), or *αNrxn3* (f) mRNA in Md-DA (green), LC-NA (orange), and NTS-NA (orange) neurons. Signals are compared to hippocampal CA3 pyramidal neurons (CA3-Py) obtained from the same section (aqua). The number in the parentheses next to each column indicates the number of cells analyzed. Data are represented as means ± SEM. ns, not significant; * $P < 0.05$; ** $P < 0.01$; *** $P < 0.001$ (Kruskal-Wallis test with post hoc Dunn's test). Scale bars, 20 μm.

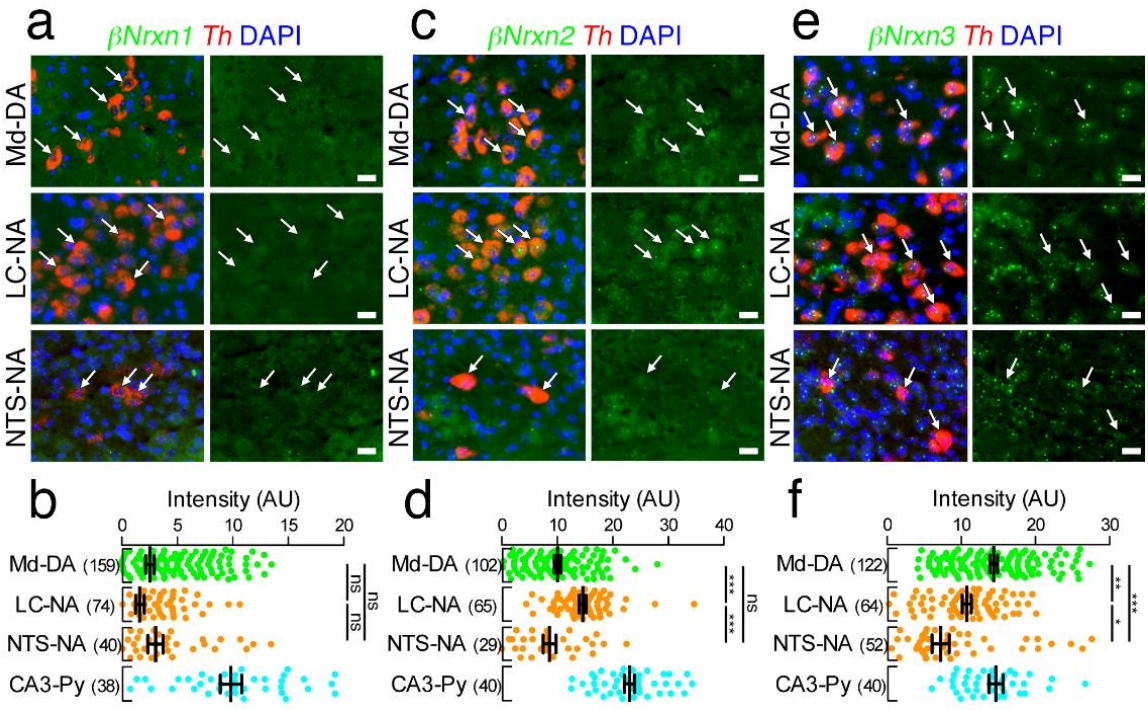

Figure 2.15 | Distinct expression of *βNrxn* mRNAs in catecholaminergic neurons. (a, c, e) Double FISH for *βNrxn1* (a), *βNrxn2* (c), or *βNrxn3* (e) and *Th* mRNAs showing distinct expression patterns of *Nrxn* mRNAs (green) in *Th* mRNA (red)-labeled DA neurons in the midbrain (Md-DA, top) and NA neurons in the LC (LC-NA, middle) and NTS (NTS-NA, bottom). Arrows indicate catecholaminergic neurons. Nuclei are stained with DAPI (blue). (b, d, f) Summary scatter plots for *βNrxn1* (b), *βNrxn2* (d), or *βNrxn3* (f) mRNA in Md-DA (green), LC-NA (orange), and NTS-NA (orange) neurons. Signals are compared to hippocampal CA3 pyramidal neurons (CA3-Py) obtained from the same section (aqua). The number in the parentheses next to each column indicates the number of cells analyzed. Data are represented as means ± SEM. ns, not significant; * $P < 0.05$; ** $P < 0.01$; *** $P < 0.001$ (Kruskal-Wallis test with post hoc Dunn's test). Scale bars, 20 μm.

4. Non-neuronal expression of αNrxn1 and αNrxn2 mRNA

In our double FISH data, we encountered signals for *αNrxn1* and *αNrxn2* mRNA in *Gad1*(-) putative glial cells in the hippocampus and cortex. Therefore, we first addressed the expression of six *Nrxn* mRNAs in non-neuronal cells in the hippocampal CA1 region (**Figure 2.16a-f**) and somatosensory cortex layers 2/3 (**Figure 2.17a-f**). Non-neuronal *Nrxn* signal intensities were normalized to the

neuronal expression. Neuronal and non-neuronal cells were identified as pyramidal neurons and *Gad1*(-) neuropil cells in the hippocampus, and the cells with large and pale DAPI+ nuclei and small and dark DAPI+ nuclei in the somatosensory cortex, respectively. Prominent expression of *αNrxn1* and *αNrxn2* was found in non-neuronal cells in both brain areas (**Figures 2.16g and 2.17g**). Next, we performed double FISH for *αNrxn1* and *αNrxn2,* and glial markers: glutamate/aspartate transporter (*Glast*) for astrocytes, proteolipid protein (*Plp*) for oligodendrocytes, and purinergic receptor P2Y (*P2ry12*) for microglia to identify the cell type expressing *αNrxn1* and *αNrxn2* (**Figures 2.16h-o and 2.17h-o**). Signals for *αNrxn1* mRNA frequently overlapped with those for *Glast* mRNA, but not *Plp* or *P2ry12* mRNA, in the hippocampal CA1 (**Figure 2.16h-k**), somatosensory cortex (**Figure 2.17h-k**), and other brain regions examined (data not shown), thus demonstrating *αNrxn1* expression in astrocytes. In contrast, signals for *αNrxn2* mRNA overlapped with those for *Glast* or *Plp*, but not *P2ry12* mRNA, in the hippocampal CA1 (**Figure 2.16l-o**), somatosensory cortex (**Figure 2.17l-o**) and other brain regions examined (data not shown), thus revealing *αNrxn2* expression in astrocytes and oligodendrocytes.

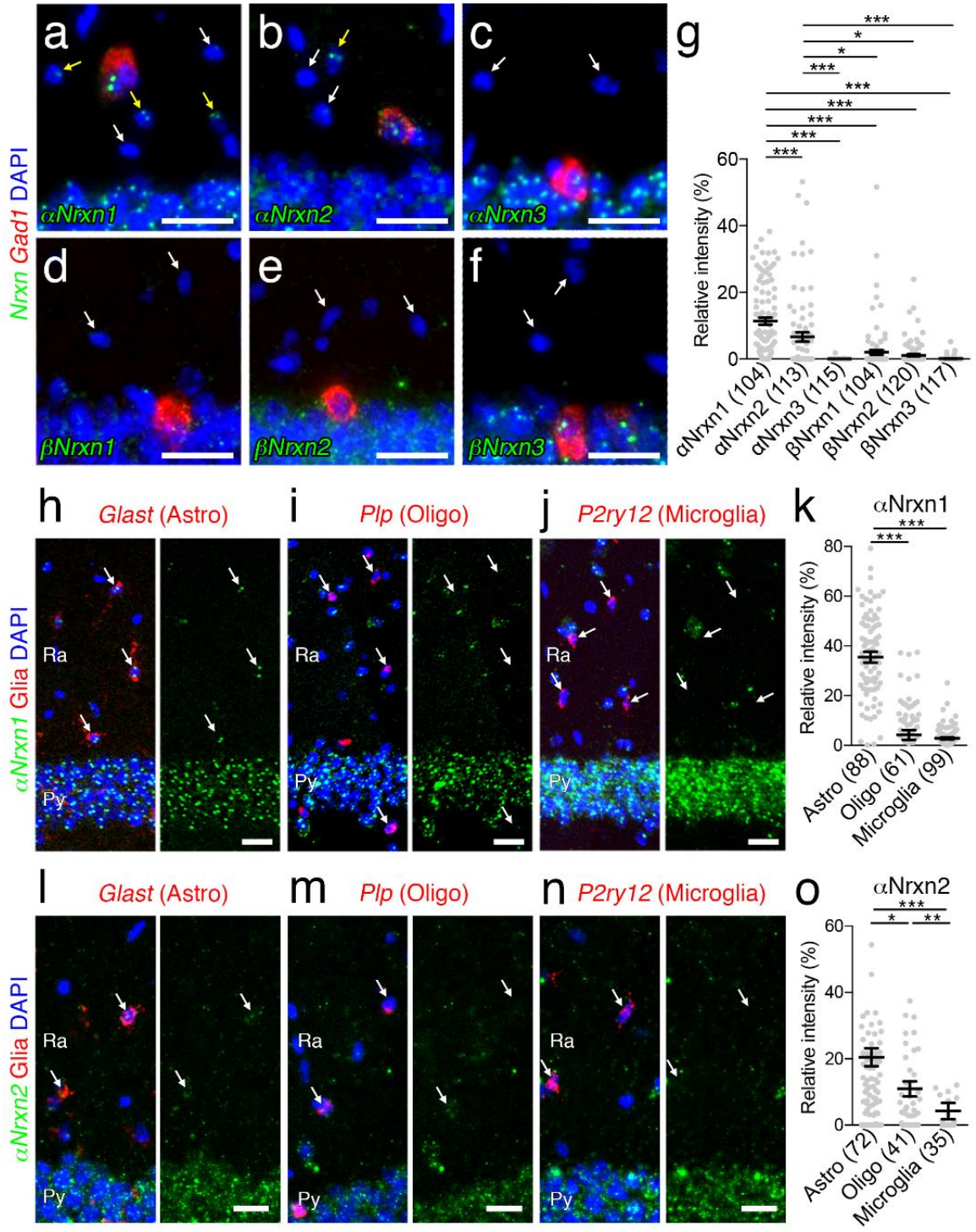

Figure 2.16 | Non-neuronal *αNrxn1* and *αNrxn2* expression in the hippocampal CA1 subregion. (a - f) Double FISH for *αNrxn1* (a), *αNrxn2* (b), *αNrxn3* (c), *βNrxn1* (d), *βNrxn2* (e), or *βNrxn3* (f) and *Gad1* mRNAs in the hippocampus CA1 region showing different expression patterns of *Nrxn* mRNAs (green) in non-neuronal cells identified by neuropil

cells negative for *Gad1* mRNA (red). Yellow and white arrows indicate non-neuronal cells with or without *Nrxn* expression, respectively. (g) Summary scatter plot for six *Nrxn* mRNAs in non-neuronal cells. The signal intensity in each cell is normalized to that in CA1 pyramidal cells. (h-j, l-n) Double FISH for *αNrxn1* (h-j) or *αNrxn2* (l-n) mRNA (green) and non-neuronal markers (red), including *Glast* (h, l), *Plp* (i, m), and *P2ry12* (j, n) for astrocytes (Astro), oligodendrocytes (Oligo), and microglia, respectively. Arrows indicate non-neuronal cells. Nuclei were stained with DAPI (blue). Ra, stratum radiatum; Py, Pyramidal cell layer. (k, o) Summary scatter plot for *αNrxn1* (k) or *αNrxn2* (o) mRNA in astrocytes, oligodendrocytes, and microglia. The signal intensity in each cell is normalized to that in CA1 pyramidal cells. The number in the parentheses below the scatter plot indicates the number of cells analyzed. Data are represented as means ± SEM. * $P < 0.05$; ** $P < 0.01$; *** $P < 0.001$ (Kruskal-Wallis test with post hoc Dunn's test). Scale bars, 20 μm.

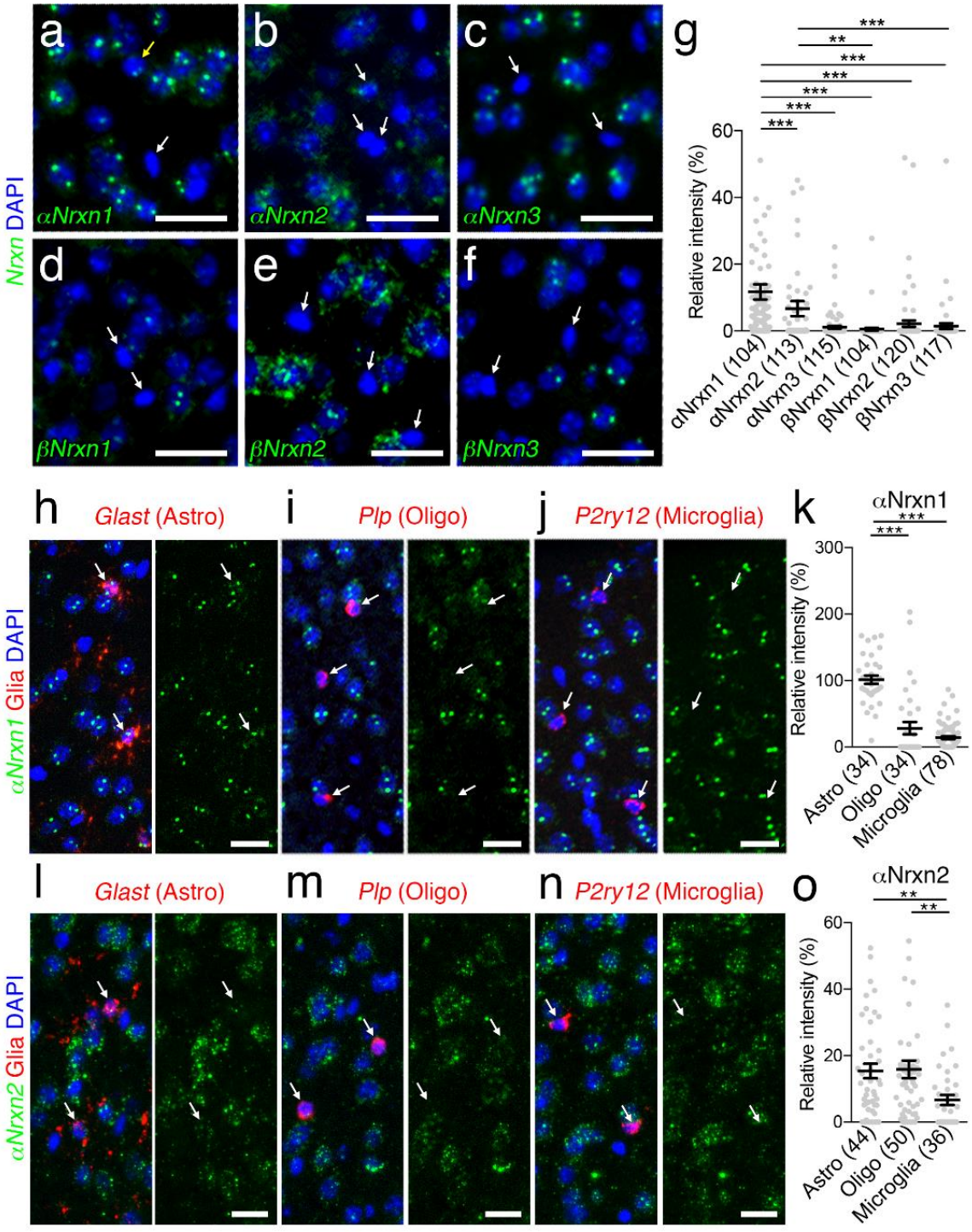

Figure 2.17 | Non-neuronal *αNrxn1* and *αNrxn2* expression in the somatosensory cortex. (a - f) Single FISH for *αNrxn1* (a), *αNrxn2* (b), *αNrxn3* (c), *βNrxn1* (d), *βNrxn2* (e), or *βNrxn3* (f) in the somatosensory cortex showing different expression patterns of *Nrxn* mRNAs (green) in non-neuronal cells with small and dark DAPI+ nuclei. Yellow and white

arrows indicate non-neuronal cells with or without *Nrxn* expression, respectively. (g) Summary scatter plot for six *Nrxn* mRNAs in non-neuronal cells. The signal intensity in each cell is normalized to that in cortical neurons with large and pale DAPI+ nuclei. (h-j, l-n) Double FISH for *αNrxn1* (h-j) or *αNrxn2* (l-n) mRNA (green) and non-neuronal markers (red), including *Glast* (h, l), *Plp* (i, m), and *P2ry12* (j, n) for astrocytes (Astro), oligodendrocytes (Oligo), and microglia, respectively. Arrows indicate non-neuronal cells. Nuclei were stained with DAPI (blue). Ra, stratum radiatum; Py, Pyramidal cell layer. (k, o) Summary scatter plot for *αNrxn1* (k) and *αNrxn2* (o) mRNA in astrocytes, oligodendrocytes, and microglia. The signal intensity in each cell is normalized to that in cortical neurons. The number in the parentheses below the scatter plot indicates the number of cells analyzed. Data are represented as means ± SEM. * $P < 0.05$; ** $P < 0.01$; *** $P < 0.001$ (Kruskal-Wallis test with post hoc Dunn's test). Scale bars, 20 μm.

5. Gene expression of trans-synaptic Nrxn binding proteins in the brain

Both diverse expression patterns of *Nrxn* in the brain and the variety of postsynaptic Nrxn binding partners should generate massive combinations of trans-synaptic protein interactions (Sudhof, 2017). Importantly, the expression of Nrxns and their trans-synaptic binding partners have not been well compared. Therefore, we studied the expression of the genes encoding the major trans-synaptic Nrxn binding partners, *Nlgn1-3* (Ichtchenko et al., 1995; Ichtchenko et al., 1996), *Lrrtm1-4* (de Wit et al., 2009; Ko et al., 2009) and *Adgrl1-3* (Latrophilin1-3) (Boucard et al., 2012), in the brain using chromogenic *in situ* hybridization (**Figure 2.18a-j**). For this analysis, cRNA probes were designed for unique coding and/or 5´-UTR region of each *Nlgn, Lrrtm and Adgrl* isoform (total, 11 probes). No signals were found using the corresponding sense probes (**Figure 2.18a-j, insets**), indicating the specificity of hybridization signals.

5.1. *Nlgns*

Nlgn1 mRNA expression was weak throughout the brain with the highest signals in the hippocampus (**Figure 2.18a**). In contrast, we observed much stronger signals for *Nlgn2* and *Nlgn3* mRNAs. Striking expression of *Nlgn2* mRNA was noted in not only the hippocampus, but also olfactory mitral cell layer and cerebellar Purkinje cell layer (**Figure 2.18b**). *Nlgn3* mRNA was ubiquitously expressed throughout the brain with peak signal levels visualized in the hippocampus (**Figure 2.18c**).

5.2. *Lrrtms*

Lrrtm1 mRNA displayed prominent expression in the hippocampus, neocortex, thalamus, and olfactory bulb (**Figure 2.18d**). Similarly, *Lrrtm2* mRNA expression was discernible in the hippocampus, neocortex, and thalamus (**Figure 2.18e**). The hippocampus exhibited similar expression patterns of *Lrrtm1* and *Lrrtm2* mRNAs with higher intensity in the CA1 and dentate gyrus than in the CA3. In contrast, *Lrrtm3* and *Lrrtm4* mRNAs were predominant in the cerebellum (**Figure 2.18f**) and dentate gyrus (**Figure 2.18g**), respectively.

5.3. *Adgrls* (Latrophilins)

Adgrl1 mRNA was widely and richly expressed throughout the brain (**Figure 2.18h**). *Adgrl2* and *Adgrl3* mRNAs were also expressed ubiquitously (**Figure 2.18i, j**). However, the signal intensities for *Adgrl2* and *Adgrl3* mRNAs were much weaker

than that for *Adgrl1* mRNA. *Adgrl2* mRNA showed peak intensity in the hippocampal CA1 region (**Figure 2.18i**), while *Adgrl3* mRNA was highly expressed in the hippocampal CA1 and dentate gyrus regions (**Figure 2.18j**).

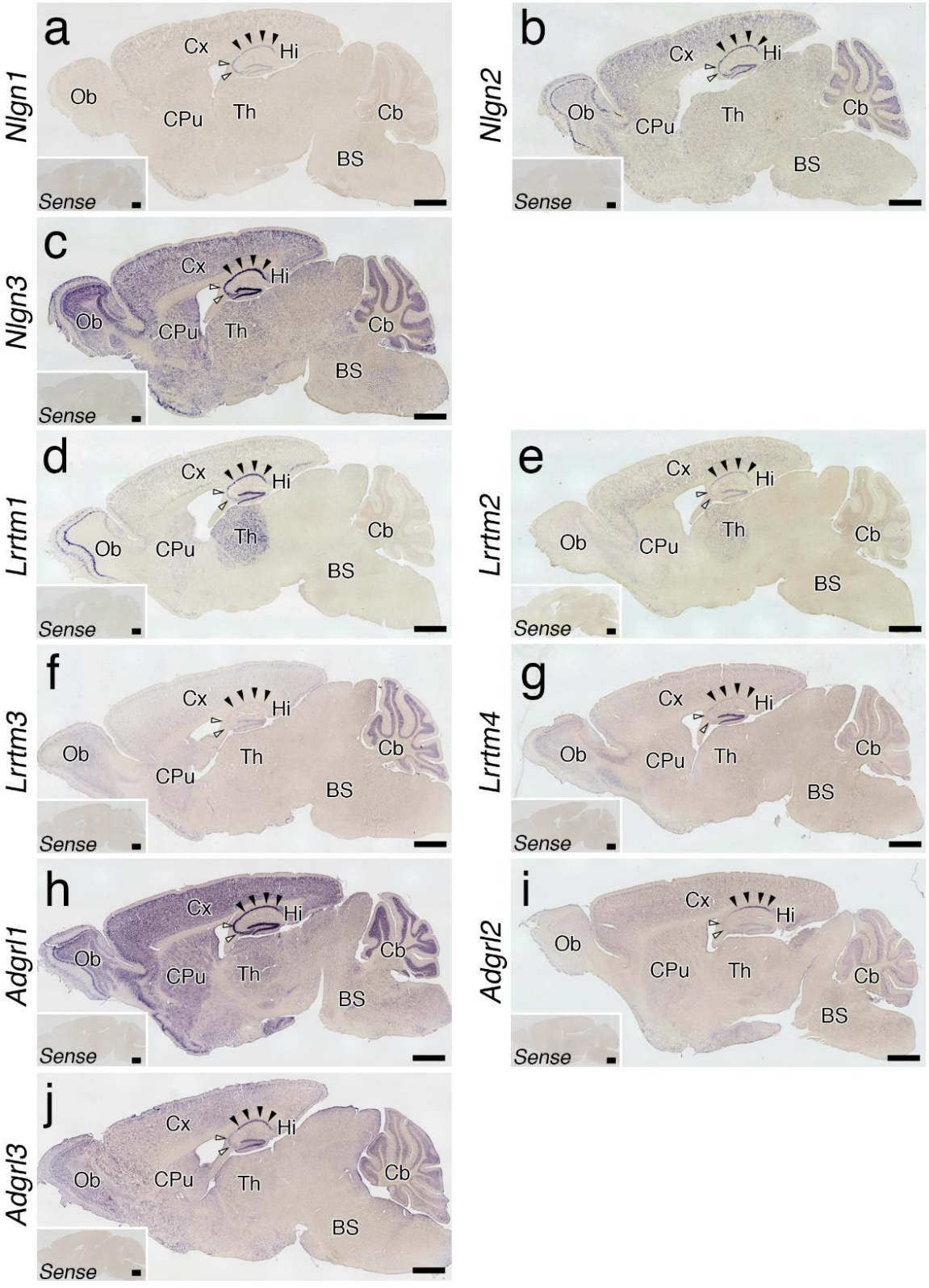
a
Nlgn1
Cx
Hi
Ob
CPu
Th
Cb
BS
Sense
b
Nlgn2
Cx
Hi
Ob
CPu
Th
Cb
BS
Sense
c
Nlgn3
Cx
Hi
Ob
CPu
Th
Cb
BS
Sense
d
Lrrtm1
Cx
Hi
Ob
CPu
Th
Cb
BS
Sense
e
Lrrtm2
Cx
Hi
Ob
CPu
Th
Cb
BS
Sense
f
Lrrtm3
Cx
Hi
Ob
CPu
Th
Cb
BS
Sense
g
Lrrtm4
Cx
Hi
Ob
CPu
Th
Cb
BS
Sense
h
Adgrl1
Cx
Hi
Ob
CPu
Th
Cb
BS
Sense
i
Adgrl2
Cx
Hi
Ob
CPu
Th
Cb
BS
Sense
j
Adgrl3
Cx
Hi
Ob
CPu
Th
Cb
BS
Sense

Figure 2.18 | **Expression of Nrxn binding partners in the brain.** (a-j) Whole brain sagittal views of chromogenic hybridization signals for *Nlgn1-3* (a-c), *Lrrtm1-3* (d-f) and *Adgrl1-4* (g-j) mRNAs. Insets showing no hybridization signals with sense cRNA probes. Filled and open arrows indicate the CA1 and CA3 pyramidal cell layers, respectively. For abbreviations, see list. Scale bars, 1 mm

Discussion

In this study, *Nrxn* mRNA expression was systematically mapped by *in situ* hybridization in the adult mouse brain. Consistent with previous reports (Gorecki et al., 1999; Puschel & Betz, 1995; Schreiner et al., 2014; Treutlein et al., 2014; Ullrich et al., 1995), we confirmed highly diverse expression profiles of *Nrxns* throughout the brain. Although the translational regulation of Nrxn proteins should be considered, our brain-wide and detailed expression analysis revealed distinct regional and cellular expression patterns of the six principal isoforms of *Nrxns* at the mRNA level.

First, we found cortical layer- or subregion- dependent differences in *Nrxn* mRNA expression in glutamatergic and GABAergic neurons. In the somatosensory cortex, the mean signal intensities for *αNrxn2*, *αNrxn3*, and *βNrxn3* mRNAs were significantly higher in GABAergic neurons than in glutamatergic neurons (**Figures 2.8f, h and 2.9f**). In the hippocampus, the mean signal intensities for all six isoforms were significantly lower in GABAergic neurons than in glutamatergic neurons (**Figures 2.10b, d, f and 2.11b, d, f**). This difference may underlie to some extent brain region-specific phenotypes on synaptic transmission in Nlgn3 KO or Nlgn3 R451C mice, which lack or decrease postsynaptic expression of Nlgn3, one of the binding partners of Nrxn proteins (Etherton et al., 2011; Tabuchi

et al., 2007). In addition, the variance of the signal intensities of *Nrxn* mRNAs appeared high in cortical GABAergic neurons (**Figures 2.8-2.11**). This is supported by the notion that distinct subsets of inhibitory neurons in cortical structures differ in their expression patterns of *Nrxn* mRNAs (L. Y. Chen et al., 2017; Fuccillo et al., 2015). In particular, we found some inhibitory neurons with high signals for *αNrxn2* mRNA in the deep cortical layer (**Figure 2.8e, f**). *αNrxn2* can selectively induce inhibitory presynaptic differentiation via its interaction with postsynaptic IgSF21, which is expressed in the deep layer neurons (Tanabe et al., 2017). This molecular interaction could contribute to synapse specification at a subset of inhibitory synapses.

Next, we found unique expression of *Nrxn* mRNAs in the hippocampus. Consistent with previous studies (Nguyen et al., 2016; Ullrich et al., 1995), the CA1 pyramidal cell layer highly expressed mRNAs for all the isoforms except *βNrxn1* (**Figures 2.3 and 2.4**). The CA2 and CA3 pyramidal layers expressed all *Nrxn* mRNAs, however, *αNrxn2* was preferentially expressed in the CA2 region (**Figures 2.1c, d, k and 2.3b**) and *βNrxn3* had septotemporal gradient expression in the CA3 region (**Figures 2.1k, l, 2.3f, and 2.4f**). Furthermore, the dentate gyrus had a septotemporal gradient of *βNrxn3* (**Figures 2.3f and 2.4f**) mRNA expression, and its upstream entorhinal cortex also had a rostrocaudal gradient of *αNrxn3* **(Figures 2.4c and 2.5c**) and *βNrxn3* (**Figures 2.4f and 2.5f**) mRNA expressions.Different parts of the entorhinal cortex project to different septotemporal levels of the dentate gyrus (Amaral & Pierre, 2006). The

rostromedial entorhinal cortex, which expresses both *αNrxn3* and *βNrxn3* mRNAs at high levels, projects to the temporal half of the dentate gyrus, which highly expresses *βNrxn3* mRNA. In contrast, the caudolateral entorhinal cortex, which expresses *αNrxn3* and *βNrxn3* mRNAs at low levels, projects to the septal half, where *βNrxn3* mRNA expression is low. This coincidence of the topographic projections and *Nrxn3* expression between the entorhinal cortex and dentate gyrus could underlie a unique function of *Nrxn3* in memory formation. Furthermore, a specific splicing variant of Nrxn3 protein can recruit postsynaptic kainate receptors via C1ql2/3 at dentate gyrus-CA3 synapses (Matsuda et al., 2016). Although we did not map splicing variants of *Nrxn3* gene in this study, our data raise a possibility of topographical differences in the postsynaptic recruitment of kainate receptors.

We also investigated the region- and cell type- dependent expression of *Nrxn* mRNAs in catecholaminergic neurons including midbrain DA neurons and LC and NTS NA neurons (**Figures 2.14 and 2.15**). Similar to glutamatergic and GABAergic neurons, midbrain DA neurons expressed multiple *Nrxn* isoforms, consistent with Nrxn protein expression at striatal DA synapses formed by midbrain DA neurons (Uchigashima et al., 2016). In addition, we found *Nrxn* mRNA expressions with different combinations in LC and NTS NA neurons. Different expression patterns of *Nrxn* mRNAs among catecholaminergic neurons may provide distinct molecular bases to control the release of each catecholamine. Indeed, pan-*Nrxn* deletion causes different phenotypes in synaptic transmissions from distinct neurons with their own repertories of *Nrxn* mRNAs (L. Y. Chen et al.,

2017). Therefore, region- and cell type- dependent expression patterns of *Nrxn* mRNAs would provide the molecular-anatomical basis for the diversity of synapse specification at various types of synapses.

We found a unique expression of the *Nrxn3* gene in the auditory system. Several auditory relay stations, including the ventral cochlear nucleus, nucleus of trapezoid body, and inferior colliculus, displayed high expressions of *αNrxn3*, *βNrxn3*, or both mRNAs (**Figures 2.5c and 2.6c, f**). The medial geniculate nucleus, which is the thalamic nucleus relaying auditory information to the neocortex, highly expressed both *αNrxn3* and *βNrxn3* mRNAs as well as other *Nrxn* isoforms (**Figure 2.4a-f**). Furthermore, the primary auditory cortex had a unique expression pattern of *βNrxn3* mRNA. *βNrxn3* mRNA was expressed with a peak density in layers 2/3 as well as layer 4 region (**Figures 2.3f and 2.4f**), while the primary somatosensory cortex exhibited peak expression in layer 4 only (**Figure 2.3f)**. Above all, the predominant expression of *αNrxn3* and *βNrxn3* mRNAs may suggest the importance of Nrxn3 in auditory function. Indeed, a patient with a rare mutation of the *Nrxn3* gene exhibited difficulty in auditory processing (Vaags et al., 2012).

In the olfactory system, all isoforms of *Nrxn* mRNAs were highly expressed in mitral cell layer neurons (**Figure 2.2a-f**), the second order neurons receiving input from olfactory cells, and in pyramidal neurons in the piriform cortex (**Figures 2.2g-l and 2.3**), which are the third order neurons receiving input from mitral cell layer neurons. We also noted striking expression of *αNrxn* mRNA in the granule cells of

the olfactory bulb (**Figure 2.2a-c**), and of *αNrxn2*, *αNrxn3*, *βNrxn1*, and *βNrxn3* mRNAs in the island of Calleja (**Figure 2.2h, i, l**), which is anatomically associated with the piriform cortex (Fallon et al., 1978). Interestingly, some ASD patients exhibit olfactory deficits (Galle et al., 2013). *α/βNrxn3* KO mice have impaired GABAergic synaptic transmission in the olfactory bulb, leading to deficits in olfactory function (Aoto et al., 2015). Interestingly, both *αNrxn1* and *αNrxn2* KO mice, which show autism-related behaviors, have been reported to have intact olfaction, highlighting the importance of *Nrxn3* in olfaction (Dachtler et al., 2014; Grayton et al., 2013).

Some nuclei in the brainstem share similar *Nrxn* mRNA expression patterns. *αNrxn2* mRNA was remarkable in facial nucleus (**Figure 2.6b**) and hypoglossal nucleus (**Figure 2.7b**), consistent with the requirement of αNrxns in high fidelity synaptic transmission at mouse neuromuscular junctions and relay synapses (Sons et al., 2006). Our findings suggest that neurons associated with particular functions could partly share a similar expression profile with the six principal isoforms of *Nrxn* mRNAs.

It is important to note that we did not find any neuronal populations that express only a single *Nrxn* isoform. This provides support for the redundancy of Nrxn proteins, which could reduce deleterious consequences of synaptic dysfunction if one of the co-expressed Nrxns has detrimental mutations. We identified brain regions that express all six *Nrxn* isoforms, including olfactory bulb mitral cell layer, hippocampal CA3 and piriform cortex pyramidal cell layers. The

expression of all *Nrxns* were particularly high in piriform cortex. Piriform cortex is the first cortical area receiving olfactory information and contains strong associational circuits (Hagiwara et al., 2012). Expression of multiple *Nrxn* isoforms may be important to maintain the connectivity of this high-fidelity circuit.

We identified *αNrxn1* as the most ubiquitous *Nrxn* isoform in any brain region. Importantly, *αNrxn1* mRNA was expressed in neuronal cell types (glutamatergic, GABAergic, catecholaminergic neurons) and astrocytes. This may explain the strong association of *αNrxn1* mutations with neurodevelopmental disorders, including ASD, ADHD, intellectual disability, schizophrenia, and Tourette syndrome (Autism Spectrum Disorders Working Group of The Psychiatric Genomics, 2017; Ching et al., 2010; Clarke et al., 2012; H. G. Kim et al., 2008; Sebat et al., 2007; Szatmari et al., 2007; Vinas-Jornet et al., 2014; Yan et al., 2008; Zahir et al., 2008).

We found the non-neuronal expressions of *αNrxn1* and *αNrxn2*. It is important to identify the cell type(s) that interacts with *αNrxn1* and *αNrxn2* mRNA-expressing astrocytes. It has been reported that Nlgns expressed in astrocytes control synaptogenesis and astrocyte morphogenesis (Stogsdill et al., 2017). It is intriguing to address the role of Nlgn-Nrxn protein interaction between astrocytes. Addressing the involvement of Nrxns on gliotransmission or exocytotic release of neurotransmitters and factors from astrocytes to neurons should help to elucidate the role of Nrxns in astrocytes (Parpura & Zorec, 2010). We found *αNrxn2* as a major *Nrxn* mRNA in oligodendrocytes (**Figures 2.16m, o and 2.17m, o**). αNrxn2

protein expression was reported in oligodendrocyte-like cells in the early developing human cerebral cortex (Harkin et al., 2017). It has been suggested that Nlgn3 expressed in oligodendrocytes and axonal Nrxn protein interactions are important for oligodendrocyte differentiation (Proctor et al., 2015). Further studies addressing the role of *αNrxn2* in oligodendrocyte development and function are required.

Lastly, we examined the mRNA expression patterns of three gene families, *Nlgns*, *Lrrtms* and *Adgrls*, that encode major Nrxn binding proteins, and compared their brain region-specific expression patterns to that of *Nrxns*. All three gene families had diverse expression profiles throughout the brain (**Figure 2.18**). In particular, hippocampal CA1 pyramidal neurons, which receive excitatory inputs from CA3 pyramidal neurons, expressed most of these genes except *Lrrtm3* and *Lrrtm4*, likely contributing to numerous combinations of trans-synaptic interactions. In contrast, CA3 pyramidal neurons, which form associational circuits with each other, expressed only *Nlgns* and *Adgrl1* at high levels. Considering the expression of multiple *Nrxn* isoforms in CA3 pyramidal cells, the differential expression of Nrxn binding partners in postsynaptic neurons could underlie the distinct distributions of different Nrxn proteins at presynaptic terminals, thus providing unique region- and cell type- specific connections important for synaptic transmission (Sudhof, 2017).

Acknowledgment

We thank Dr. Paul D. Gardner for valuable discussions and Dr. Kenji Tanaka for a gift of a Nlgn3 probe. This work was supported by grants from the Riccio Fund for Neuroscience (to K.F.), the Whitehall Foundation (to K.F.), National Institutes of Health Grant (R01NS085215 to K.F.), Grants-in-Aid for Scientific Research (15K06732 to M.U.), and The Naito Foundation (to M.U.). The authors thank Ms. Naoe Watanabe for her skillful technical assistance.

Chapter III

Deletion of all neurexins in serotonin neurons compromises serotonin release and complex behaviors

Chapter III: Deletion of all neurexins in serotonin neurons compromises serotonin release and complex behaviors

Amy Cheung[1], Aya Matsui[2], and Kensuke Futai[1]

1. Department of Neurobiology, Brudnick Neuropsychiatric Research Institute, University of Massachusetts Medical School, Worcester, Massachusetts.
2. Vollum Institute, Oregon Health & Science University, Portland, Oregon.

Abstract

Extensive serotonin (5-HT) innervation throughout the brain corroborates 5-HT's modulatory role in numerous cognitive activities. Abnormal brain 5-HT levels and function have been implicated in Autism Spectrum Disorder (ASD). Neurexin (Nrxn) genes are risk factors for ASD and encode presynaptic cell adhesion molecules important for specifying synaptic phenotypes for proper neural circuit assembly. Here, we found that Nrxn1 and Nrxn2 genes are predominantly expressed in 5-HT neurons. We generated a mouse line with the deletion of all three Nrxn genes in 5-HT neurons to study how Nrxns affect 5-HT signaling. The lack of 5-HTergic Nrxns impaired 5-HT release in the dorsal raphe nucleus and hippocampus and altered serotonin transporter distribution in specific brain areas. Removal of Nrxns from 5-HT neurons also reduced sociability and increased depressive-like behavior in male mice. Our results highlight roles for Nrxns in 5-HT neurotransmission and the execution of complex social behaviors.

Introduction

Serotonin (5-hydroxytryptamine, 5-HT) is a monoamine neurotransmitter with a near ubiquitous presence in a variety of behaviors. Clusters of 5-HT neurons reside specifically in brainstem raphe nuclei and send their fibers throughout the brain to modulate electrochemical information for arousal, social interactions, stress responses, and valence, among other processes. Abnormalities in 5-HT signaling have been extensively reported in neuropsychiatric disorders including depression, anxiety disorders, schizophrenia, and autism spectrum disorder (ASD), which are treated with pharmacological agents that act on the 5-HT system (Pourhamzeh et al., 2021).

5-HT reaches postsynaptic specializations through volume transmission (Descarries et al., 2010) or at synapses and synaptic triads (Belmer et al., 2017). 5-HT release sites are expressed in somatodendritic compartments, along axons, or at terminals juxtaposed to postsynaptic sites and can be identified by proteins that provide mechanisms for vesicle release (Belmer et al., 2017; Dudok et al., 2009; Haase et al., 2017; Jansch et al., 2021). These modes of signaling allow 5-HT to exert fast and slow message relaying effects through ion channels and G-protein coupled receptors, respectively, over a range of distances. Genetic variants of synaptic organizing and structural proteins such as scaffolding and adhesion molecules have been identified in people with ASD (Autism Spectrum Disorders Working Group of The Psychiatric Genomics, 2017; Grove et al., 2019; Yuen et al., 2017; Zoghbi & Bear, 2012). Moreover, the knockout or knock-in of synaptic genes

such as Shank3, Nlgn3, and Gabrb3 have generated autism-related phenotypes in mice (Bey & Jiang, 2014; Kazdoba et al., 2016; Silverman et al., 2010). 5-HT neuron transcriptome profiles were found to be enriched in genes for cell adhesion, including trans-synaptic molecules Neuroligin (Nlgn) 1 and Neurexin (Nrxn) 1 (Okaty et al., 2015). While much work has focused on deciphering receptor and reuptake dynamics in 5-HT signaling, the molecular framework of 5-HT release sites that facilitates communication with postsynaptic targets remains undefined.

Neurotransmission involves Nrxns, presynaptic cell adhesion molecules produced from three genes (*Nrxn1*, *Nrxn2*, and *Nrxn3*) as longer alpha- (*αNrxn1*, *αNrxn2*, *αNrxn3*), shorter beta- (*βNrxn1*, *βNrxn2*, *βNrxn3*), and Nrxn1-specific gamma (*γNrxn1*) isoforms (Sudhof, 2017; Ushkaryov et al., 1992). These diverse expressions, with further variation mediated through alternative splicing, help define Nrxns as critical regulators of synapse specification. Nrxns interact with ligands across the synaptic cleft to promote synapse differentiation (Anderson et al., 2015; Graf et al., 2004; Uchigashima, Konno, et al., 2020) and modulate presynaptic neurotransmitter release with neuronal (F. Luo et al., 2020; Missler et al., 2003) and nonneuronal (Sons et al., 2006) postsynaptic partners. Additionally, the functions of Nrxns depend on the circuits and brain regions in which they reside (Aoto et al., 2015; L. Y. Chen et al., 2017). Knockout of αNrxn1 (Etherton et al., 2009; Grayton et al., 2013) and αNrxn2 (Born et al., 2015) in mice caused core symptoms of ASD, notably deficits in social and repetitive behaviors, and co-occurring anxiety-like behavior. Mice lacking the ability to synthesize 5-HT also

exhibited autism-related behaviors (Kane et al., 2012). While 5-HT and Nrxn dysfunction have been studied separately as molecular factors that contribute to the development of ASD, the effects of Nrxns at 5-HT release sites and on animal behavior is still unknown.

In this study, we elucidated the functions of Nrxns in the 5-HT system by assessing signaling properties and behaviors of knockout mice with absent Nrxn expression in 5-HT neurons. We demonstrated that the loss of Nrxn genes reduced 5-HT release in the dorsal raphe nucleus and hippocampus and altered 5-HT connectivity in the mouse brain. Moreover, the lack of Nrxns in 5-HT neurons produced social behavioral and depressive-like phenotypes in males. These results highlight Nrxns as regulators of neurotransmission and complex behaviors in the neuromodulatory 5-HT system.

Materials and Methods

Animals

All experiments were conducted with approved animal protocols from the Institutional Animal Care and Use Committee (IACUC) at the University of Massachusetts Medical School. 5-HT neuron-specific tdTomato mice (Fev/RFP) were generated by crossing $^{lox\text{-}STOP\text{-}lox}$tdTomato (Jax #007905) and Fev^{Cre} mice (ePet^{Cre}: Jax #012712) (Scott et al., 2005). Fev/RFP mice were crossed with Nrxn1$^{f/f}$/2$^{f/f}$/3$^{f/f}$ mouse line (Uchigashima, Konno, et al., 2020; Uemura et al., 2020) to generate serotonin neuron-specific triple Nrxn knockout mouse line (Fev^{Cre}/$^{lox\text{-}STOP\text{-}lox}$tdTomato/Nrxn1$^{f/f}$/2$^{f/f}$/3$^{f/f}$: Fev/RFP/NrxnTKO). The Fev/RFP/NrxnTKO line was maintained by breeding Fev/RFP/NrxnTKO mice with Cre-negative ($^{lox\text{-}STOP\text{-}lox}$tdTomato/Nrxn1$^{f/f}$/2$^{f/f}$/3$^{f/f}$: WT) mice. Unless specified, Cre-negative littermates were used as wildtype controls. Male mice were used in all experiments, whereas females were tested only in behavioral studies. For social behavioral experiments, juvenile stimuli consisted of 4- to 6- week-old sex-matched mice on a C57BL/6J background.

Mice were group housed (2-5 per cage) and maintained in ventilated cages with *ad libitum* access to food and water on a standard 12-hour light/dark cycle (lights ON at 7 A.M.) in a temperature-controlled (20-26°C) facility. One to two weeks prior to experimentation, mice were acclimated to a reverse 12-hour light/dark cycle (lights ON at 7 P.M.). Mice were water restricted or individually housed before some tests as indicated.

Single-cell RNA extraction

Using whole cell patch-clamp approach as described previously (Mao et al., 2018; Uchigashima, Konno, et al., 2020; Uchigashima, Leung, et al., 2020), cytosol from RFP+ serotonin neurons in the dorsal and median raphe nuclei in Fev/RFP and Fev/RFP/NrxnTKO mice was harvested. Briefly, glass patch pipettes were filled with DEPC-treated internal solution containing RNase inhibitor (1 U/ µl, Ambion) and the following (in mM): 140 K-methanesulfonate, 0.2 EGTA, 2 $MgCl_2$ and 10 HEPES, pH-adjusted to 7.3 with KOH. Before the electrode was filled with RNase inhibitor-containing solution (4.5 µl), a small volume of internal solution (~0.5 µl) was loaded in the tip to form a smooth seal. After establishing whole-cell mode, the cytosol of the recorded cell was aspirated into the glass electrode and expelled into an RNase-free 0.5-ml tube (Ambion).

Single-cell RT-qPCR

A SMART-Seq® HT Kit (TAKARA Bio) was used to prepare the cDNA libraries following the manufacturer's instructions. Briefly, single-cell templates underwent reverse transcription reaction at 42°C for 90 min followed by regular PCR amplification: 95°C for 1 min, 98°C for 10 s, 65°C for 30 sec, and 68°C for 3 min for 25 cycles. To validate the Fev/RFP/NrxnTKO mouse line, the following TaqMan gene expression assays (Applied Biosystems) were used: *Nrxn1* (Mm03808857_m1), *Nrxn2* (Mm01236856_m1), *Nrxn3* (Mm00553213_m1), *Tph2* (Mm00557715_m1) and *Gapdh* (Mm99999915_g1). The PCR reactions and

analyses were performed blind. The relative expression of *Nrxns* or *Tph2* were calculated as: Relative expression = $2^{Ct,Gapdh}/2^{Ct,Nrxns\ or\ Tph2}$; Ct, threshold cycle for target gene amplification.

Fluorescence *in situ* hybridization

Double fluorescence *in situ* hybridization was performed as previously described (Uchigashima et al., 2019; Uchigashima, Konno, et al., 2020). Unless otherwise noted, all procedures were performed at room temperature. Briefly, fresh frozen sections prepared from two 10-week-old male C57BL/6 mice were fixed with 4% paraformaldehyde (PFA) / 0.1 M phosphate buffer (PB, pH 7.4) for 30 min, acetylated with 0.25% acetic anhydride in 0.1 M triethanolamine-HCl (pH 8.0) for 10 min and prehybridized with hybridization buffer for 30 min. Hybridization and post-hybridization were performed at 75°C. Sections were hybridized in a mixture of fluorescein- (1:1000) or DIG- (1:10,000) labeled cRNA probes in hybridization buffer overnight and washed in saline-sodium citrate buffers post-hybridization. Sections were pre-treated with DIG blocking solution for 30 min and 0.5% tryamide signal amplification (TSA) blocking reagent in Tris-NaCl-Tween 20 (TNT) buffer for 30 min before signal visualization using a two-step detection method. For the first step, sections were incubated with peroxidase-conjugated anti-fluorescein antibody (1:500, Roche Diagnostics) for 1 hr and TSA Plus Fluorescein amplification kit (PerkinElmer) for 10 min. Immediately after, residual peroxidase activity was inactivated with 3% H_2O_2 in TNT buffer for 30 min. In the second step,

the same times were used for incubating sections with peroxidase-conjugated anti-DIG antibody (1:500, Roche Diagnostics) and TSA Plus Cy3 amplification kit. For nuclear counterstaining, sections were incubated in DAPI (1:5000, Sigma-Aldrich) for 10 min. Dorsal raphe nucleus and median raphe nucleus were imaged at 20x (NA 0.75) using a fluorescence microscope (BZ-X710, Keyence). ImageJ software (National Institutes of Health) was used to quantify the co-localization of Nrxn-positive puncta in 5-HT neurons.

Immunohistochemistry

All mice were transcardially perfused with ice-cold 4% paraformaldehyde (PFA) / 0.1 M phosphate buffer (PB, pH 7.4) under isoflurane anesthesia. Brains were dissected and post-fixed at 4°C in in PFA for 2 hours, then cryo-protected in 30% sucrose / 0.1 M PB to prepare 40 µm-thick coronal brain sections on a cryostat (CM3050 S, Leica Biosystems). All immunohistochemical incubations were carried out at room temperature. Sections were permeabilized for 10 min in 0.1% Tween 20 / 0.01 M phosphate-buffered saline (PBS, pH 7.4), blocked for 30 min in 10% normal donkey serum and incubated overnight in guinea pig polyclonal anti-serotonin transporter antibody (1 µg/ml, Frontier Institute). The following day, sections were incubated in donkey anti-guinea pig-Alexa488 antibody for 2 hours at a dilution of 1:500 (Jackson ImmunoResearch Laboratories).

SERT density analysis

To assess the density of SERT fiber inputs, which labels 5-HT neuron projections, four stained sections from three or four male WT and Fev/RFP/NrxnTKO brains containing the medial prefrontal cortex, nucleus accumbens, amygdala, hippocampus, or raphe nuclei were imaged (1024 x 1024 pixels) using a laser scanning confocal microscope (LSM700, Zeiss) with a 63x oil-immersed objective (NA 1.4) at an optical zoom of 1.6 and Zen black acquisition software (Zeiss). For each brain, six randomly chosen 100x fields of view within the region of interest were acquired with seven z-stack steps at 0.35 µm spacing to generate maximum intensity projections (MIPs) of the z-stacks. Images from all brains for a particular region were acquired using identical settings and data analyses were performed using ImageJ as previously described (Werneburg et al., 2020). The six images from each region per animal were analyzed and averaged to generate a group mean (n=3-4). A consistent threshold range was determined by subjecting images, blinded to genotype, to background subtraction and manual thresholding for each MIP within one experiment (IsoData segmentation method, 15-225). Using the analyze particles function, the thresholded images were used to calculate the total area of SERT fiber inputs.

Electrophysiology

Slice preparation

Mice were anesthetized with isoflurane and decapitated to remove their brains. Brains were quickly cooled in ice-cold, pre-oxygenated (95% O_2/5% CO_2) aCSF containing the following (in mM): 126 NaCl, 2.5 KCl, 1.2 NaH_2PO_4, 1.2 $MgCl_2$, 2.4 $CaCl_2$, 25 $NaHCO_3$, 20 HEPES, 11 D-glucose, 0.4 ascorbic acid, pH adjusted to 7.4 with NaOH. Coronal slices (400 µm) containing hippocampus or dorsal raphe nucleus were prepared in ice-cold aCSF using a vibratome (VT1200 S, Leica Biosystems). Slices were recovered in oxygenated aCSF at room temperature (22-24°C) for at least 1 hour before use. Slices were then transferred to a recording chamber perfused at a rate of 1 ml/min with room temperature, oxygenated aCSF.

Fast scan cyclic voltammetry

5-HT measurements were performed in the radiatum of dorsal CA3 and dorsal raphe nucleus. All experiments and analyses were performed blind to genotype. To detect 5-HT release, carbon fiber electrodes were prepared as previously described (Hashemi et al., 2009; Matsui & Alvarez, 2018). Carbon fiber electrodes consisted of 7-µm diameter carbon fibers (Goodfellow) inserted into a glass pipette (A-M Systems, cat# 602500) with ~150-200 µm of exposed fiber. The exposed carbon fibers were soaked in isopropyl alcohol for 30 min to clean the surface. Next, the exposed fibers were coated with Nafion solution (Sigma) to improve detection sensitivity by inserting the carbon fiber into Nafion solution dropped in a 3 mm diameter circle of twisted reference Ag/AgCl wire for 30 sec with constant application of +1.0 V potential. The carbon fiber electrodes were air dried for 5 min

and then placed in a 70°C oven for 10 min. A modified 5-HT voltage ramp was used, in which the carbon fiber electrode was held at +0.2 V and scanned to +1.0 V, down to -0.1 V, and back to +0.2 V at 1,000 V/s delivered every 100 ms. Prior to recording, the electrodes were conditioned in aCSF with a voltage ramp delivered at 60 Hz for 10 min.

5-HT release was evoked with electrical stimulation (30 pulses, 30 Hz, 150 or 250 µA, 1 ms) from an adjacent custom-made bipolar tungsten electrode every 10 min. The stimulating electrode was placed ~100-200 µm away from the carbon fiber electrode (John et al., 2006). Recordings were performed using a Chem-Clamp amplifier (Dagan Corporation) and Digidata 1550B after low-pass filter at 3 kHz and digitization at 100 kHz. Data were acquired using pClamp10 (Molecular Devices) and analyzed with custom written VIGOR software using Igor Pro 8 (32-bit; Wavemetrics) running mafPC (courtesy of M.A. Xu-Friedman). Carbon fiber electrodes were calibrated with 1 µM 5-HT at the end of the experiment to convert peak current amplitude of 5-HT transients to concentration. Three consecutive traces were obtained and averaged from each recording condition to generate sample traces. Background subtracted peak 5-HT transients and area were determined by subtracting the current remaining after TTX application from the maximum current measured.

Drugs

Serotonin HCl, dopamine HCl, and fluoxetine HCl were obtained from Sigma.

Behavioral assays

All behavioral experiments were performed on male and female mice aged 8 weeks or older during the dark cycle (8 A.M. to 6 P.M.). Animals were habituated to the testing room for 30 minutes before each experiment and all tests were conducted under dim red light conditions and white noise to maintain a constant ambient sound unless otherwise noted. The full behavioral schedule is described in **Table 3.1**. All experiments and analyses were performed in a blind manner. Animals were tested in this order with at least two days of rest in between experiments 1-5 and at least 7 days of rest in between experiments 6 and 7: 1) locomotor activity, 2) open field, 3) elevated plus-maze, 4) grooming, and 5) marble burying, 6) tail suspension test, and 7) forced swim test. Another group of animals was tested with at least two days of rest in between experiments in this order: 1) object interaction test, 2) three-chamber social interaction test, 3) social conditioned place preference, 4) rotarod, and 5) sucrose preference test and quinine preference test. Following rotarod, mice were single housed for at least one week prior to sucrose preference and quinine preference tests. Animals were used in only one behavioral paradigm for the direct social interaction test with the same juvenile conspecific (familiar), direct social interaction test with two different social stimuli (novel), and fear conditioning. Behavioral testing apparatuses were cleaned with 0.1% Micro-90 (International Products Corporation) between each mouse and males and females were tested separately to eliminate odor cues.

Table 3.1 | Behavioral experiment schedule

Group	Experiment
1	≥2 days of rest in between: 1. Locomotor activity 2. Open field 3. Elevated plus-maze 4. Grooming 5. Marble burying ≥7 days of rest in between: 6. Tail suspension test 7. Forced swim test
2	Direct social interaction test (familiar)
3	Direct social interaction test (novel)
4	≥2 days of rest in between: 1. Object interaction test 2. Three-chamber social interaction test 3. Social conditioned place preference 4. Rotarod Single house (≥7 days): 5. Sucrose and quinine preference tests
5	Fear conditioning

Locomotor activity: Locomotor activity of each mouse was tracked in photobeam activity chambers (San Diego Instruments) for 90 minutes. Total horizontal movement was measured in 5-minute bins.

Open field: Mice were placed in the center of an open arena (41 x 38 x 30.5 cm) facing the furthest wall and allowed to freely explore the arena for 10 min. Time spent in the center of the arena (20.5 x 19 cm) as compared with the periphery was automatically tracked with EthoVision XT 11.5 (Noldus).

Elevated plus-maze: The apparatus (Med Associates) consists of four arms, two enclosed with black walls (19 cm high) and two open (35 x 6 cm), connected by a

central axis (6 x 6 cm) and elevated 74 cm above the floor. Mice were placed in the intersection of the maze facing the furthest open arm and allowed to freely explore the maze for 5 min. Time spent in the open and closed arms (index of anxiety-like behavior) and total entries into the open and closed arms (index of locomotor activity) were automatically measured with MED-PC IV software.

Grooming: Self-grooming behavior was scored as previously described (McFarlane et al., 2008; Yang et al., 2007). Mice were habituated for 5 min in an empty mouse cage with no bedding, then grooming behavior was observed for 10 min by an experimenter sitting approximately 2 meters from the testing cage. Cumulative time spent grooming during the 10 min session was recorded using a silenced stopwatch.

Marble burying: 15 sterilized 1.5-cm glass marbles evenly spaced 2 cm apart in three rows of five were placed in a standard mouse cage with 5-6 cm layer of bedding. A mouse was placed in the test for 30 min, then returned to its home cage, and the number of marbles buried to 2/3 of their depth with bedding was counted.

Tail suspension test: Mice were placed in a rectangular TST apparatus (28 x 28 x 42 cm) and suspended by their tails which were wrapped in red lab tape at around 3/4 the distance from the base. Movement was monitored for 6 min and the last 4 min were scored for immobility behavior (absence of righting attempt).

Forced swim test: Mice were placed in a plexiglass cylinder (20 cm diameter, 40 cm height) containing 22±1°C water at a depth of 20 cm to prevent them from escaping and touching the bottom. Immobility, measured as floating in the absence

of movement except for those necessary to keep the head above water, was measured during the last 4 min of a 6 min session. Following the test, mice were gently dried with a clean paper towel and placed in a fresh cage on top of a heating pad for around 10-15 minutes after which they were returned to their home cage (Yankelevitch-Yahav et al., 2015).

Direct social interaction test: The test was adapted from *Hitti et al.* (Hitti & Siegelbaum, 2014). Mice were placed in a standard mouse cage and allowed to habituate for 5 minutes followed by the introduction of a novel sex-matched juvenile mouse. Activity was monitored for 10 min and social behavior initiated by the subject mouse was measured by an experimenter sitting approximately 2 meters from the testing cage with a silenced stopwatch. Scored behaviors were described previously (Kogan et al., 2000): direct contact with the juvenile including grooming and pawing, sniffing including the ano-genital area and mouth and close following (within 1 cm) of the juvenile. After 24 hours, the 10 min test was run again with the previously encountered mouse (familiar) or a second mouse (novel). Any aggressive encounters observed between animals led to exclusion of the subject mouse from analysis.

Object interaction test: The test was adapted from *Molas et al.* (Molas et al., 2017). The apparatus consisted of a custom-made white Plexiglass T-shaped maze (three arms, each 9 x 29.5 x 20 cm, connected through a central 9 x 9 cm zone). Mice were placed in the start arm to habituate to the apparatus for 5 min. Following habituation, they were presented with identical inanimate objects for 5 min/day

located at opposite ends of the T-maze arms for two consecutive days. On day 3, the mice were presented with a new inanimate object that was placed in the same location as the one of the previous objects (counterbalanced) for 5 min. The preference ratio was calculated as: (total novel stimulus investigation – total familiar stimulus investigation) / (total investigation).

Three-chamber social interaction test: Using a standard three-chamber design (Moy et al., 2004), the apparatus consisted of a neutral central zone (18 x 40.5 x 22 cm) connecting two identical compartments (each 19.5 x 40.5 x 22 cm) (Molas et al., 2017). Each of the outer compartments housed a caged cylinder (8 cm diameter, 18 cm height; 1 cm between each vertical rod) to allow limited, but direct physical contact between the subject and stimulus animals. Subject mice were placed in the central zone and habituated to a completely empty apparatus for 5 min then briefly removed to place a juvenile mouse under one of the two caged cylinders while the other caged cylinder remained empty (counterbalanced). The subject mouse was then returned to the apparatus to freely explore all three compartments for 5 min/day for three consecutive days using the same juvenile placed in the same compartment. On Day 3, a novel juvenile mouse was placed in the empty caged cylinder. On days 1 and 2, the preference ratio was calculated as: (total social stimulus investigation – total nonsocial stimulus investigation) / (total investigation). On day 3, the preference ratio was calculated as: (total novel stimulus investigation – total familiar stimulus investigation) / (total investigation).

Social conditioned place preference: The CPP apparatus (Med Associates) consisted of a central neutral zone (10 x 12.5 x 12.5 cm) connecting two outer conditioning chambers (each 16.5 x 12.5 x 12.5 cm), one with black walls and a striped metal floor and the other with white walls and a grid metal floor. The experiment was designed as a three-phase protocol: pre-test, acquisition, and test, and conducted under dim light and sound-attenuated conditions (Molas et al., 2017). An inverted plastic cup (7 cm diameter, 9 cm height) was placed in each of the outer chambers during the acquisition phase. In the pre-test (day 1) and test (day 5) phases, mice were placed in the central zone and allowed to explore the entire apparatus for 20 min. A biased procedure was used in which the least preferred chamber in the pre-test was paired with a social stimulus during the acquisition phase. 24 hours after the pre-test session, the acquisition phase was initiated and consisted of two conditioning trials each day which were separated by 5-6 hours and performed over three consecutive days. During the acquisition phase (days 2, 3, and 4), mice were confined to one chamber in the presence of either a social juvenile stimulus or a nonsocial stimulus (empty cup) for 10 min (counterbalanced for morning and afternoon trials). The preference ratio was calculated as: (time spent in social chamber) / (total time spent in social and nonsocial chambers).

Rotarod: Motor coordination and balance were evaluated on a rotarod apparatus (San Diego Instruments) with an accelerating rotarod test. In each trial, mice were habituated to a rod rotating at 6 rpm for 30 sec, then the rotation was increased to

60 rpm over 5 min. The latency to fall was measured over five trials with an interval of 10 min between each trial. Any mice that remained on the apparatus after 5 min were removed and their time was scored as 5 min.

Sucrose and quinine preference tests: Hedonia/anhedonia was measured in sucrose and quinine preference tests as previously described (Angoa-Perez et al., 2014; Olney et al., 2018). Single- housed mice were habituated to the presence of two 50 ml drinking bottles containing water for 2 days. A stopper with a ball sipper tube was attached to the drinking bottles to minimize loss of fluid. Over the next 4 days, the mice underwent a two-bottle choice with 3% sucrose in water vs water. After a two-day washout period with water, mice were similarly tested with a two-bottle choice of 0.06 mM quinine in water vs water. The bottles were switched daily to prevent potential side preferences. Consumption of water and sucrose or water and quinine were measured once daily. Preference for sucrose was calculated as: (% of consumed sucrose) / (total volume of liquid consumed). Preference for quinine was determined using the same formula.

Fear conditioning: The fear conditioning paradigm was adapted from *Herry et al.* (Herry et al., 2008). Animals were not habituated in the testing room to avoid untimely association with auditory cues. Using the ANY-maze fear conditioning system (Ugo Basile SRL), mice were placed in a fear conditioning cage (17 x 17 x 25 cm) in a sound-attenuating box. The paradigm was performed under no light conditions using two different contexts (context A and B). Mice underwent four phases with 24 hours in between each session: habituation, acquisition, auditory

recall, and contextual recall. On day 1 (context A), mice were habituated to five 30 sec presentations of the CS+ and CS- (white noise) at 80 dB sound pressure level. The inter-cue interval was pseudorandomized and each session with the CS+ or CS- was 10 min. The presentation order of the CS+ and CS- trials were counterbalanced across animals. On day 2 (context A), discriminative fear conditioning was performed by pairing the CS+ with a US (1 sec foot shock, 0.75 mA, 5 CS+/US pairings; intertrial interval: 22-125 s). The onset of the US coincided with the last second of the CS+. On day 3, auditory recall was measured in context B with 5 presentations of CS+ and CS-. On day 4, contextual recall was measured in context A for 10 min. ANY-maze software was used to analyze freezing behavior (no movement detected for 1 sec), which was scored automatically with an infrared photobeam assay in the fear conditioning cage.

Statistical analyses

Results are represented as mean ± SEM. Statistical significance was set at $p < 0.05$ and evaluated using unpaired or paired two-tailed Student's t-tests and two-way ANOVA or two-way repeated measures ANOVA with Šidák's post hoc testing for normally distributed data. Mann Whitney U tests were used for nonparametric data. Analyses were carried out with Graphpad (Graphpad Software).

Results

5-HT neuron-specific expression of Nrxn isoforms and validation of the Fev/RFP/NrxnTKO mouse line

To understand the expression frequency of Nrxn isoforms in 5-HT neurons, we performed double FISH for *Nrxns* (*αNrxn1-3*, *βNrxn1-3*) and tryptophan hydroxylase 2 (*Tph2*), a marker of 5-HT neurons, and measured the colocalization of *Nrxn* mRNA-positive signals observed in *Tph2*+ 5-HT neurons in the dorsal raphe nucleus (DRN) (**Figure 3.1A, B**) and median raphe nucleus (MRN) (**Figure 3.1C, D**). *αNrxn1* and *αNrxn2* were the predominantly expressed isoforms in both the DRN and MRN. *βNrxn3*/*Tph2*+ neurons consisted of 40-50% of the total number of *Tph2*+ cells in the DRN and MRN. Less than 20% of *Tph2*+ 5-HT neurons overlapped with *αNrxn3*, *βNrxn1*, and *βNrxn2* signals. These results indicate that αNrxn1 and αNrxn2 are the major Nrxn isoforms in the DRN and MRN.

To test *in vivo* and *in vitro* roles of Nrxns in 5-HT neurons, we generated a 5-HT neuron-specific *Nrxn* triple knockout (TKO) mouse line by crossing 5-HT neuron-specific Cre, tdTomato reporter, and triple Nrxn1/2/3 floxed lines (Fev^{Cre}/$^{lox\text{-}STOP\text{-}lox}$tdTomato/$Nrxn1^{f/f}/2^{f/f}/3^{f/f}$: Fev/RFP/NrxnTKO). Cre-negative littermates and Fev/RFP mice were used as WT controls. The specific deletion of Nrxns in 5-HT neurons was confirmed by single-cell RT-qPCR (**Figure 3.1E-H**) in Fev/RFP (WT) and Fev/RFP/NrxnTKO mice. The Fev/RFP/NrxnTKO line was fertile and viable and did not demonstrate obvious differences in gross appearance.

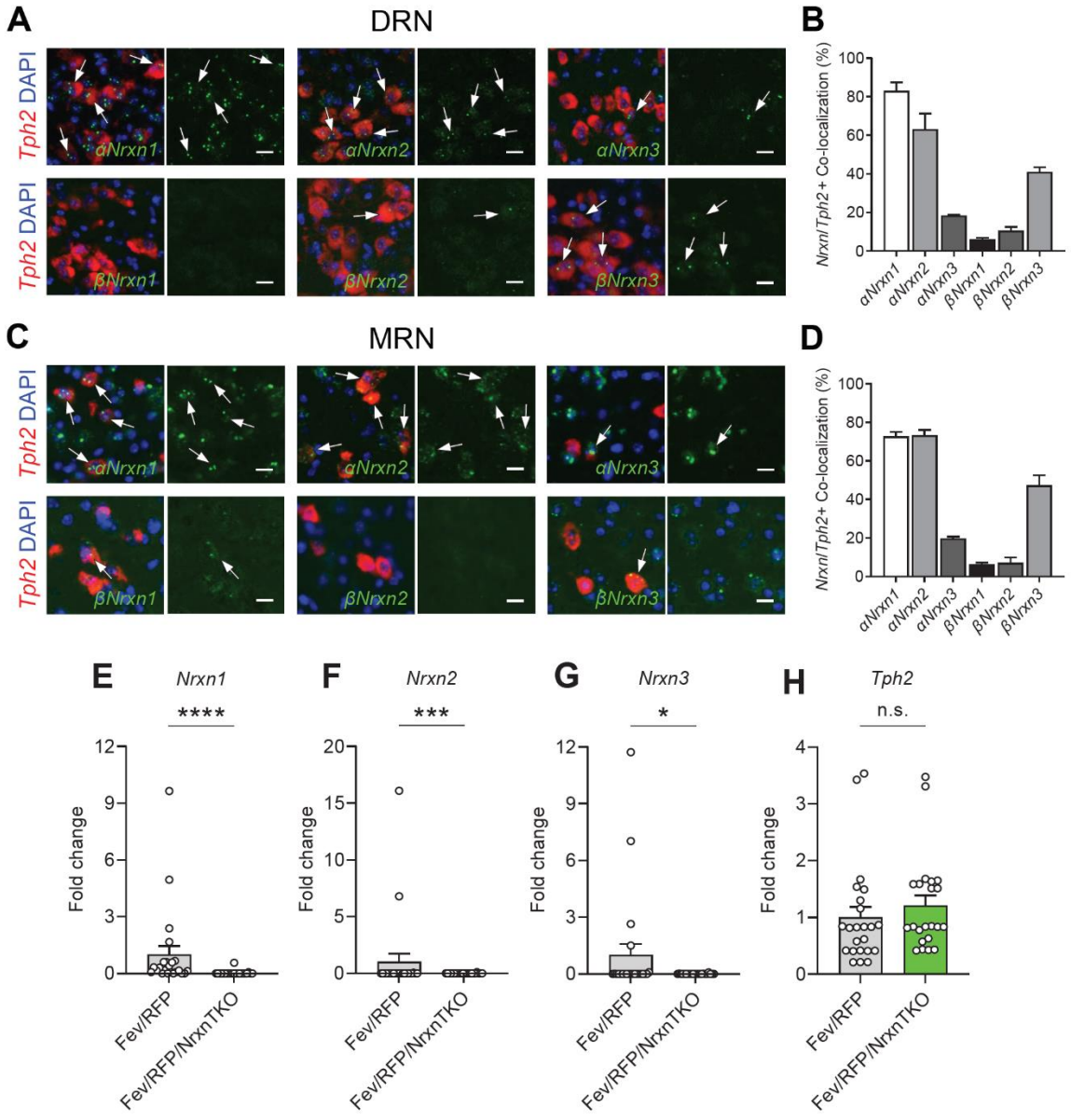

Figure 3.1 | Nrxn mRNA expression in the raphe nuclei and confirmation of Nrxn deletion in Fev/RFP/NrxnTKO mice. (**A, C**) Expression of *Nrxn* mRNA in the dorsal raphe nucleus (DRN) and median raphe nucleus (MRN). Double FISH for *Nrxn* mRNA (green) and *Tph2*+ 5-HT neurons (red). Arrows represent *Nrxn* puncta in *Tph2*-positive neurons. Nuclei were stained with DAPI (blue). (**B, D**) Co-localization quantification was based on the expression of at least 1 *Nrxn* puncta in *Tph2*+ neurons (n = 2). (**E, F, G, H**) Validation of the Fev/RFP/NrxnTKO mouse line. Expression of *Nrxn* genes were compared between tdTomato-positive 5-HT+ neurons prepared from Fev/RFP and Fev/RFP/NrxnTKO mice. qPCRs against *Nrxn 1, 2, 3*, *Tph2*, and *Gapdh* (internal control) were performed for single-cell cDNA libraries prepared from tdTomato-positive neurons. Number of neurons: Fev/RFP (n = 23, 4 mice) and Fev/RFP/NrxnTKO (22, 4). Data are

reported as mean ± SEM. n.s., not significant, * $p < 0.05$, *** $p < 0.001$, **** $p < 0.0001$; Mann-Whitney U test. Scale bars, 20 µm.

Reduced 5-HT release in Fev/RFP/NrxnTKO mice

Deletion of Nrxns has been shown to impair neurotransmitter release including glutamate, GABA, and acetylcholine (Born et al., 2015; L. Y. Chen et al., 2017; F. Luo et al., 2020; Missler et al., 2003; Sons et al., 2006; W. Zhang et al., 2005). To test whether Nrxns are involved in modulatory 5-HT release, we measured 5-HT transients in the DRN and hippocampus using fast scan cyclic voltammetry (FSCV). 5-HT release was recorded with a voltage ramp (**Figure 3.2A**) delivered through Nafion-coated carbon-fiber electrodes (Hashemi et al., 2009; Matsui & Alvarez, 2018). We confirmed 5-HT detection through direct application of 5-HT and DA (**Figure 3.2B**). No significant current was produced from DA and current-voltage (CV) plots displayed the expected currents for 5-HT oxidation and reduction peak potentials (0.6 V and -0.1 V; **Figure 3.2B insets**), indicating selective recording of 5-HT with minimal contribution from DA.

5-HT transients were recorded in the DRN of adult male WT and Fev/RFP/NrxnTKO mice. Electrical stimulation (30 pulses, 30 Hz, 1 ms) (John et al., 2006) was applied at two different stimulus strengths (150 and 250 µA) to evoke 5-HT release in acute brain slices containing the DRN. We confirmed that FSCV transients were mediated by electrically evoked 5-HT by applying the selective serotonin reuptake inhibitor fluoxetine (FLX; 10 µM) and sodium channel blocker tetrodotoxin (TTX; 1 µM). The expected oxidation peaks for 5-HT in the CV

plots acquired from WT (**Figure 3.2C**) and Fev/RFP/NrxnTKO (**Figure 3.2D,**) mice were similar to those recorded during exogenous 5-HT application. A reduction in the peak 5-HT amplitude was observed in Fev/RFP/NrxnTKO mice (**Figure 3.2E**). FLX application prolonged 5-HT transient area which verified that the FSCV transients detected 5-HT signals. WT and Fev/RFP/NrxnTKO mice showed similar responses to FLX (**Figure 3.2F**). TTX completely abolished peak transients indicating that FSCV measurements were mediated by action potential-induced 5-HT release (Carboni & Di Chiara, 1989).

Next, we performed FSCV recordings in the hippocampus to determine whether differences in 5-HT release could be detected in distal regions receiving 5-HT fiber projections. Dorsal hippocampal CA3 stratum radiatum was chosen because of its dense 5-HT innervation (Awasthi et al., 2021; Moore & Halaris, 1975). As we observed in the DRN, the CV plots for WT (**Figure 3.2G**) and Fev/RFP/NrxnTKO mice (**Figure 3.2H**) demonstrated the expected 5-HT oxidation peak potential. 5-HT currents were significantly reduced in Fev/RFP/NrxnTKO mice compared with WT mice at both stimulus strengths (**Figure 3.2J**). FLX application increased 5-HT transient area in WT but not Fev/RFP/NrxnTKO mice (**Figure 3.2J**). Taken together, these findings indicate that Nrxns are important for 5-HT release.

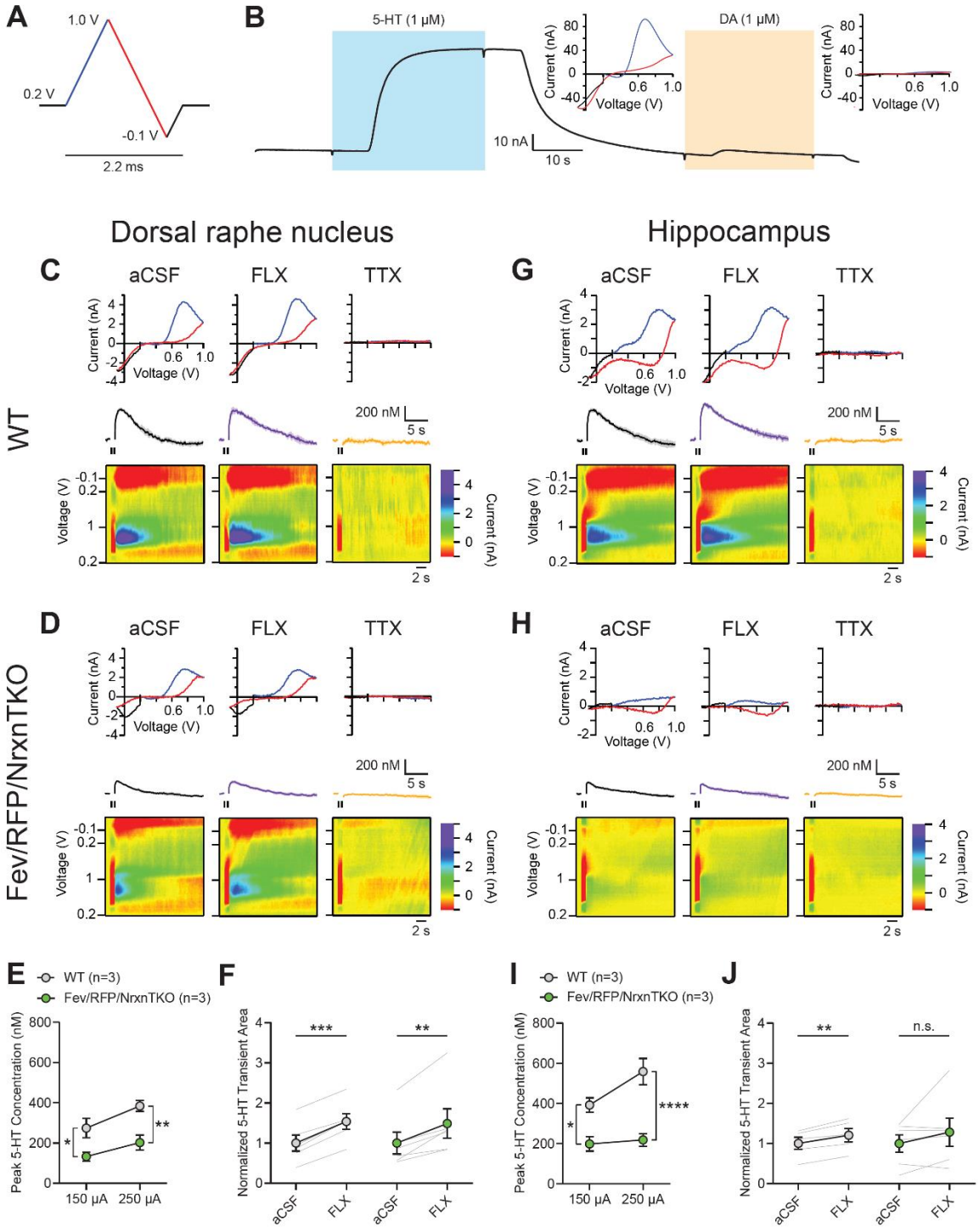

Figure 3.2 | The lack of Nrxns in 5-HT neurons reduces evoked 5-HT release in the dorsal raphe nucleus and hippocampus. (**A**) Voltage ramp protocol for detecting 5-HT with FSCV. (**B**) Representative current traces when measuring 5-HT (1 μM, blue) or dopamine (DA; 1 μM, orange) using Nafion-coated carbon-fiber microelectrodes

calibrated on a 5-HT voltage ramp. Insets: Background-subtracted CV plots of the electrochemical current when 5-HT (left) or DA (right) was applied. (**C, D**) Electrically evoked 5-HT transients detected in the dorsal raphe nucleus (DRN) of WT (n = 3) (**C**) and Fev/RFP/NrxnTKO (n = 3) (**D**) mice during perfusion with aCSF (left), SERT blocker FLX (10 µM, middle), and action potential-blocking TTX (1 µM, right). Top: representative CV plots of the electrochemical current in aCSF, FLX, and TTX. Middle: average 5-HT transients under each condition. Bottom: background-subtracted 3D voltammograms (false color scale) as a function of time (x axis, 20 s) and voltage applied (y axis). (**E**) Peak amplitude of 5-HT transients evoked using a 150 µA or 250 µA stimulation train in the DRN of WT (gray) and Fev/RFP/NrxnTKO (green) mice. 5-HT release was significantly different between genotypes (two-way repeated measures ANOVA: genotype main effect, $F_{1,10}$ = 12.02, $^{\#\#}$ p = 0.006; stimulation strength main effect, $F_{1,10}$ = 26.89, p = 0.0004; stimulus strength x genotype interaction, $F_{1,10}$ = 1.936, p = 0.2648). (**F**) Normalized area of 5-HT transients recorded in the DRN before and after FLX application. Gray lines represent paired measurements. 5-HT transient area before and after FLX was significantly different in WT (paired two-tailed Student's t-test: t_5 = 11.05, *** p = 0.0001) and Fev/RFP/NrxnTKO mice (paired two-tailed Student's t-test: t_5 = 4.111, ** p = 0.0093). (**G, H**) Electrically evoked 5-HT transients detected in the hippocampus of WT (n = 3) (**G**) and Fev/RFP/NrxnTKO (n = 3) (**H**) mice during perfusion with aCSF (left), SERT blocker FLX (10 µM, middle), and action potential-blocking TTX (1 µM, right). Top: representative CV plots of the electrochemical current in aCSF, FLX, and TTX. Middle: average 5-HT transients under each condition. Bottom: background-subtracted 3D voltammograms (false color scale) as a function of time (x axis, 20 s) and voltage applied (y axis). (**I**) Peak amplitude of 5-HT transients evoked using a 150 µA or 250 µA stimulation train in the hippocampus of WT and Fev/RFP/NrxnTKO mice. 5-HT release at each stimulation strength was significantly different between groups (two-way repeated measures ANOVA with Šidák's post hoc test following significant stimulation strength x genotype interaction, $F_{1,9}$ = 6.982, p = 0.0268; stimulation strength main effect, $F_{1,9}$ = 11.24, p = 0.0085; genotype main effect, $F_{1,9}$ = 24.56, p = 0.0008). (**J**) Normalized area of 5-HT transients recorded in the hippocampus before and after FLX application. Gray lines represent paired measurements. 5-HT transient area before and after FLX was significantly different in WT (paired two-tailed Student's t-test: t_4 = 5.591, ** p = 0.005) whereas no differences in 5-HT transient area before and after FLX were found in Fev/RFP/NrxnTKO mice (paired two-tailed Student's t-test: t_5 = 1.244, p = 0.2686). Data are expressed as mean ± SEM. n.s. not significant, * p < 0.05, ** p < 0.01, *** p < 0.001, **** p < 0.0001.

Altered 5-HT fiber connectivity in Fev/NrxnTKO/RFP mice

5-HT fibers are distributed throughout the brain to modulate diverse physiological functions and behaviors (Okaty et al., 2019; Ren et al., 2018; Ren et al., 2019). We sought to identify 5-HT projection patterns in areas known to integrate 5-HT signals and regulate complex behaviors, particularly the prefrontal cortex (Garcia-

Garcia et al., 2017; Puig et al., 2005), nucleus accumbens (Dolen et al., 2013; Walsh et al., 2018), amygdala (Jiang et al., 2009; Quah et al., 2020), hippocampus (Hitti & Siegelbaum, 2014; Okuyama et al., 2016), and dorsal raphe nucleus (Balazsfi et al., 2018; J. Luo et al., 2017). In adult male WT and Fev/RFP/NrxnTKO mice, we analyzed serotonin transporter (SERT) innervation to the medial prefrontal cortex (mPFC; Bregma 2.1 ± 0.3 mm), nucleus accumbens core and shell (NAcc, NAcSh; Bregma 1.18 ± 0.3 mm), basolateral and medial amygdala (BLA, MeA; Bregma -1.64 ± 0.4 mm), stratum oriens of the CA1, CA2, and CA3 subregions of the dorsal hippocampus (dCA1, dCA2, dCA3; Bregma -1.46 ± 0.4 mm), stratum oriens of the CA1 subregion of the ventral hippocampus (vCA1; -3.16 ± 0.4 mm), and dorsal raphe nucleus (DRN; Bregma -4.56 ± 0.4 mm). We found that SERT-positive fibers were reduced in the dorsal hippocampus (**Figure 3.3F-H**) and DRN (**Figure 3.3J**) and elevated in the mPFC (**Figure 3.3A**) and BLA (**Figure 3.3AE**). dCA3 showed the greatest SERT area among the dorsal hippocampal subregions which is consistent with other reports (Awasthi et al., 2021; Muzerelle et al., 2016). The DRN contained the highest SERT-positive fiber density followed by the BLA (**Figure 3.3K**) in WT mice. The BLA demonstrated 18.1% SERT area innervation (vs. 22.9% in the DRN) which supports previous work that it is one of the most densely labeled areas in the brain (Awasthi et al., 2021). In contrast, Fev/RFP/NrxnTKO mice showed the highest area of SERT in the BLA given the reduction of DRN fibers. DRN innervation was reduced the most (24.8% decrease) and mPFC received more SERT inputs (41% increase) in 5-HT

neurons lacking Nrxns. No differences were seen in projection density in the NAcc, NAcSh, MeA, and vCA1 (**Figure 3.3B-D, I**) indicating that SERT inputs are not globally altered. Fibers to the vCA1 showed a nonsignificant trend for decreased SERT innervation in the absence of 5-HTergic Nrxns. These findings suggest that Nrxns selectively mediate SERT-positive fiber area depending on the innervated circuit.

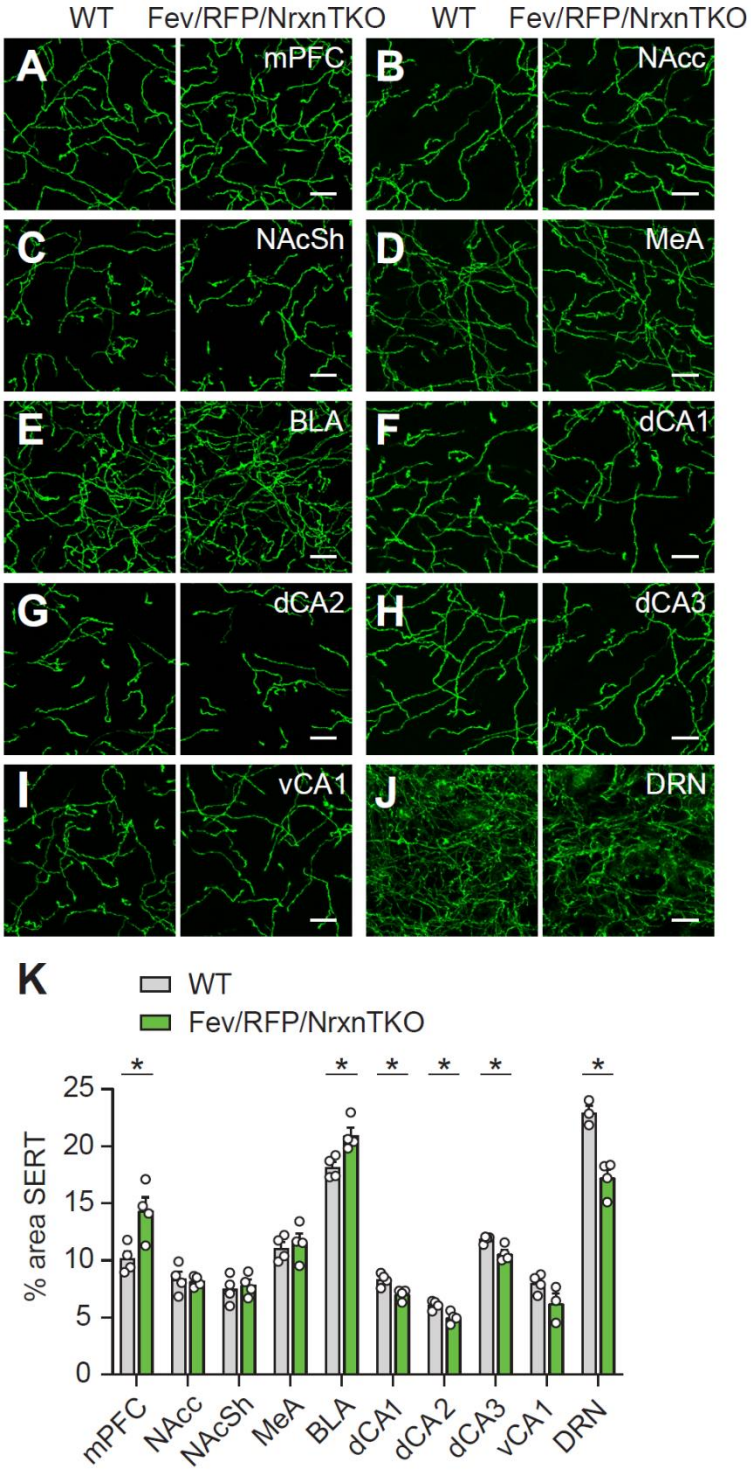

Figure 3.3 | The loss of Nrxns in 5-HT neurons alters 5-HT connectivity. (**A-H**) Representative 100x images of SERT-positive fibers in the medial prefrontal cortex (mPFC) (**A**), nucleus accumbens core (NAcc) (**B**), nucleus accumbens shell (NAcSh) (**C**),

medial amygdala (MeA) (**D**), basolateral amygdala (BLA) (**E**), dorsal hippocampal CA1-3 subregions (dCA1, 2, 3) (**F-H**), ventral hippocampal CA1 (vCA1) (**I**), and dorsal raphe nucleus (DRN) (**J**). The images are maximum intensity projections of 21 z-stacks across a 7 µm z-depth using 0.35 µm z-steps. (**K**) Quantification of the area of SERT-positive fibers revealed that the absence of Nrxns altered 5-HT innervation in specific brain regions (n = 3-4 mice/genotype). Data are expressed as mean ± SEM. * $p < 0.05$; unpaired two-tailed Student's t-test. Scale bars, 10 µm.

Behavioral testing of the Fev/NrxnTKO/RFP mouse line

To assess the behavioral effects of selective Nrxn deletion in 5-HT neurons, we compared the performance of adult (>8-week-old) male and female WT and Fev/RFP/NrxnTKO mice in studies of motor skills, anxiety, social behavior, learning and memory, repetitive behaviors, and depression. First, spontaneous locomotion was examined over a 90-min period. There were no differences in locomotor activity between WT and Fev/RFP/NrxnTKO mice (**Figure 3.S1A, B**). Females in general moved more than males (**Figure 3.S1C**). Rotarod was used to assess motor coordination and the latency to fall was comparable in both males and females regardless of genotype (**Figure 3.S1D, E**). The absence of Nrxns in 5-HT neurons also did not affect anxiety-like behaviors in the mouse line (**Figure 3.S2**). Compared with males, females spent less time in the center of an open field (**Figure 3.S2A**) and were more active in the elevated plus-maze (**Figure 3.S2E**). These results suggest that 5-HTergic Nrxns are not involved in exploratory locomotor and anxiety-related behaviors although baseline locomotor activity and anxiety levels differed by sex.

Given these normal behaviors that could have confounded differences detected between genotypes, we next assessed 5-HTergic Nrxns in social

behavior. WT and Fev/RFP/NrxnTKO underwent a direct social interaction test to examine naturally occurring interaction between a subject mouse and a sex-matched juvenile (4- to 6- week-old) stimulus mouse. In trial 1, the stimulus mouse was unfamiliar to the subject mouse. After 24 hours, the subject mouse was re-exposed to the same stimulus mouse from trial 1 (**Figure 3.2A**) or introduced to a new unfamiliar stimulus mouse (**Figure 3.2D**). Social memory was measured as a reduction in time that the subject mouse spent investigating the stimulus mouse in trial 2. We found that male Fev/RFP/NrxnTKO mice spent less time exploring the stimulus mouse in trial 1 compared with WT mice, demonstrating impaired sociability (**Figure 3.2B**). Male WT mice reduced their investigation of the familiar conspecific on trial 2 whereas Fev/RFP/NrxnTKO mice similarly investigated the juvenile mouse across both trials. These results suggest that Fev/RFP/NrxnTKO mice have social memory deficits, however, the effect is unclear in the context of reduced sociability. Among females, Fev/RFP/NrxnTKO mice displayed no differences in interaction for the familiar stimulus mouse compared with WT mice (**Figure 3.2C**) and both groups showed reduced investigation of the familiar conspecific in trial 2. During the direct social interaction test with two unfamiliar juvenile mice across the two trials (**Figure 3.2D**), male WT and Fev/RFP/NrxnTKO mice exhibited similar investigation of the stimulus mice, indicating intact social novelty preference (**Figure 3.2E**). Both groups spent less time with the second conspecific compared with the first. Unexpectedly, interaction with the juvenile stimulus mouse on day 1 was similar between WT and Fev/RFP/NrxnTKO mice.

The lack of reproducible sociability deficits could be due to variable social exploratory behavior displayed by WT mice. During the first trial of the direct social interaction test, WT investigation was 79.32 ± 12.05 sec (mean ± SEM) prior to re-introduction of the same conspecific (familiar) whereas investigation was 59 ± 7.442 sec prior to exposure to a new juvenile mouse (novel). In contrast, Fev/RFP/NrxnTKO mice showed similar investigation of the stimulus mice in trial 1 between experiments: 49.9 ± 8.485 sec (familiar) and 54.18 ± 6.106 sec (novel). For females tested in the direct social interaction test with two novel conspecifics, no genotype differences were observed and both groups showed significant reduction of interaction with the second stimulus mouse (**Figure 3.2F**). These findings suggest that the absence of Nrxns in 5-HT neurons specifically impacts social approach behavior in males.

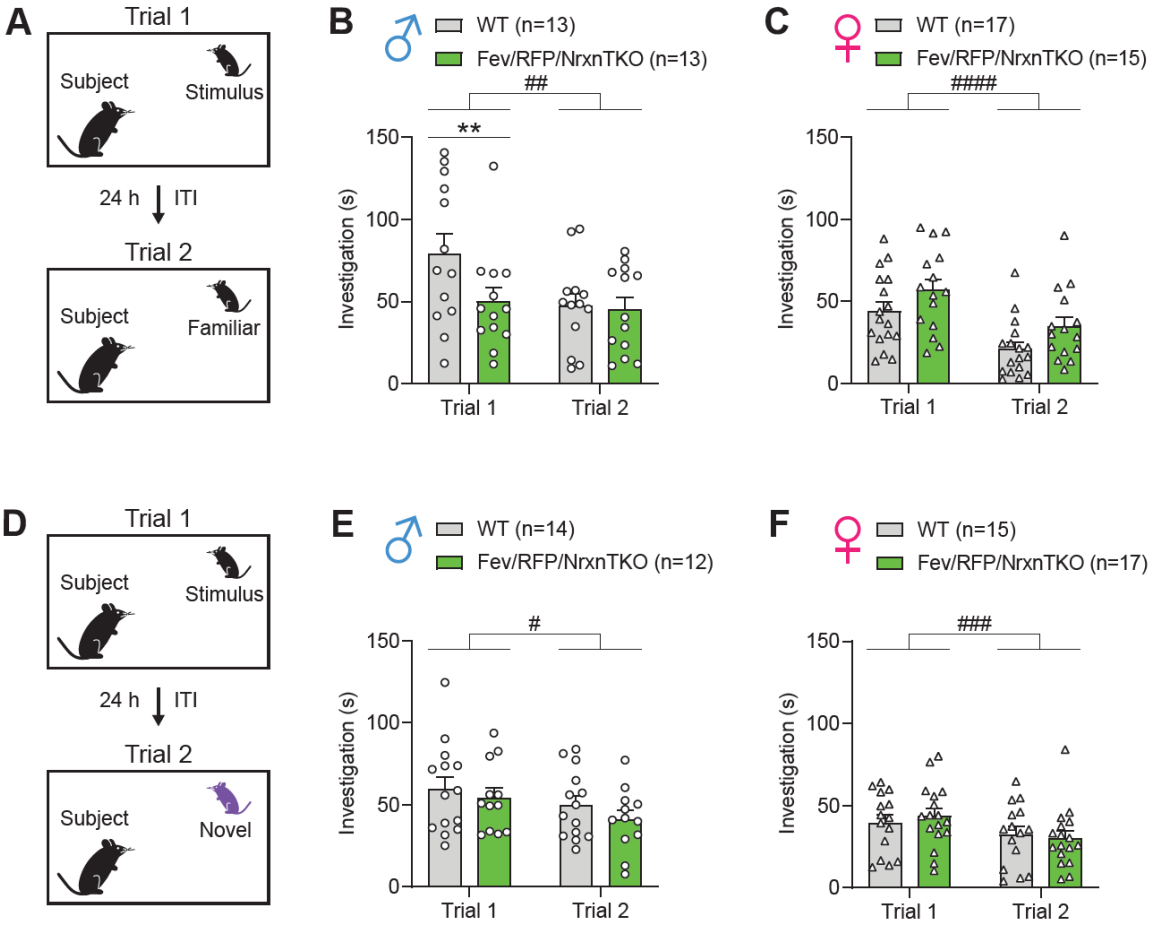

Figure 3.4 | Nrxn-deficient 5-HT signaling impairs social behavior in males. (**A**) Direct social interaction test using the same juvenile stimulus across two trials. (**B**) Male (circular border) WT (gray, n = 13) and Fev/RFP/NrxnTKO (green, n = 13) mice differed in their investigation of the juvenile stimulus across the two trials (two-way repeated measures ANOVA with Šidák's post hoc test following significant trial x genotype interaction, $F_{1,24}$ = 4.344, p = 0.0479, ** p = 0.0024). Both groups spent less time exploring the juvenile stimulus during trial 2 than in trial 1 (two-way repeated measures ANOVA: trial main effect, $F_{1,24}$ = 7.855, $^{\#\#}$ p = 0.0099; genotype main effect, $F_{1,24}$ = 2.086, p = 0.1616). (**C**) Female (triangular border) WT (n = 17) and Fev/RFP/NrxnTKO (n = 15) mice did not differ in their investigation of the juvenile stimulus (two-way repeated measures ANOVA: trial x genotype interaction, $F_{1,30}$ = 0.0242, p = 0.8774). The investigation of the juvenile stimulus was reduced in both groups (two-way repeated measures ANOVA: trial main effect, $F_{1,30}$ = 30.08, $^{\#\#\#\#}$ p < 0.0001; genotype main effect, $F_{1,30}$ = 4.161, p = 0.0502). (**D**) Direct social interaction test using novel juvenile stimuli across two trials. (**E**) Male WT (n = 14) and Fev/RFP/NrxnTKO (n = 12) mice explored the two novel juvenile stimuli similarly (two-way repeated measures ANOVA: trial x genotype interaction, $F_{1,24}$ = 0.141, p = 0.7106). Both groups spent less time investigating the novel juvenile stimulus in trial 2 (two-way repeated measures ANOVA: trial main effect, $F_{1,24}$ = 6.608, $^{\#}$ p = 0.0168; genotype main effect, $F_{1,24}$ = 0.8833, p = 0.3567). (**F**) Female WT (n = 15) and Fev/RFP/NrxnTKO (n = 17) mice did

not spend different amounts of time exploring the juvenile stimuli (two-way repeated measures ANOVA: trial x genotype interaction, $F_{1,30} = 1.586$, $p = 0.2177$). Both groups decreased their investigation of the second novel stimulus compared with the first (two-way repeated measures ANOVA: trial main effect, $F_{1,30} = 17.79$, $^{\#\#\#}$ $p = 0.0002$; genotype main effect, $F_{1,30} = 0.01552$, $p = 9017$). Data are expressed as mean ± SEM. ** $p < 0.01$; Trial 1 vs. trial 2: $^{\#}$ $p < 0.05$, $^{\#\#}$ $p < 0.01$, $^{\#\#\#}$ $p < 0.001$, $^{\#\#\#\#}$ $p < 0.0001$.

To further study sociability and social novelty in the Fev/RFP/NrxnTKO mouse line, we conducted a three-chamber social interaction test, in which a stimulus mouse was confined to a cylinder to limit direct interaction (**Figure 3.S3A**). Both male (**Figure 3.S3B, C**) and female (**Figure 3.S3D, E**) WT and Fev/RFP/NrxnTKO mice showed similar preferences for a stimulus mouse than for a second empty cylinder in a different chamber (days 1 and 2) and for a novel stimulus mouse than for the previously encountered juvenile conspecific (day 3). Male WT and Fev/RFP/NrxnTKO mice showed different investigation behavior on day 1. However, there were no differences in exploration of the cylinder-contained social stimulus between groups which contrasts the sociability deficits observed in the direct social interaction test. Male Fev/RFP/NrxnTKO mice also displayed intact social novelty preference on day 3, where we would expect to see similar exploration times of both the novel and familiar conspecifics or reduced investigation time. Social reward preference was also assessed in a social conditioned preference test (**Figure 3.S4A**). Mice were conditioned to associate one chamber of the apparatus with a social stimulus placed underneath a cup and another chamber with an empty cup representing a nonsocial stimulus. No genotype differences were observed among males (**Figure 3.S4B**) and females

(**Figure 3.S4C**). Across sexes, both groups demonstrated increased preference for the social stimulus-paired chamber during the post-test. These results suggest that social behavior and social reward preference in the context of limited direct interaction are intact in Fev/RFP/NrxnTKO mice.

We examined whether aspects of memory were affected by the loss of Nrxns in 5-HT neurons. We performed a 3-day object interaction test (**Figure 3.S5A**) and found that both male (**Figure 3.S5B, C**) and female (**Figure 3.S5D, E**) WT and Fev/RFP/NrxnTKO mice demonstrated no differences in investigation of identical objects on days 1 and 2 and a novel object over a familiar one on day 3. Associative memory was tested through fear conditioning (**Figure 3.S6A**). Male WT and Fev/RFP/NrxnTKO mice showed no differences in learning the foot shock-cue association (**Figure 3.S6B**) and recalling the specific cue (**Figure 3.S6C**) and context (**Figure 3.S6D**) that they received the shock. Female Fev/RFP/NrxnTKO mice showed elevated fear learning acquisition (**Figure 3.S6E**), however, no differences in memory recall (**Figure 3.S6F, G**) were observed. These results suggest that Fev/RFP/NrxnTKO mice have normal object and associative memory and females have heightened fear learning during associative foot shock administration.

We next tested repetitive behaviors, a core feature of ASD, in the Fev/RFP/NrxnTKO mouse line. No significant differences between genotypes across both sexes were found in marble burying (**Figure 3.S7A**) and self-grooming (**Figure 3.SB, C**) tests. In general, females spent less time grooming than males.

These results suggest that 5-HT neuron-specific TKO of Nrxns does not affect repetitive behaviors. Lastly, we examined depressive-like behaviors using assays that measure coping strategies in response to despair-related stress and anhedonia. In a tail suspension test, both male (**Figure 3.5A**) and female (**Figure 3.5B**) WT and Fev/RFP/NrxnTKO mice showed no differences in immobility during the 6 min session. In contrast, male Fev/RFP/NrxnTKO mice demonstrated increased immobility behavior compared with WT mice in the forced swim test (**Figure 3.5C**). No differences in the number of immobile episodes were seen across genotypes in both sexes (**Figure 3.5D**). Anhedonia was assessed using sucrose and quinine preference tests. We found that male and female WT and Fev/RFP/NrxnTKO mice showed similar preferences for sucrose (**Figure 3.S8A, B**). No differences were seen among males for quinine preference (**Figure 3.S8C**) whereas female Fev/RFP/NrxnTKO mice showed a nonsignificant trend for reduced quinine consumption compared with WT mice (**Figure 3.S8D**). These results demonstrate impaired coping responses to behavioral despair in male Fev/RFP/NrxnTKO mice and no involvement of 5-HTergic Nrxns in depressive-related anhedonia.

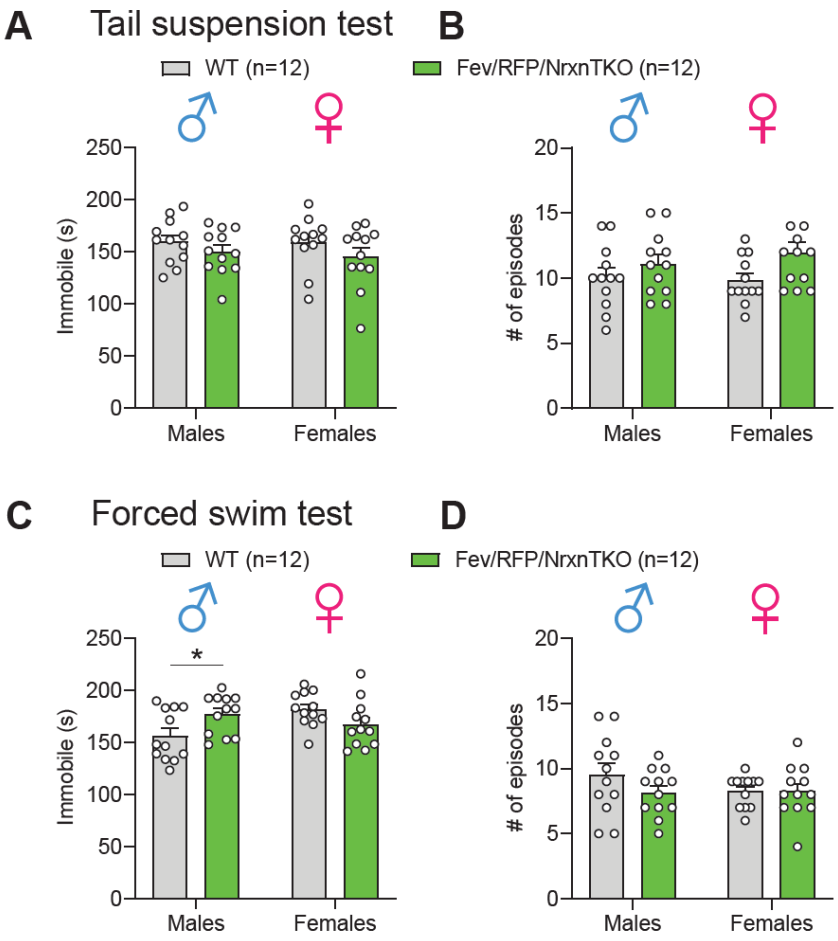

Figure 3.5 | Removal of Nrxns in 5-HT neurons generates depressive-like behavior. (**A**) Male WT (n = 12) and Fev/RFP/NrxnTKO (n = 12) mice and female WT (n = 12) and Fev/RFP/NrxnTKO (n = 12) mice showed no differences in despair-associated coping strategies in the tail suspension test (two-way ANOVA: genotype main effect, $F_{1,44} = 2.681$, $p = 0.1087$; sex main effect, $F_{1,44} = 0.1299$, $p = 0.7203$; interaction, $F_{1,44} = 0.09853$, $p = 0.7551$). (**B**) No differences in the number of immobile episodes were observed although there was an effect of genotype (two-way ANOVA: genotype main effect, $F_{1,44} = 4.819$, $p = 0.0335$; interaction, sex main effect, $F_{1,44} = 0.1725$, 0.6799; interaction, $F_{1,44} = 0.5949$, $p = 0.4447$). (**C**) A significant interaction between sex and genotype was observed for immobile behavior in the forced swim test that was driven by male Fev/RFP/NrxnTKO mice (two-way repeated measures ANOVA with Šidák's post hoc test following significant interaction, $F_{1,44} = 8.699$, $p = 0.0051$, * $p = 0.0375$; sex main effect, $F_{1,44} = 1.678$, $p = 0.202$; genotype main effect, $F_{1,44} = 0.2465$, $p = 0.622$). Data are expressed as mean ± SEM, * $p < 0.05$.

Discussion

Although much progress has been made in characterizing the functions of genes that increase the risk of ASD (Autism Spectrum Disorders Working Group of The Psychiatric Genomics, 2017; Grove et al., 2019; Yuen et al., 2017; Zoghbi & Bear, 2012), the etiology of ASD remains elusive. Nrxn variants (Tromp et al., 2021; J. Wang et al., 2018) and 5-HT dysfunction (C. L. Muller et al., 2016; Nakamura et al., 2010) have separately been found to be involved in ASD. Collectively, our study demonstrates three ways in which Nrxns act in the 5-HT system through the selective deletion of Nrxns in 5-HT neurons. First, our FSCV experiments showed that the absence of Nrxns decreased 5-HT release with no differences in FLX-mediated uptake in the DRN. Just as Nrxns affect neurotransmitter release at excitatory and inhibitory synapses (Born et al., 2015; L. Y. Chen et al., 2017; F. Luo et al., 2020; Missler et al., 2003; W. Zhang et al., 2005), our results demonstrate that Nrxns are required for normal 5-HT release. Second, the lack of 5-HTergic Nrxns reduced SERT-positive projections to the DRN and dorsal hippocampus, increased innervation to the mPFC and BLA, and did not affect 5-HT fibers to the nucleus accumbens, MeA, and ventral hippocampus. These findings suggest that Nrxns affect the distribution of SERT-positive 5-HT fibers in distinct brain regions. Third, sociability and despair-associated coping responses were impaired in male Fev/RFP/NrxnTKO mice. Female Fev/RFP/NrxnTKO mice behaved similarly to WT mice although they demonstrated a specific elevation in fear learning acquisition. No other alterations in behaviors were observed,

suggesting a sex-dependent phenotype in social and depressive-like behaviors. Taken together, Nrxns modulate multiple aspects of 5-HT signaling viewed through molecular, physiological, and behavioral standpoints.

While Nxns have non-canonical roles at different synapses (L. Y. Chen et al., 2017), many studies have highlighted its role in efficient neurotransmitter release by coupling Ca^{2+} channels to presynaptic release machinery (Anderson et al., 2015; F. Luo et al., 2020; Missler et al., 2003; Sudhof, 2017). In one of the earliest studies defining Nrxns in the neurotransmitter release process, αNrxn TKO led to early postnatal death and impaired excitatory and inhibitory neurotransmitter release due to reduced Ca^{2+} channel function (Missler et al., 2003). Pan-Nrxn deletion in the calyx of Held synapse suppressed glutamate release by reducing the function of Ca^{2+}-activated big potassium channels and decreased active zone-associated proteins although Ca^{2+} channel number and function remained intact (F. Luo et al., 2020). βNrxn KO was shown to decrease glutamate release probability and action potential-induced Ca^{2+} influx but did not alter the readily releasable vesicle pool (Anderson et al., 2015).

Here we provided evidence that Nrxns influence neuromodulatory 5-HT release. FLX-mediated uptake kinetics were unchanged in the DRN between genotypes whereas application of FLX in the hippocampus increased 5-HT transient area in WT but not Fev/RFP/NrxnTKO mice. The lack of change following FLX treatment in Fev/RFP/NrxnTKO mice appears to be due to the low levels of 5-HT that may not be sufficient to alter extracellular 5-HT detected following SERT

blockade. It is important to consider the precise mechanisms through which Nrxns influence release events and the specific sites that express Nrxns to control 5-HT neurotransmission. In the hippocampus, approximately 80% of varicosities are extra-synaptic, while the remaining 20% form synapses (Oleskevich et al., 1991). Indeed, Nrxns have been found to modify acetylcholine release at neuromuscular junctions which lack postsynaptic neuronal partners (Sons et al., 2006). Given the predominance of non-junctional specializations, we speculate that Nrxns reside at 5-HT release sites that lack a direct postsynaptic target. Utilization of SLENDR (single-cell labeling of endogenous proteins by CRISPR-Cas9-mediated homology-directed repair) could allow us to explore the subcellular localization of Nrxns in 5-HT fibers (Mikuni et al., 2016). Moreover, the ability of Nrxns to couple with release machinery triggering 5-HT vesicle exocytosis and its role in postsynaptic differentiation at synapses is yet to be explored.

The distribution of 5-HT fibers from the raphe nuclei to practically all brain regions allows 5-HT to modify neurotransmission in the specific circuits it innervates. SERT acts in close proximity to sites with vesicle proteins to facilitate 5-HT reuptake (Haase et al., 2017; H. K. Muller et al., 2014). The molecular architecture of 5-HT release sites is not well-defined, however, studies have demonstrated presynaptic proteins in different compartments of 5-HT neurons. Human induced pluripotent stem cell-derived 5-HT neurons expressed the active zone protein Bassoon evenly along the soma and extensions (Jansch et al., 2021). Synaptophysin puncta in SERT-labeled axons were found to interact with

excitatory and inhibitory synapses (Belmer et al., 2017) and co-localize with vesicular glutamate transporter type 3 (VGluT3) for dual 5-HT and glutamate release (H. L. Wang et al., 2019). A more direct evaluation of synaptic players in 5-HT release sites and postsynaptic specializations could be performed to better define structural aspects of 5-HT signaling.

We found that the DRN and hippocampus displayed a profound reduction in 5-HT exocytosis and were innervated by fewer SERT-positive fibers. Decreased SERT innervation suggests that 5-HTergic Nrxns reduce fiber formation, regulate the abundance of SERT itself, or that inefficient 5-HT release requires less SERT as a compensatory mechanism. Indeed, sparse pan-Nrxn deletion has been shown to blunt inferior olive neuron climbing fiber projections in the cerebellum while complete removal of Nrxns at the climbing fiber synapse did not alter climbing fiber axons but impaired synaptic transmission (L. Y. Chen et al., 2017). Unexpectedly, SERT fiber density in the mPFC and BLA was increased in 5-HT neurons that lack Nrxns. This suggests a primary disturbance in 5-HT signaling that results in increased innervation or a response to attenuate perturbed circuits. The DRN has been shown to decrease activity in the mPFC (Puig et al., 2005) and BLA (Jiang et al., 2009). A recent study found that SERT innervation to the amygdala was increased in participants with ASD (Lew et al., 2020) and PET-visualized metabolism was higher in the prefrontal cortex of participants with major depression (Brody et al., 2001). Treatment with the selective serotonin reuptake inhibitor paroxetine attenuated hyperactivity in the mPFC and alleviated

depressive symptoms. It is possible that reduced 5-HT release requires more SERT-positive fibers to increase available 5-HT (and its reuptake) to alleviate impaired inhibitory control from raphe nuclei or maintain signaling homeostasis. 5-HT release in the mPFC was not directly tested and it is not clear if our FSCV findings can be extended to other brain areas. The complex interplay between 5-HT concentration, clearance, autoreceptor-mediated feedback inhibition, and postsynaptic responses that contributes to 5-HT neurotransmission must be considered to address these considerations.

We utilized the Cre/LoxP system to remove Nrxns specifically in 5-HT neurons. 5-HT signaling is known to influence brain development including neuron migration (Frazer et al., 2015; Jacobshagen et al., 2014) and circuit formation (E. Deneris & Gaspar, 2018; Migliarini et al., 2013; Vitalis et al., 2013). It is possible that the decrease in SERT-positive fibers could be attributed to altered 5-HT projection patterns during the prenatal period when 5-HT circuits begin to take shape. A knock-in mouse line that replaced TPH2 with an enhanced green fluorescent protein (eGFP) reporter demonstrated that mice lacking the ability to synthesize 5-HT showed an elevation of SERT fiber density in the hippocampus and nucleus accumbens compared with heterozygous knock-in mice (Migliarini et al., 2013). In contrast, our mouse line showed no differences in SERT innervation to the nucleus accumbens and reduced SERT distribution to the hippocampus. It appears that the potential developmental contribution of 5-HTergic Nrxns cannot

fully explain the molecular differences we observed. An inducible knockout mouse line could be generated to investigate postnatal effects of Nrxns in the 5-HT system.

The loss of Nrxns in 5-HT neurons generated specific behavioral phenotypes despite extensive 5-HT innervation throughout the brain. In contrast, global KO of αNrxn1 (Etherton et al., 2009; Grayton et al., 2013) and αNrxn2 (Born et al., 2015; Dachtler et al., 2014) produced ASD-associated behaviors and elevated anxiety. Although αNrxn1 is highly expressed in 5-HT neurons (**Figure 3.1**) and global αNrxn1 KO mice showed increased grooming behavior (Etherton et al., 2009), no abnormalities in repetitive behaviors were found in the mouse line. It appears that the absence of Nrxns in the 5-HT system is not sufficient to broadly alter behavior, suggesting that overall network function remains intact. Reduced sociability was only observed in the direct social interaction test and not in other social behavioral tests. This deficit was not reproduced in the direct social interaction test with two novel juvenile stimuli suggesting that any presumed social behavioral phenotypes due to the loss of Nrxns in 5-HT neurons are subtle.

The increase in immobile behavior observed in males supports a relationship between low DRN activity due in part to low extracellular 5-HT and depressive-like behaviors (Bambico et al., 2009; Lira et al., 2003). Moreover, DRN 5-HT hyperactivity has been associated with active coping responses to depressive-like stress (Nishitani et al., 2019; Teissier et al., 2015). We found that floating behavior was only altered in the forced swim test. One possibility is that Fev/RFP/NrxnTKO mice are more susceptible to stress because the forced swim

test was performed following the tail suspension test. Stress effects could be evaluated by subjecting mice to a chronic unpredictable stress paradigm prior to testing in the tail suspension or forced swim tests (Monteiro et al., 2015). Another explanation is that the forced swim test may model negative symptoms (e.g., loss of motivation, anhedonia) more accurately than the tail suspension test (Chatterjee et al., 2012), however, no differences in anhedonia were observed in the mouse line. Additionally, female Fev/RFP/NrxnTKO mice displayed a specific impairment in fear learning. This behavior could be due to heightened pain sensitivity because freezing behavior during cued and contextual memory recall was similar between WT and Fev/RFP/NrxnTKO mice. Indeed, the 5-HT system is implicated in pain modulation (Paredes et al., 2019; Sommer, 2010) and pain behaviors can be evaluated using nociception assays (Deuis et al., 2017).

We present evidence that Nrxns control critical aspects of 5-HT signaling that were observed following their selective deletion in 5-HT neurons. An important finding was that Nrxns impaired 5-HT release in the DRN and hippocampus, which also received fewer SERT-positive fibers. Increased SERT innervation was observed in the mPFC and BLA which reiterates the role of Nrxns as organizers of distinct synaptic properties in specific circuits. The observed deficits in sociability and depressive-related behaviors are relevant to ASD which often presents with co-occurring conditions. These results reveal that Nrxns expressed in the neuromodulatory 5-HT system are important for maintaining the presynaptic molecular function of 5-HT release sites. Correlating physiological events with the

output of complex behaviors is essential for gaining greater insights on disorders with enigmatic origins like ASD. New investigations can examine the precise signaling consequences of Nrxn deletion in raphe nuclei-innervated circuits and whether 5-HT therapeutics can improve behavioral deficits. Deciphering the contributions of brain-wide signaling mechanisms paves the way for personalized interventions especially when considering the heterogenous presentations of ASD.

Supplemental Information

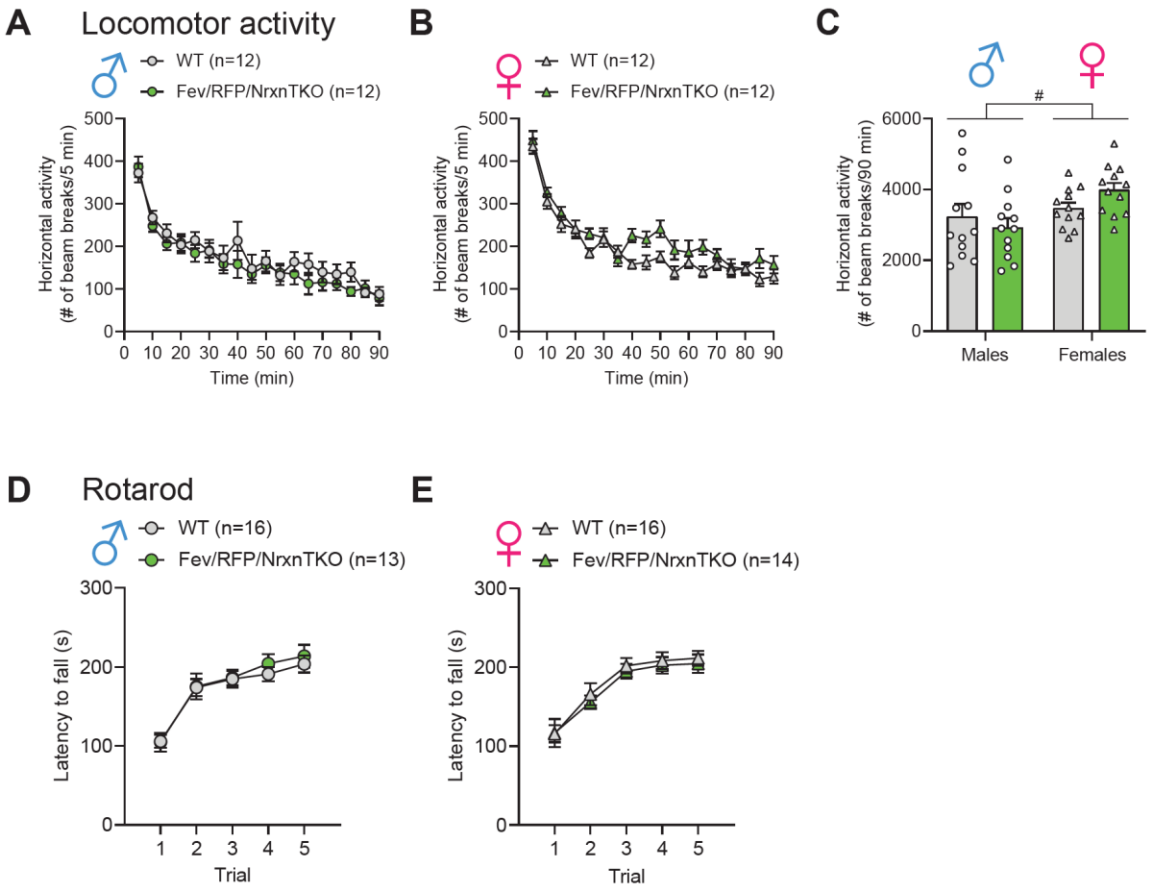

Figure 3.S1 | Locomotor activity and rotarod performance are unaffected by the deletion of Nrxns in 5-HT neurons. (**A**) Male WT (n = 12) and Fev/RFP/NrxnTKO (n = 12) mice showed no differences in horizontal locomotor activity (two-way repeated measures ANOVA: genotype main effect, $F_{1,22}$ = 0.4666, p = 0.5017; time x genotype interaction, $F_{17,374}$ = 0.9467, p = 0.5188). (**B**) No differences in horizontal locomotor activity were detected between female WT (n = 12) and Fev/RFP/NrxnTKO (n = 12) mice (two-way repeated measures ANOVA: genotype main effect, $F_{1,22}$ = 4.035, p = 0.057; trial x genotype interaction, $F_{17,374}$ = 1.559, p = 0.0724). (**C**) Cumulative locomotor activity did not differ between WT and Fev/RFP/NrxnTKO mice over the 90 min period (two-way ANOVA: genotype main effect, $F_{1,44}$ = 0.1682, p = 0.6837; sex x genotype interaction, $F_{1,44}$ = 2.541, p = 0.1181). Females moved significantly more than males (two-way ANOVA: sex main effect, $F_{1,44}$ = 6.302, $^{\#}$ p = 0.0158). (**D**) Male WT (n = 16) and Fev/RFP/NrxnTKO (n = 13) mice showed no differences in latency to fall over 5 trials of accelerating rotarod (two-way repeated measures ANOVA: genotype main effect, $F_{1,27}$ = 0.2204, p = 0.6425; trial x genotype interaction, $F_{4,108}$ = 0.2161, p = 0.929). (**E**) Female WT (n = 16) and Fev/RFP/NrxnTKO (n = 14) mice showed no differences in latency to fall over 5 trials of accelerating rotarod (two-way repeated measures ANOVA: genotype main effect, $F_{1,28}$ =

0.1803, p = 0.6743; trial x genotype interaction, $F_{4,112}$ = 0.1747, p = 0.951). Data are expressed as mean ± SEM. Males vs. females: $^{\#}$ p < 0.05.

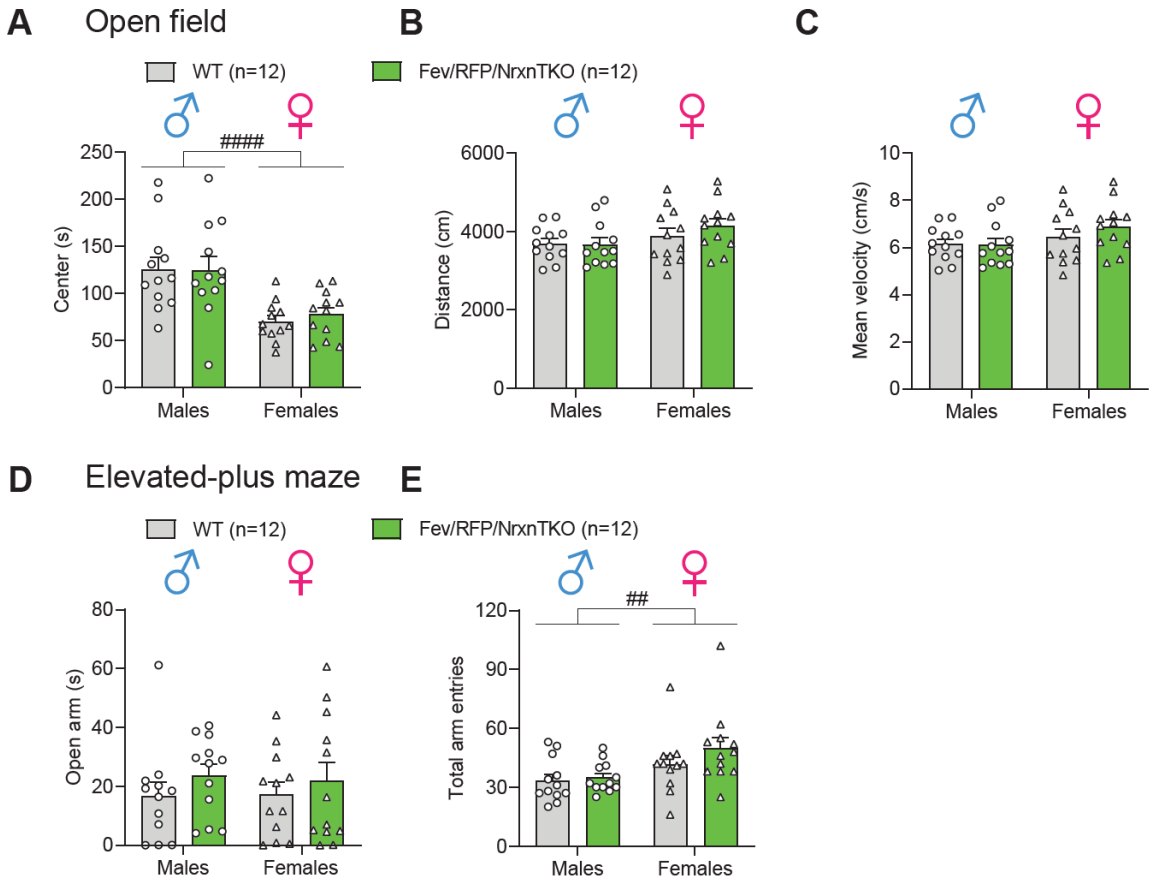

Figure 3.S2 | Anxiety-like behavior is unaltered by the lack of Nrxns in 5-HT neurons. (**A**) Male WT (n = 12) and Fev/RFP/NrxnTKO (n = 12) mice and female WT (n = 12) and Fev/RFP/NrxnTKO (n = 12) mice showed no differences in time spent in the center of the open field arena (two-way ANOVA: genotype main effect, $F_{1,44} = 0.09494$, $p = 0.7594$; sex x genotype interaction, $F_{1,44} = 0.1537$, $p = 0.6969$). Females spent less time in the center than males (two-way ANOVA: sex main effect, $F_{1,44} = 21.75$, $^{\#\#\#\#}$ $p < 0.0001$). (**B**) There were no differences across both sexes for the distance traveled during open field (two-way ANOVA: genotype main effect, $F_{1,44} = 0.5135$, $p = 0.4774$; sex main effect, $F_{1,44} = 3.736$, $p = 0.597$; sex x genotype interaction, $F_{1,44} = 0.7166$, $p = 0.4018$). (**C**) No differences were observed for both sexes for the mean velocity the mice moved during open field (two-way ANOVA: genotype main effect, $F_{1,44} = 0.5135$, $p = 0.4774$; sex main effect, $F_{1,44} = 3.736$, $p = 0.597$; sex x genotype interaction, $F_{1,44} = 0.7166$, $p = 0.4018$). (**D**) The time the mice spent in the open arms during the elevated plus-maze was similar between genotypes for both sexes (two-way ANOVA: genotype main effect, $F_{1,44} = 1.458$, $p = 0.2338$; sex main effect, $F_{1,44} = 0.02036$, $p = 0.8872$; sex x genotype interaction, $F_{1,44} = 0.06707$, $p = 0.7969$). (**E**) WT and Fev/RFP/NrxnTKO mice both demonstrated similar total arm entries (two-way ANOVA: genotype main effect, $F_{1,44} = 1.385$, $p = 0.2456$; sex x genotype interaction, $F_{1,44} = 0.682$, $p = 0.4134$). Females demonstrated more movement during the session than males (two-way ANOVA: sex main effect, $F_{1,44} = 8.354$, $^{\#\#}$ $p < 0.006$). Data are expressed as mean ± SEM. Males vs. females: $^{\#\#}$ $p < 0.01$, $^{\#\#\#\#}$ $< p < 0.0001$.

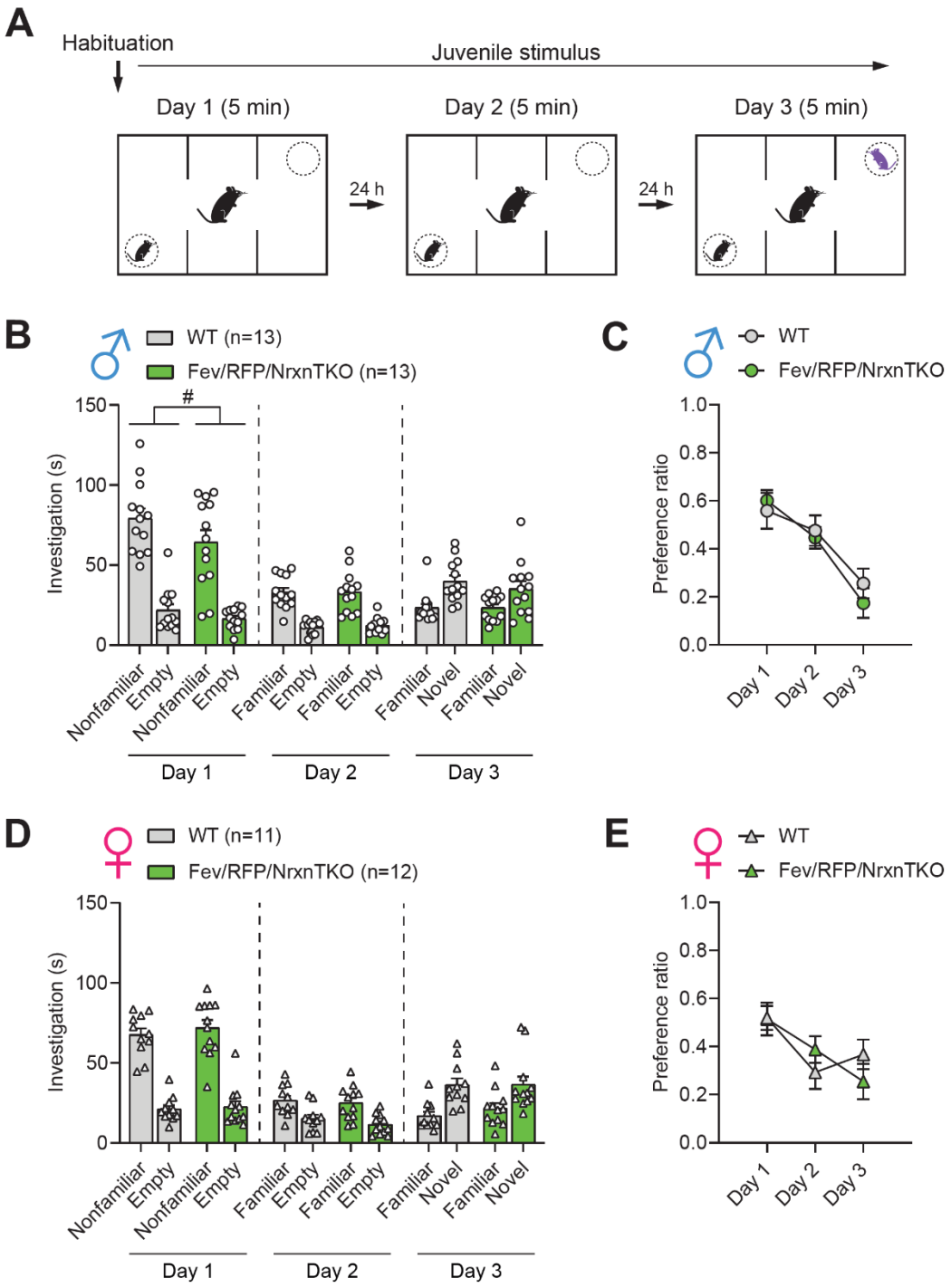

Figure 3.S3 | Social behavior in the three-chamber social interaction test is preserved in Fev/RFP/NrxnTKO mice. (**A**) Protocol for three-chamber social interaction test. (**B**) Male WT (n = 13) and Fev/RFP/NrxnTKO (n = 13) preferred the social stimulus over the nonsocial stimulus on day 1 (two-way repeated measures ANOVA: stimulus main effect, $F_{1,24} = 77.08$, $p < 0.0001$; stimulus x genotype interaction, $F_{1,24} = 0.6324$, $p = 0.4243$)

and day 2 (two-way repeated measures ANOVA: stimulus main effect, $F_{1,24} = 83.16$, $p < 0.0001$; stimulus x genotype interaction, $F_{1,24} = 0.03609$, $p = 0.8509$). Both groups preferred the novel stimulus over the familiar stimulus on day 3 (two-way repeated measures ANOVA: stimulus main effect, $F_{1,24} = 18.3$, $p = 0.0003$; stimulus x genotype interaction, $F_{1,24} = 0.4758$, $p = 0.4969$). Genotype differences were observed only on day 1 (two-way repeated measures ANOVA on day 1: genotype main effect, $F_{1,24} = 4.798$, $^{\#}$ $p = 0.0384$; day 2: genotype main effect, $F_{1,24} = 0.05209$, $p = 0.8214$; day 3: genotype main effect, $F_{1,24} = 0.4063$, $p = 0.5299$). (**C**) The preference ratio for a social stimulus differed across days (two-way repeated measures ANOVA: day main effect, $F_{1.951,46.82} = 20.67$, $p < 0.0001$), but no differences were seen between groups (two-way repeated measures ANOVA: genotype main effect, $F_{1,24} = 0.1992$, $p = 0.6594$; day x genotype interaction, $F_{2,48} = 0.5837$, $p = 0.5617$). (**D**) Female WT (n = 11) and Fev/RFP/NrxnTKO (n = 12) preferred the social stimulus over the nonsocial stimulus and novel stimulus over the familiar stimulus (two-way repeated measures ANOVA on day 1: stimulus main effect, $F_{1,21} = 110.4$, $p < 0.0001$; genotype main effect, $F_{1,21} = 0.8124$, $p = 0.3776$; stimulus x genotype interaction, $F_{1,21} = 0.8984$, $p = 0.7673$; day 2: stimulus main effect, $F_{1,21} = 38.33$, $p < 0.0001$; genotype main effect, $F_{1,21} = 0.7325$, $p = 0.4017$; stimulus x genotype interaction, $F_{1,21} = 0.3221$, $p = 0.5764$; day 3: stimulus main effect, $F_{1,21} = 31.66$, $p < 0.0001$; genotype main effect, $F_{1,21} = 0.294$, $p = 0.5934$; stimulus x genotype interaction, $F_{1,21} = 0.5623$, $p = 0.4616$). (**E**) The preference ratio for a social stimulus differed across days (two-way repeated measures ANOVA: day main effect, $F_{1.983,41.64} = 5.084$, $p = 0.0108$), but no differences were seen between groups (two-way repeated measures ANOVA: genotype main effect, $F_{1,21} = 0.03346$, $p = 0.8566$; day x genotype interaction, $F_{2,42} = 1.103$, $p = 0.3412$). Data are expressed as mean ± SEM. WT vs. Fev/RFP/NrxnTKO: $^{\#}$ $p < 0.05$.

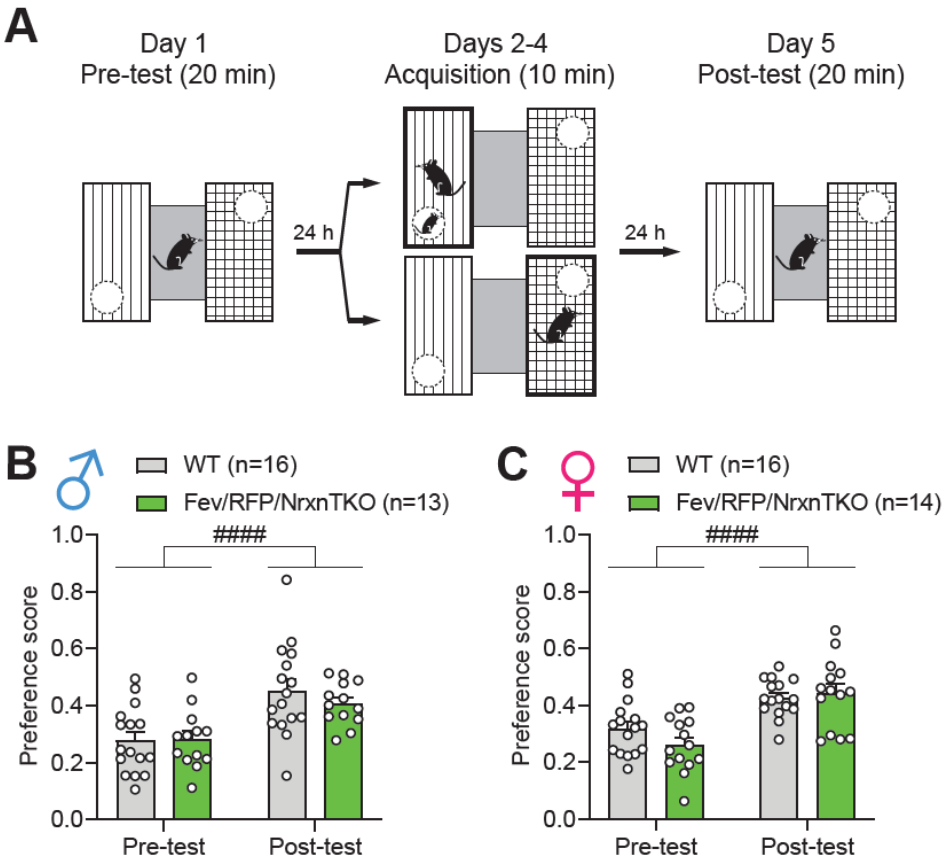

Figure 3.S4 | Removal of Nrxns in 5-HT neurons does not alter social reward behavior. (**A**) Protocol for social conditioned place preference. (**B**) Male WT (n = 16) and Fev/RFP/NrxnTKO (n = 13) preferred the social stimulus-paired over the nonsocial stimulus-paired chamber following the test (two-way repeated measures ANOVA: test phase main effect, $F_{1,27} = 54.18$, #### $p < 0.0001$; genotype main effect, $F_{1,27} = 0.2351$, $p = 0.6317$; test phase x genotype interaction, $F_{1,27} = 1.395$, $p = 0.2479$). (**C**) Female WT (n = 16) and Fev/RFP/NrxnTKO (n = 14) preferred the social stimulus-paired over the nonsocial stimulus-paired chamber following the test (two-way repeated measures ANOVA: test phase main effect, $F_{1,28} = 52.31$, #### $p < 0.0001$; genotype main effect, $F_{1,28} = 0.5395$, $p = 0.4687$; test phase x genotype interaction, $F_{1,28} = 3.415$, $p = 0.0752$). Data are expressed as mean ± SEM. Pre-test vs. post-test: #### $p < 0.0001$.

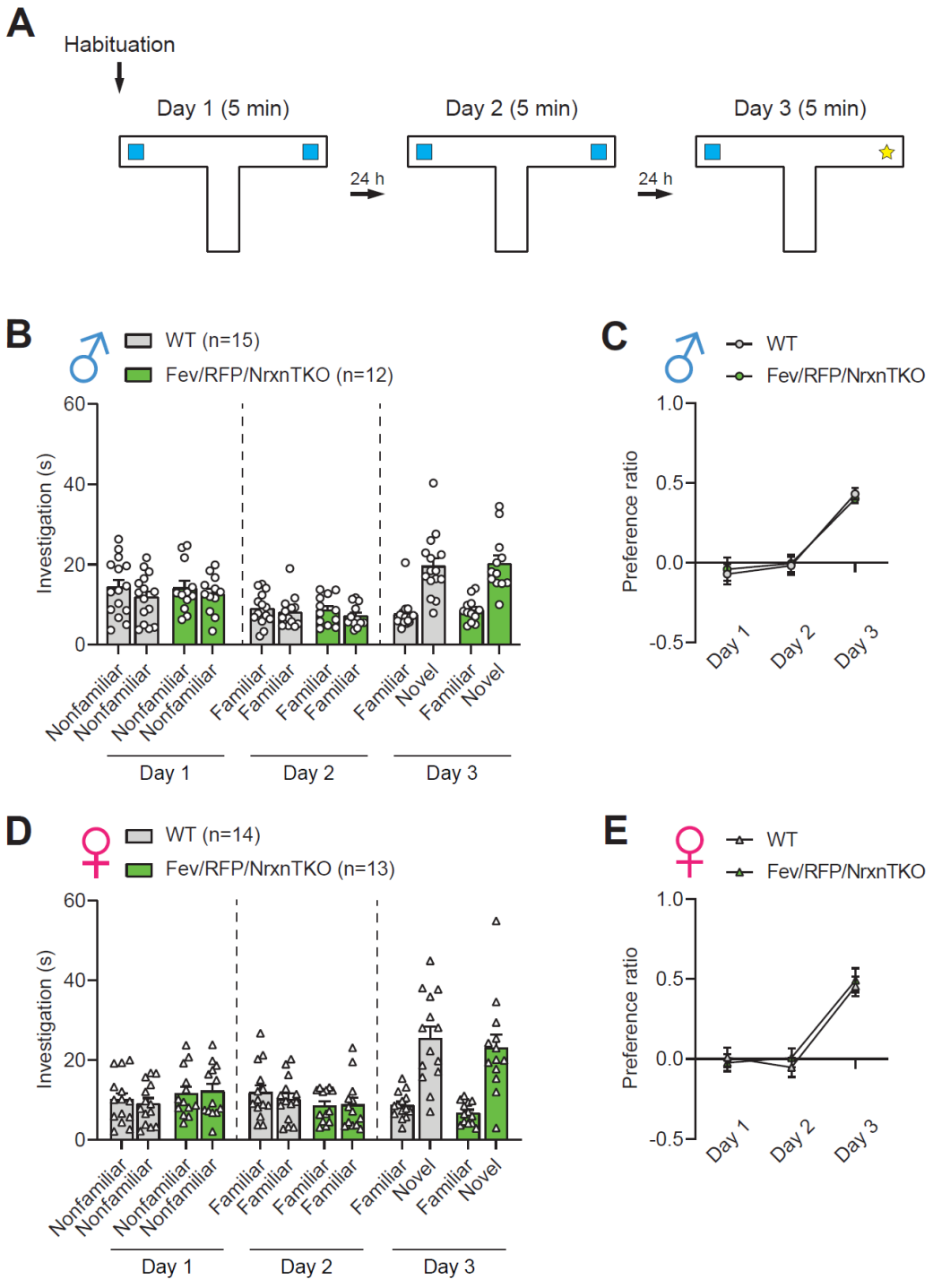

Figure 3.S5 | Object recognition is not affected by the loss of Nrxns in 5-HT neurons. (**A**) Protocol for object interaction test. (**B**) Male WT (n = 15) and Fev/RFP/NrxnTKO (n = 12) showed no preference for identical objects on day 1 (two-way repeated measures ANOVA: stimulus main effect, $F_{1,25}$ = 2.606, p = 0.119; genotype main effect, $F_{1,25}$ =

0.02422, p = 0.8776; stimulus x genotype interaction, $F_{1,25}$ = 0.1923, p = 0.6648) and day 2 (two-way repeated measures ANOVA: stimulus main effect, $F_{1,25}$ = 3.18, p = 0.0867; genotype main effect, $F_{1,25}$ = 0.27, p = 0.6079; stimulus x genotype interaction, $F_{1,25}$ = 0.1825, p = 0.6729) and preferred the novel object over the familiar object on day 3 (two-way repeated measures ANOVA: stimulus main effect, $F_{1,25}$ = 129.6, p < 0.0001; genotype main effect, $F_{1,25}$ = 0.1452, p = 0.7064; stimulus x genotype interaction, $F_{1,25}$ = 0.03164, p = 0.8603). (**C**) The preference ratio for the objects differed across days (two-way repeated measures ANOVA: day main effect, $F_{1.932,48.3}$ = 47.7, p < 0.0001), but no differences were seen between groups (two-way repeated measures ANOVA: genotype main effect, $F_{2,50}$ = 0.008519, p = 0.9272; day x genotype interaction, $F_{2,50}$ = 0.1781, p = 0.8374). (**D**) Female WT (n = 14) and Fev/RFP/NrxnTKO (n = 13) showed no preference for identical objects and preferred the novel object over the familiar object (two-way repeated measures ANOVA on day 1: stimulus main effect, $F_{1,25}$ = 0.05374, p = 0.8186; genotype main effect, $F_{1,25}$ = 1.167, p = 0.2904; stimulus x genotype interaction, $F_{1,25}$ = 0.876, p = 0.3583; day 2: stimulus main effect, $F_{1,25}$ = 0.5898, p = 0.4497; genotype main effect, $F_{1,25}$ = 1.372, p = 0.2525; stimulus x genotype interaction, $F_{1,25}$ = 0.9663, p = 0.335; day 3: stimulus main effect, $F_{1,25}$ = 64.01, p < 0.0001; genotype main effect, $F_{1,25}$ = 0.6659, p = 0.4222; stimulus x genotype interaction, $F_{1,25}$ = 0.01182, p = 0.9143). (**E**) The preference ratio for the objects differed across days (two-way repeated measures ANOVA: day main effect, $F_{1.996,49.9}$ = 43.36, p < 0.0001), but no differences were seen between groups (two-way repeated measures ANOVA: genotype main effect, $F_{1,25}$ = 0.1566, p = 0.6957; day x genotype interaction; $F_{2,50}$ = 0.3318, p = 0.7192). Data are expressed as mean ± SEM.

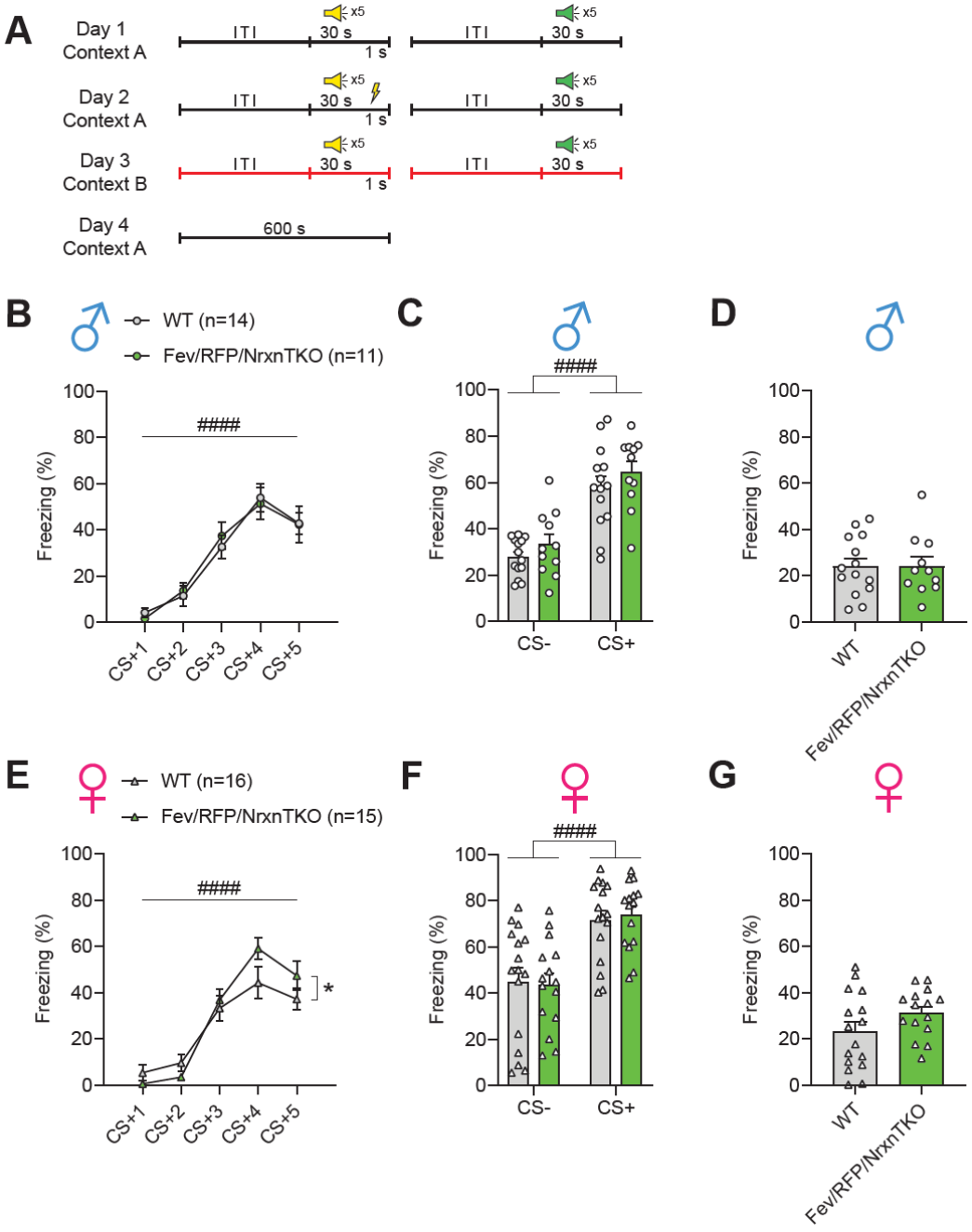

Figure 3.S6 | Fev/RFP/NrxnTKO mice show preserved fear conditioning responses and female-specific deficits in fear learning. (**A**) Protocol for fear conditioning. (**B**) Male WT (n = 14) and Fev/RFP/NrxnTKO (n = 11) mice both showed differences in freezing behavior across the presentations associated with the foot shock (CS+) (two-way repeated measures ANOVA: stimulus main effect, $F_{2.607,59.97} = 45.06$, $^{\#\#\#\#}$ $p < 0.0001$). No differences were seen between groups (two-way repeated measures ANOVA: genotype main effect, $F_{1,23} = 0.00339$, $p = 0.9541$; stimulus x genotype interaction, $F_{4,92} = 0.2652$, p

= 0.8996). (**C**) Among males, freezing to the CS+ was increased relative to the CS- (stimulus with no association between auditory cue and foot shock) (two-way repeated measures ANOVA: stimulus main effect, $F_{1,23} = 85.22$, #### $p < 0.0001$), but no differences were detected between groups (two-way repeated measures ANOVA: genotype main effect, $F_{1,23} = 1.67$, $p = 0.2091$; stimulus x genotype interaction, $F_{1,23} = 0.03121$, $p = 0.8613$). (**D**) Male mice showed no altered freezing behavior during contextual recall (unpaired two-tailed Student's t-test: $t_{23} = 0.01457$, $p = 0.9885$). (**E**) Female WT (n = 16) and Fev/RFP/NrxnTKO (n = 15) mice showed differences in freezing to the CS+ after consecutive presentations with shock (two-way repeated measures ANOVA: stimulus main effect, $F_{2.723,78.96} = 62.16$, #### $p < 0.0001$; genotype main effect, $F_{1,29} = 0.6774$, $p = 0.4172$; stimulus x genotype interaction, $F_{4,116} = 2.728$, * $p = 0.0325$). (**F**) Among females, freezing to the CS+ was increased relative to the CS- (two-way repeated measures ANOVA: stimulus main effect, $F_{1,29} = 38.92$, #### $p < 0.0001$), but no differences were detected between groups (two-way repeated measures ANOVA: genotype main effect, $F_{1,29} = 0.02049$, $p = 0.8872$; stimulus x genotype interaction, $F_{1,29} = 0.1367$, $p = 0.7142$). (**G**) Female mice showed no altered freezing behavior during contextual recall (unpaired two-tailed Student's t-test: $t_{29} = 1.662$, $p = 0.1073$). Data are expressed as mean ± SEM. * $p < 0.05$; stimulus effect: #### $p < 0.0001$ (**B, E**); CS- vs. CS+: #### $p < 0.0001$ (**C, F**).

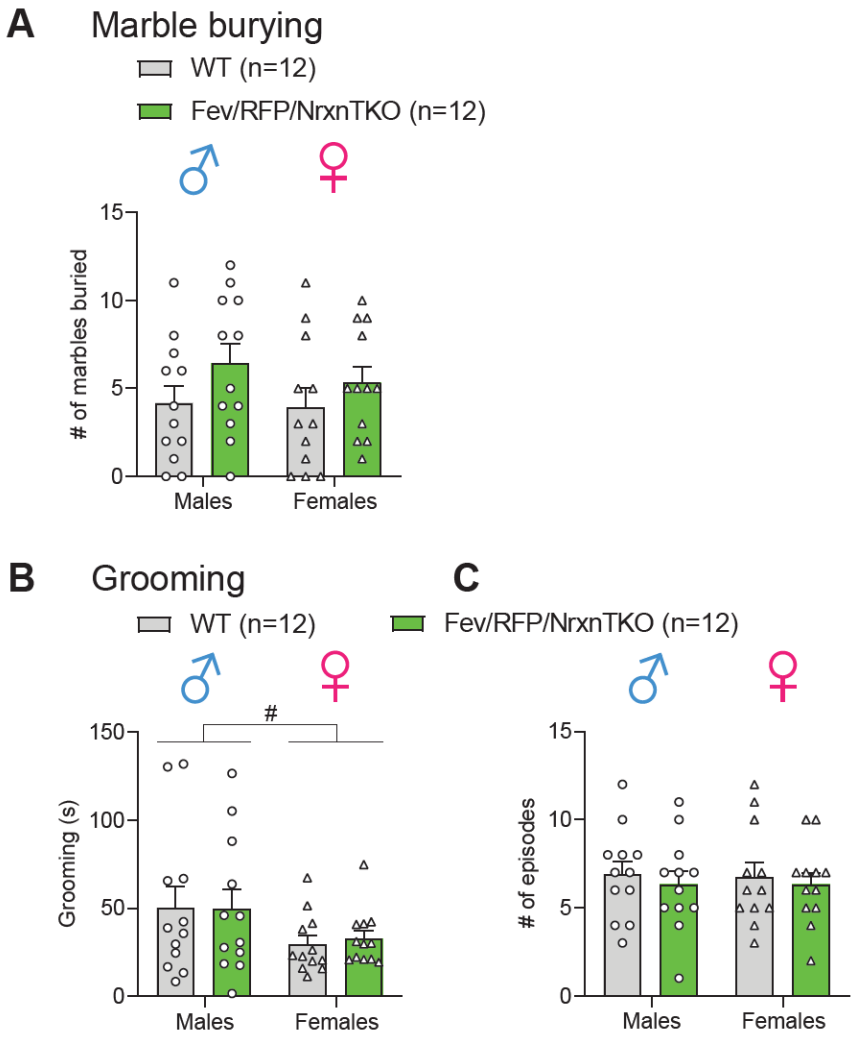

Figure 3.S7 | Repetitive behaviors are not altered in the absence of Nrxns in 5-HT neurons. (**A**) Male WT (n = 12) and Fev/RFP/NrxnTKO (n = 12) mice and female WT (n = 12) and Fev/RFP/NrxnTKO (n = 12) mice showed no differences in the number of marbles buried (two-way ANOVA: genotype main effect, $F_{1,44}$ = 3.179, p = 0.0815; sex main effect, $F_{1,44}$ = 0.4204, p = 0.5201; interaction, $F_{1,44}$ = 0.1642, p = 0.6873). (**B**) No differences in grooming time were observed between groups (two-way ANOVA: genotype main effect, $F_{1,44}$ = 0.02373, p = 0.8783; interaction $F_{1,44}$ = 0.05298, p = 0.819). Males spent more time grooming than females (two-way ANOVA: sex main effect, $F_{1,44}$ = 4.499, $^{\#}$ p = 0.0396). (**C**) The number of grooming episodes was similar between groups across both sexes (two-way ANOVA: genotype main effect, $F_{1,44}$ = 0.4452, p = 0.5081; sex main effect, $F_{1,44}$ = 0.01237, p = 0.912; interaction $F_{1,44}$ = 0.01237, p = 0.912). Data are expressed as mean ± SEM. Males vs. females: $^{\#}$ p < 0.05.

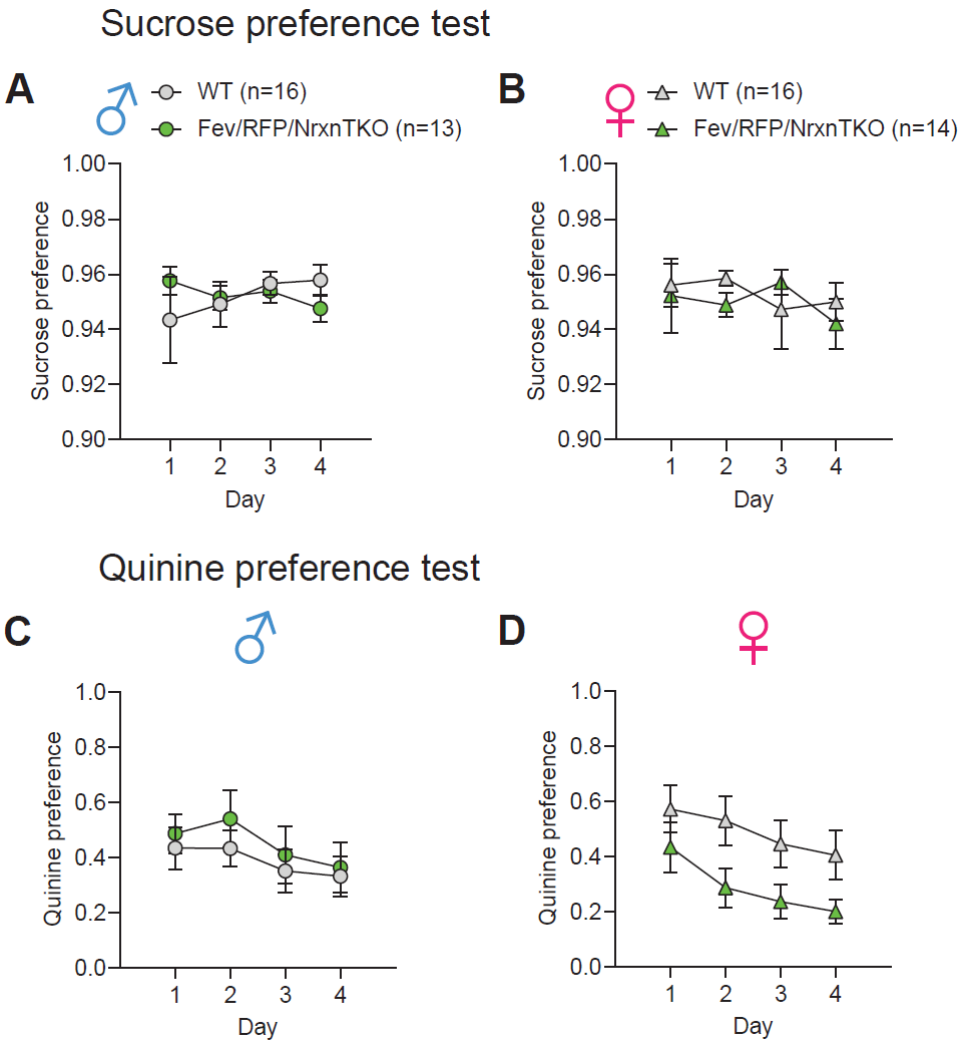

Figure 3.S8 | Anhedonia is unaffected by the lack of Nrxns in 5-HT neurons. (**A**) Male WT (n = 16) and Fev/RFP/NrxnTKO (n = 13) mice showed no differences in preference for sucrose (two-way repeated measures ANOVA: genotype main effect, $F_{1,27}$ = 0.01733, p = 0.8962; day main effect, $F_{1.568,42.35}$ = 0.1959, p = 0.7692; day x genotype interaction, $F_{3,81}$ = 0.9707, p = 0.4107). (**B**) Female WT (n = 16) and Fev/RFP/NrxnTKO (n = 14) mice showed similar preferences for sucrose (two-way repeated measures ANOVA: genotype main effect, $F_{1,28}$ = 0.1157, p = 0.7363; day main effect, $F_{2.346,65.68}$ = 0.4739, p = 0.6551; day x genotype interaction, $F_{3,84}$ = 0.6535, p = 0.5829). (**C**) Male mice showed no differences in preference for quinine (two-way repeated measures ANOVA: genotype main effect, $F_{1,27}$ = 0.3662, p = 0.5501; day x genotype interaction, $F_{3,81}$ = 0.2499, p = 0.8612). The volume of quinine consumed was different across days (two-way repeated measures ANOVA: day main effect, $F_{2.192,59.2}$ = 4.078, p = 0.019). (**D**) Quinine preference was similar between groups in females (two-way repeated measures ANOVA: genotype main effect, $F_{1,28}$ = 3.481, p = 0.0726; day x genotype interaction, $F_{3,84}$ = 0.89, p = 0.4498). (two-way repeated measures ANOVA: day main effect, $F_{2.192,59.2}$ = 4.078, p = 0.019). Data are expressed as mean ± SEM.

Chapter IV

Discussion

Chapter IV: Discussion

Summary

This thesis sought to integrate an investigation of neurexins (Nrxns) in the mouse brain in two ways: looking at brain-wide expression of the six principal Nrxns in different cell types and brain regions (Chapter II) and characterizing electrophysiological, molecular, and behavioral phenotypes of Nrxns in serotonin (5-HT) neurons (Chapter III).

Chapter II focused on mapping α and β isoforms of *Nrxn1*, *Nrxn2*, and *Nrxn3* mRNA using *in situ* hybridization to describe the diverse expression patterns of Nrxns in the adult mouse brain. Previous studies have assessed alternative splicing of Nrxns (Schreiner et al., 2014; Treutlein et al., 2014; Ullrich et al., 1995), which provide a detailed view of sites that can produce thousands of isoforms, and the mRNA expression of *Nrxns* in specific brain regions in the developing brain (Gorecki et al., 1999; Puschel & Betz, 1995). Our study is in line with these previous reports and confirmed unique profiles of Nrxns in different cell types and brain regions. Moreover, we provided an unbiased whole brain-wide study to outline Nrxn expression patterns. We emphasize *Nrxn* mRNA expression in excitatory and inhibitory neurons in layer-dependent somatosensory neocortex (**Figure 2.8, 2.9**) and subregion-dependent hippocampus (**Figure 2.10, 2.11**). Specific cell types in cerebellar cortex (**Figure 2.12, 2.13**), catecholaminergic (DAergic and noradrenergic) neurons (**Figure 2.14, 2.15**), and non-neuronal (astrocytes and oligodendrocytes) cells (**Figure 2.16, 2.17**) were found to express

distinct *Nrxn* signals. Trans-synaptic Nrxn binding partners, notably neuroligins (Nlgns), leucine-rich repeat transmembrane proteins (Lrrtms), and Adgrls (Latrophilins) were differentially expressed in the brain (**Figure 2.18**). **Table 2.2** provides an overview of the expression levels of *Nrxn* mRNAs in the brain regions studied. While descriptive in nature, these findings underscore the numerous combinations of trans-synaptic interactions that can occur between presynaptic Nrxns and Nrxn binding molecules.

Chapter III demonstrated that Nrxns serve as a molecular code that can functionally specify properties at 5-HT release sites. In Chapter II, we found that *αNrxn1* and *αNrxn2* were consistently and predominantly expressed in the dorsal raphe nucleus (DRN) (**Figure 2.5**). In Chapter III, we performed *in situ* hybridization for the six Nrxn isoforms in 5-HT neurons and found that the mRNA expression of *αNrxn1* and *αNrxn2* were highly expressed in 5-HT neurons in the DRN and median raphe nucleus (MRN) (**Figure 3.1**). Using a mouse model with specific KO of all Nrxns in 5-HT neurons, we showed that the loss of Nrxns in males reduced 5-HT release by roughly 50-60% compared with the peak concentrations of 5-HT seen in the DRN and hippocampus of wildtype (WT) mice (**Figure 3.2**). SERT-labeled 5-HT fiber innervation was altered in regions including the medial prefrontal cortex (mPFC) and basolateral amygdala (BLA) (increased fiber density) as well as the dorsal hippocampus and DRN (decreased fiber density) (**Figure 3.3**). Moreover, impaired sociability and coping responses to behavioral despair were observed in male but not female mice (**Figure 3.4, 3.5**). These results reveal that

Nrxns regulate neuromodulatory 5-HT signaling and allow us to further appreciate the role of Nrxns as presynaptically-positioned synaptic organizers. The remainder of this chapter will interpret the results of Chapter III and discuss implications for future studies.

Comments on the Fev/RFP/NrxnTKO mouse line

We demonstrated physiological and molecular characteristics of Nrxns in the 5-HT system: Nrxn-deficient 5-HT release sites were correlated with 1) a robust decrease in 5-HT release and 2) altered SERT innervation in specific brain areas. 5-HT release was reduced in male Fev/RFP/NrxnTKO mice in the DRN and hippocampus (**Figure 3.2**). Fluoxetine (FLX) was used to confirm that evoked transient areas would increase when the action of the serotonin transporter (SERT) was blocked, leading to more 5-HT available for detection. This was observed in the DRN but not hippocampus. One explanation is that since the hippocampus is innervated by fewer SERT-positive fibers than the DRN, blocking SERT would not generate a robust difference in 5-HT uptake kinetics. It is possible that increasing the number of slices recorded will allow us to detect differences in the evoked 5-HT transients before and after selective serotonin reuptake inhibitor (SSRI) application. WT and Fev/RFP/NrxnTKO mice showed a trend for drug effect on the transient area due to FLX treatment ($F_{1,9}$ = 3.711, p = 0.0862). Alternatively, a higher concentration of FLX could be attempted or a different SSRI like paroxetine, which has a higher SERT binding affinity, or escitalopram, which is more selective

for SERT, could be used to investigate their effects on 5-HT availability in the hippocampus (Sanchez et al., 2003; Sanchez & Hyttel, 1999). Indeed, acute administration of escitalopram for *in vivo* fast scan cyclic voltammetry (FSCV) reduced reuptake of 5-HT resulting in increased extracellular 5-HT concentration (Saylor et al., 2019).

The removal of Nrxns in 5-HT neurons resulted in fewer SERT-positive fibers in the DRN and hippocampus. SERT signals were differentially affected in the brain areas investigated (**Figure 3.3**). We observed increased fiber innervation in the mPFC and BLA and no differences in SERT distribution to the nucleus accumbens (NAc) and ventral hippocampus. It is possible that using SERT to label 5-HT fibers may not fully capture information on the breadth of 5-HT projections. This is particularly relevant in the NAc, which is innervated by SERT-positive and to a smaller extent SERT-negative 5-HT fibers (Brown & Molliver, 2000). SERT-negative axons are preferentially distributed in the caudal NAcSh and we may have underestimated SERT density in this area. Additionally, there is a possibility that Nrxns regulate the distribution of SERT rather than the abundance of 5-HT fibers. 5-HT itself can be used as another phenotypic marker of 5-HT fibers to compare 5-HT innervation between WT and Fev/RFP/NrxnTKO mice. Of note, *Nielsen et al.* reported that SERT labeling is more reliable than 5-HT staining because of the rapid metabolism of 5-HT leading to underdetection of 5-HT fibers (Nielsen et al., 2006). Sparse deletion of all Nrxns in climbing fiber synapses led to blunted green fluorescent protein (GFP)-labeled fibers (L. Y. Chen et al., 2017). We can use this

same approach to evaluate red fluorescent protein (RFP) innervation, dictated by the presence or absence of Nrxns, and its overlap with SERT or 5-HT signals in Fev/RFP and Fev/RFP/NrxnTKO mice to further examine 5-HT connectivity.

Global knockout (KO) of αNrxn1 (Asede et al., 2020; Esclassan et al., 2015; Etherton et al., 2009; Grayton et al., 2013; Twining et al., 2017) βNrxn1 (Rabaneda et al., 2014), αNrxn2 (Born et al., 2015; Dachtler et al., 2014; Dachtler et al., 2015), Nrxn3 (Keum et al., 2018), and βNrxns (Anderson et al., 2015) have led to impairments in locomotor activity, anxiety, social behaviors, restrictive behaviors, olfaction, and fear learning and memory. In our mouse model with pan-Nrxn deletion in 5-HT neurons, sociability was reduced (**Figure 3.4**) and depressive-like behavior increased (**Figure 3.5**) in male mice. Unexpectedly, sociability was not altered in other social behavioral tests (**Figure 3.4E, 3.S3, 3.S4**). In females, only fear learning acquisition was elevated in Fev/RFP/NrxnTKO mice (**Figure 3.S6E**). No other differences in behaviors were observed across sexes (**Figure 3.S1-S8**). Some sex-specific responses were seen such as increased movement by females in the locomotor activity assay (**Figure 3.S1C**) and elevated plus-maze (**Figure 3.S2E**) compared with males. The specific deletion of Nrxns in 5-HT neurons induced a subtle change in behavior despite the physiological and molecular phenotypes we observed. Existing circuits or molecules appear to compensate for the perturbation in the 5-HT system so that behaviors are executed normally. While 5-HT modulates fast-acting excitatory and inhibitory neurotransmission, 5-HT signals should be viewed as a part of a network of information deciphered across

circuits to generate complex behaviors. A summary of characteristics observed in the Fev/RFP/NrxnTKO mouse line is shown in **Figure 4.1**, which specifically highlights the raphe-hippocampal circuit in males.

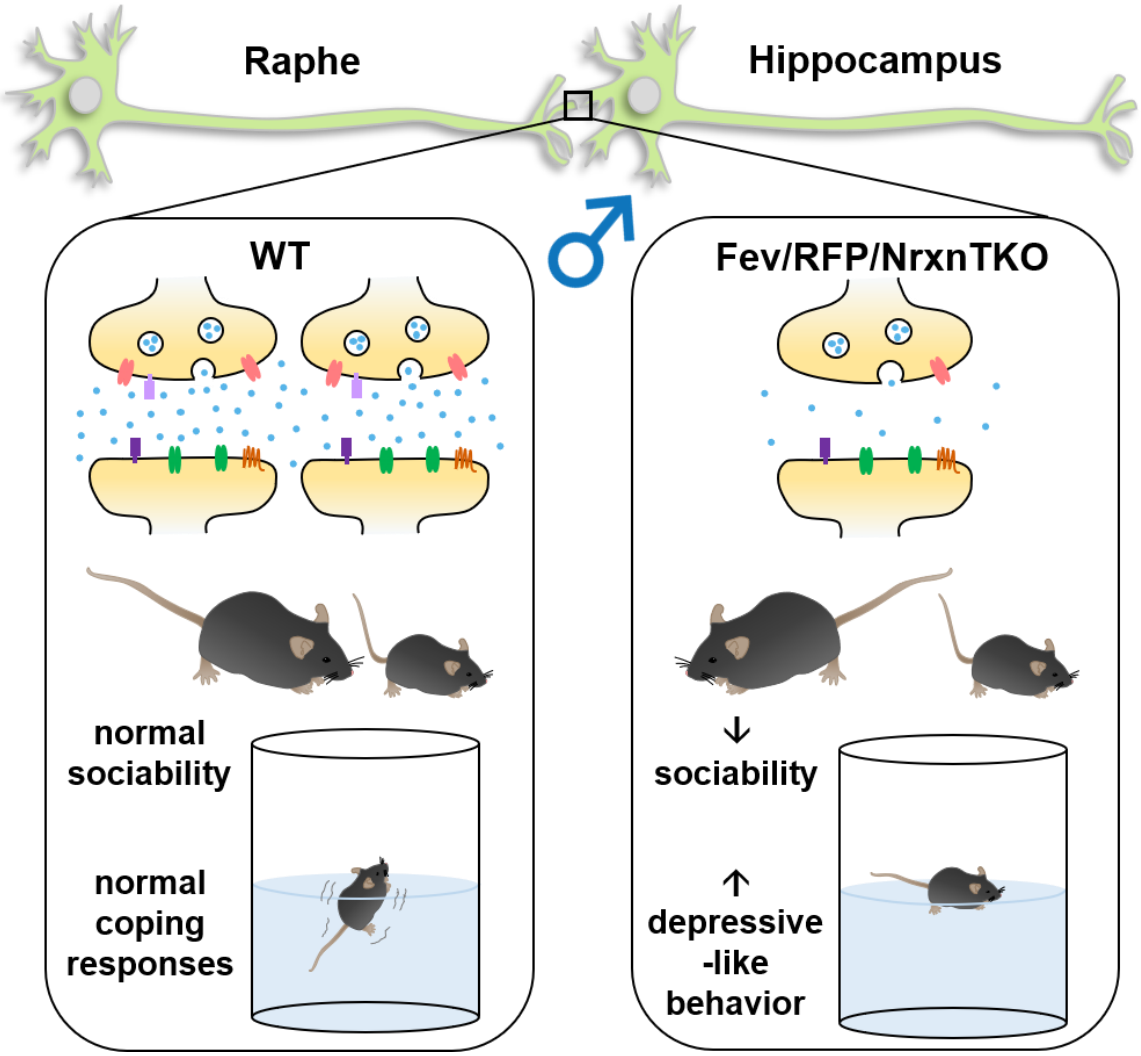

Figure 4.1 | Working model of the Fev/RFP/NrxnTKO mouse line. (**Top**) The loss of Nrxns in 5-HT neurons disrupts innervation in the raphe-hippocampal circuit in males. Compared with WT mice (left), 5-HT release and SERT fibers are reduced in the hippocampus of Fev/RFP/NrxnTKO mice (right). Given that volume transmission is the major mode of 5-HT signaling, 5-HT release sites are shown near but not directly apposed to postsynaptic specializations. Transmission at 5-HT synapses is not displayed although Nrxns binding to Nrxn ligands could modify synapse properties. Presynaptic components: 5-HT (green), SERT (pink), and Nrxns (light purple). Postsynaptic components: ionotropic receptors (brown), metabotropic receptors (blue), and Nrxn ligands (dark purple). (**Middle**): Fev/RFP/NrxnTKO mice spent less time exploring a sex-matched juvenile conspecific, indicating deficits in sociability compared with WT mice. (**Bottom**): Fev/RFP/NrxnTKO mice demonstrated greater immobility than WT mice, suggesting that 5-HT neurons that lack Nrxns increased depressive-like behavior.

Because sociability was reduced in male Fev/RFP/NrxnTKO mice (**Figure 3.4B**), we tested whether single Nrxn KO in 5-HT neurons was sufficient to reproduce these findings. αNrxn1 and αNrxn2 are the major Nrxn isoforms expressed in the DRN and MRN and we therefore generated mouse lines with single deletion of Nrxn1 (Fev/RFP/Nrxn1KO) and Nrxn2 (Fev/RFP/Nrxn2KO). Using the same experimental protocol (**Figure 4.2A**), we found that male Fev/RFP/Nrxn1KO (**Figure 4.2B**) and Fev/RFP/Nrxn2KO (**Figure 4.2C**) mice showed no differences in investigation of the stimulus mouse on day 1 compared with WT mice. Moreover, both groups similarly reduced their exploration of the familiar conspecific in trial 2. These results suggest that Nrxn1 and Nrxn2 are not involved in social behavior. The inconsistent sociability deficits seen in the direct social interaction test are perplexing. Male WT mice appeared to show slightly lower average investigation time of the stimulus mouse on trial 1 of the direct social interaction test with different conspecifics (**Figure 3.4E**) compared with trial 1 of the test with the same conspecific over the two trials (**Figure 3.4B**). This suggests variability between cohorts in the mouse line. No differences between genotypes were observed in the three-chamber social interaction test and social conditioned place preference. However, a significant genotype effect was observed on day 1 of the three-chamber social interaction test in male mice ($F_{1,24} = 4.798$, $p = 0.0384$). Differences in social behavior may exist but are difficult to capture. Social behavioral tests could be repeated with longer habituation times (from 5 to 10 min) to reduce novelty of the testing environment and increase predictable responses

during the test. In the three-chamber social interaction test, stimulus mice could be habituated to the cylinders prior to testing to minimize abnormal behaviors or agitation (Yang et al., 2011). Additionally, mice could be habituated to both cylinders prior to the test phase of the experiment. It is possible that when the empty cylinder (nonsocial stimulus) and cylinder-contained mouse (social stimulus) are presented concurrently after the habituation phase, subject mice inherently prefer the social stimulus because it represents two novel stimuli: the mouse and the cylinder itself (Rein et al., 2020). Therefore, modifying social behavioral tests to account for these variables could yield different results.

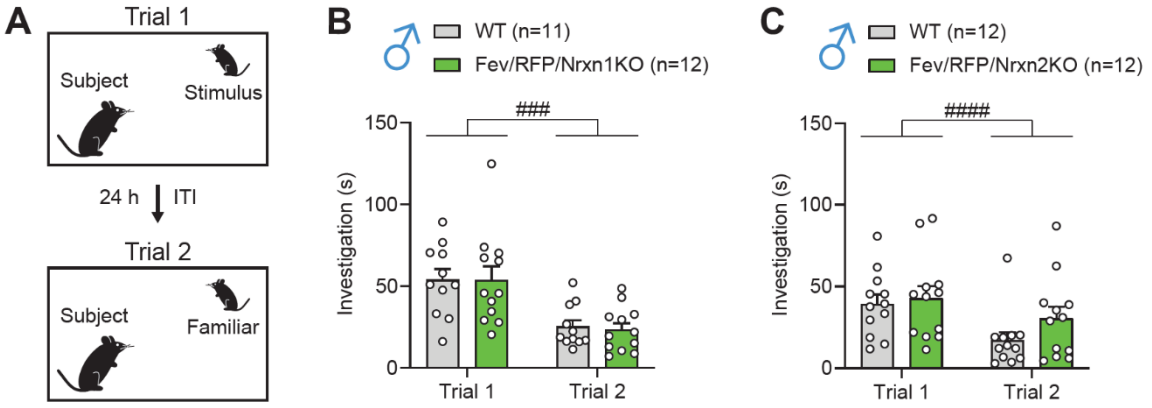

Figure 4.2 | Single Nrxn KO in 5-HT neurons does not alter social behavior in males. (**A**) Direct social interaction test using the same juvenile stimulus across two trials. (**B**) Male WT (gray, n = 11) and Fev/RFP/Nrxn1KO (green, n = 12) both similarly decreased investigation of a familiar juvenile stimulus in trial 2 although no differences between groups were observed (two-way repeated measures ANOVA: trial main effect, $F_{1,21}$ = 42.86, #### p < 0.0001; genotype main effect, $F_{1,21}$ = 0.01797, p = 0.8946; trial x genotype interaction, $F_{1,21}$ = 0.03666, p = 0.85). (**C**) Male WT (n = 12) and Fev/RFP/Nrxn2KO (n = 12) showed no differences in their investigation of the juvenile stimulus (two-way repeated measures ANOVA: genotype main effect, $F_{1,22}$ = 1.081, p = 0.3097; trial x genotype interaction, $F_{1,22}$ = 1.345, p = 0.2586). Both groups spent less time investigating the familiar juvenile stimulus in trial 2 (two-way repeated measures ANOVA: trial main effect, $F_{1,22}$ = 15.94, ### p = 0.0006). Data are expressed as mean ± SEM. Trial 1. vs. trial 2: ### p < 0.001, #### p < 0.0001.

The lack of behavioral phenotype in female mice is another unanswered observation. A single difference in fear learning acquisition was observed in which Fev/RFP/NrxnTKO mice showed heightened freezing behavior during auditory cue-foot shock associations (CS+) compared with WT mice (**Figure 3.S6E**). Because cued and contextual memory recall were not affected, we speculate that female Fev/RFP/NrxnTKO mice are more sensitive to pain. Increased nociceptive responses to the shock itself could explain the exclusive deficit in fear learning acquisition that did not result in increased freezing behavior during memory recall when the shock was no longer delivered. 5-HT has a well-known role in pain processing (Sommer, 2010). To test whether deletion of Nrxns in 5-HT neurons alters pain behaviors in females, we can perform nociceptive assays like the Radall-Selitto (paw pressure) test (mechanical nociception) or hot-plate test (thermal nociception) (Deuis et al., 2017).

While it is evident that autism spectrum disorder (ASD) is more prevalent in males than females, the mechanism that drives this sex difference is still unclear. Many Nrxn KO studies have used only males, pooled male and female data, or found diverging behavioral phenotypes between males and females. For example, female αNrxn1 KO mice showed reduced locomotor activity and increased social novelty preference, male αNrxn1 KO mice demonstrated increased anxiety behavior and aggression, and both male and female mutant mice had normal sociability but impaired nest building (Grayton et al., 2013). *Laarakker et al.* found that male but not female mice with heterozygous KO of αNrxn1 were quicker to

habituate to novel stimuli compared with sex-matched WT mice (Laarakker et al., 2012). Additionally, female αNrxn1 heterozygous KO mice showed poor associative memory in a passive avoidance test while both male and female αNrxn1 heterozygous KO mice displayed impaired social memory. In the same study, female αNrxn2 heterozygous KO mice displayed a lack of object discrimination memory (Dachtler et al., 2015). These differences are often reported with little interpretation provided. Emerging evidence suggests that there are protective mechanisms in females that shield them from the development of ASD symptoms (Werling & Geschwind, 2013). More gene mutations such as deleterious missense mutations and loss of function variants were found in females with ASD compared with males with ASD. Male-specific candidate genes outnumber female-specific ones, and some shared pathology include mutations in postsynaptic proteins like Shank3 and Nlgn1 (Y. Zhang et al., 2020).

A neuronal-hormonal relationship for Nrxns as well as other risk genes for ASD is yet to be explored. In rhesus macques, estrogen therapy increased Nrxn3 expression in TPH-positive neurons (Bethea & Reddy, 2012) while testosterone interrupted Nrxn-Nlgn interactions in *Octodon degus* (Yagishita-Kyo et al., 2021). Fetal steroidogenic activity has been found to be elevated in children who were later diagnosed with ASD (Baron-Cohen et al., 2015), however, our understanding of the connection between sex steroids and Nrxns is still immature. In the Fev/RFP/NrxnTKO mouse line, female mice appear to benefit from currently unknown factors that reduce their susceptibility to impaired patterns of behavior.

While the loss of Nrxns in 5-HT neurons did not alter behavior in females, it is possible that electrophysiological and molecular phenotypes exist like in male Fev/RFP/NrxnTKO mice. The same experiments (FSCV and SERT density analysis) could be performed in females to examine differences between groups.

Physiological importance of 5-HTergic Nrxns

Effect on molecular machinery?

It is still unclear what molecular role Nrxns plays at 5-HT release sites. Ultrastructural analysis of SERT-labeled fiber profiles revealed that SERT is mainly targeted to extrasynaptic sites rather than within synaptic membrane specializations (Zhou et al., 1998). SERT was also often found near large dense core vesicles that contain storage and release machinery (Pickel & Chan, 1999). These dense core vesicles store neuropeptides like galanin which coexists in 5-HT neurons and modulates 5-HT signaling in depressive-like behaviors (Barde et al., 2016; Hokfelt et al., 1998; Lu et al., 2005; Zhu et al., 1986). Given that galanin has been found to regulate 5-HT release (Kehr et al., 2002; Yoshitake et al., 2004), it will be interesting to investigate Nrxn-galanin interactions and determine whether they exert synergistic or antagonistic effects. Additionally, immunohistochemical analysis of SERT with vesicular monoamine transporter 2 (VMAT2), which packages monoamines like 5-HT into vesicles (Eiden & Weihe, 2011), and active zone proteins like Bassoon and Munc13 (Dresbach et al., 2001) could be performed to determine whether the absence of Nrxns affects the density or

colocalization of these proteins at 5-HT release sites. This would allow us to better understand how Nrxns impact the architecture of 5-HT release sites. In the DA system, roughly 30% of DA varicosities on DA axons were shown to contain active zone-like sites that expressed active zone proteins including Bassoon and RIM (regulating synaptic membrane exocytosis protein) (Liu et al., 2018). 5-HT release sites may also demonstrate similar release machinery for 5-HT exocytosis. If Nrxns alter components of 5-HT release sites, this would allude to a functional role for Nrxns in organizing features of the active zone that are important for efficient 5-HT release. Indeed, pan-Nrxn deletion in the calyx of Held synapse has been shown to reduce Bassoon signals in presynaptic terminals without affecting synapse formation, calcium (Ca^{2+}) channel number or function, and the readily releasable pool of vesicles (F. Luo et al., 2020). Future studies could also examine the involvement of Nrxns in postsynaptic differentiation at synapses.

Effect on synapse physiology?

Nrxns play a critical role in the organization of excitatory and inhibitory synapses (Sudhof, 2017). αNrxnTKO mice display decreased ultrastructural inhibitory synaptic density with no effect on excitatory synaptic density, and reduced frequency of miniature excitatory postsynaptic currents (mEPSCs) and miniature inhibitory postsynaptic currents (mIPSCs) (Missler et al., 2003). Mice with conditional deletion of all βNrxns in the hippocampus demonstrated decreased frequency of mEPSCs with no change in mIPSCs indicating specific impairment in

glutamate release (L. Y. Chen et al., 2017). A shift in the ratio between synaptic excitation and inhibition (E-I ratio) in favor of excitation was found in a 15q11-13 duplication mouse model of ASD with low 5-HT levels (Nakai et al., 2017). Other mouse models targeting ASD risk genes also show increased E-I ratio due in part to deficits in feedforward excitation and inhibition (Antoine et al., 2019; Selten et al., 2018). These findings highlight: 1) the diverse roles of Nrxns on neurotransmission and that 2) normal 5-HT levels maintain E-I ratio in neuronal circuits. It is possible that Nrxns deficient at 5-HT release sites cause abnormal synaptic excitation and inhibition in areas with altered physiological or molecular properties like the hippocampus. An immunohistochemical assay could be performed to identify differences in the distribution of excitatory (vesicular glutamate transporter type 1 [VGluT1]) and inhibitory (vesicular GABA transporter [VGAT]) protein markers in the Fev/RFP/NrxnTKO mouse line. Additionally, the ability of 5-HTergic Nrxns to regulate excitatory and inhibitory synaptic transmission could be explored. Previous studies have shown that application of 5-HT in the hippocampus potentiates synaptic transmission at the mossy fiber-CA3 (Kobayashi et al., 2008) and CA3-CA1 (Teixeira et al., 2018) synapses. Electrophysiological recordings to measure field excitatory postsynaptic potentials could be performed to determine whether the loss of 5-HTergic Nrxns decreases neuronal excitation.

Behavioral impact of 5-HTergic Nrxns

Therapeutic rescue?

A previous study found that chronic administration of the SSRI FLX was sufficient to improve sociability in a 15q11-13 duplication mouse model of ASD (Nakai et al., 2017). FLX also restored the low extracellular 5-HT levels seen in midbrain samples containing the raphe nuclei. Decreased sociability in another mouse model of ASD with 16p11.2 deletion was rescued following activation of 5-HT terminals in the NAc (Walsh et al., 2018). Additionally, the tail suspension and forced swim tests are commonly used to evaluate the effects of antidepressant drugs (Cryan et al., 2005; Slattery & Cryan, 2012). Would augmenting extracellular 5-HT be sufficient to reinstate altered behaviors in male Fev/RFP/NrxnTKO mice? Chronic administration of SSRIs, either through the drinking solution or injections, could be given to the Fev/RFP/NrxnTKO mouse line to determine whether increasing 5-HT levels is sufficient to restore social and depressive-like behaviors.

Of note, SSRI-induced elevation of 5-HT levels provides little information about specific 5-HT receptor action. Activation of 5-HT_{1B} receptors in the NAc using CP-93129 increased sociability in 16p11.2 deletion mice (Walsh et al., 2018), while injection of the 5-HT_{1A} receptor agonist 8OH-DPAT improved social interaction deficits in 15q11-13 duplication mice (Nagano et al., 2018). Administration of 5-HT_{1A} or 5-HT_{1B} receptor agonists could be performed to determine whether activation of either of these 5-HT receptors is sufficient to improve sociability in male Fev/RFP/NrxnTKO mice. These findings would indicate that 5-HT action,

through 5-HT receptor subtype activation, is necessary for social behavior. Moreover, while antidepressants are the standard therapeutic agents for depression, 5-HT_{1A} receptors are suggested as targets for treatment (Celada et al., 2013). 5-HT_{1A} receptor agonists have been shown to decrease depressive-like behavior in the forced swim test (Wieland & Lucki, 1990). *Gu et al.* reported that the herb *Angelicae dahuricae* has antidepressant-like effects which could be suppressed by administration of 5-HT_{1A} receptor antagonist (Gu et al., 2014). SSRIs affect 5-HT_{1A} receptor activity through their regulation of extracellular 5-HT availability. The increase in 5-HT levels activates presynaptic 5-HT_{1A} receptor-mediated autoinhibition of 5-HT neuron firing and desensitizes autoreceptors but not heteroreceptors with chronic treatment (Celada et al., 2013; F. Chen et al., 2003). Postsynaptic 5-HT_{2A} receptor antagonists have also been shown to synergize with SSRIs to increase therapeutic effects in people with depression or OCD (G. J. Marek et al., 2003). Treatment with 5-HT_{1A} receptor agonist or 5-HT_{2A} receptor antagonist could be attempted in male Fev/RFP/NrxnTKO mice to test whether targeting 5-HT receptors is sufficient to improve despair-associated responses. Given the variability observed with the social behavioral phenotype, future studies can first focus on ameliorating depressive-like behavior.

Specific Nrxn involvement?

The deletion of all three Nrxns led to deficits in sociability and depressive-like behavior in males. It is still unknown which Nrxn isoform (α or βNrxn) is important

for driving these aberrant behaviors. αNrxn1 or αNrxn2 may be important for social and depressive behaviors given the low expression of other Nrxn isoforms in DRN and MRN 5-HT neurons. αNrxn2 KO mice exhibit reduced sociability and social novelty (Dachtler et al., 2014). No behavioral studies on βNrxn1 and βNrxn2 KO mice are currently published in the literature. Additionally, there are no reports that have studied depressive-like behavior in Nrxn KO mice. It is unclear which Nrxn isoform contributes to the depressive-like phenotype. We can first perform the forced swim test in the Fev/RFP/Nrxn1KO and Fev/RFP/Nrxn2KO mouse lines to determine whether single Nrxn KO is sufficient to reproduce this impairment.

The impact of the absence of Nrxns in the developing 5-HT system cannot be excluded. Our mouse line utilizes the Cre/loxP system to specifically delete Nrxns in 5-HT neurons which begins during development. Nrxns are expressed before extensive synapse formation occurs in the early developing brain and likely help to organize an assembly of molecules for synapse differentiation or mediate cell-cell or cell-extracellular environment interactions (Harkin et al., 2017; Puschel & Betz, 1995). It is possible that the loss of Nrxns affects how 5-HT neurons form circuits and make contacts with other cells or regions in the brain. Of note, Nrxns are viewed as critical organizers of synaptic properties and not central regulators of synapse formation (F. Luo et al., 2020; Sudhof, 2017). While a potential developmental influence of Nrxns may more closely resemble pathophysiological processes that occur in neurodevelopmental disorders, it also complicates how we define the underlying mechanisms by which Nrxns modulate 5-HT signaling. An

inducible mouse line like Cre-ERT (tamoxifen-inducible Cre/loxP estrogen receptor) mice could be used to focus on the effect of Nrxns in 5-HT circuits after development. For example, tryptophan hydroxylase 2 (TPH2)-iCreER (Jax #016584) or Fev-iCreER (Liu et al., 2010) mice could be bred with Nrxn1$^{f/f}$/2$^{f/f}$/3$^{f/f}$ mice to generate mice with tamoxifen-dependent postnatal deletion of Nrxns. If single or double Nrxn KO mice produced using a breeding approach display altered behaviors, a viral construct that knocks down specific Nrxn gene(s) could be expressed in Fev/RFP mice. Input-specific Nrxn knockdown could be achieved by using a Cre-dependent retrograde adeno-associated virus (retroAAV) vector (Lin et al., 2020) in areas like the mPFC, hippocampus, BLA, or DRN which exhibited aberrant SERT innervation and are part of circuits involved in social and depressive behaviors. These mice could undergo the same experiments performed in the Fev/RFP/NrxnTKO line to compare similarities and differences in phenotypes. We could also pursue molecular and physiological studies to connect behavior to specific 5-HT circuits.

Nrxns in neuromodulatory systems

There are a few studies that have evaluated Nlgns (Nrxn ligands) in DAergic and 5-HTergic pathways. Presynaptic DA terminals were found to form contacts with postsynaptic GABAergic structures that express Nlgn2. Interestingly, Nrxns were detected at presynaptic DA terminals that directly apposed dendritic spines of medium spiny neurons in the striatum (Uchigashima et al., 2016). Additionally, the

somatodendritic compartment of 5-HT neurons in the DRN but not fibers in the hippocampus were shown to form *cis* Nlgn2 interactions. Nrxns were also found to complex with SERT, but through *trans* (presynaptic) interactions (Ye et al., 2015). *Sons et al.* demonstrated that double KO of αNrxn at neuromuscular junctions impairs acetylcholine release (Sons et al., 2006), indicating the ability of Nrxns to control efficient presynaptic neurotransmitter exocytosis. Taken together, it is evident that Nrxns exist in or interact with neuromodulatory systems.

Just as Nrxns shape the properties of synapses, neuromodulators adjust signaling dynamics. Neuromodulators can affect presynaptic neurotransmitter release by altering Ca^{2+} influx or vesicle number or fusion (Higley & Sabatini, 2010; Patzke et al., 2019; Photowala et al., 2006) and regulate postsynaptic responses and transcriptional activity (Feng et al., 2001; Kobayashi et al., 2020; Sun et al., 2005). While we have investigated Nrxns in the 5-HT system, Nrxns likely play a role at acetylcholine, DA, epinephrine, and norepinephrine release sites in the central nervous system. Addressing Nrxns in neuromodulation will be a new avenue of study to highlight their functions in diverse signaling pathways.

Bibliography

Abela, A. R., Browne, C. J., Sargin, D., Prevot, T. D., Ji, X. D., Li, Z., et al. (2020). Median raphe serotonin neurons promote anxiety-like behavior via inputs to the dorsal hippocampus. *Neuropharmacology, 168*, 107985. https://doi.org/10.1016/j.neuropharm.2020.107985

Adamsen, D., Ramaekers, V., Ho, H. T., Britschgi, C., Rufenacht, V., Meili, D., et al. (2014). Autism spectrum disorder associated with low serotonin in CSF and mutations in the SLC29A4 plasma membrane monoamine transporter (PMAT) gene. *Mol Autism, 5*, 43. https://doi.org/10.1186/2040-2392-5-43

Amaral, D., & Pierre, L. (2006). Hippocampal Neuroanatomy. *The Hippocampus Book*. https://doi.org/10.1093/acprof:oso/9780195100273.001.0001

American Psychiatric Association. (2013). Diagnostic and statistical manual of mental disorders, 5th edition.

Anderson, G. R., Aoto, J., Tabuchi, K., Foldy, C., Covy, J., Yee, A. X., et al. (2015). beta-Neurexins Control Neural Circuits by Regulating Synaptic Endocannabinoid Signaling. *Cell, 162*(3), 593-606. https://doi.org/10.1016/j.cell.2015.06.056

Andersson, M., Tangen, A., Farde, L., Bolte, S., Halldin, C., Borg, J., et al. (2020). Serotonin transporter availability in adults with autism-a positron emission tomography study. *Mol Psychiatry*. https://doi.org/10.1038/s41380-020-00868-3

Angoa-Perez, M., Kane, M. J., Briggs, D. I., Herrera-Mundo, N., Sykes, C. E., Francescutti, D. M., et al. (2014). Mice genetically depleted of brain serotonin do not display a depression-like behavioral phenotype. *ACS Chem Neurosci, 5*(10), 908-919. https://doi.org/10.1021/cn500096g

Antoine, M. W., Langberg, T., Schnepel, P., & Feldman, D. E. (2019). Increased Excitation-Inhibition Ratio Stabilizes Synapse and Circuit Excitability in Four Autism Mouse Models. *Neuron, 101*(4), 648-661 e644. https://doi.org/10.1016/j.neuron.2018.12.026

Aoto, J., Foldy, C., Ilcus, S. M., Tabuchi, K., & Sudhof, T. C. (2015). Distinct circuit-dependent functions of presynaptic neurexin-3 at GABAergic and glutamatergic synapses. *Nat Neurosci, 18*(7), 997-1007. https://doi.org/10.1038/nn.4037

Aoto, J., Martinelli, D. C., Malenka, R. C., Tabuchi, K., & Sudhof, T. C. (2013). Presynaptic neurexin-3 alternative splicing trans-synaptically controls postsynaptic AMPA receptor trafficking. *Cell, 154*(1), 75-88. https://doi.org/10.1016/j.cell.2013.05.060

Arango, V., Underwood, M. D., & Mann, J. J. (2002). Serotonin brain circuits involved in major depression and suicide. *Prog Brain Res, 136*, 443-453. https://doi.org/10.1016/s0079-6123(02)36037-0

Asede, D., Joseph, A., & Bolton, M. M. (2020). Deletion of NRXN1alpha impairs long-range and local connectivity in amygdala fear circuit. *Transl Psychiatry, 10*(1), 242. https://doi.org/10.1038/s41398-020-00926-y

Autism Genome Project, C., Szatmari, P., Paterson, A. D., Zwaigenbaum, L., Roberts, W., Brian, J., et al. (2007). Mapping autism risk loci using genetic linkage and chromosomal rearrangements. *Nat Genet, 39*(3), 319-328. https://doi.org/10.1038/ng1985

Autism Spectrum Disorders Working Group of The Psychiatric Genomics, C. (2017). Meta-analysis of GWAS of over 16,000 individuals with autism spectrum disorder highlights a novel locus at 10q24.32 and a significant overlap with schizophrenia. *Mol Autism, 8*, 21. https://doi.org/10.1186/s13229-017-0137-9

Awasthi, J. R., Tamada, K., Overton, E. T. N., & Takumi, T. (2021). Comprehensive topographical map of the serotonergic fibers in the male mouse brain. *J Comp Neurol, 529*(7), 1391-1429. https://doi.org/10.1002/cne.25027

Baghdadli, A., Assouline, B., Sonie, S., Pernon, E., Darrou, C., Michelon, C., et al. (2012). Developmental trajectories of adaptive behaviors from early childhood to adolescence in a cohort of 152 children with autism spectrum disorders. *J Autism Dev Disord, 42*(7), 1314-1325. https://doi.org/10.1007/s10803-011-1357-z

Bai, D., Yip, B. H. K., Windham, G. C., Sourander, A., Francis, R., Yoffe, R., et al. (2019). Association of Genetic and Environmental Factors With Autism in a 5-Country Cohort. *JAMA Psychiatry, 76*(10), 1035-1043. https://doi.org/10.1001/jamapsychiatry.2019.1411

Baio, J., Wiggins, L., Christensen, D. L., Maenner, M. J., Daniels, J., Warren, Z., et al. (2018). Prevalence of Autism Spectrum Disorder Among Children Aged 8 Years - Autism and Developmental Disabilities Monitoring Network, 11 Sites, United States, 2014. *MMWR Surveill Summ, 67*(6), 1-23. https://doi.org/10.15585/mmwr.ss6706a1

Balazsfi, D., Zelena, D., Demeter, K., Miskolczi, C., Varga, Z. K., Nagyvaradi, A., et al. (2018). Differential Roles of the Two Raphe Nuclei in Amiable Social Behavior and Aggression - An Optogenetic Study. *Front Behav Neurosci, 12*, 163. https://doi.org/10.3389/fnbeh.2018.00163

Bambico, F. R., Nguyen, N. T., & Gobbi, G. (2009). Decline in serotonergic firing activity and desensitization of 5-HT1A autoreceptors after chronic unpredictable stress. *Eur Neuropsychopharmacol, 19*(3), 215-228. https://doi.org/10.1016/j.euroneuro.2008.11.005

Barde, S., Ruegg, J., Prud'homme, J., Ekstrom, T. J., Palkovits, M., Turecki, G., et al. (2016). Alterations in the neuropeptide galanin system in major depressive disorder involve levels of transcripts, methylation, and peptide. *Proc Natl Acad Sci U S A, 113*(52), E8472-E8481. https://doi.org/10.1073/pnas.1617824113

Baron-Cohen, S., Auyeung, B., Norgaard-Pedersen, B., Hougaard, D. M., Abdallah, M. W., Melgaard, L., et al. (2015). Elevated fetal steroidogenic activity in autism. *Mol Psychiatry, 20*(3), 369-376. https://doi.org/10.1038/mp.2014.48

Baxter, A. J., Brugha, T. S., Erskine, H. E., Scheurer, R. W., Vos, T., & Scott, J. G. (2015). The epidemiology and global burden of autism spectrum disorders. *Psychol Med, 45*(3), 601-613. https://doi.org/10.1017/S003329171400172X

Beliveau, V., Svarer, C., Frokjaer, V. G., Knudsen, G. M., Greve, D. N., & Fisher, P. M. (2015). Functional connectivity of the dorsal and median raphe nuclei at rest. *Neuroimage, 116*, 187-195. https://doi.org/10.1016/j.neuroimage.2015.04.065

Belmer, A., Klenowski, P. M., Patkar, O. L., & Bartlett, S. E. (2017). Mapping the connectivity of serotonin transporter immunoreactive axons to excitatory and inhibitory neurochemical synapses in the mouse limbic brain. *Brain Struct Funct, 222*(3), 1297-1314. https://doi.org/10.1007/s00429-016-1278-x

Berger, M., Gray, J. A., & Roth, B. L. (2009). The expanded biology of serotonin. *Annu Rev Med, 60*, 355-366. https://doi.org/10.1146/annurev.med.60.042307.110802

Bethea, C. L., & Reddy, A. P. (2012). Effect of ovarian steroids on gene expression related to synapse assembly in serotonin neurons of macaques. *J Neurosci Res, 90*(7), 1324-1334. https://doi.org/10.1002/jnr.23004

Bey, A. L., & Jiang, Y. H. (2014). Overview of mouse models of autism spectrum disorders. *Curr Protoc Pharmacol, 66*, 5 66 61-26. https://doi.org/10.1002/0471141755.ph0566s66

Born, G., Grayton, H. M., Langhorst, H., Dudanova, I., Rohlmann, A., Woodward, B. W., et al. (2015). Genetic targeting of NRXN2 in mice unveils role in excitatory cortical synapse function and social behaviors. *Front Synaptic Neurosci, 7*, 3. https://doi.org/10.3389/fnsyn.2015.00003

Boucard, A. A., Chubykin, A. A., Comoletti, D., Taylor, P., & Sudhof, T. C. (2005). A splice code for trans-synaptic cell adhesion mediated by binding of neuroligin 1 to alpha- and beta-neurexins. *Neuron, 48*(2), 229-236. https://doi.org/10.1016/j.neuron.2005.08.026

Boucard, A. A., Ko, J., & Sudhof, T. C. (2012). High affinity neurexin binding to cell adhesion G-protein-coupled receptor CIRL1/latrophilin-1 produces an intercellular adhesion complex. *J Biol Chem, 287*(12), 9399-9413. https://doi.org/10.1074/jbc.M111.318659

Bradley, W. E., Raelson, J. V., Dubois, D. Y., Godin, E., Fournier, H., Prive, C., et al. (2010). Hotspots of large rare deletions in the human genome. *PLoS One, 5*(2), e9401. https://doi.org/10.1371/journal.pone.0009401

Brody, A. L., Saxena, S., Stoessel, P., Gillies, L. A., Fairbanks, L. A., Alborzian, S., et al. (2001). Regional brain metabolic changes in patients with major depression treated with either paroxetine or interpersonal therapy: preliminary findings. *Arch Gen Psychiatry, 58*(7), 631-640. https://doi.org/10.1001/archpsyc.58.7.631

Brown, P., & Molliver, M. E. (2000). Dual serotonin (5-HT) projections to the nucleus accumbens core and shell: relation of the 5-HT transporter to amphetamine-induced neurotoxicity. *J Neurosci, 20*(5), 1952-1963. Retrieved from https://www.ncbi.nlm.nih.gov/pubmed/10684896

Bruns, D., & Jahn, R. (1995). Real-time measurement of transmitter release from single synaptic vesicles. *Nature, 377*(6544), 62-65. https://doi.org/10.1038/377062a0

Bruns, D., Riedel, D., Klingauf, J., & Jahn, R. (2000). Quantal release of serotonin. *Neuron, 28*(1), 205-220. https://doi.org/10.1016/s0896-6273(00)00097-0

Canli, T., & Lesch, K. P. (2007). Long story short: the serotonin transporter in emotion regulation and social cognition. *Nat Neurosci, 10*(9), 1103-1109. https://doi.org/10.1038/nn1964

Carboni, E., & Di Chiara, G. (1989). Serotonin release estimated by transcortical dialysis in freely-moving rats. *Neuroscience, 32*(3), 637-645. https://doi.org/10.1016/0306-4522(89)90285-6

Celada, P., Bortolozzi, A., & Artigas, F. (2013). Serotonin 5-HT1A receptors as targets for agents to treat psychiatric disorders: rationale and current status of research. *CNS Drugs, 27*(9), 703-716. https://doi.org/10.1007/s40263-013-0071-0

Charnay, Y., & Leger, L. (2010). Brain serotonergic circuitries. *Dialogues Clin Neurosci, 12*(4), 471-487. Retrieved from https://www.ncbi.nlm.nih.gov/pubmed/21319493

Chatterjee, M., Jaiswal, M., & Palit, G. (2012). Comparative evaluation of forced swim test and tail suspension test as models of negative symptom of schizophrenia in rodents. *ISRN Psychiatry, 2012*, 595141. https://doi.org/10.5402/2012/595141

Chen, F., Rezvani, A. H., & Lawrence, A. J. (2003). Autoradiographic quantification of neurochemical markers of serotonin, dopamine and opioid systems in rat brain mesolimbic regions following chronic St John's wort treatment. *Naunyn Schmiedebergs Arch Pharmacol, 367*(2), 126-133. https://doi.org/10.1007/s00210-002-0666-3

Chen, L. Y., Jiang, M., Zhang, B., Gokce, O., & Sudhof, T. C. (2017). Conditional Deletion of All Neurexins Defines Diversity of Essential Synaptic Organizer Functions for Neurexins. *Neuron, 94*(3), 611-625 e614. https://doi.org/10.1016/j.neuron.2017.04.011

Chih, B., Gollan, L., & Scheiffele, P. (2006). Alternative splicing controls selective trans-synaptic interactions of the neuroligin-neurexin complex. *Neuron, 51*(2), 171-178. https://doi.org/10.1016/j.neuron.2006.06.005

Ching, M. S., Shen, Y., Tan, W. H., Jeste, S. S., Morrow, E. M., Chen, X., et al. (2010). Deletions of NRXN1 (neurexin-1) predispose to a wide spectrum of developmental disorders. *Am J Med Genet B Neuropsychiatr Genet, 153B*(4), 937-947. https://doi.org/10.1002/ajmg.b.31063

Chugani, D. C., Muzik, O., Behen, M., Rothermel, R., Janisse, J. J., Lee, J., et al. (1999). Developmental changes in brain serotonin synthesis capacity in autistic and nonautistic children. *Ann Neurol, 45*(3), 287-295. https://doi.org/10.1002/1531-8249(199903)45:3<287::aid-ana3>3.0.co;2-9

Clarke, R. A., Lee, S., & Eapen, V. (2012). Pathogenetic model for Tourette syndrome delineates overlap with related neurodevelopmental disorders including Autism. *Transl Psychiatry, 2*, e158. https://doi.org/10.1038/tp.2012.75

Coleman, D. M., Adams, J. B., Anderson, A. L., & Frye, R. E. (2019). Rating of the Effectiveness of 26 Psychiatric and Seizure Medications for Autism Spectrum Disorder: Results of a National Survey. *J Child Adolesc Psychopharmacol, 29*(2), 107-123. https://doi.org/10.1089/cap.2018.0121

Colgan, L. A., Cavolo, S. L., Commons, K. G., & Levitan, E. S. (2012). Action potential-independent and pharmacologically unique vesicular serotonin release from dendrites. *J Neurosci, 32*(45), 15737-15746. https://doi.org/10.1523/JNEUROSCI.0020-12.2012

Cook, E. H., Jr., Courchesne, R., Lord, C., Cox, N. J., Yan, S., Lincoln, A., et al. (1997). Evidence of linkage between the serotonin transporter and autistic disorder. *Mol Psychiatry, 2*(3), 247-250. https://doi.org/10.1038/sj.mp.4000266

Cryan, J. F., Mombereau, C., & Vassout, A. (2005). The tail suspension test as a model for assessing antidepressant activity: review of pharmacological and genetic studies in mice. *Neurosci Biobehav Rev, 29*(4-5), 571-625. https://doi.org/10.1016/j.neubiorev.2005.03.009

Dachtler, J., Glasper, J., Cohen, R. N., Ivorra, J. L., Swiffen, D. J., Jackson, A. J., et al. (2014). Deletion of alpha-neurexin II results in autism-related behaviors in mice. *Transl Psychiatry, 4*, e484. https://doi.org/10.1038/tp.2014.123

Dachtler, J., Ivorra, J. L., Rowland, T. E., Lever, C., Rodgers, R. J., & Clapcote, S. J. (2015). Heterozygous deletion of alpha-neurexin I or alpha-neurexin II results in behaviors relevant to autism and schizophrenia. *Behav Neurosci, 129*(6), 765-776. https://doi.org/10.1037/bne0000108

De-Miguel, F. F., Leon-Pinzon, C., Noguez, P., & Mendez, B. (2015). Serotonin release from the neuronal cell body and its long-lasting effects on the nervous system. *Philos Trans R Soc Lond B Biol Sci, 370*(1672). https://doi.org/10.1098/rstb.2014.0196

de Bartolomeis, A., Tomasetti, C., & Iasevoli, F. (2015). Update on the Mechanism of Action of Aripiprazole: Translational Insights into Antipsychotic Strategies Beyond Dopamine Receptor Antagonism. *CNS Drugs, 29*(9), 773-799. https://doi.org/10.1007/s40263-015-0278-3

de la Torre-Ubieta, L., Won, H., Stein, J. L., & Geschwind, D. H. (2016). Advancing the understanding of autism disease mechanisms through genetics. *Nat Med, 22*(4), 345-361. https://doi.org/10.1038/nm.4071

De Rubeis, S., He, X., Goldberg, A. P., Poultney, C. S., Samocha, K., Cicek, A. E., et al. (2014). Synaptic, transcriptional and chromatin genes disrupted in autism. *Nature, 515*(7526), 209-215. https://doi.org/10.1038/nature13772

de Wit, J., Sylwestrak, E., O'Sullivan, M. L., Otto, S., Tiglio, K., Savas, J. N., et al. (2009). LRRTM2 interacts with Neurexin1 and regulates excitatory synapse formation. *Neuron, 64*(6), 799-806. https://doi.org/10.1016/j.neuron.2009.12.019

Deneris, E., & Gaspar, P. (2018). Serotonin neuron development: shaping molecular and structural identities. *Wiley Interdiscip Rev Dev Biol, 7*(1). https://doi.org/10.1002/wdev.301

Deneris, E. S., & Wyler, S. C. (2012). Serotonergic transcriptional networks and potential importance to mental health. *Nat Neurosci, 15*(4), 519-527. https://doi.org/10.1038/nn.3039

Descarries, L., Riad, M., & Parent, M. (2010). CHAPTER 1.4 - Ultrastructure of the Serotonin Innervation in the Mammalian Central Nervous System. In C. P. Müller & B. L. Jacobs (Eds.), *Handbook of Behavioral Neuroscience* (Vol. 21, pp. 65-101): Elsevier.

Deuis, J. R., Dvorakova, L. S., & Vetter, I. (2017). Methods Used to Evaluate Pain Behaviors in Rodents. *Front Mol Neurosci, 10*, 284. https://doi.org/10.3389/fnmol.2017.00284

Ding, Y. Q., Marklund, U., Yuan, W., Yin, J., Wegman, L., Ericson, J., et al. (2003). Lmx1b is essential for the development of serotonergic neurons. *Nat Neurosci, 6*(9), 933-938. https://doi.org/10.1038/nn1104

Dolen, G., Darvishzadeh, A., Huang, K. W., & Malenka, R. C. (2013). Social reward requires coordinated activity of nucleus accumbens oxytocin and serotonin. *Nature, 501*(7466), 179-184. https://doi.org/10.1038/nature12518

Doshi-Velez, F., Ge, Y., & Kohane, I. (2014). Comorbidity clusters in autism spectrum disorders: an electronic health record time-series analysis. *Pediatrics, 133*(1), e54-63. https://doi.org/10.1542/peds.2013-0819

Dresbach, T., Qualmann, B., Kessels, M. M., Garner, C. C., & Gundelfinger, E. D. (2001). The presynaptic cytomatrix of brain synapses. *Cell Mol Life Sci, 58*(1), 94-116. https://doi.org/10.1007/PL00000781

Dudok, J. J., Groffen, A. J., Witter, M. P., Voorn, P., & Verhage, M. (2009). Chronic activation of the 5-HT(2) receptor reduces 5-HT neurite density as studied in organotypic slice cultures. *Brain Res, 1302*, 1-9. https://doi.org/10.1016/j.brainres.2009.08.071

Eiden, L. E., & Weihe, E. (2011). VMAT2: a dynamic regulator of brain monoaminergic neuronal function interacting with drugs of abuse. *Ann N Y Acad Sci, 1216*, 86-98. https://doi.org/10.1111/j.1749-6632.2010.05906.x

Esclassan, F., Francois, J., Phillips, K. G., Loomis, S., & Gilmour, G. (2015). Phenotypic characterization of nonsocial behavioral impairment in

neurexin 1alpha knockout rats. *Behav Neurosci, 129*(1), 74-85. https://doi.org/10.1037/bne0000024

Etherton, M. R., Blaiss, C. A., Powell, C. M., & Sudhof, T. C. (2009). Mouse neurexin-1alpha deletion causes correlated electrophysiological and behavioral changes consistent with cognitive impairments. *Proc Natl Acad Sci U S A, 106*(42), 17998-18003. https://doi.org/10.1073/pnas.0910297106

Etherton, M. R., Tabuchi, K., Sharma, M., Ko, J., & Sudhof, T. C. (2011). An autism-associated point mutation in the neuroligin cytoplasmic tail selectively impairs AMPA receptor-mediated synaptic transmission in hippocampus. *EMBO J, 30*(14), 2908-2919. https://doi.org/10.1038/emboj.2011.182

Fallon, J. H., Riley, J. N., Sipe, J. C., & Moore, R. Y. (1978). The islands of Calleja: organization and connections. *J Comp Neurol, 181*(2), 375-395. https://doi.org/10.1002/cne.901810209

Feng, J., Cai, X., Zhao, J., & Yan, Z. (2001). Serotonin receptors modulate GABA(A) receptor channels through activation of anchored protein kinase C in prefrontal cortical neurons. *J Neurosci, 21*(17), 6502-6511. Retrieved from https://www.ncbi.nlm.nih.gov/pubmed/11517239

Feng, J., Schroer, R., Yan, J., Song, W., Yang, C., Bockholt, A., et al. (2006). High frequency of neurexin 1beta signal peptide structural variants in patients with autism. *Neurosci Lett, 409*(1), 10-13. https://doi.org/10.1016/j.neulet.2006.08.017

Fernandez, S. P., Muzerelle, A., Scotto-Lomassese, S., Barik, J., Gruart, A., Delgado-Garcia, J. M., et al. (2017). Constitutive and Acquired Serotonin Deficiency Alters Memory and Hippocampal Synaptic Plasticity. *Neuropsychopharmacology, 42*(2), 512-523. https://doi.org/10.1038/npp.2016.134

Francken, B. J., Jurzak, M., Vanhauwe, J. F., Luyten, W. H., & Leysen, J. E. (1998). The human 5-ht5A receptor couples to Gi/Go proteins and inhibits adenylate cyclase in HEK 293 cells. *Eur J Pharmacol, 361*(2-3), 299-309. https://doi.org/10.1016/s0014-2999(98)00744-4

Frazer, S., Otomo, K., & Dayer, A. (2015). Early-life serotonin dysregulation affects the migration and positioning of cortical interneuron subtypes. *Transl Psychiatry, 5*, e644. https://doi.org/10.1038/tp.2015.147

Fuccillo, M. V., Foldy, C., Gokce, O., Rothwell, P. E., Sun, G. L., Malenka, R. C., et al. (2015). Single-Cell mRNA Profiling Reveals Cell-Type-Specific Expression of Neurexin Isoforms. *Neuron, 87*(2), 326-340. https://doi.org/10.1016/j.neuron.2015.06.028

Futai, K., Doty, C. D., Baek, B., Ryu, J., & Sheng, M. (2013). Specific trans-synaptic interaction with inhibitory interneuronal neurexin underlies differential ability of neuroligins to induce functional inhibitory synapses. *J Neurosci, 33*(8), 3612-3623. https://doi.org/10.1523/JNEUROSCI.1811-12.2013

Futai, K., Kim, M. J., Hashikawa, T., Scheiffele, P., Sheng, M., & Hayashi, Y. (2007). Retrograde modulation of presynaptic release probability through signaling mediated by PSD-95-neuroligin. *Nat Neurosci, 10*(2), 186-195. https://doi.org/10.1038/nn1837

Gabriele, S., Sacco, R., & Persico, A. M. (2014). Blood serotonin levels in autism spectrum disorder: a systematic review and meta-analysis. *Eur Neuropsychopharmacol, 24*(6), 919-929. https://doi.org/10.1016/j.euroneuro.2014.02.004

Galle, S. A., Courchesne, V., Mottron, L., & Frasnelli, J. (2013). Olfaction in the autism spectrum. *Perception, 42*(3), 341-355. https://doi.org/10.1068/p7337

Garcia-Garcia, A. L., Meng, Q., Canetta, S., Gardier, A. M., Guiard, B. P., Kellendonk, C., et al. (2017). Serotonin Signaling through Prefrontal Cortex 5-HT1A Receptors during Adolescence Can Determine Baseline Mood-Related Behaviors. *Cell Rep, 18*(5), 1144-1156. https://doi.org/10.1016/j.celrep.2017.01.021

Gaspar, P., Cases, O., & Maroteaux, L. (2003). The developmental role of serotonin: news from mouse molecular genetics. *Nat Rev Neurosci, 4*(12), 1002-1012. https://doi.org/10.1038/nrn1256

Gauthier, J., Siddiqui, T. J., Huashan, P., Yokomaku, D., Hamdan, F. F., Champagne, N., et al. (2011). Truncating mutations in NRXN2 and NRXN1 in autism spectrum disorders and schizophrenia. *Hum Genet, 130*(4), 563-573. https://doi.org/10.1007/s00439-011-0975-z

Gibson, J. R., Bartley, A. F., Hays, S. A., & Huber, K. M. (2008). Imbalance of neocortical excitation and inhibition and altered UP states reflect network hyperexcitability in the mouse model of fragile X syndrome. *J Neurophysiol, 100*(5), 2615-2626. https://doi.org/10.1152/jn.90752.2008

Giovedi, S., Corradi, A., Fassio, A., & Benfenati, F. (2014). Involvement of synaptic genes in the pathogenesis of autism spectrum disorders: the case of synapsins. *Front Pediatr, 2*, 94. https://doi.org/10.3389/fped.2014.00094

Gomez, A. M., Traunmuller, L., & Scheiffele, P. (2021). Neurexins: molecular codes for shaping neuronal synapses. *Nat Rev Neurosci, 22*(3), 137-151. https://doi.org/10.1038/s41583-020-00415-7

Gonzalez-Lozano, M. A., Klemmer, P., Gebuis, T., Hassan, C., van Nierop, P., van Kesteren, R. E., et al. (2016). Dynamics of the mouse brain cortical synaptic proteome during postnatal brain development. *Sci Rep, 6*, 35456. https://doi.org/10.1038/srep35456

Gorecki, D. C., Szklarczyk, A., Lukasiuk, K., Kaczmarek, L., & Simons, J. P. (1999). Differential seizure-induced and developmental changes of neurexin expression. *Mol Cell Neurosci, 13*(3), 218-227. Retrieved from http://www.ncbi.nlm.nih.gov/pubmed/10408888

Gould, G. G., Hensler, J. G., Burke, T. F., Benno, R. H., Onaivi, E. S., & Daws, L. C. (2011). Density and function of central serotonin (5-HT) transporters, 5-

HT1A and 5-HT2A receptors, and effects of their targeting on BTBR T+tf/J mouse social behavior. *J Neurochem, 116*(2), 291-303. https://doi.org/10.1111/j.1471-4159.2010.07104.x

Graf, E. R., Zhang, X., Jin, S. X., Linhoff, M. W., & Craig, A. M. (2004). Neurexins induce differentiation of GABA and glutamate postsynaptic specializations via neuroligins. *Cell, 119*(7), 1013-1026. https://doi.org/10.1016/j.cell.2004.11.035

Grailhe, R., Grabtree, G. W., & Hen, R. (2001). Human 5-HT(5) receptors: the 5-HT(5A) receptor is functional but the 5-HT(5B) receptor was lost during mammalian evolution. *Eur J Pharmacol, 418*(3), 157-167. https://doi.org/10.1016/s0014-2999(01)00933-5

Grayton, H. M., Missler, M., Collier, D. A., & Fernandes, C. (2013). Altered social behaviours in neurexin 1alpha knockout mice resemble core symptoms in neurodevelopmental disorders. *PLoS One, 8*(6), e67114. https://doi.org/10.1371/journal.pone.0067114

Grove, J., Ripke, S., Als, T. D., Mattheisen, M., Walters, R. K., Won, H., et al. (2019). Identification of common genetic risk variants for autism spectrum disorder. *Nat Genet, 51*(3), 431-444. https://doi.org/10.1038/s41588-019-0344-8

Gu, X., Zhou, Y., Wu, X., Wang, F., Zhang, C. Y., Du, C., et al. (2014). Antidepressant-like effects of auraptenol in mice. *Sci Rep, 4*, 4433. https://doi.org/10.1038/srep04433

Guilmatre, A., Dubourg, C., Mosca, A. L., Legallic, S., Goldenberg, A., Drouin-Garraud, V., et al. (2009). Recurrent rearrangements in synaptic and neurodevelopmental genes and shared biologic pathways in schizophrenia, autism, and mental retardation. *Arch Gen Psychiatry, 66*(9), 947-956. https://doi.org/10.1001/archgenpsychiatry.2009.80

Haase, J., Grudzinska-Goebel, J., Muller, H. K., Munster-Wandowski, A., Chow, E., Wynne, K., et al. (2017). Serotonin Transporter Associated Protein Complexes Are Enriched in Synaptic Vesicle Proteins and Proteins Involved in Energy Metabolism and Ion Homeostasis. *ACS Chem Neurosci, 8*(5), 1101-1116. https://doi.org/10.1021/acschemneuro.6b00437

Hagiwara, A., Pal, S. K., Sato, T. F., Wienisch, M., & Murthy, V. N. (2012). Optophysiological analysis of associational circuits in the olfactory cortex. *Front Neural Circuits, 6*, 18. https://doi.org/10.3389/fncir.2012.00018

Haider, S., Khaliq, S., Tabassum, S., & Haleem, D. J. (2012). Role of somatodendritic and postsynaptic 5-HT(1)A receptors on learning and memory functions in rats. *Neurochem Res, 37*(10), 2161-2166. https://doi.org/10.1007/s11064-012-0839-5

Hallmayer, J., Cleveland, S., Torres, A., Phillips, J., Cohen, B., Torigoe, T., et al. (2011). Genetic heritability and shared environmental factors among twin pairs with autism. *Arch Gen Psychiatry, 68*(11), 1095-1102. https://doi.org/10.1001/archgenpsychiatry.2011.76

Han, S., Tai, C., Westenbroek, R. E., Yu, F. H., Cheah, C. S., Potter, G. B., et al. (2012). Autistic-like behaviour in Scn1a+/- mice and rescue by enhanced GABA-mediated neurotransmission. *Nature, 489*(7416), 385-390. https://doi.org/10.1038/nature11356

Hansen, S. N., Schendel, D. E., & Parner, E. T. (2015). Explaining the increase in the prevalence of autism spectrum disorders: the proportion attributable to changes in reporting practices. *JAMA Pediatr, 169*(1), 56-62. https://doi.org/10.1001/jamapediatrics.2014.1893

Harkin, L. F., Lindsay, S. J., Xu, Y., Alzu'bi, A., Ferrara, A., Gullon, E. A., et al. (2017). Neurexins 1-3 Each Have a Distinct Pattern of Expression in the Early Developing Human Cerebral Cortex. *Cereb Cortex, 27*(1), 216-232. https://doi.org/10.1093/cercor/bhw394

Hashemi, P., Dankoski, E. C., Petrovic, J., Keithley, R. B., & Wightman, R. M. (2009). Voltammetric detection of 5-hydroxytryptamine release in the rat brain. *Anal Chem, 81*(22), 9462-9471. https://doi.org/10.1021/ac9018846

Hegarty, J. P., 2nd, Pegoraro, L. F. L., Lazzeroni, L. C., Raman, M. M., Hallmayer, J. F., Monterrey, J. C., et al. (2020). Genetic and environmental influences on structural brain measures in twins with autism spectrum disorder. *Mol Psychiatry, 25*(10), 2556-2566. https://doi.org/10.1038/s41380-018-0330-z

Hendricks, T., Francis, N., Fyodorov, D., & Deneris, E. S. (1999). The ETS domain factor Pet-1 is an early and precise marker of central serotonin neurons and interacts with a conserved element in serotonergic genes. *J Neurosci, 19*(23), 10348-10356. https://doi.org/10.1523/jneurosci.19-23-10348.1999

Hernandez-Hernandez, O. T., Martinez-Mota, L., Herrera-Perez, J. J., & Jimenez-Rubio, G. (2019). Role of Estradiol in the Expression of Genes Involved in Serotonin Neurotransmission: Implications for Female Depression. *Curr Neuropharmacol, 17*(5), 459-471. https://doi.org/10.2174/1570159X16666180628165107

Herry, C., Ciocchi, S., Senn, V., Demmou, L., Muller, C., & Luthi, A. (2008). Switching on and off fear by distinct neuronal circuits. *Nature, 454*(7204), 600-606. https://doi.org/10.1038/nature07166

Higley, M. J., & Sabatini, B. L. (2010). Competitive regulation of synaptic Ca2+ influx by D2 dopamine and A2A adenosine receptors. *Nat Neurosci, 13*(8), 958-966. https://doi.org/10.1038/nn.2592

Hirsch, L. E., & Pringsheim, T. (2016). Aripiprazole for autism spectrum disorders (ASD). *Cochrane Database Syst Rev*(6), CD009043. https://doi.org/10.1002/14651858.CD009043.pub3

Hitti, F. L., & Siegelbaum, S. A. (2014). The hippocampal CA2 region is essential for social memory. *Nature, 508*(7494), 88-92. https://doi.org/10.1038/nature13028

Hokfelt, T., Xu, Z. Q., Shi, T. J., Holmberg, K., & Zhang, X. (1998). Galanin in ascending systems. Focus on coexistence with 5-hydroxytryptamine and

noradrenaline. *Ann N Y Acad Sci, 863*, 252-263. https://doi.org/10.1111/j.1749-6632.1998.tb10700.x

Holmes, A., Yang, R. J., Lesch, K. P., Crawley, J. N., & Murphy, D. L. (2003). Mice lacking the serotonin transporter exhibit 5-HT(1A) receptor-mediated abnormalities in tests for anxiety-like behavior. *Neuropsychopharmacology, 28*(12), 2077-2088. https://doi.org/10.1038/sj.npp.1300266

Hu, Z., Xiao, X., Zhang, Z., & Li, M. (2019). Genetic insights and neurobiological implications from NRXN1 in neuropsychiatric disorders. *Mol Psychiatry, 24*(10), 1400-1414. https://doi.org/10.1038/s41380-019-0438-9

Ichtchenko, K., Hata, Y., Nguyen, T., Ullrich, B., Missler, M., Moomaw, C., et al. (1995). Neuroligin 1: a splice site-specific ligand for beta-neurexins. *Cell, 81*(3), 435-443. Retrieved from http://www.ncbi.nlm.nih.gov/pubmed/7736595

Ichtchenko, K., Nguyen, T., & Sudhof, T. C. (1996). Structures, alternative splicing, and neurexin binding of multiple neuroligins. *J Biol Chem, 271*(5), 2676-2682. Retrieved from http://www.ncbi.nlm.nih.gov/pubmed/8576240

Ishimura, K., Takeuchi, Y., Fujiwara, K., Tominaga, M., Yoshioka, H., & Sawada, T. (1988). Quantitative analysis of the distribution of serotonin-immunoreactive cell bodies in the mouse brain. *Neurosci Lett, 91*(3), 265-270. https://doi.org/10.1016/0304-3940(88)90691-x

Jacobshagen, M., Niquille, M., Chaumont-Dubel, S., Marin, P., & Dayer, A. (2014). The serotonin 6 receptor controls neuronal migration during corticogenesis via a ligand-independent Cdk5-dependent mechanism. *Development, 141*(17), 3370-3377. https://doi.org/10.1242/dev.108043

Jansch, C., Ziegler, G. C., Forero, A., Gredy, S., Waldchen, S., Vitale, M. R., et al. (2021). Serotonin-specific neurons differentiated from human iPSCs form distinct subtypes with synaptic protein assembly. *J Neural Transm (Vienna), 128*(2), 225-241. https://doi.org/10.1007/s00702-021-02303-5

Jesner, O. S., Aref-Adib, M., & Coren, E. (2007). Risperidone for autism spectrum disorder. *Cochrane Database Syst Rev*(1), CD005040. https://doi.org/10.1002/14651858.CD005040.pub2

Jiang, X., Xing, G., Yang, C., Verma, A., Zhang, L., & Li, H. (2009). Stress impairs 5-HT2A receptor-mediated serotonergic facilitation of GABA release in juvenile rat basolateral amygdala. *Neuropsychopharmacology, 34*(2), 410-423. https://doi.org/10.1038/npp.2008.71

John, C. E., Budygin, E. A., Mateo, Y., & Jones, S. R. (2006). Neurochemical characterization of the release and uptake of dopamine in ventral tegmental area and serotonin in substantia nigra of the mouse. *J Neurochem, 96*(1), 267-282. https://doi.org/10.1111/j.1471-4159.2005.03557.x

Kane, M. J., Angoa-Perez, M., Briggs, D. I., Sykes, C. E., Francescutti, D. M., Rosenberg, D. R., et al. (2012). Mice genetically depleted of brain serotonin display social impairments, communication deficits and

repetitive behaviors: possible relevance to autism. *PLoS One, 7*(11), e48975. https://doi.org/10.1371/journal.pone.0048975

Kang, Y., Zhang, X., Dobie, F., Wu, H., & Craig, A. M. (2008). Induction of GABAergic postsynaptic differentiation by alpha-neurexins. *J Biol Chem, 283*(4), 2323-2334. https://doi.org/10.1074/jbc.M703957200

Kasem, E., Kurihara, T., & Tabuchi, K. (2018). Neurexins and neuropsychiatric disorders. *Neurosci Res, 127*, 53-60. https://doi.org/10.1016/j.neures.2017.10.012

Kazdoba, T. M., Leach, P. T., Yang, M., Silverman, J. L., Solomon, M., & Crawley, J. N. (2016). Translational Mouse Models of Autism: Advancing Toward Pharmacological Therapeutics. *Curr Top Behav Neurosci, 28*, 1-52. https://doi.org/10.1007/7854_2015_5003

Kehr, J., Yoshitake, T., Wang, F. H., Razani, H., Gimenez-Llort, L., Jansson, A., et al. (2002). Galanin is a potent in vivo modulator of mesencephalic serotonergic neurotransmission. *Neuropsychopharmacology, 27*(3), 341-356. https://doi.org/10.1016/S0893-133X(02)00309-3

Kempton, M. J., Salvador, Z., Munafo, M. R., Geddes, J. R., Simmons, A., Frangou, S., et al. (2011). Structural neuroimaging studies in major depressive disorder. Meta-analysis and comparison with bipolar disorder. *Arch Gen Psychiatry, 68*(7), 675-690. https://doi.org/10.1001/archgenpsychiatry.2011.60

Keum, S., Kim, A., Shin, J. J., Kim, J. H., Park, J., & Shin, H. S. (2018). A Missense Variant at the Nrxn3 Locus Enhances Empathy Fear in the Mouse. *Neuron, 98*(3), 588-601 e585. https://doi.org/10.1016/j.neuron.2018.03.041

Kim, H. G., Kishikawa, S., Higgins, A. W., Seong, I. S., Donovan, D. J., Shen, Y., et al. (2008). Disruption of neurexin 1 associated with autism spectrum disorder. *Am J Hum Genet, 82*(1), 199-207. https://doi.org/10.1016/j.ajhg.2007.09.011

Kim, J. H., & Huganir, R. L. (1999). Organization and regulation of proteins at synapses. *Curr Opin Cell Biol, 11*(2), 248-254. https://doi.org/10.1016/s0955-0674(99)80033-7

Kirov, G., Gumus, D., Chen, W., Norton, N., Georgieva, L., Sari, M., et al. (2008). Comparative genome hybridization suggests a role for NRXN1 and APBA2 in schizophrenia. *Hum Mol Genet, 17*(3), 458-465. https://doi.org/10.1093/hmg/ddm323

Kiser, D., Steemers, B., Branchi, I., & Homberg, J. R. (2012). The reciprocal interaction between serotonin and social behaviour. *Neurosci Biobehav Rev, 36*(2), 786-798. https://doi.org/10.1016/j.neubiorev.2011.12.009

Ko, J., Fuccillo, M. V., Malenka, R. C., & Sudhof, T. C. (2009). LRRTM2 functions as a neurexin ligand in promoting excitatory synapse formation. *Neuron, 64*(6), 791-798. https://doi.org/10.1016/j.neuron.2009.12.012

Kobayashi, K., Ikeda, Y., Haneda, E., & Suzuki, H. (2008). Chronic fluoxetine bidirectionally modulates potentiating effects of serotonin on the

hippocampal mossy fiber synaptic transmission. *J Neurosci, 28*(24), 6272-6280. https://doi.org/10.1523/JNEUROSCI.1656-08.2008

Kobayashi, K., Mikahara, Y., Murata, Y., Morita, D., Matsuura, S., Segi-Nishida, E., et al. (2020). Predominant Role of Serotonin at the Hippocampal Mossy Fiber Synapse with Redundant Monoaminergic Modulation. *iScience, 23*(4), 101025. https://doi.org/10.1016/j.isci.2020.101025

Koehnke, J., Katsamba, P. S., Ahlsen, G., Bahna, F., Vendome, J., Honig, B., et al. (2010). Splice form dependence of beta-neurexin/neuroligin binding interactions. *Neuron, 67*(1), 61-74. https://doi.org/10.1016/j.neuron.2010.06.001

Kogan, J. H., Frankland, P. W., & Silva, A. J. (2000). Long-term memory underlying hippocampus-dependent social recognition in mice. *Hippocampus, 10*(1), 47-56. https://doi.org/10.1002/(SICI)1098-1063(2000)10:1<47::AID-HIPO5>3.0.CO;2-6

Kosofsky, B. E., & Molliver, M. E. (1987). The serotoninergic innervation of cerebral cortex: different classes of axon terminals arise from dorsal and median raphe nuclei. *Synapse, 1*(2), 153-168. https://doi.org/10.1002/syn.890010204

Kudo, T., Uchigashima, M., Miyazaki, T., Konno, K., Yamasaki, M., Yanagawa, Y., et al. (2012). Three types of neurochemical projection from the bed nucleus of the stria terminalis to the ventral tegmental area in adult mice. *J Neurosci, 32*(50), 18035-18046. https://doi.org/10.1523/JNEUROSCI.4057-12.2012

Laarakker, M. C., Reinders, N. R., Bruining, H., Ophoff, R. A., & Kas, M. J. (2012). Sex-dependent novelty response in neurexin-1alpha mutant mice. *PLoS One, 7*(2), e31503. https://doi.org/10.1371/journal.pone.0031503

Lee, J. J., Hahm, E. T., Lee, C. H., & Cho, Y. W. (2008). Serotonergic modulation of GABAergic and glutamatergic synaptic transmission in mechanically isolated rat medial preoptic area neurons. *Neuropsychopharmacology, 33*(2), 340-352. https://doi.org/10.1038/sj.npp.1301396

Levy, S. E., Giarelli, E., Lee, L. C., Schieve, L. A., Kirby, R. S., Cunniff, C., et al. (2010). Autism spectrum disorder and co-occurring developmental, psychiatric, and medical conditions among children in multiple populations of the United States. *J Dev Behav Pediatr, 31*(4), 267-275. https://doi.org/10.1097/DBP.0b013e3181d5d03b

Lew, C. H., Groeniger, K. M., Hanson, K. L., Cuevas, D., Greiner, D. M. Z., Hrvoj-Mihic, B., et al. (2020). Serotonergic innervation of the amygdala is increased in autism spectrum disorder and decreased in Williams syndrome. *Mol Autism, 11*(1), 12. https://doi.org/10.1186/s13229-019-0302-4

Leyfer, O. T., Folstein, S. E., Bacalman, S., Davis, N. O., Dinh, E., Morgan, J., et al. (2006). Comorbid psychiatric disorders in children with autism: interview development and rates of disorders. *J Autism Dev Disord, 36*(7), 849-861. https://doi.org/10.1007/s10803-006-0123-0

Li, Y., Zhong, W., Wang, D., Feng, Q., Liu, Z., Zhou, J., et al. (2016). Serotonin neurons in the dorsal raphe nucleus encode reward signals. *Nat Commun, 7*, 10503. https://doi.org/10.1038/ncomms10503

Lin, K., Zhong, X., Li, L., Ying, M., Yang, T., Zhang, Z., et al. (2020). AAV9-Retro mediates efficient transduction with axon terminal absorption and blood-brain barrier transportation. *Mol Brain, 13*(1), 138. https://doi.org/10.1186/s13041-020-00679-1

Lira, A., Zhou, M., Castanon, N., Ansorge, M. S., Gordon, J. A., Francis, J. H., et al. (2003). Altered depression-related behaviors and functional changes in the dorsal raphe nucleus of serotonin transporter-deficient mice. *Biol Psychiatry, 54*(10), 960-971. https://doi.org/10.1016/s0006-3223(03)00696-6

Liu, C., Kershberg, L., Wang, J., Schneeberger, S., & Kaeser, P. S. (2018). Dopamine Secretion Is Mediated by Sparse Active Zone-like Release Sites. *Cell, 172*(4), 706-718 e715. https://doi.org/10.1016/j.cell.2018.01.008

Liu, C., Maejima, T., Wyler, S. C., Casadesus, G., Herlitze, S., & Deneris, E. S. (2010). Pet-1 is required across different stages of life to regulate serotonergic function. *Nat Neurosci, 13*(10), 1190-1198. https://doi.org/10.1038/nn.2623

Lu, X., Barr, A. M., Kinney, J. W., Sanna, P., Conti, B., Behrens, M. M., et al. (2005). A role for galanin in antidepressant actions with a focus on the dorsal raphe nucleus. *Proc Natl Acad Sci U S A, 102*(3), 874-879. https://doi.org/10.1073/pnas.0408891102

Luo, F., Sclip, A., Jiang, M., & Sudhof, T. C. (2020). Neurexins cluster Ca(2+) channels within the presynaptic active zone. *EMBO J, 39*(7), e103208. https://doi.org/10.15252/embj.2019103208

Luo, J., Feng, Q., Wei, L., & Luo, M. (2017). Optogenetic activation of dorsal raphe neurons rescues the autistic-like social deficits in Shank3 knockout mice. *Cell Res, 27*(7), 950-953. https://doi.org/10.1038/cr.2017.52

Makkonen, I., Riikonen, R., Kokki, H., Airaksinen, M. M., & Kuikka, J. T. (2008). Serotonin and dopamine transporter binding in children with autism determined by SPECT. *Dev Med Child Neurol, 50*(8), 593-597. https://doi.org/10.1111/j.1469-8749.2008.03027.x

Mao, W., Salzberg, A. C., Uchigashima, M., Hasegawa, Y., Hock, H., Watanabe, M., et al. (2018). Activity-Induced Regulation of Synaptic Strength through the Chromatin Reader L3mbtl1. *Cell Rep, 23*(11), 3209-3222. https://doi.org/10.1016/j.celrep.2018.05.028

Mao, W., Watanabe, T., Cho, S., Frost, J. L., Truong, T., Zhao, X., et al. (2015). Shank1 regulates excitatory synaptic transmission in mouse hippocampal parvalbumin-expressing inhibitory interneurons. *Eur J Neurosci, 41*(8), 1025-1035. https://doi.org/10.1111/ejn.12877

Marek, G. J. (2010). CHAPTER 2.2 - Electrophysiology of Serotonin Receptors. In C. P. Müller & B. L. Jacobs (Eds.), *Handbook of Behavioral Neuroscience* (Vol. 21, pp. 163-182): Elsevier.

Marek, G. J., Carpenter, L. L., McDougle, C. J., & Price, L. H. (2003). Synergistic action of 5-HT2A antagonists and selective serotonin reuptake inhibitors in neuropsychiatric disorders. *Neuropsychopharmacology, 28*(2), 402-412. https://doi.org/10.1038/sj.npp.1300057

Martin, E. I., Ressler, K. J., Binder, E., & Nemeroff, C. B. (2009). The neurobiology of anxiety disorders: brain imaging, genetics, and psychoneuroendocrinology. *Psychiatr Clin North Am, 32*(3), 549-575. https://doi.org/10.1016/j.psc.2009.05.004

Matsuda, K., Budisantoso, T., Mitakidis, N., Sugaya, Y., Miura, E., Kakegawa, W., et al. (2016). Transsynaptic Modulation of Kainate Receptor Functions by C1q-like Proteins. *Neuron, 90*(4), 752-767. https://doi.org/10.1016/j.neuron.2016.04.001

Matsui, A., & Alvarez, V. A. (2018). Cocaine Inhibition of Synaptic Transmission in the Ventral Pallidum Is Pathway-Specific and Mediated by Serotonin. *Cell Rep, 23*(13), 3852-3863. https://doi.org/10.1016/j.celrep.2018.05.076

Matsumoto, R., Ichise, M., Ito, H., Ando, T., Takahashi, H., Ikoma, Y., et al. (2010). Reduced serotonin transporter binding in the insular cortex in patients with obsessive-compulsive disorder: a [11C]DASB PET study. *Neuroimage, 49*(1), 121-126. https://doi.org/10.1016/j.neuroimage.2009.07.069

McFarlane, H. G., Kusek, G. K., Yang, M., Phoenix, J. L., Bolivar, V. J., & Crawley, J. N. (2008). Autism-like behavioral phenotypes in BTBR T+tf/J mice. *Genes Brain Behav, 7*(2), 152-163. https://doi.org/10.1111/j.1601-183X.2007.00330.x

Meneses, A. (2003). A pharmacological analysis of an associative learning task: 5-HT(1) to 5-HT(7) receptor subtypes function on a pavlovian/instrumental autoshaped memory. *Learn Mem, 10*(5), 363-372. https://doi.org/10.1101/lm.60503

Migliarini, S., Pacini, G., Pelosi, B., Lunardi, G., & Pasqualetti, M. (2013). Lack of brain serotonin affects postnatal development and serotonergic neuronal circuitry formation. *Mol Psychiatry, 18*(10), 1106-1118. https://doi.org/10.1038/mp.2012.128

Mikuni, T., Nishiyama, J., Sun, Y., Kamasawa, N., & Yasuda, R. (2016). High-Throughput, High-Resolution Mapping of Protein Localization in Mammalian Brain by In Vivo Genome Editing. *Cell, 165*(7), 1803-1817. https://doi.org/10.1016/j.cell.2016.04.044

Miner, L. H., Schroeter, S., Blakely, R. D., & Sesack, S. R. (2000). Ultrastructural localization of the serotonin transporter in superficial and deep layers of the rat prelimbic prefrontal cortex and its spatial relationship to dopamine terminals. *J Comp Neurol, 427*(2), 220-234. https://doi.org/10.1002/1096-9861(20001113)427:2<220::aid-cne5>3.0.co;2-p

Missler, M., Hammer, R. E., & Sudhof, T. C. (1998). Neurexophilin binding to alpha-neurexins. A single LNS domain functions as an independently folding ligand-binding unit. *J Biol Chem, 273*(52), 34716-34723. Retrieved from http://www.ncbi.nlm.nih.gov/pubmed/9856994

Missler, M., Zhang, W., Rohlmann, A., Kattenstroth, G., Hammer, R. E., Gottmann, K., et al. (2003). Alpha-neurexins couple Ca2+ channels to synaptic vesicle exocytosis. *Nature, 423*(6943), 939-948. https://doi.org/10.1038/nature01755

Molas, S., Zhao-Shea, R., Liu, L., DeGroot, S. R., Gardner, P. D., & Tapper, A. R. (2017). A circuit-based mechanism underlying familiarity signaling and the preference for novelty. *Nat Neurosci, 20*(9), 1260-1268. https://doi.org/10.1038/nn.4607

Monteiro, S., Roque, S., de Sa-Calcada, D., Sousa, N., Correia-Neves, M., & Cerqueira, J. J. (2015). An efficient chronic unpredictable stress protocol to induce stress-related responses in C57BL/6 mice. *Front Psychiatry, 6*, 6. https://doi.org/10.3389/fpsyt.2015.00006

Moore, R. Y., & Halaris, A. E. (1975). Hippocampal innervation by serotonin neurons of the midbrain raphe in the rat. *J Comp Neurol, 164*(2), 171-183. https://doi.org/10.1002/cne.901640203

Moreau, C. A., Urchs, S. G. W., Kuldeep, K., Orban, P., Schramm, C., Dumas, G., et al. (2020). Mutations associated with neuropsychiatric conditions delineate functional brain connectivity dimensions contributing to autism and schizophrenia. *Nat Commun, 11*(1), 5272. https://doi.org/10.1038/s41467-020-18997-2

Moy, S. S., Nadler, J. J., Perez, A., Barbaro, R. P., Johns, J. M., Magnuson, T. R., et al. (2004). Sociability and preference for social novelty in five inbred strains: an approach to assess autistic-like behavior in mice. *Genes Brain Behav, 3*(5), 287-302. https://doi.org/10.1111/j.1601-1848.2004.00076.x

Muller, C. L., Anacker, A. M. J., & Veenstra-VanderWeele, J. (2016). The serotonin system in autism spectrum disorder: From biomarker to animal models. *Neuroscience, 321*, 24-41. https://doi.org/10.1016/j.neuroscience.2015.11.010

Muller, H. K., Kragballe, M., Fjorback, A. W., & Wiborg, O. (2014). Differential regulation of the serotonin transporter by vesicle-associated membrane protein 2 in cells of neuronal versus non-neuronal origin. *PLoS One, 9*(5), e97540. https://doi.org/10.1371/journal.pone.0097540

Muller, J. F., Mascagni, F., & McDonald, A. J. (2007). Serotonin-immunoreactive axon terminals innervate pyramidal cells and interneurons in the rat basolateral amygdala. *J Comp Neurol, 505*(3), 314-335. https://doi.org/10.1002/cne.21486

Muzerelle, A., Scotto-Lomassese, S., Bernard, J. F., Soiza-Reilly, M., & Gaspar, P. (2016). Conditional anterograde tracing reveals distinct targeting of individual serotonin cell groups (B5-B9) to the forebrain and brainstem.

Brain Struct Funct, 221(1), 535-561. https://doi.org/10.1007/s00429-014-0924-4

Nag, A., Bochukova, E. G., Kremeyer, B., Campbell, D. D., Muller, H., Valencia-Duarte, A. V., et al. (2013). CNV analysis in Tourette syndrome implicates large genomic rearrangements in COL8A1 and NRXN1. *PLoS One, 8*(3), e59061. https://doi.org/10.1371/journal.pone.0059061

Nagano, M., Takumi, T., & Suzuki, H. (2018). Critical roles of serotonin-oxytocin interaction during the neonatal period in social behavior in 15q dup mice with autistic traits. *Sci Rep, 8*(1), 13675. https://doi.org/10.1038/s41598-018-32042-9

Nakai, N., Nagano, M., Saitow, F., Watanabe, Y., Kawamura, Y., Kawamoto, A., et al. (2017). Serotonin rebalances cortical tuning and behavior linked to autism symptoms in 15q11-13 CNV mice. *Sci Adv, 3*(6), e1603001. https://doi.org/10.1126/sciadv.1603001

Nakamura, K., Sekine, Y., Ouchi, Y., Tsujii, M., Yoshikawa, E., Futatsubashi, M., et al. (2010). Brain serotonin and dopamine transporter bindings in adults with high-functioning autism. *Arch Gen Psychiatry, 67*(1), 59-68. https://doi.org/10.1001/archgenpsychiatry.2009.137

Nam, C. I., & Chen, L. (2005). Postsynaptic assembly induced by neurexin-neuroligin interaction and neurotransmitter. *Proc Natl Acad Sci U S A, 102*(17), 6137-6142. https://doi.org/10.1073/pnas.0502038102

Nelson, S. B., & Valakh, V. (2015). Excitatory/Inhibitory Balance and Circuit Homeostasis in Autism Spectrum Disorders. *Neuron, 87*(4), 684-698. https://doi.org/10.1016/j.neuron.2015.07.033

Nguyen, T. M., Schreiner, D., Xiao, L., Traunmuller, L., Bornmann, C., & Scheiffele, P. (2016). An alternative splicing switch shapes neurexin repertoires in principal neurons versus interneurons in the mouse hippocampus. *Elife, 5*. https://doi.org/10.7554/eLife.22757

Nielsen, K., Brask, D., Knudsen, G. M., & Aznar, S. (2006). Immunodetection of the serotonin transporter protein is a more valid marker for serotonergic fibers than serotonin. *Synapse, 59*(5), 270-276. https://doi.org/10.1002/syn.20240

Nishitani, N., Nagayasu, K., Asaoka, N., Yamashiro, M., Andoh, C., Nagai, Y., et al. (2019). Manipulation of dorsal raphe serotonergic neurons modulates active coping to inescapable stress and anxiety-related behaviors in mice and rats. *Neuropsychopharmacology, 44*(4), 721-732. https://doi.org/10.1038/s41386-018-0254-y

Nishizawa, S., Benkelfat, C., Young, S. N., Leyton, M., Mzengeza, S., de Montigny, C., et al. (1997). Differences between males and females in rates of serotonin synthesis in human brain. *Proc Natl Acad Sci U S A, 94*(10), 5308-5313. https://doi.org/10.1073/pnas.94.10.5308

Ohmura, Y., Tanaka, K. F., Tsunematsu, T., Yamanaka, A., & Yoshioka, M. (2014). Optogenetic activation of serotonergic neurons enhances anxiety-

like behaviour in mice. *Int J Neuropsychopharmacol, 17*(11), 1777-1783. https://doi.org/10.1017/S1461145714000637

Okaty, B. W., Commons, K. G., & Dymecki, S. M. (2019). Embracing diversity in the 5-HT neuronal system. *Nat Rev Neurosci, 20*(7), 397-424. https://doi.org/10.1038/s41583-019-0151-3

Okaty, B. W., Freret, M. E., Rood, B. D., Brust, R. D., Hennessy, M. L., deBairos, D., et al. (2015). Multi-Scale Molecular Deconstruction of the Serotonin Neuron System. *Neuron, 88*(4), 774-791. https://doi.org/10.1016/j.neuron.2015.10.007

Okuyama, T., Kitamura, T., Roy, D. S., Itohara, S., & Tonegawa, S. (2016). Ventral CA1 neurons store social memory. *Science, 353*(6307), 1536-1541. https://doi.org/10.1126/science.aaf7003

Oleskevich, S., Descarries, L., Watkins, K. C., Seguela, P., & Daszuta, A. (1991). Ultrastructural features of the serotonin innervation in adult rat hippocampus: an immunocytochemical description in single and serial thin sections. *Neuroscience, 42*(3), 777-791. https://doi.org/10.1016/0306-4522(91)90044-o

Olney, J. J., Marshall, S. A., & Thiele, T. E. (2018). Assessment of depression-like behavior and anhedonia after repeated cycles of binge-like ethanol drinking in male C57BL/6J mice. *Pharmacol Biochem Behav, 168*, 1-7. https://doi.org/10.1016/j.pbb.2018.03.006

Pandya, M., Altinay, M., Malone, D. A., Jr., & Anand, A. (2012). Where in the brain is depression? *Curr Psychiatry Rep, 14*(6), 634-642. https://doi.org/10.1007/s11920-012-0322-7

Paredes, S., Cantillo, S., Candido, K. D., & Knezevic, N. N. (2019). An Association of Serotonin with Pain Disorders and Its Modulation by Estrogens. *Int J Mol Sci, 20*(22). https://doi.org/10.3390/ijms20225729

Parent, M., & Descarries, L. (2020). Chapter 4 - Ultrastructure of the serotonin innervation in mammalian central nervous system. In C. P. Müller & K. A. Cunningham (Eds.), *Handbook of Behavioral Neuroscience* (Vol. 31, pp. 49-90): Elsevier.

Parent, M., Wallman, M. J., & Descarries, L. (2010). Distribution and ultrastructural features of the serotonin innervation in rat and squirrel monkey subthalamic nucleus. *Eur J Neurosci, 31*(7), 1233-1242. https://doi.org/10.1111/j.1460-9568.2010.07143.x

Parpura, V., & Zorec, R. (2010). Gliotransmission: Exocytotic release from astrocytes. *Brain Res Rev, 63*(1-2), 83-92. https://doi.org/10.1016/j.brainresrev.2009.11.008

Patel, K. R., Cherian, J., Gohil, K., & Atkinson, D. (2014). Schizophrenia: overview and treatment options. *P T, 39*(9), 638-645. Retrieved from https://www.ncbi.nlm.nih.gov/pubmed/25210417

Patzke, C., Brockmann, M. M., Dai, J., Gan, K. J., Grauel, M. K., Fenske, P., et al. (2019). Neuromodulator Signaling Bidirectionally Controls Vesicle

Numbers in Human Synapses. *Cell, 179*(2), 498-513 e422. https://doi.org/10.1016/j.cell.2019.09.011

Penagarikano, O., Abrahams, B. S., Herman, E. I., Winden, K. D., Gdalyahu, A., Dong, H., et al. (2011). Absence of CNTNAP2 leads to epilepsy, neuronal migration abnormalities, and core autism-related deficits. *Cell, 147*(1), 235-246. https://doi.org/10.1016/j.cell.2011.08.040

Photowala, H., Blackmer, T., Schwartz, E., Hamm, H. E., & Alford, S. (2006). G protein betagamma-subunits activated by serotonin mediate presynaptic inhibition by regulating vesicle fusion properties. *Proc Natl Acad Sci U S A, 103*(11), 4281-4286. https://doi.org/10.1073/pnas.0600509103

Pickel, V. M., & Chan, J. (1999). Ultrastructural localization of the serotonin transporter in limbic and motor compartments of the nucleus accumbens. *J Neurosci, 19*(17), 7356-7366. Retrieved from https://www.ncbi.nlm.nih.gov/pubmed/10460242

Pinto, D., Delaby, E., Merico, D., Barbosa, M., Merikangas, A., Klei, L., et al. (2014). Convergence of genes and cellular pathways dysregulated in autism spectrum disorders. *Am J Hum Genet, 94*(5), 677-694. https://doi.org/10.1016/j.ajhg.2014.03.018

Pithadia, A. B., & Jain, S. M. (2009). 5-Hydroxytryptamine Receptor Subtypes and their Modulators with Therapeutic Potentials. *J Clin Med Res, 1*(2), 72-80. https://doi.org/10.4021/jocmr2009.05.1237

Pourhamzeh, M., Moravej, F. G., Arabi, M., Shahriari, E., Mehrabi, S., Ward, R., et al. (2021). The Roles of Serotonin in Neuropsychiatric Disorders. *Cell Mol Neurobiol*. https://doi.org/10.1007/s10571-021-01064-9

Proctor, D. T., Stotz, S. C., Scott, L. O. M., de la Hoz, C. L. R., Poon, K. W. C., Stys, P. K., et al. (2015). Axo-glial communication through neurexin-neuroligin signaling regulates myelination and oligodendrocyte differentiation. *Glia, 63*(11), 2023-2039. https://doi.org/10.1002/glia.22875

Puig, M. V., Artigas, F., & Celada, P. (2005). Modulation of the activity of pyramidal neurons in rat prefrontal cortex by raphe stimulation in vivo: involvement of serotonin and GABA. *Cereb Cortex, 15*(1), 1-14. https://doi.org/10.1093/cercor/bhh104

Puschel, A. W., & Betz, H. (1995). Neurexins are differentially expressed in the embryonic nervous system of mice. *J Neurosci, 15*(4), 2849-2856. Retrieved from https://www.ncbi.nlm.nih.gov/pubmed/7722633

Quah, S. K. L., McIver, L., Roberts, A. C., & Santangelo, A. M. (2020). Trait Anxiety Mediated by Amygdala Serotonin Transporter in the Common Marmoset. *J Neurosci, 40*(24), 4739-4749. https://doi.org/10.1523/JNEUROSCI.2930-19.2020

Quentin, E., Belmer, A., & Maroteaux, L. (2018). Somato-Dendritic Regulation of Raphe Serotonin Neurons; A Key to Antidepressant Action. *Front Neurosci, 12*, 982. https://doi.org/10.3389/fnins.2018.00982

Rabaneda, L. G., Robles-Lanuza, E., Nieto-Gonzalez, J. L., & Scholl, F. G. (2014). Neurexin dysfunction in adult neurons results in autistic-like

behavior in mice. *Cell Rep, 8*(2), 338-346. https://doi.org/10.1016/j.celrep.2014.06.022

Rein, B., Ma, K., & Yan, Z. (2020). A standardized social preference protocol for measuring social deficits in mouse models of autism. *Nat Protoc, 15*(10), 3464-3477. https://doi.org/10.1038/s41596-020-0382-9

Reissner, C., Klose, M., Fairless, R., & Missler, M. (2008). Mutational analysis of the neurexin/neuroligin complex reveals essential and regulatory components. *Proc Natl Acad Sci U S A, 105*(39), 15124-15129. https://doi.org/10.1073/pnas.0801639105

Ren, J., Friedmann, D., Xiong, J., Liu, C. D., Ferguson, B. R., Weerakkody, T., et al. (2018). Anatomically Defined and Functionally Distinct Dorsal Raphe Serotonin Sub-systems. *Cell, 175*(2), 472-487 e420. https://doi.org/10.1016/j.cell.2018.07.043

Ren, J., Isakova, A., Friedmann, D., Zeng, J., Grutzner, S. M., Pun, A., et al. (2019). Single-cell transcriptomes and whole-brain projections of serotonin neurons in the mouse dorsal and median raphe nuclei. *Elife, 8*. https://doi.org/10.7554/eLife.49424

Rice, C. E., Rosanoff, M., Dawson, G., Durkin, M. S., Croen, L. A., Singer, A., et al. (2012). Evaluating Changes in the Prevalence of the Autism Spectrum Disorders (ASDs). *Public Health Rev, 34*(2), 1-22. https://doi.org/10.1007/BF03391685

Richardson-Jones, J. W., Craige, C. P., Nguyen, T. H., Kung, H. F., Gardier, A. M., Dranovsky, A., et al. (2011). Serotonin-1A autoreceptors are necessary and sufficient for the normal formation of circuits underlying innate anxiety. *J Neurosci, 31*(16), 6008-6018. https://doi.org/10.1523/JNEUROSCI.5836-10.2011

RK, C. Y., Merico, D., Bookman, M., J, L. H., Thiruvahindrapuram, B., Patel, R. V., et al. (2017). Whole genome sequencing resource identifies 18 new candidate genes for autism spectrum disorder. *Nat Neurosci, 20*(4), 602-611. https://doi.org/10.1038/nn.4524

Rylaarsdam, L., & Guemez-Gamboa, A. (2019). Genetic Causes and Modifiers of Autism Spectrum Disorder. *Front Cell Neurosci, 13*, 385. https://doi.org/10.3389/fncel.2019.00385

Sachs, B. D., Ni, J. R., & Caron, M. G. (2015). Brain 5-HT deficiency increases stress vulnerability and impairs antidepressant responses following psychosocial stress. *Proc Natl Acad Sci U S A, 112*(8), 2557-2562. https://doi.org/10.1073/pnas.1416866112

Sanchez, C., Bergqvist, P. B., Brennum, L. T., Gupta, S., Hogg, S., Larsen, A., et al. (2003). Escitalopram, the S-(+)-enantiomer of citalopram, is a selective serotonin reuptake inhibitor with potent effects in animal models predictive of antidepressant and anxiolytic activities. *Psychopharmacology (Berl), 167*(4), 353-362. https://doi.org/10.1007/s00213-002-1364-z

Sanchez, C., & Hyttel, J. (1999). Comparison of the effects of antidepressants and their metabolites on reuptake of biogenic amines and on receptor

binding. *Cell Mol Neurobiol, 19*(4), 467-489. https://doi.org/10.1023/a:1006986824213

Saylor, R. A., Hersey, M., West, A., Buchanan, A. M., Berger, S. N., Nijhout, H. F., et al. (2019). In vivo Hippocampal Serotonin Dynamics in Male and Female Mice: Determining Effects of Acute Escitalopram Using Fast Scan Cyclic Voltammetry. *Front Neurosci, 13*, 362. https://doi.org/10.3389/fnins.2019.00362

Schreiner, D., Nguyen, T. M., Russo, G., Heber, S., Patrignani, A., Ahrne, E., et al. (2014). Targeted combinatorial alternative splicing generates brain region-specific repertoires of neurexins. *Neuron, 84*(2), 386-398. https://doi.org/10.1016/j.neuron.2014.09.011

Schreiner, D., Simicevic, J., Ahrne, E., Schmidt, A., & Scheiffele, P. (2015). Quantitative isoform-profiling of highly diversified recognition molecules. *Elife, 4*, e07794. https://doi.org/10.7554/eLife.07794

Scott, M. M., Wylie, C. J., Lerch, J. K., Murphy, R., Lobur, K., Herlitze, S., et al. (2005). A genetic approach to access serotonin neurons for in vivo and in vitro studies. *Proc Natl Acad Sci U S A, 102*(45), 16472-16477. https://doi.org/10.1073/pnas.0504510102

Sebat, J., Lakshmi, B., Malhotra, D., Troge, J., Lese-Martin, C., Walsh, T., et al. (2007). Strong association of de novo copy number mutations with autism. *Science, 316*(5823), 445-449. https://doi.org/10.1126/science.1138659

Selten, M., van Bokhoven, H., & Nadif Kasri, N. (2018). Inhibitory control of the excitatory/inhibitory balance in psychiatric disorders. *F1000Res, 7*, 23. https://doi.org/10.12688/f1000research.12155.1

Selvaraj, S., Arnone, D., Cappai, A., & Howes, O. (2014). Alterations in the serotonin system in schizophrenia: a systematic review and meta-analysis of postmortem and molecular imaging studies. *Neurosci Biobehav Rev, 45*, 233-245. https://doi.org/10.1016/j.neubiorev.2014.06.005

Silverman, J. L., Yang, M., Lord, C., & Crawley, J. N. (2010). Behavioural phenotyping assays for mouse models of autism. *Nat Rev Neurosci, 11*(7), 490-502. https://doi.org/10.1038/nrn2851

Singh, S. K., Stogsdill, J. A., Pulimood, N. S., Dingsdale, H., Kim, Y. H., Pilaz, L. J., et al. (2016). Astrocytes Assemble Thalamocortical Synapses by Bridging NRX1alpha and NL1 via Hevin. *Cell, 164*(1-2), 183-196. https://doi.org/10.1016/j.cell.2015.11.034

Slattery, D. A., & Cryan, J. F. (2012). Using the rat forced swim test to assess antidepressant-like activity in rodents. *Nat Protoc, 7*(6), 1009-1014. https://doi.org/10.1038/nprot.2012.044

Sommer, C. (2010). CHAPTER 3.11 - Serotonin in Pain and Pain Control. In C. P. Müller & B. L. Jacobs (Eds.), *Handbook of Behavioral Neuroscience* (Vol. 21, pp. 457-471): Elsevier.

Sons, M. S., Busche, N., Strenzke, N., Moser, T., Ernsberger, U., Mooren, F. C., et al. (2006). alpha-Neurexins are required for efficient transmitter release and synaptic homeostasis at the mouse neuromuscular junction.

Neuroscience, 138(2), 433-446. https://doi.org/10.1016/j.neuroscience.2005.11.040

Sterky, F. H., Trotter, J. H., Lee, S. J., Recktenwald, C. V., Du, X., Zhou, B., et al. (2017). Carbonic anhydrase-related protein CA10 is an evolutionarily conserved pan-neurexin ligand. *Proc Natl Acad Sci U S A, 114*(7), E1253-E1262. https://doi.org/10.1073/pnas.1621321114

Stogsdill, J. A., Ramirez, J., Liu, D., Kim, Y. H., Baldwin, K. T., Enustun, E., et al. (2017). Astrocytic neuroligins control astrocyte morphogenesis and synaptogenesis. *Nature, 551*(7679), 192-197. https://doi.org/10.1038/nature24638

Sudhof, T. C. (2017). Synaptic Neurexin Complexes: A Molecular Code for the Logic of Neural Circuits. *Cell, 171*(4), 745-769. https://doi.org/10.1016/j.cell.2017.10.024

Sugita, S., Saito, F., Tang, J., Satz, J., Campbell, K., & Sudhof, T. C. (2001). A stoichiometric complex of neurexins and dystroglycan in brain. *J Cell Biol, 154*(2), 435-445. Retrieved from http://www.ncbi.nlm.nih.gov/pubmed/11470830

Sun, X., Zhao, Y., & Wolf, M. E. (2005). Dopamine receptor stimulation modulates AMPA receptor synaptic insertion in prefrontal cortex neurons. *J Neurosci, 25*(32), 7342-7351. https://doi.org/10.1523/JNEUROSCI.4603-04.2005

Szatmari, P., Paterson, A. D., Zwaigenbaum, L., Roberts, W., Brian, J., Liu, X. Q., et al. (2007). Mapping autism risk loci using genetic linkage and chromosomal rearrangements. *Nat Genet, 39*(3), 319-328. https://doi.org/10.1038/ng1985

Tabuchi, K., Blundell, J., Etherton, M. R., Hammer, R. E., Liu, X., Powell, C. M., et al. (2007). A neuroligin-3 mutation implicated in autism increases inhibitory synaptic transmission in mice. *Science, 318*(5847), 71-76. https://doi.org/10.1126/science.1146221

Tabuchi, K., & Sudhof, T. C. (2002). Structure and evolution of neurexin genes: insight into the mechanism of alternative splicing. *Genomics, 79*(6), 849-859. https://doi.org/10.1006/geno.2002.6780

Tanabe, Y., Naito, Y., Vasuta, C., Lee, A. K., Soumounou, Y., Linhoff, M. W., et al. (2017). IgSF21 promotes differentiation of inhibitory synapses via binding to neurexin2alpha. *Nat Commun, 8*(1), 408. https://doi.org/10.1038/s41467-017-00333-w

Tanaka, M., Sato, A., Kasai, S., Hagino, Y., Kotajima-Murakami, H., Kashii, H., et al. (2018). Brain hyperserotonemia causes autism-relevant social deficits in mice. *Mol Autism, 9*, 60. https://doi.org/10.1186/s13229-018-0243-3

Taylor, M. J., Rosenqvist, M. A., Larsson, H., Gillberg, C., D'Onofrio, B. M., Lichtenstein, P., et al. (2020). Etiology of Autism Spectrum Disorders and Autistic Traits Over Time. *JAMA Psychiatry, 77*(9), 936-943. https://doi.org/10.1001/jamapsychiatry.2020.0680

Teissier, A., Chemiakine, A., Inbar, B., Bagchi, S., Ray, R. S., Palmiter, R. D., et al. (2015). Activity of Raphe Serotonergic Neurons Controls Emotional Behaviors. *Cell Rep, 13*(9), 1965-1976. https://doi.org/10.1016/j.celrep.2015.10.061

Teixeira, C. M., Rosen, Z. B., Suri, D., Sun, Q., Hersh, M., Sargin, D., et al. (2018). Hippocampal 5-HT Input Regulates Memory Formation and Schaffer Collateral Excitation. *Neuron, 98*(5), 992-1004 e1004. https://doi.org/10.1016/j.neuron.2018.04.030

Thomas, D. R., Melotto, S., Massagrande, M., Gribble, A. D., Jeffrey, P., Stevens, A. J., et al. (2003). SB-656104-A, a novel selective 5-HT7 receptor antagonist, modulates REM sleep in rats. *Br J Pharmacol, 139*(4), 705-714. https://doi.org/10.1038/sj.bjp.0705290

Tian, Z., Yamanaka, M., Bernabucci, M., Zhao, M. G., & Zhuo, M. (2017). Characterization of serotonin-induced inhibition of excitatory synaptic transmission in the anterior cingulate cortex. *Mol Brain, 10*(1), 21. https://doi.org/10.1186/s13041-017-0303-1

Treutlein, B., Gokce, O., Quake, S. R., & Sudhof, T. C. (2014). Cartography of neurexin alternative splicing mapped by single-molecule long-read mRNA sequencing. *Proc Natl Acad Sci U S A, 111*(13), E1291-1299. https://doi.org/10.1073/pnas.1403244111

Tromp, A., Mowry, B., & Giacomotto, J. (2021). Neurexins in autism and schizophrenia-a review of patient mutations, mouse models and potential future directions. *Mol Psychiatry, 26*(3), 747-760. https://doi.org/10.1038/s41380-020-00944-8

Trotter, J. H., Hao, J., Maxeiner, S., Tsetsenis, T., Liu, Z., Zhuang, X., et al. (2019). Synaptic neurexin-1 assembles into dynamically regulated active zone nanoclusters. *J Cell Biol, 218*(8), 2677-2698. https://doi.org/10.1083/jcb.201812076

Twining, R. C., Vantrease, J. E., Love, S., Padival, M., & Rosenkranz, J. A. (2017). An intra-amygdala circuit specifically regulates social fear learning. *Nat Neurosci, 20*(3), 459-469. https://doi.org/10.1038/nn.4481

Uchigashima, M., Cheung, A., Suh, J., Watanabe, M., & Futai, K. (2019). Differential expression of neurexin genes in the mouse brain. *J Comp Neurol, 527*(12), 1940-1965. https://doi.org/10.1002/cne.24664

Uchigashima, M., Konno, K., Demchak, E., Cheung, A., Watanabe, T., Keener, D. G., et al. (2020). Specific Neuroligin3-alphaNeurexin1 signaling regulates GABAergic synaptic function in mouse hippocampus. *Elife, 9*. https://doi.org/10.7554/eLife.59545

Uchigashima, M., Leung, M., Watanabe, T., Cheung, A., Le, T., Pallat, S., et al. (2020). Neuroligin3 splice isoforms shape inhibitory synaptic function in the mouse hippocampus. *J Biol Chem, 295*(25), 8589-8595. https://doi.org/10.1074/jbc.AC120.012571

Uchigashima, M., Ohtsuka, T., Kobayashi, K., & Watanabe, M. (2016). Dopamine synapse is a neuroligin-2-mediated contact between dopaminergic

presynaptic and GABAergic postsynaptic structures. *Proc Natl Acad Sci U S A, 113*(15), 4206-4211. https://doi.org/10.1073/pnas.1514074113

Ucok, A., & Gaebel, W. (2008). Side effects of atypical antipsychotics: a brief overview. *World Psychiatry, 7*(1), 58-62. https://doi.org/10.1002/j.2051-5545.2008.tb00154.x

Uemura, T., Lee, S. J., Yasumura, M., Takeuchi, T., Yoshida, T., Ra, M., et al. (2010). Trans-synaptic interaction of GluRdelta2 and Neurexin through Cbln1 mediates synapse formation in the cerebellum. *Cell, 141*(6), 1068-1079. https://doi.org/10.1016/j.cell.2010.04.035

Uemura, T., Suzuki, E., Kawase, S., Kurihara, T., Yasumura, M., Yoshida, T., et al. (2020). Neurexins play a crucial role in cerebellar granule cell survival by organizing autocrine machinery for neurotrophins *Submitted*.

Ullrich, B., Ushkaryov, Y. A., & Sudhof, T. C. (1995). Cartography of neurexins: more than 1000 isoforms generated by alternative splicing and expressed in distinct subsets of neurons. *Neuron, 14*(3), 497-507. https://doi.org/10.1016/0896-6273(95)90306-2

Unichenko, P., Yang, J. W., Kirischuk, S., Kolbaev, S., Kilb, W., Hammer, M., et al. (2018). Autism Related Neuroligin-4 Knockout Impairs Intracortical Processing but not Sensory Inputs in Mouse Barrel Cortex. *Cereb Cortex, 28*(8), 2873-2886. https://doi.org/10.1093/cercor/bhx165

Ushkaryov, Y. A., Petrenko, A. G., Geppert, M., & Sudhof, T. C. (1992). Neurexins: synaptic cell surface proteins related to the alpha-latrotoxin receptor and laminin. *Science, 257*(5066), 50-56. Retrieved from http://www.ncbi.nlm.nih.gov/pubmed/1621094

Vaags, A. K., Lionel, A. C., Sato, D., Goodenberger, M., Stein, Q. P., Curran, S., et al. (2012). Rare deletions at the neurexin 3 locus in autism spectrum disorder. *Am J Hum Genet, 90*(1), 133-141. https://doi.org/10.1016/j.ajhg.2011.11.025

Varga, V., Losonczy, A., Zemelman, B. V., Borhegyi, Z., Nyiri, G., Domonkos, A., et al. (2009). Fast synaptic subcortical control of hippocampal circuits. *Science, 326*(5951), 449-453. https://doi.org/10.1126/science.1178307

Vicari, S., Napoli, E., Cordeddu, V., Menghini, D., Alesi, V., Loddo, S., et al. (2019). Copy number variants in autism spectrum disorders. *Prog Neuropsychopharmacol Biol Psychiatry, 92*, 421-427. https://doi.org/10.1016/j.pnpbp.2019.02.012

Vinas-Jornet, M., Esteba-Castillo, S., Gabau, E., Ribas-Vidal, N., Baena, N., San, J., et al. (2014). A common cognitive, psychiatric, and dysmorphic phenotype in carriers of NRXN1 deletion. *Mol Genet Genomic Med, 2*(6), 512-521. https://doi.org/10.1002/mgg3.105

Vitalis, T., Ansorge, M. S., & Dayer, A. G. (2013). Serotonin homeostasis and serotonin receptors as actors of cortical construction: special attention to the 5-HT3A and 5-HT6 receptor subtypes. *Front Cell Neurosci, 7*, 93. https://doi.org/10.3389/fncel.2013.00093

Vrijenhoek, T., Buizer-Voskamp, J. E., van der Stelt, I., Strengman, E., Genetic, R., Outcome in Psychosis, C., et al. (2008). Recurrent CNVs disrupt three candidate genes in schizophrenia patients. *Am J Hum Genet, 83*(4), 504-510. https://doi.org/10.1016/j.ajhg.2008.09.011

Waider, J., Popp, S., Mlinar, B., Montalbano, A., Bonfiglio, F., Aboagye, B., et al. (2019). Serotonin Deficiency Increases Context-Dependent Fear Learning Through Modulation of Hippocampal Activity. *Front Neurosci, 13*, 245. https://doi.org/10.3389/fnins.2019.00245

Walsh, J. J., Christoffel, D. J., Heifets, B. D., Ben-Dor, G. A., Selimbeyoglu, A., Hung, L. W., et al. (2018). 5-HT release in nucleus accumbens rescues social deficits in mouse autism model. *Nature, 560*(7720), 589-594. https://doi.org/10.1038/s41586-018-0416-4

Wang, H. L., Zhang, S., Qi, J., Wang, H., Cachope, R., Mejias-Aponte, C. A., et al. (2019). Dorsal Raphe Dual Serotonin-Glutamate Neurons Drive Reward by Establishing Excitatory Synapses on VTA Mesoaccumbens Dopamine Neurons. *Cell Rep, 26*(5), 1128-1142 e1127. https://doi.org/10.1016/j.celrep.2019.01.014

Wang, J., Gong, J., Li, L., Chen, Y., Liu, L., Gu, H., et al. (2018). Neurexin gene family variants as risk factors for autism spectrum disorder. *Autism Res, 11*(1), 37-43. https://doi.org/10.1002/aur.1881

Werling, D. M., & Geschwind, D. H. (2013). Sex differences in autism spectrum disorders. *Curr Opin Neurol, 26*(2), 146-153. https://doi.org/10.1097/WCO.0b013e32835ee548

Werneburg, S., Jung, J., Kunjamma, R. B., Ha, S. K., Luciano, N. J., Willis, C. M., et al. (2020). Targeted Complement Inhibition at Synapses Prevents Microglial Synaptic Engulfment and Synapse Loss in Demyelinating Disease. *Immunity, 52*(1), 167-182 e167. https://doi.org/10.1016/j.immuni.2019.12.004

Wieland, S., & Lucki, I. (1990). Antidepressant-like activity of 5-HT1A agonists measured with the forced swim test. *Psychopharmacology (Berl), 101*(4), 497-504. https://doi.org/10.1007/BF02244228

Williams, K., Brignell, A., Randall, M., Silove, N., & Hazell, P. (2013). Selective serotonin reuptake inhibitors (SSRIs) for autism spectrum disorders (ASD). *Cochrane Database Syst Rev*(8), CD004677. https://doi.org/10.1002/14651858.CD004677.pub3

Won, H., Mah, W., & Kim, E. (2013). Autism spectrum disorder causes, mechanisms, and treatments: focus on neuronal synapses. *Front Mol Neurosci, 6*, 19. https://doi.org/10.3389/fnmol.2013.00019

Yagishita-Kyo, N., Ikai, Y., Uekita, T., Shinohara, A., Koshimoto, C., Yoshikawa, K., et al. (2021). Testosterone interrupts binding of Neurexin and Neuroligin that are expressed in a highly socialized rodent, Octodon degus. *Biochem Biophys Res Commun, 551*, 54-62. https://doi.org/10.1016/j.bbrc.2021.03.015

Yamasaki, M., Matsui, M., & Watanabe, M. (2010). Preferential localization of muscarinic M1 receptor on dendritic shaft and spine of cortical pyramidal cells and its anatomical evidence for volume transmission. *J Neurosci, 30*(12), 4408-4418. https://doi.org/10.1523/JNEUROSCI.5719-09.2010

Yamasaki, M., Yamada, K., Furuya, S., Mitoma, J., Hirabayashi, Y., & Watanabe, M. (2001). 3-Phosphoglycerate dehydrogenase, a key enzyme for l-serine biosynthesis, is preferentially expressed in the radial glia/astrocyte lineage and olfactory ensheathing glia in the mouse brain. *J Neurosci, 21*(19), 7691-7704. Retrieved from http://www.ncbi.nlm.nih.gov/pubmed/11567059

Yan, J., Noltner, K., Feng, J., Li, W., Schroer, R., Skinner, C., et al. (2008). Neurexin 1alpha structural variants associated with autism. *Neurosci Lett, 438*(3), 368-370. https://doi.org/10.1016/j.neulet.2008.04.074

Yang, M., Silverman, J. L., & Crawley, J. N. (2011). Automated three-chambered social approach task for mice. *Curr Protoc Neurosci, Chapter 8*, Unit 8 26. https://doi.org/10.1002/0471142301.ns0826s56

Yang, M., Zhodzishsky, V., & Crawley, J. N. (2007). Social deficits in BTBR T+tf/J mice are unchanged by cross-fostering with C57BL/6J mothers. *Int J Dev Neurosci, 25*(8), 515-521. https://doi.org/10.1016/j.ijdevneu.2007.09.008

Yankelevitch-Yahav, R., Franko, M., Huly, A., & Doron, R. (2015). The forced swim test as a model of depressive-like behavior. *J Vis Exp*(97). https://doi.org/10.3791/52587

Ye, R., Quinlan, M. A., Iwamoto, H., Wu, H. H., Green, N. H., Jetter, C. S., et al. (2015). Physical Interactions and Functional Relationships of Neuroligin 2 and Midbrain Serotonin Transporters. *Front Synaptic Neurosci, 7*, 20. https://doi.org/10.3389/fnsyn.2015.00020

Yoshitake, T., Wang, F. H., Kuteeva, E., Holmberg, K., Yamaguchi, M., Crawley, J. N., et al. (2004). Enhanced hippocampal noradrenaline and serotonin release in galanin-overexpressing mice after repeated forced swimming test. *Proc Natl Acad Sci U S A, 101*(1), 354-359. https://doi.org/10.1073/pnas.0307042101

Yu, P., McKinney, E. C., Kandasamy, M. M., Albert, A. L., & Meagher, R. B. (2015). Characterization of brain cell nuclei with decondensed chromatin. *Dev Neurobiol, 75*(7), 738-756. https://doi.org/10.1002/dneu.22245

Yuen, R., Merico, D., Bookman, M., J, L. H., Thiruvahindrapuram, B., Patel, R. V., et al. (2017). Whole genome sequencing resource identifies 18 new candidate genes for autism spectrum disorder. *Nat Neurosci, 20*(4), 602-611. https://doi.org/10.1038/nn.4524

Zahir, F. R., Baross, A., Delaney, A. D., Eydoux, P., Fernandes, N. D., Pugh, T., et al. (2008). A patient with vertebral, cognitive and behavioural abnormalities and a de novo deletion of NRXN1alpha. *J Med Genet, 45*(4), 239-243. https://doi.org/10.1136/jmg.2007.054437

Zhang, C., Atasoy, D., Arac, D., Yang, X., Fucillo, M. V., Robison, A. J., et al. (2010). Neurexins physically and functionally interact with GABA(A)

receptors. *Neuron, 66*(3), 403-416. https://doi.org/10.1016/j.neuron.2010.04.008

Zhang, D., Cheng, L., Qian, Y., Alliey-Rodriguez, N., Kelsoe, J. R., Greenwood, T., et al. (2009). Singleton deletions throughout the genome increase risk of bipolar disorder. *Mol Psychiatry, 14*(4), 376-380. https://doi.org/10.1038/mp.2008.144

Zhang, L., Ma, W., Barker, J. L., & Rubinow, D. R. (1999). Sex differences in expression of serotonin receptors (subtypes 1A and 2A) in rat brain: a possible role of testosterone. *Neuroscience, 94*(1), 251-259. https://doi.org/10.1016/s0306-4522(99)00234-1

Zhang, W., Rohlmann, A., Sargsyan, V., Aramuni, G., Hammer, R. E., Sudhof, T. C., et al. (2005). Extracellular domains of alpha-neurexins participate in regulating synaptic transmission by selectively affecting N- and P/Q-type Ca2+ channels. *J Neurosci, 25*(17), 4330-4342. https://doi.org/10.1523/JNEUROSCI.0497-05.2005

Zhang, Y., Li, N., Li, C., Zhang, Z., Teng, H., Wang, Y., et al. (2020). Genetic evidence of gender difference in autism spectrum disorder supports the female-protective effect. *Transl Psychiatry, 10*(1), 4. https://doi.org/10.1038/s41398-020-0699-8

Zhou, F. C., Tao-Cheng, J. H., Segu, L., Patel, T., & Wang, Y. (1998). Serotonin transporters are located on the axons beyond the synaptic junctions: anatomical and functional evidence. *Brain Res, 805*(1-2), 241-254. https://doi.org/10.1016/s0006-8993(98)00691-x

Zhu, P. C., Thureson-Klein, A., & Klein, R. L. (1986). Exocytosis from large dense cored vesicles outside the active synaptic zones of terminals within the trigeminal subnucleus caudalis: a possible mechanism for neuropeptide release. *Neuroscience, 19*(1), 43-54. https://doi.org/10.1016/0306-4522(86)90004-7

Zoghbi, H. Y., & Bear, M. F. (2012). Synaptic dysfunction in neurodevelopmental disorders associated with autism and intellectual disabilities. *Cold Spring Harb Perspect Biol, 4*(3). https://doi.org/10.1101/cshperspect.a009886

Zweier, C. (2012). Severe Intellectual Disability Associated with Recessive Defects in CNTNAP2 and NRXN1. *Mol Syndromol, 2*(3-5), 181-185. https://doi.org/10.1159/000331270